2022

Long-Term Durability of Rooftop Grid-Connected Solar Photovoltaic Systems

Chibuisi Chinasaokwu Okorieimoh
Technological University Dublin, nasachibuisi@outlook.com

Recommended Citation

Long-Term Durability of Rooftop Grid-Connected Solar Photovoltaic Systems

by

Chibuisi Chinasaokwu Okorieimoh

Thesis submitted in fulfilment of the requirements for the degree of

Doctor of Philosophy

June 2022

ABSTRACT

Compared to their initial performance, solar photovoltaic (PV) arrays show long-term performance degradation, resulting in lower like-for-like efficiencies and performance ratios. The long-term durability of polycrystalline silicon (p-Si) solar PV modules in three roof-top grid-connected arrays has been examined. Electrical output, ambient temperature, cell temperature, solar irradiance, solar irradiation, and wind speed data were collected at hourly intervals from 2017 to 2021 from three 50 kWp PV installations in Northern Ireland. The results show the extent to which higher PV temperatures associated with more intense solar radiation decrease efficiency, fill factor and maximum power output for PV arrays in a temperate climate.

Long-term durability trends for grid-connected roof-top solar photovoltaic systems can be obscured by diurnal and seasonal changes in environmental conditions. To reduce the influence of variable conditions, performance ratios (PR_{corr}) were "corrected" using the measured annual average cell temperature (T_{cell_avg}). Introduction of this temperature-correction reduced the seasonal variation of the performance ratio.

Using temperature-corrected performance ratios, long-term (in this case those seen after five-years operation) performance degradation trends become evident with high confidence after six months for one PV array and within three years for the two other arrays. If lower statistical confidence in trends is acceptable, long-term degradation rates can be identified within one year of operation for all PV arrays examined.

These results have the important implication that relatively short-duration outdoor PV performance monitoring may be reliably used to estimate long-term degradation and/or to calibrate normally-conducted accelerated testing.

DECLARATION PAGE

I certify that this thesis which I now submit for examination for the award of PhD is entirely my work. All the works taken from the research journals, conference papers, research reports, books and periodicals have been duly cited.

I hereby affirm that this thesis has been prepared following the regulations of the Graduate Research School of Technological University Dublin and has not been submitted in whole or in part for another award in any Institution. The work reported on in this thesis conforms to the principles and requirements of the University's guidelines for ethics in research. Therefore, the University has permission to keep, lend or copy this thesis in whole or in part, on condition that any such use of the material of the thesis is duly acknowledged.

Signature _____ Date _____

ACKNOWLEDGEMENT

I wish to sincerely thank my thesis supervisors Prof. Brian Norton and Prof. Michael Conlon for their novel and expert contributions with an update of recent research papers and information which led to the completion of this project. I am grateful to ESB Networks especially Mr Desmond Lalor for their approval of using their PV site portals for this research study. I also thank Dr Marek Rebow, the Head of Research for always responding to emails promptly when the need for research queries arises.

My sincere gratitude goes to Technological University Dublin for awarding me with Fiosraigh Scholarship which assists in funding this research. Dublin Energy Lab and ESHI, Grangegorman are not left out in my hearty gratitude for they have contributed immensely through their research colloquiums where I have gained more research insight and advice.

I also wish to thank my beloved wife Mrs Ezinne O. Okorieimoh who will always provide me with domestic support and ensure that I am emotionally strong to get the research going and controlled our little children during the research meetings via MS teams, especially in the era of COVID-19 lockdown.

Above all, I give all Glory and Honour to God Almighty through him I have strong faith that this journey will end smoothly without a problem.

DEDICATION

I dedicate this work to my late parents who are lovers of Education. Their support of my academic journey has been a trademark.

Table of Contents

List of Tables

xiii

List of Figures

xvii

Nomenclature

$\emptyset$	Latitude (^{o})
Δn	Excess carrier concentration (m^{-3})
a	Annum
A	Area (m^2)
a_c	Temperature-dependent diode non-ideality factor (K^{-1})
A_{cell}	Area of the solar PV cell (m^2)
A_m	Module area (m^2)
di	Difference between corrected absolute and relative performance loss rates
n	Diode's ideality factor
$D_{PLRcorr}$	Differences in temperature-corrected performance loss rates in arrays and systems
$D_{PLRuncorr}$	Differences in uncorrected performance loss rates in arrays and systems
$E_{AC,d}$	Average monthly daily total AC output (kWh)
$E_{DC,d}$	Average monthly daily total DC output (kWh)
q	Electronic charge (1.60218×10^{-19}C)
FF	Fill factor
G	Generation rate (in Photons$A^{-1}s^{-1}m^{-1}$)
G_R/G_{STC}	Reference solar irradiance (1000 Wm^{-2})
G_R/POA	Incident solar radiation at the plane of the arrays (Wm^{-2})
h	Altitude (m)
I	Current (A)
I_L	Light generated current (A)

I_o	Low reverse diode saturation current (A)
I_{ph}	Photo-current (A)
I_{SC}	Short-circuit current (A)
J	Current density (Am^{-2})
J_{SC}	Short-current density (Am^{-2})
L_C	DC array capture loss (hour/day)
N_A	Doping concentration (at.%)
η_{cell}	Solar PV cell efficiency
$\mathbf{n}_i$	Intrinsic carrier concentration (m^{-3})
η_{inv}	Inverter efficiency
$\eta_{inv, m}$	Monthly inverter efficiency
η_{module}	Solar energy conversion efficiency of a PV module
$\eta_{module,STC}$	Module efficiency at standard test conditions
η_{module_m}	Average monthly PV module conversion efficiency
n_p	Number of solar PV cells in parallel
n_s	Number of solar PV cells in series
N_s	Number of solar cells connected in series which constitutes a PV module
η_{Sys}	System efficiency
O	Probability of occurrence of defect
V_{OC}	Open-circuit voltage (V)
V	Operating voltage at the terminal of a PV module (V)
P_{AC}	AC power output (W)
P_{DC}	Module capacity (W)
P_{DCd}	Average monthly daily total DC output (W)

PF	Packing factor
P_{in}	Input power (W)
PLR_{abs}	Absolute performance loss rate
$PLR_{abs.corr}$	Absolute temperature-corrected performance loss rates in arrays and systems
$PLR_{abs.uncorr}$	Absolute uncorrected performance loss rates in arrays and systems
$PLR_{rel.corr}$	Relative temperature-corrected performance loss rate
PLR_{corr_abs}	Absolute weather-corrected performance loss rates
PLR_{rel}	Relative performance loss rate
$PLR_{rel.corr}$	Relative temperature-corrected performance loss rates in arrays and systems
$PLR_{rel.uncorr}$	Relative uncorrected performance loss rates in arrays and systems
PLR_{uncorr}	Relative weather-corrected performance loss rate
P_{Max}	Maximum power (W)
P_o	Power output (W)
$P_{PV},rated$	Installed PV module capacity (W)
PR	Performance ratio
PR_A	Array performance ratio
PR_{avg}	Monthly average system performance ratios
$PR_{corrected}$	Temperature-corrected performance ratio
PR_{Syst}	System performance ratio
$PR_{uncorrected}$	Weather-uncorrected performance ratio
T_{cell}	PV module operating temperature/cell temperature (K)

k	Stefan Boltzmann constant ($1.38066 \times 10^{-23} JK^{-1}$)
t	Data collection period (s)
t_{cal}	Calculated t-value
T_{cell_avg}	Average annual PV cell temperature (^{o}C)
L_n	Electron diffusion length (µm)
L_p	Hole diffusion length (µm)
V_T	Thermal voltage of a diode (V)
y	Proportionality constant
y_A	Array yield (hour/day)
y_f	Final yield (hour/day)
y_r	Reference yield (hour/day)
Yt	Time-series linear regression model
α	Sun elevation angle (^{o})
β_1	Gradient of linear trend line for PLR
β_o	y-intercept of the linear trend line for PLR
$\boldsymbol{\beta}_{ref}$	Temperature coefficient of a PV cell (K^{-1})
δ	Declination angle (^{o})
θz	Zenith angle (^{o})
$\boldsymbol{\omega\_sr}$	Hour angle of sunrise (^{o})
$\boldsymbol{\omega\_ss}$	Hour angle of sunset (^{o})
d	Inter-row spacing (m)
D	Likelihood that available data can detect failure modes
DF	Degree of freedom
L_{SH}	Shadow length (m)
N	Number of days

R_{th}	Equivalent thermal resistance ($^{o}CW^{-1}$)
S	Severity of damage
R	Resistance (Ω)
R^2	Coefficient of determination
RPN	Risk priority number
R_S	Series resistance (Ω)
R_{SH}	Shunt or parallel resistance (Ω)

Abbreviation

μ_{abs}	Absolute averages of the temperature-corrected performance loss rates
μ_{rel}	Relative averages of the temperature-corrected performance loss rates
AC	Alternating current
AET	Accelerated environmental testing
Ag	Silver
ALT	Accelerated life testing
AR	Anti-reflective
a-Si	Amorphous-silicon
a-Si:H	Hydrogenated amorphous silicon
CdTe	Cadmium telluride
Ce	Cerium
CIS	Copper indium diselenide
DC	Direct current
EL	Electroluminescence
ESB	Electricity Supply Board
EVA	Ethyl vinyl acetate
FMEA	Failure modes and effects analysis
IEC	International Electrotechnical Commission
ILD	Initial light degradation
IR	Infrared
LID	Light-induced degradation
LIPD	Light-induced power degradation

MPP	Maximum power point
m-Si	Mono-crystalline silicon
NISE	National Institute of Solar Energy
OPV	Organic photovoltaic
Pb-Sn	Tin-Lead
PDMS	Poly dimethyl siloxane
PET	Polyethylene terephthalate
PID	Potential induced degradation
PL	Photoluminescence
PLR	Performance loss rate
PR_{AC}	AC performance ratio
PR_{DC}	DC performance ratio
p-Si	Poly-crystalline silicon
PV	Photovoltaic
PVB	Polyvinyl butyral
R_S	Series resistance (Ω)
R_{SH}	Shunt or parallel resistance (Ω)
SC	Short-circuited
Si-HIT	Silicon hetero-junction with an intrinsic thin layer
SLP	Service life prediction
SnO_2	Tin dioxide
S_W	Wind speed (ms^{-1})
T_{amb}	Ambient temperature (^oC)
TCO	Transparent conductive oxides
T_{Module}	PV module temperature (^oC)

TPEs   Thermoplastic elastomers

TPOs   Thermoplastic polyolefins

UL   Underwriters laboratories

UV   Ultraviolet

σ_{abs} Absolute standard deviations of the temperature-corrected

                 performance loss rates

σ_{rel} Relative standard deviations of the temperature-corrected

                 performance loss rate

CHAPTER 1

OBJECTIVES AND SCOPE

The interrelated research questions that this thesis addresses are:

(i) Do similar PV arrays in the same climate show different measured performance, if so, why?

(ii) Over what period of elapsed PV array operation does it become possible to disaggregate long-term performance degradation from diurnal and seasonal performance changes?

To answer these questions, the long-term performance of three large-scale roof-mounted PV arrays in three locations in Northern Ireland has been examined. This is reported in Chapter 3. The disaggregation of long-term performance degradation from transient performance changes using the measured data from these three arrays is reported in Chapter 4. The monitored data obtained from these three large-scale PV arrays were analysed to determine:

- Array, final, and reference yields.

- Array, inverter, and system losses.

- Relative and absolute system-level performance degradation over five years

using linear regressions for weather-uncorrected performance ratio ($PR_{uncorrected}$) and temperature-corrected performance ratio ($PR_{corrected}$).

- Effect of solar irradiance and solar cell temperature on normalised output power efficiency, system conversion efficiency, fill factor and maximum power output and AC power output.

- How variations in geographical site location, weather conditions and time of day influence power output profiles.

- Develop and assess analytical techniques to disaggregate long-term performance degradation from short-term transient performance changes using both relative and absolute performance loss rates equations.

This research is intended to inform:

i.   PV system design for long-term durability.

ii.   PV operation and maintenance strategies and procedures; and

iii. development of tools for PV performance evaluation.

The data used for this research was from large-scale roof-mounted PV arrays located in Belfast (Longitude: 5.94^{o}W and Latitude: 54.57^{o}N), Newry (Longitude: 6.32^{o}W and Latitude: 54.18^{o}N) and Warrenpoint (Longitude: 6.26^{o}W and Latitude: 54.11^{o}N) in Northern Ireland.

Accomplishing the overall objectives of this research required acquisition of a comprehensive appreciation of the causes and consequences of PV degradation. The presentation of this forms Chapter 2 of this thesis.

CHAPTER 2

REVIEW OF RELEVANT PREVIOUS LITERATURE

2.1 PV Array Performance Metrics

2.1.1   Photovoltaic Equivalent Circuit

Solar energy conversion efficiency of a PV module η_{module} is given by;

$$\eta_{module} = \frac{P}{G} \qquad\qquad (1)$$

where;

G is the incident solar radiation (Wm^{-2}); and

P is the electrical output (W) per unit module surface area (m^2).
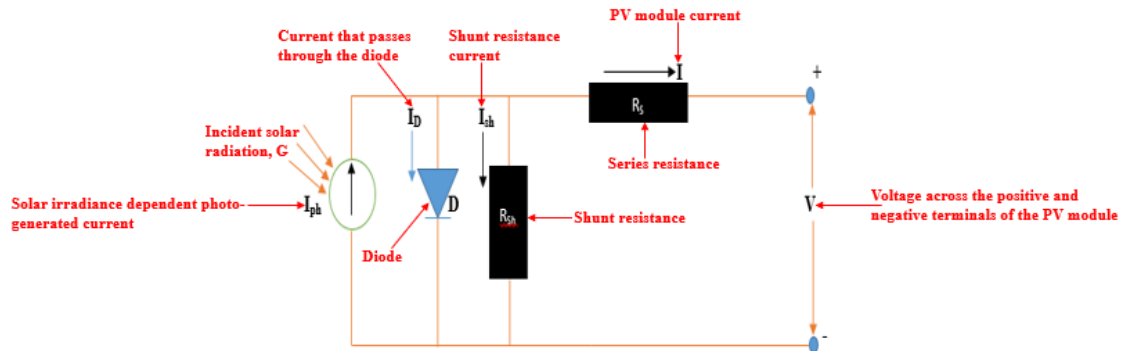
Figure 1. Equivalent circuit of a PV module

In the electrical equivalent circuit of a PV module shown in Figure 1 and the current characteristic equation shown in equation (2), the PV cells can be modelled electrically with five key elements such as diode constants (I_o, V_T), photocurrent (I_{ph}), series resistance, R_S (Ω), and shunt resistance, R_{SH} (Ω) respectively. Hence, the current, I (A) for the PV cell equivalent circuit diagram shown in Figure 1 is given by:

$$I = I_{ph} - I_o \left[\exp\left(\frac{V + I.R_S}{ac}\right) - 1 \right] - \frac{V + I.R_S}{R_{SH}} \qquad (2)$$

where a_c is given by

$$a_c = \frac{Ns.n.K.Tcell}{q} = N_s.n.V_T \qquad (3)$$

where;

I_{ph} is solar irradiance-dependent photo-generated current (A);

I_o is reverse diode saturation current (A);

a_c is a temperature-dependent diode non-ideality factor (K^{-1});

N_s is the number of solar cells connected in series constituting a PV module;

n is the diode's ideality factor;

k is Stefan Boltzmann constant $= 1.38066 \times 10^{-23} JK^{-1}$;

T_{cell} is the PV module operating temperature (K);

q is an electronic charge ($1.60218 \times 10^{-19} C$);

V_T is the thermal voltage of a diode (V);

V is the operating voltage at the terminal of a PV module (V).

Equation [1] produces a current-voltage characteristic curve (I-V curve) for a PV cell as illustrated in Figure 2.
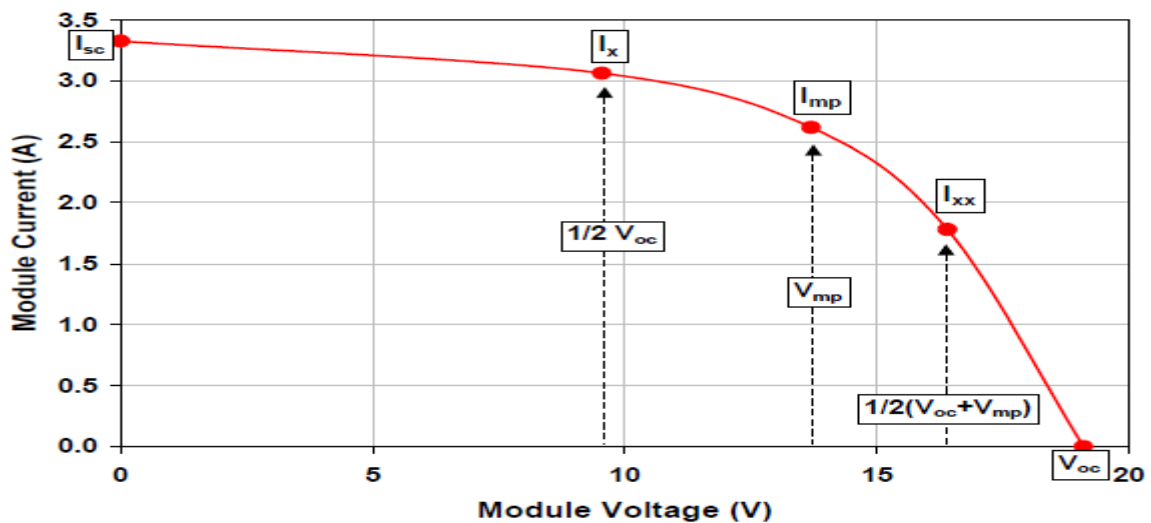
Figure 2. PV Current-Voltage (I-V) characteristic curve *[2]*

4

2.1.2 Short-circuit Current

A short-circuit current (I_{SC}) passes through a solar cell when the voltage (V) across that solar cell is zero as shown in green in Figure 3.
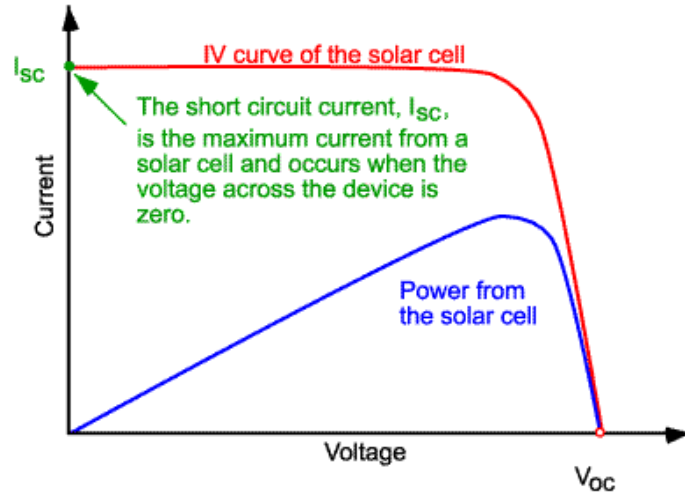
Figure 3. Current-Voltage (I-V) curve of a solar cell showing a short-circuit current *[3]*

For a high-quality solar PV cell with low series resistance (R_S) low reverse diode saturation current (I_o), and high shunt (i.e., parallel) resistance, (R_{SH}), the short-circuit current (I_{SC}) approximates photo-current, (I_{Ph}), that is, $I_{SC} \approx I_{Ph}$.

Short-current density, J_{SC} (A/m^2) is defined as,

$$J_{SC} = \frac{I_{SC}}{A} \tag{4}$$

In a cell with a perfectly passivated surface, electrons and holes do not recombine prematurely with one another on the wafer surface, so short-circuit current, (I_{SC}) (A) can then be approximated to [4]:

$$I_{SC} = qG(L_n + L_p) \tag{5}$$

where:

G is the generation rate (Photons $A^{-1}s^{-1}m^{-1}$).

L_n (μm) and L_p (μm) are the electron and hole diffusion lengths respectively; and

q is the electronic charge (i.e., $1.602176634 \times 10^{-19}$ C).

2.1.3 Open-circuit Voltage

Open-circuit voltage (V_{OC}) is the maximum voltage from a solar PV cell when the total current is zero as illustrated in green in Figure 4.
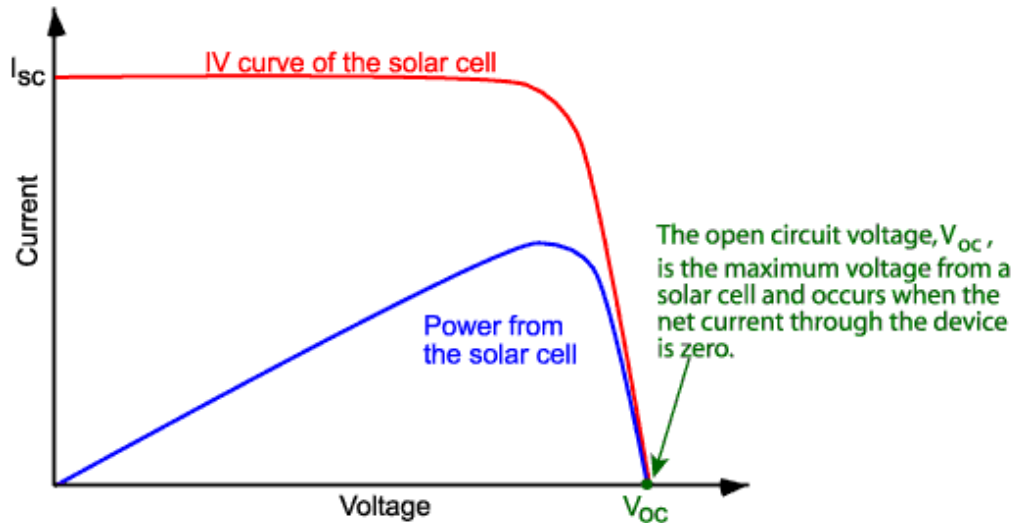
Figure 4. Current-Voltage (I-V) curve of a solar cell showing an open-circuit voltage *[3]*

V_{OC} (V) is found by setting the net current equal to zero in the solar PV cell equation (3) to give:

$$V_{OC} = \frac{nKT}{q} \ln \left(\frac{I_{ph}}{I_o} \right) \tag{6}$$

Equation (6) shows the dependency of V_{OC} on I_o and I_{ph}. V_{OC} is a measure of the amount of recombination of electrons and holes in a solar PV cell. High-quality single-crystalline material silicon solar cells have a V_{OC} of approximately 764 mV under AM 1.5 conditions [5], while commercial multi-crystalline silicon devices typically have V_{OC} of approximately 600 mV [6]. V_{OC} can also be found from the intrinsic carrier concentration (i.e., thermal excitation of a carrier across bands from the valence band to the conduction band) [7], [8] from;

$$V_{OC} = \frac{KT}{q} \ln \left[\frac{(N_A + \Delta n)\Delta n}{n_i^2} \right] \tag{7}$$

6

where:

kT/q is the thermal voltage (V_T).

N_A is doping concentration (at.%).

Δn is the excess carrier concentration (m^{-3}).

n_i is the intrinsic carrier concentration (m^{-3}).

2.1.4   Fill Factor

Fill factor, FF is the ratio of maximum power, P_{Max} from a solar PV cell to the product of V_{OC} and I_{SC}. Graphically, the FF is a measure of the "squareness" of a solar PV cell IV-curve as shown in Figure 5.
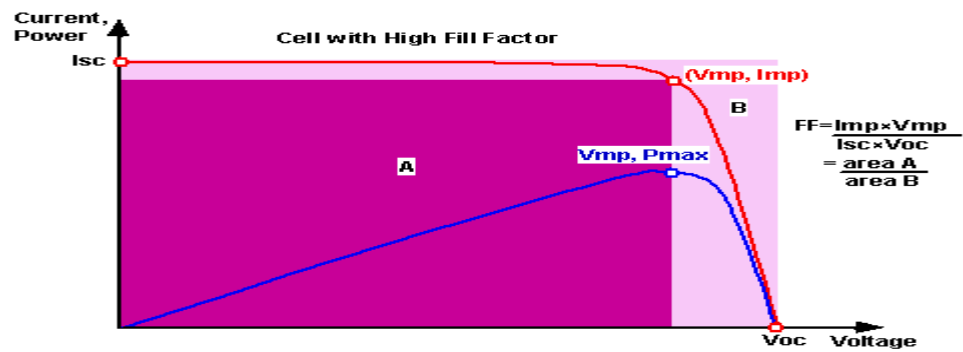
Figure 5. Fill factor diagram *[3]*

As the P_{max} of a solar PV cell decreases, its FF also decreases, i.e.,

$$FF = \frac{P_{Max}}{V_{OC} \times I_{SC}} = \frac{I_{mp} \times V_{mp}}{V_{OC} \times I_{SC}} = \frac{\text{area A}}{\text{area B}} \qquad (8)$$

Ideality factor, n, is defined by;

$$n = \frac{(qV)V}{[\ln(I) - \ln(I_o)]kT} \qquad (9)$$

7

Achieving high FF requires low recombination with ideality factors close to 1 [9]. For PV cells with high recombination, the ideality factor will be greater than 1 so, the FF value will be lower [9].

2.1.4.1 Series resistance in a PV cell

Electrical resistance in a solar PV cell decreases cell efficiency by dissipating power. A PV cell series resistance (R_S) is shown in red in Figure 6.
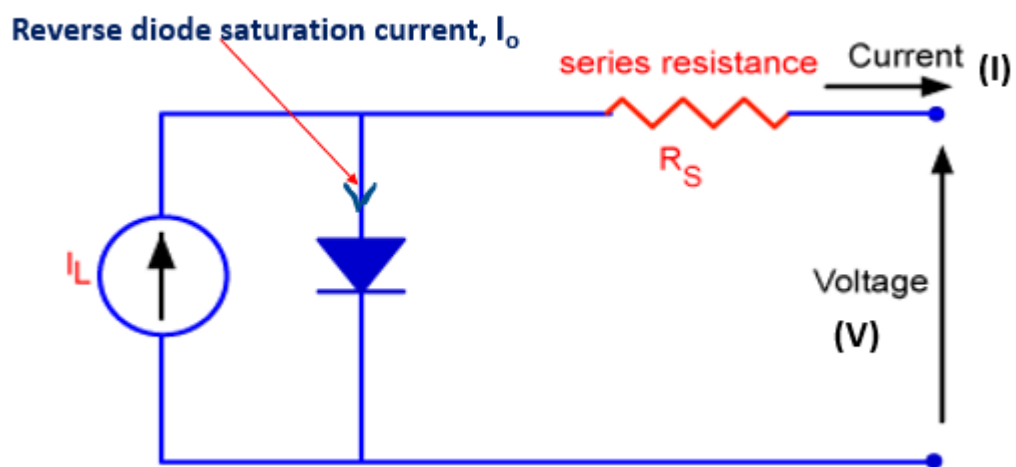
Figure 6. Effect of R_S on solar PV cell *[3]*

Such a series resistance reduces the current, as given by;

$$I = I_L - I_o \exp[\frac{q(V+IR_S)}{nkT}] \tag{10}$$

where:

I is the output current (A);

I_L is the light-generated current or photo-generated current, I_{ph} (A);

V is the voltage across the solar cell terminals (V);

R_S is the series resistance (Ω).

8

R_S does not affect the solar PV cell at V_{OC}, because there is no current flowing through the solar PV cell, so, therefore, R_S is zero. Close to V_{OC}, an I-V curve is strongly affected by series resistance.

In general, resistance (R) is proportional to the area (A) of the solar PV cell, that is:

$$R = yA \qquad (11)$$

where y is a proportionality constant known as resistance density (Ωm^{-2}) or area-normalised resistance.

Defining current density (Am^{-2}) as, $J = \dfrac{I}{A}$, from Ohm's law equation (11) becomes:

$$V = IR \qquad (12)$$

$$J = \dfrac{V}{y} \text{ or } y = \dfrac{V}{J} \qquad (13)$$

Series resistance reduces FF, though too high R_S values may also degrade the I_{SC} [9].

2.1.4.2 Parallel resistance in a PV cell

Power losses caused by a parallel (or shunt) resistance R_{SH}, are usually due to manufacturing defects rather than poor cell design. A decrease in R_{SH} causes power losses in PV cells by allowing an additional photocurrent path that lowers the current flowing through the solar cell so decreasing the solar cell voltage. The effect caused by shunt resistance is particularly critical at low solar radiation intensities since less current is generated. At lower voltages where the effective resistance of the solar cell is high, the impact of an R_{SH} is small. The equation for solar PV cell current in presence of R_{SH} as illustrated in red in Figure 7 is given by:

$$I = I_L - I_o \exp[\dfrac{qV}{nKT}] - \dfrac{V}{R_{SH}} \qquad (14)$$
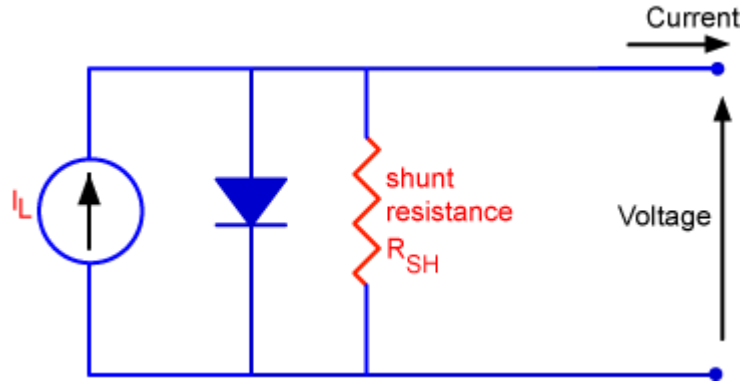
Figure 7. Effect of R_{SH} on solar PV cells *[3]*

2.1.5 Solar PV Cell Efficiency

Solar PV cell efficiency is the ratio of energy output from a solar PV cell to solar radiation input. Solar PV cell efficiency is dependent on the spectrum and intensity of the incident solar radiation and the PV cell temperature [10]. Solar PV cell efficiency is given by:

$$\eta_{cell} = \frac{P_o}{P_{in}} = \frac{P_{Max}}{P_{in}} = \frac{V_m I_m}{G_{R/POA} A_{cell}} \times 100\% \tag{15}$$

where:

    P_o is the power output (W).

    P_{Max} is the maximum power (W).

    P_{in} is the input power (W).

    G_{POA} is the incident solar radiation at the plane of the array (Wm^{-2}).

    A_{cell} is the solar PV cell area (m^2).

Efficiency of a solar cell (η_{cell}) can be expressed as:

$$\eta_{cell} = \frac{P_{mp}}{P_{input}} \tag{16}$$

For $\qquad\qquad P_{Max} = V_{OC} I_{SC} FF \tag{17}$

$$\eta_{cell} = \frac{V_{OC} I_{SC} FF}{P_{in}} \tag{18}$$

10

2.1.5.1 Bypass diodes

PV systems are usually faced with a shading effect, especially when one cell of the module is shaded by fallen leaves, trees or buildings. To reduce this shading effect and increase the PV power output, bypass diodes are connected to the sub-strings of the PV module in series.

Failure of an individual cell is affected by module temperature. To avoid this, bypass diodes are used that "open" when the voltage in a reverse direction due to cell failure exceeds a threshold voltage. The bypass diode is not applied for every single solar cell in actual PV modules but forms an antiparallel connection to a group of serially connected cells (usually 20-24 solar cells) [11]. The practicality of the bypass diode is also evident from the I-V curve, where "stairs" can occur, which can alter the detection of MPP because more than one local optimum is present in the I-V curve [12].   This is illustrated in Figure 8.
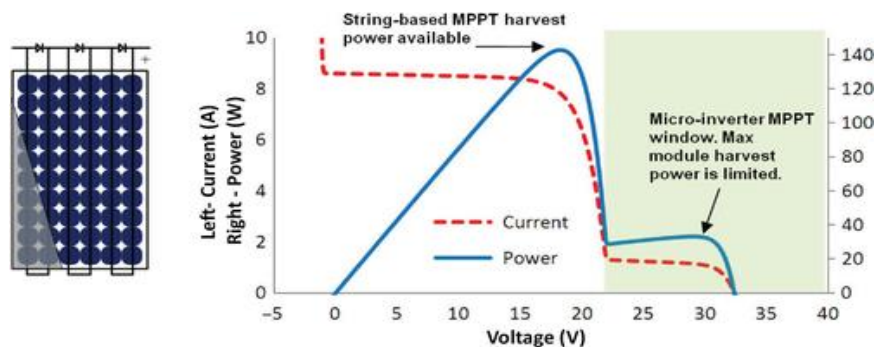
Figure 8. Shading on one submodule string *[13]*

2.1.6 Photovoltaic Module and System Efficiencies

PV system solar energy conversion efficiency at a particular instant can be calculated from [14]:

$$\eta_{Sys} = \frac{P_{AC}}{G_{POA} A_a} \qquad (19)$$

where:

P_{AC} is the average monthly AC power output (W).

η_{Sys} is the PV system efficiency.

The instantaneous module efficiency is computed using [14]:

$$\eta_{PV} = \frac{P_{DC}}{G_{POA} A_a} \qquad (20)$$

where:

P_{DC} is the average monthly DC power output (W).

η_{PV} is the instantaneous module efficiency.

The monthly PV module efficiency is given by [15]:

$$\eta_{PV\_m} = \frac{E_{DC\_d}}{G_{POA} A_a} \qquad (21)$$

where:

η_{PV_m} is the average monthly PV module conversion efficiency.

E_{DC_d} is the average monthly daily total DC output energy (Wh).

A_a is the area of the array (m^2).

2.1.7 Introduction to Inverter Function

Solar inverters are used to convert the direct current (DC) output from the solar PV modules to alternating current (AC). Hence, the AC then flows into the distribution panel to be utilised in various homes or transmit to the utility grid for public use [16]. Apart from the conversion role played by the inverter, it also regulates the PV system [17]. Inverter functions may be through electronic processes or a combination of electronic and mechanical properties, such as a switch [16]. A simple design of the inverter switch shows that it consists of four transistors labelled A, B, C and D in an H-bridge as shown in Figure 9. This Figure shows that when A and D are closed, the DC receives power and spins in one direction. When C and B are closed, the direction of the DC changes and spins in the opposite direction. If A, B, C and D are open, or any of the A, B, C or D is closed, the DC will receive no power [16]. If both A and C are closed, or B and D are closed, the DC is powered to resist motion and brakes if currently spinning. Therefore, the opening and closing of transistors on both sides of the circuit will make the current flow in an alternative direction to the load, M [16].
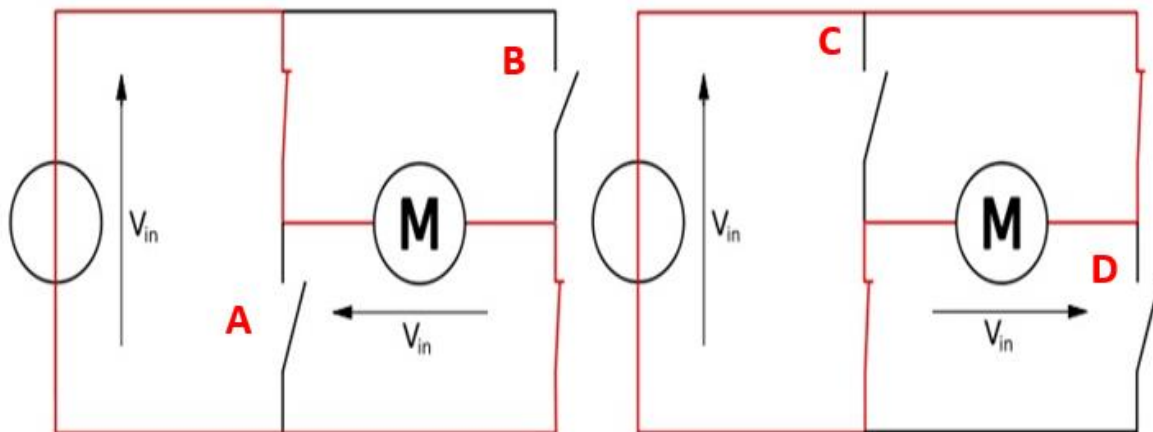
Figure 9. H-Bridge Circuit Design for Inverters *[16]*

In larger photovoltaic systems many PV modules feed into a single inverter where they are converted. This is done to prevent or reduce the overall cost of the inverter system and to prevent conversion losses due to resistance through the circuit. When designing an inverter the

maximum output of voltage, current and power generated by the PV modules must be considered. A good and well-designed inverter will always withstand the maximum output of voltage, current, and power generated by the PV modules [16].

Therefore, when sizing inverters the following requirements needs to be met [16], [18]:

i. the maximum open circuit voltage of the PV system does not exceed the required voltage.

ii. the minimum voltage required by the inverter must be met for the PV system to function accurately.

iii. the maximum power output of the PV modules must be less than the rating of the inverter.

iv. the maximum current at the point of operation must be less than the rating of the inverter.

Data published by inverter manufacturers have shown that the overall inverter efficiency ranges from 95 – 98%. This range of efficiencies under standard operating conditions is for a system whose array is properly sized for the inverter [18]. Vignola and Mavromatakis [17] found that inverter efficiency declines slowly after reaching the maximum incident energy levels of 400 – 700 W/m^2 of one-year data. This according to them is caused by an increase in operating temperature generated by the inverter when it carries loads with more power [17].

2.1.8 Inverter Efficiency

The maximum efficiency of an inverter is strongly dependent on the inverter's operating temperature. For instance, the inverter efficiency reaches its peak value of 96.5 – 97% when the inverter operating temperature is less and shows a drop of 2 – 4% when the temperature increases above 37°C [19]. Inverter efficiency variation is dependent on the input power and voltage of the PV array [20]. The study carried out by Ketjoy et al [20] showed that the inverter connected to polycrystalline silicon (p-Si) modules operated the highest inverter efficiency at 91% and their analyses showed that PV module technology had less influence on inverter efficiency. They concluded that it was the power input from the PV module that has an impact on the inverter efficiency.

Inverter efficiency (η_{inv}) at a particular instant is *[15]*;

$$\eta_{inv} = \frac{P_{AC}}{P_{DC}} \times 100\% \qquad (22)$$

Monthly inverter efficiency ($\eta_{inv, m}$) is [15]:

$$\eta_{inv, m} = \frac{E_{AC,d}}{E_{DCd}} \times 100\% \qquad (23)$$

where:

P_{AC} is the AC power output (Watt);

$E_{AC,d}$ is the average daily total AC output (kWh); and

$E_{DC,d}$ is the average daily total DC output (kWh)

2.1.9 Packing factor of a solar PV cell

The packing factor (PF) of a solar PV cell is defined as the fraction of the total module area occupied by PV cells given by [21]:

$$PF = \frac{(n_s + n_p)A_{cell}}{A_m} \qquad (24)$$

15

where:

n$_s$ is the number of solar PV cells in series.

n$_p$ is the number of solar PV cells in parallel.

A$_{cell}$ is the cell area (m^2); and

A$_m$ is the module area (m^2).

High packing factors obviously give high electrical output per unit collector area.

2.1.10 Temperature co-efficient of a PV cell

When PV temperature increases, the efficiency of a solar PV will decrease. Many relations are available to calculate the effect of cell temperature (T$_{cell}$) on the efficiency of the solar PV cell (Ƞ$_{cell}$). In practical applications, equation (25) can be applied without significant loss in accuracy [22], [23]. Hence, this approach is adopted because the availability of the measured parameters fits in equation (25).

$$\text{Ƞ}_{cell} = \text{Ƞ}_{ref} \left[1 - \beta_{ref} (T_{cell} - T_{ref})\right] \qquad (25)$$

where:

Ƞ$_{ref}$ is a reference value for solar PV cell efficiency usually at standard test conditions;

T$_{ref}$ is a temperature at standard test conditions (25°C or 298K); and

β$_{ref}$ is the temperature coefficient of a PV cell (K^{-1}).

β$_{ref}$ is usually provided in the manufacturer's datasheet. Table 1 shows the typical β$_{ref}$ value for various solar PV technologies.

Table 1. Temperature coefficients for silicon PV cells *[24]*

		β_{ref} ($^{o}C^{-1}$)
PV cell type	Mono c-Si	0.003-0.005
	Multi c-Si	0.004
	a-Si	0.0011-0.0026

2.1.11 Yields

Array yield (y_A) is the ratio of daily, monthly, or yearly direct current (DC) energy output from a PV array to the rated PV array power computed from [25];

$$y_A = \frac{E_{DC}}{P_{PV,rated}} \tag{26}$$

where E_{DC} is the total DC energy output from the PV arrays (kWh) and $P_{PV,}$rated is the rated output power of the PV system (kWp).

Reference yield (y_r) is the ratio of total daily in-plane solar irradiation (G) (kWh/m^2) over its reference solar irradiance (G_{STC}) [26];

$$y_r = \frac{G}{G_{STC}} \tag{27}$$

Final yield (y_f) is the total AC energy during a given period divided by the rated PV array power [27]:

$$y_f = \frac{E_{AC}}{P_{PV,rated}} \tag{28}$$

where E_{AC} is the total AC energy output from the inverter generated by the PV power system for a specific period (kWh).

2.1.1 PV Performance Ratio

Performance Ratio (PR) compares actual and theoretical energy outputs of a PV system [28]. PR is a measure of the quality of a solar PV system independent of location or solar irradiance. It is often referred to as a quality factor. The nearer a PV system's PR approaches 100%, the more efficiently the array has utilised the available solar energy. Because of optical losses, PV array losses, DC to AC conversion losses, cabling losses, dust, shade, wind velocity and high module temperatures, measured PR values are typically about 80% for well-operating PV systems [29].

Array and system PR values are calculated from [30]:

$$PR_A = \frac{y_A}{y_r} \times 100\% \qquad\qquad (29)$$

$$PR_{Syst.} = \frac{y_f}{y_r} \times 100\% \qquad\qquad (30)$$

The array PR (PR_A) is the ratio of the DC array yield (y_A) to reference yield (y_r) as expressed in equation (29). It is also known as the DC performance ratio (PR_{DC}) because it evaluates the performance of the DC-rated power of the PV array. DC array capture loss (L_C) is the common loss associated with PR_{DC}. The DC array capture losses are associated with PV conversion, ageing, module quality, mismatch, and wiring and it is expressed in equation (31) [25].

$$L_C = y_r - y_A \qquad\qquad (31)$$
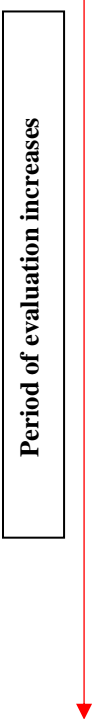
The system PR ($PR_{Syst.}$) is the ratio of the AC final yield (y_f) to reference yield (y_r) as seen in equation (30) [25]. This is also called the AC performance ratio (PR_{AC}) because it measures the output performance of the PV system. PR_{AC} is affected by an AC system loss (L_S). It is associated with system losses due to inverter conversion efficiency in grid-connected arrays and is given by equation (32) [25].

$$L_S = y_A - y_f \qquad\qquad (32)$$

The equivalent PR at STC is computed by adjusting the power to a temperature-corrected power using a temperature-correction factor (α) at each recording interval in the STC reference condition. Equivalent PR is the difference between PR at the actual PV module temperature (T_{Module}) and the STC reference temperature, (T_{ref}) (25°C). This procedure is normally used only when the system PR is to be measured for a short duration of a day [31].

PR is influenced by the factors listed in Table 2.

Table 2. Environmental, measurement and system factors that influence PR *[31]*

			Effect
Period of evaluation increases	**Short-term environmental**	PV module temperature	When the temperature of PV modules increases, efficiencies decreases, thus, lowering PR.
		Shade	Shading results in a PV module receiving less solar irradiation than expected, so PR reduces.
	Measurement period		If the recorded measurement period is short (say less than one month), there will be insufficient measurements for reliable computation of PR.
	Short-term system operational	Conduction losses	Optical losses occur when light is reflected off the PV panel surface instead of being absorbed into the panel surface to interact with electrons.
		Inverter losses	With the conversion of energy from DC to AC via an inverter and injection into the grid, conduction losses occur that reduce PR.
		Efficiency of the inverter	A highly efficient inverter leads to high PR values. For instance, inverters with an efficiency of 90% enable PR values of over 80%.
	Long-term environmental and operational	PV cell degradation	Age-related degradation of solar cells lowers PR values over time.

2.2 PV Degradation and Failure

2.2.1 Key Concepts

PV arrays exhibit long-term performance degradation, resulting in lower like-for-like efficiency and performance ratios compared to their initial performance. Understanding degradation is critical for operation, maintenance, and repair [32]. PV module failures and performance losses are caused by a gradual accumulation of damage from long-term outdoor exposure referred to as weathering [33]. Faults observed in any PV component are either (i) early failures, (ii) intrinsic/random failure, and/or (iii) deterioration [34], [35]. PV degradation can be determined by long-term outdoor testing of PV modules and by accelerated indoor exposure to thermal cycling, humidity-freeze cycles, damp, static and dynamic mechanical loads and ultraviolet light [36]. Accelerated test methodologies either use:

(i)   higher levels of stress (such as ultraviolet intensity) that normally apply to predict longer-term performance. A disadvantage is that this may induce failures that would not naturally occur, or

(ii)   use near-normal stresses but cycle them more frequently over a much shorter time.

Atlas [33] developed a test methodology to predict the likelihood of 25+ years of PV durability. Its characteristics are summarised in Table 3.
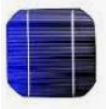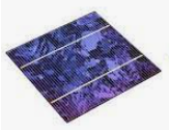
Table 3. Characteristics of a durability test method *[33]*

Representative range of weather conditions	Parameters are chosen based on three major climatic zones, (arid desert, tropical/subtropical, and northern or temperate).
Local modification of conductors as necessary	Additional test modifiers for particular urban or industrial locations (such as hydrocarbons, soot, windblown dust or dirt; acid rain; mechanical loading; and coastal or marine).
Combining stressors	Combining multiple stresses into a single test cycle, (for example, temperature and humidity cycling with solar radiation).
Inspection	Periodic visual inspections, current-voltage (I-V) curve measurements, and thermal imaging.

Allen and David [33] proposed a variety of accelerated environmental testing (AET) methodologies at realistic climate-specific stress levels delivered in cycles that mimic the natural environment, that could be run before, concurrently, or after IEC qualification tests.

There are three main groups of solar PV technologies: mono-crystalline silicon (m-Si), poly-crystalline silicon (p-Si), and thin film as shown in Table 4 [37].

Table 4. Silicon PV technologies *[37]*

Technology type	Weight/area	Efficiency (%)	Cost (€/m²) $$\frac{\text{Cost } [€]}{m^2} = \frac{\text{Cost } [€]}{[\text{Watt}_{\text{Peak}}]} \times \frac{\text{Solar Panel Power}[\text{Watt}_{\text{Peak}}]}{\text{Solar Panel}_{\text{Length}}\{m\}\text{Solar Panel}_{\text{Width}}[m]}$$
Monocrystalline silicon (m-Si)	About 0.317 kg/m² per cell	About 20-22.6%	Expensive: about 111.0
Polycrystalline silicon (p-Si)	About 0.318 kg/m² per cell	About 17-20%	Medium: 73.5
Thin film	About 0.053 kg/m² per cell	About 7-18.7%	Cheap: 37.5

Zhengpeng et al. [38] investigated the durability of five thin-film technologies and five silicon-wafer-based PV technologies. The PV modules were subjected to accelerated ageing tests in a climate dark chamber for 650 hours ($27\frac{1}{12}$ days) at temperatures of 85ºC, relative humidity of 85%, and electrical bias. They used a bias voltage of 1000V DC between each module's active circuit and the module frame. Depending on the module type and bias polarity, damp heat stressing conditions significantly degraded electrical performance causing delamination, glass surface deterioration, frame corrosion, and metal grid discolouration.

The "bathtub" reliability curve shown in Figures 10 and 11 [39] represents the failure rate of a group of PV modules over time. The curve assists PV manufacturers in identifying root causes

of failure [33]. The curve is divided into three parts: failure mode A (infant mortality), failure mode C (normal life), and failure mode B (end-of-life failure). These are elaborated on in Figure 11. The typical faults associated with PV modules are illustrated in Table 5.
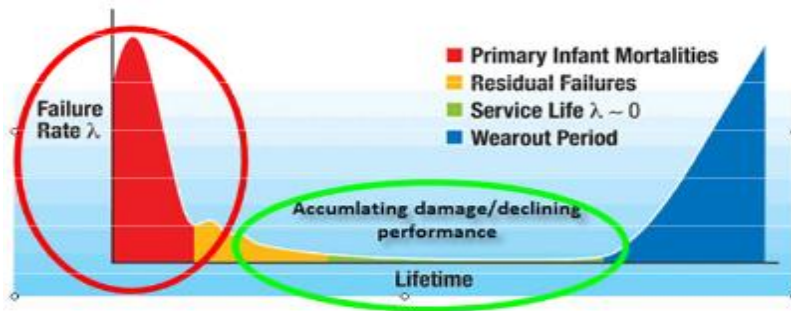
Figure 10. "Bathtub" curve for PV Durability and Reliability *[34]*
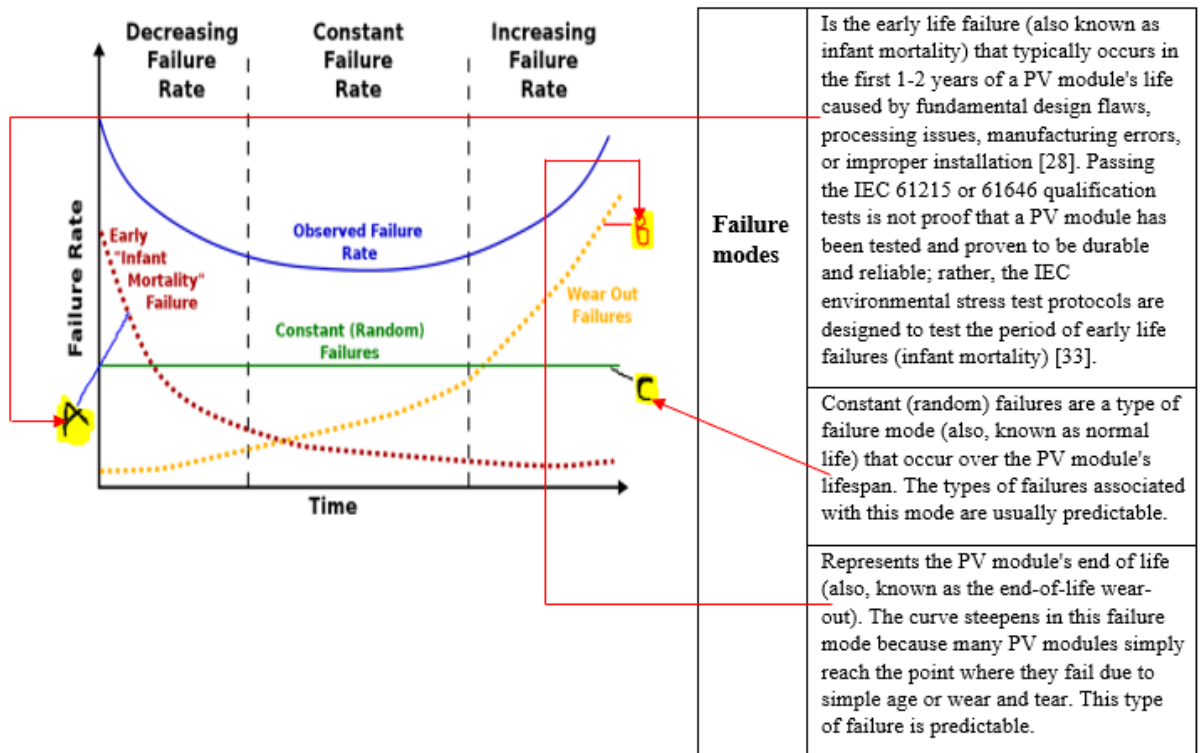
Figure 11. The multiple failure modes overlap in solar PV modules *[34]*

Table 5. Typical faults associated with PV arrays

Manufacturing defects	Hot spots (bad soldering) [40].
	Micro-cracks "snail trail" [41].
	Contamination (discolouration) [41].
Installation faults [42]	Incorrect design of the PV system.
	Poor inverter and module ventilation.
	Damage in transport to installation.
	Loose or very tight cables.
	Sensors placed badly.
	Lack of lightning protection.
	Actions that lead to corrosion.
Degradation	Connection issues with solder bonds [32].
	Sensor drifting and packaging of materials [32].
	Delamination [38].
	Micro-cracks [41].
Catastrophic failure	Fire outbreak.
	Failing of tree branches.
	Hail/stone impact.

Typically 2% of new PV modules do not comply with their warranties [34] [35]. Interconnection defects and PV module glass breakage failures are the major causes of extrinsic failures [43]. DeGraaff et al [44] found that after 8 years, the maximum working life of a PV module ends if a safety problem occurs or the module power drops under a certain level, which is defined as between 80% and 70% of the initial power rating [44]. Freire et al [45] found the most common failures in a PV module within 10 years were laminate discolouration, isolation of cell parts due to cracks, and delamination. These failures resulted in about 10% mean power loss [45]. In crystalline silicon PV modules, a boron oxygen compound is used to prevent light-induced power degradation (LIPD). Insufficient introduction of boron oxygen may result in LIPD [45]. Amorphous silicon (a-Si) PV modules are prone to light-induced degradation that can account for a power loss of 10%-30% during operation [46]. PV modules can fail due to

external causes were transportation failure, clamping, cable failure, connector failure, and lightning [47]. Breakage of the glass cover and lamination damage due to shocks and vibrations can occur during transportation [48]. Most transportation failures of PV modules can be identified neither visually nor by observing power ratings [48]. In PV module installation, clamping can cause glass breakage in frameless PV modules [48]. Clamping failures such as those shown in Figure 12 can be detected by thermographic or electroluminescence imaging.
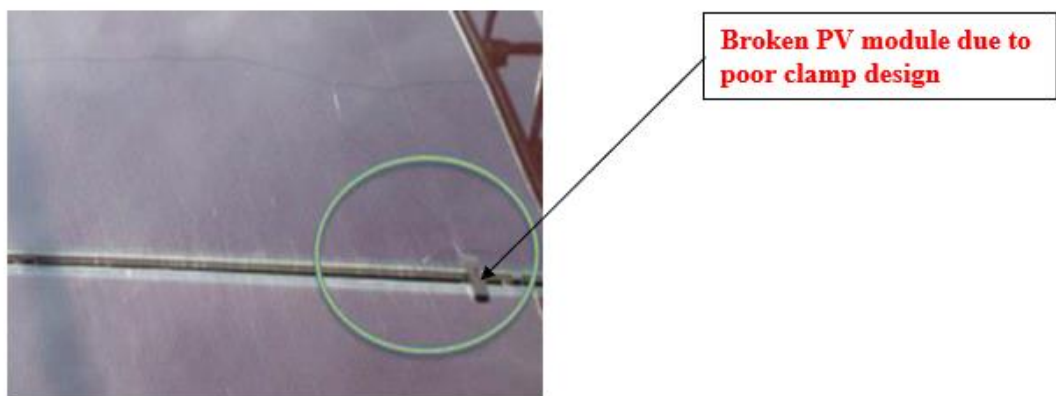
Figure 12. Broken PV module due to poor clamp design *[49]*

A finite element analysis of the stresses on PV modules, during the installation, showed sharp-edged clamps design (as illustrated in Figure 12), narrow clamps, improper positioning, and excessive tightening of screws on clamps of PV modules can cause stress on PV modules leading to breakage [49].

2.2.2 Influence of Component Materials on Degradation of Solar PV Modules

PV modules are multilayer systems comprised of adhesively bonded interfaces of glass/encapsulant, encapsulant/cell, interconnections/encapsulant, and encapsulant/backsheet as shown in Figure 13 [50].
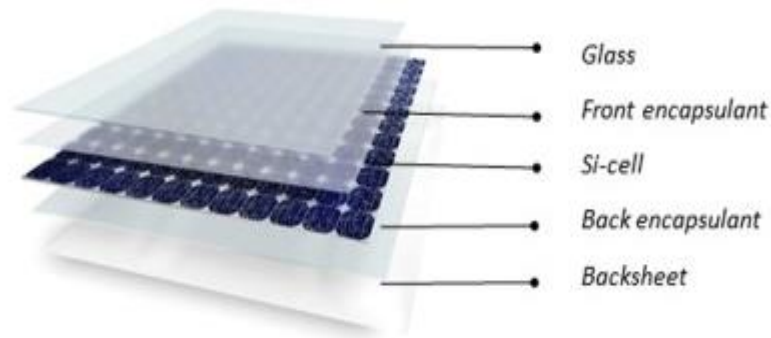
Figure 13. Component of a standard PV module *[50]*

These interfaces are possible paths for ingress contamination and interfacial reactions, that can result in degradation and current leakage [51]. For 1,919,000 solar PV modules installed in different climates, solar cells, and metallisation degradation showed limited dependency on climatic conditions, while degradation of polymer components showed a stronger dependence [52]. Polymeric material degradation was highest in hot arid climates, lower in tropical climates and least in temperate climates.

International Electrotechnical Commission (IEC) and Underwriters Laboratories (UL) initial PV qualification tests do not predict long-term performance. For this reason, there has been a development of accelerated life testing (ALT) and accelerated environmental testing (AET) for service life prediction (SLP) of PV modules and systems [53].

2.2.3 Issues Surrounding Photovoltaic Durability and Reliability

Product warranties generally require PV modules that will perform reliably for ~25 years [53].

There is no clear means by which a PV manufacturer can prove a 25-year life so it is unclear how the same warranty applies to all varied outdoor conditions for the same PV modules [54].

The reliability of the PV array is affected by the factors in Table 6 [55]:

Table 6. Factors affecting PV array reliability *[55]*

		Effects
Factors	Corrosion	loss of grounding
	Improper insulation	loss of grounding
	Delamination	plastics (on the back) and the glass (on the front) separate
		falling of rocks, hailstones, thermal fracture [56], glass fracture, shock and fatigue
	Bypass diode failure	Constant leakage of current [57]
	Inverter failure	Extreme temperatures and frequent thermal cycling and load stress [58]
	Moisture ingress	power degradation, corrosion, delamination, discolouration, potentially induced degradation, optical and adhesion losses [59]

Reliability issues linked with individual technologies are ranked according to their performance issues in Table 7 [55]:

Table 7. PV reliability issues linked with individual technologies *[55]*

Individual PV technologies	Reliability issues
Wafer silicon	Light-induced degradation (LID), front surface soiling, the effect of glass on encapsulation performance, reduced adhesion leading to corrosion and/or delamination, busbar adhesion degradation, and junction box failure.
Cadmium telluride (CdTe)	interlayer adhesion and delamination, electrochemical corrosion of SnO_2:F, shunt hot spots at scribe lines (before and after stress).
Copper indium diselenide (CIS)	interlayer adhesion, busbar mechanical adhesion and electrical, notable sensitivity of transparent conductive oxides (TCO) to moisture, moisture ingress failure of the package.
Organic photovoltaic (OPV)	photolytic instability, moisture-induced degradation, moisture ingress failure of package.
Thin-film silicon	electrochemical corrosion of tin dioxide (SnO_2), initial light degradation (ILD).

2.2.4   PV Encapsulation and Backsheet Durability

Polymeric backsheets serve as the outer layer of solar panels, protecting solar PV modules over their expected life span [60]. The backsheet of the solar PV located on the outermost layer of the solar PV module is designed to shield the inner components of the PV module, from external stresses. The backsheet must provide high-quality voltage protection insulating electrical components to safely generate electricity. Backsheets performance can be assessed by the tests in Table 8.

Table 8. Backsheet tests *[60]*

Test	Breakdown voltage	Measures the voltage level that causes permanent failure of the backsheet and substantial loss of electrical safety. Hence, the higher the breakdown voltage rating, the safer the backsheet. However, low breakdown voltage affects module safety thereby resulting in potential shock or fire hazards.
	Wet leakage	Evaluate the solar panel's ability to keep electricity separated within the proper components of the solar panel. Therefore, if a solar panel fails a wet leakage test, it means that the solar module's safety can be compromised in very wet conditions, such as melting snow, heavy rainfalls, condensing humidity, and panel cleanings.
	UV irradiation	a UV ageing test analysis to find whether a backsheet is more likely to degrade and become yellowish. If the backsheets degrade and turn yellow, it can lead to a compromise in reflectivity, which reduces performance.
	Embrittlement	Polyethylene terephthalate **(PET) layer:** A brittle backsheet may crack under mechanical stress, causing the solar PV module to fail.
	Backsheet delamination	Delamination of the backsheet layers or/and adhesive can reduce solar PV module performance, particularly in harsh weather conditions.

Solar cell performance decreases when the backsheet is subjected to defects such as cracking, yellowing, and delamination. Yellowing of the backsheet is known to be an early potential predictor of backsheet failure. Qualification tests such as IEC 61215 and UL1703 [61] assess the susceptibility of PV modules to early degradation mechanisms; however, they are not effective in assessing long-term durability. However, the ultraviolet (UV) resistance and weatherability stress testing performed as part of these PV module qualification tests do correspond to a relatively short period (roughly 70 days) in the outdoor environment [62]. These tests are insufficient for determining the durability of the backsheet in outdoor conditions. Accelerated testing of PV backsheet UV and weathering durability is used to estimate expected long-term performance [60]. Backsheets are subjected to a variety of failure modes, including cracking and delamination. With PV modules warrantied to last 20 years or

more in the field, components used in their construction must be thoroughly tested to ensure lifetime performance [60].

Optical degradation may result from the discolouration of encapsulating materials. Ultraviolet (UV) exposure, temperature, and humidity lead to yellowing of encapsulating materials after (i) extended exposure, (ii) diffusion of dirt from front surface soiling and (iii) moisture ingress from failed edge seals. The lifespan of Ethylene Vinyl Acetate (EVA) encapsulants can be increased by UV stabilisers and antioxidants [63]. Though stabiliser concentration reduces gradually at inclusion of elevated temperatures and when exposed to UV radiation [64]. When stabiliser concentration drops below a critical value, rapid degradation of the encapsulant ensues yellowing the EVA, accompanied by production of acetic acid that eventually causes the EVA to become brown. Brown EVA absorbs a significant fraction of solar radiation in the UV and visible region thereby decreasing the photons available for electric current production. Encapsulant browning can reduce PV module performance by as much as 50% [65]. Lighting a PV module with a 375 nm UV lamp regions of EVA that have started to degrade to have a nearly white colour [66].

Encapsulating PV modules provide structural support, optical coupling, electrical isolation, physical isolation/protection, from exposure to hazardous or degrading environmental factors [50] and thermal conduction for the brittle silicon solar cell and associated circuit components [67], [68], [69], [70]. Encapsulant quality has an influence on heat dissipation amongst various layers of PV modules, which can be significant for PV modules operating at a higher temperature [71], [72]. Because of demanding requirements, only polymers such as EVA, polyvinyl butyral (PVB), poly dimethyl siloxane (PDMS), ionomers, silicones, thermoplastic elastomers (TPEs), and thermoplastic polyolefins (TPOs) are suitable for PV encapsulation [69]. EVA (in glass-polymer backsheet modules) and PVB (in glass-glass modules) are the main encapsulants used in the PV industry [50], [73], [74], [75], [76].

Increased opacity of EVA over time can lead to an increase in surface temperature due to radiation absorption resulting in lower PV solar energy conversion efficiencies [75]. An increase in surface temperature due to discolouration impacts the rate of degradation. For instance, if oxygen is allowed to diffuse through PV module edges and/or permeable a backsheet, oxidation of chromophore species that is responsible for increased opacity (i.e., discolouration) is noticed on a PV module surface. This photo-bleaching effect [67], [77], produces a circular area of the yellow-to-brown encapsulant. If cracks are present, oxygen can diffuse through them leaving an uneven discolouration as seen in Figure 14.
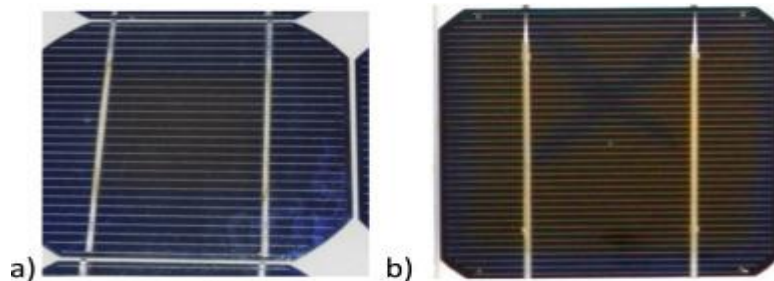
Figure 14. (a) Shows a bleaching effect because of oxygen permeation through the edges; (b) the effect of photobleaching due to the oxygen permeation through cracks *[78]*.

As shown in Figure 15, discolouration is usually followed by delamination of glass/encapsulant, encapsulant/cell, encapsulant/backsheet, encapsulant/ribbon interface, and/or within backsheet layers [79]. Delamination can originate from changes in thermal and thermos-mechanical properties of EVA upon field exposure [80], [81]. Wang et al [81] believed that UV exposure favours EVA crystallisation resulting in a higher elastic modulus of the encapsulants (that is, increased stiffness). The existence of "snail trails" is related to discolouration of the encapsulant; the type of encapsulant, backsheet, and cell metallisation play important roles in the occurrence of this phenomenon [82], [83], [84], [85].

Table 9. Properties of encapsulants *[70]*

Polymer	Polymer type	Parameter				
		T_g [ºC]	E [MPa]	Refractive index (n)	Volume resistivity@23ºC [Ωcm]	Moisture ingression [g/d]
EVA	Elastomer	-40 to -34	≤ 68	1.48 – 1.49	10^{14}	115
Silicone		-50	≤ 10	1.38 – 1.58	$10^{14} – 10^{15}$	310
PVB	Thermoplastic	+12 to +50	≤ 11	1.48	$10^{10} - 10^{12}$	310
	Ionomer	-100	≤ 300	1.49	10^{16}	55
TPSE	Thermoplastic	-60 to -40	≤ 280	1.42	10^{16}	-
TPO	Elastomer		≤ 32	1.48	$10^{14} - 10^{18}$	-

where:

E is the instantaneous Young's modulus (in megapascal, MPa).

T_g is the glass transition temperature (^oC).

g/d is the weight of moisture (g)/ingress (d).

Therefore, different polymers can be rated based on their instantaneous Young's modulus values which measure the strength of the polymers.
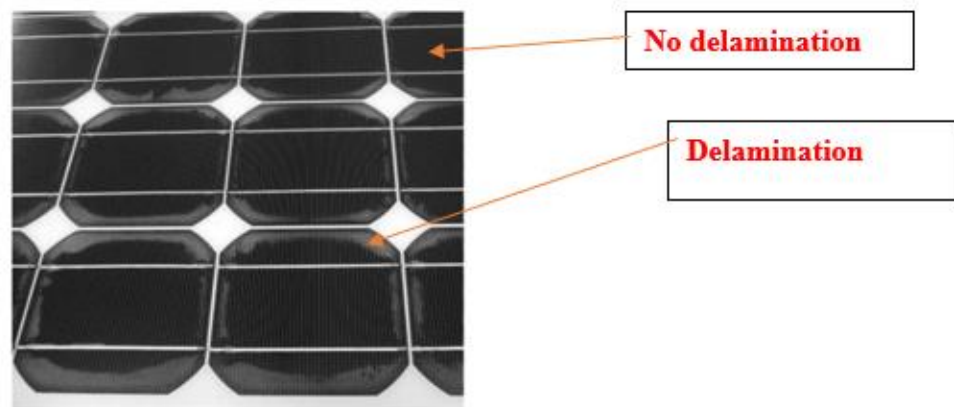
Figure 15. Front encapsulant delamination *[78]*

Potential induced degradation (PID) seems to be influenced by the encapsulant properties. In this failure mode, the volume resistivity of material is highly significant since it influences ionic current flow through the encapsulant. Higher volume resistivity decreases ion mass transfer. EVA has a high-volume resistivity that reduces with temperature [86]. Materials like PVB, thermoplastic polyolefin (TPO), silicones, or ionomers are good alternatives to EVA as seen in Table 9. The occurrence of PID is highly influenced by environmental conditions with higher temperatures and humidity values accelerating degradation [86], [87].

Lamination failures result in optical reflection losses [88]. Kleiss et al [89] reported that 90% of PV modules are prone to delamination. Zhu et al [90] noted the requirements for lamination adhesion that should be met by PV module manufacturers. Delamination can be observed with a reflectometer [91] lock-in thermography, pulse thermography, X-Ray thermography, or an ultrasonic scanner [92], [93]. Tang et al [94] presented a double-glass PV module that could withstand varied environmental conditions because its low moisture-permeable rate gave long-term stability and reliability. Dhimish et al [95] found solar cell cracks were either multi-directional cracks, diagonal cracks, or cracks parallel and perpendicular to bus bars.

Kajari-Schroder et al [96] noted that under artificial ageing cracks in PV modules gave unstable power output. In 667 cracked PV cells in 27 PV modules, 50% of crack orientations were parallel to busbar cracks considered to be highly critical [96].

Meyer et al [85] examined PV modules with "snail tracks" formed due to outdoor exposure of defected PV modules using detailed microscopic imaging of discolourations. Snail trails were mostly located at solar cell edges or near micro-cracks. The optical impression of a snail trail is a brownish discolouration of the grid finger position that becomes further imprinted on the EVA foil. The formation of snail tracks in a PV module is an electromechanical degradation process but is not deemed to be a direct cause of power loss.

Fairbrother et al [97] noted that in a particular PV array, 3% of the PV modules had burn-marks occupying 5% of the back sheet area. Mohammed et al [98] found 1.5% caused an annual average of burn-marks, cell-cracks, PV module power degradation and delamination. Potential induced degradation (PID) caused by surface polarisation or chemical corrosion is dependent on the polarity and level of potential difference between the PV cell and ground [99]. Generally, PID is seen when high voltages force sodium ions to spread out from the glass through the

encapsulation to accumulate on the cell surface resulting in surface recombination, lower fill factor and increased local shunting.

Nonreversible PID occurs because electrochemical reactions result in electro-corrosion of transparent conducting oxide. Reversible PID (also known as surface polarisation) accumulates a positive charge on a PV cell resulting in a leakage current that degrades current generation capability. The grounding configuration of a PV array determines the amount of leakage current. Typical circumstances of PID occurrence are dependent on the temperature, humidity, system voltage, type of material used, and cell refractive index [47].

2.2.5 Structure and materials used in crystalline silicon (c-Si) PV modules

The structure and materials used in c-Si PV modules as shown in Figure 16:

i. **Backsheet:** This is a polymeric material which adheres to the backside of a PV module for the provision of electrical insulation and protection from environmental factors such as moisture and ultraviolet or solar radiation. When backsheet faces reliability issues visible problematic signs such as yellowing, cracking, bubbling and delamination are noticed. This visible failure will lead to PV module failure and electric shock hazards due to the leakage of electricity [60].

ii. **EVA:** The encapsulation of PV devices using ethylene-vinyl acetate (EVA) is done to provide mechanical support, optical coupling, electrical isolation, and protection against environmental exposure. Under exposure to atmospheric water and ultraviolet or solar radiation, EVA decomposes to produce acetic acid, which lowers the pH and increases the surface corrosion rates of enclosed metallic parts of PV devices [100].

iii. **Connection box:** Failures associated with the connection box or junction box are due to system installation faults, burnt bypass diode, burnt junction or connection box, and low power generation from the system. Stresses from the generation of energy from the system can result in connection box failure [101].

iv. **Tempered glass:** Tempered glass suffered reliability issues due to mechanical contact cleaning and sand particle deposition influence during operation in outdoor environments resulting in optical efficiency loss and a decrease in mechanical integrity, durability and reliability [102].

v. **Frame:** Although the frame of solar panels has nothing to do with the watertightness and the ability of PV arrays to overcome outdoor weather conditions rather its role relies on its mechanical characteristics that bring several benefits such as handling, storage, grounding, fixation, resistance against mechanical loads such as wind and snow. The solar frame reliability issue may be due to installation problems such as too much clamping. Therefore, all the PV modules do not behave alike under mechanical load due to variations in frames.
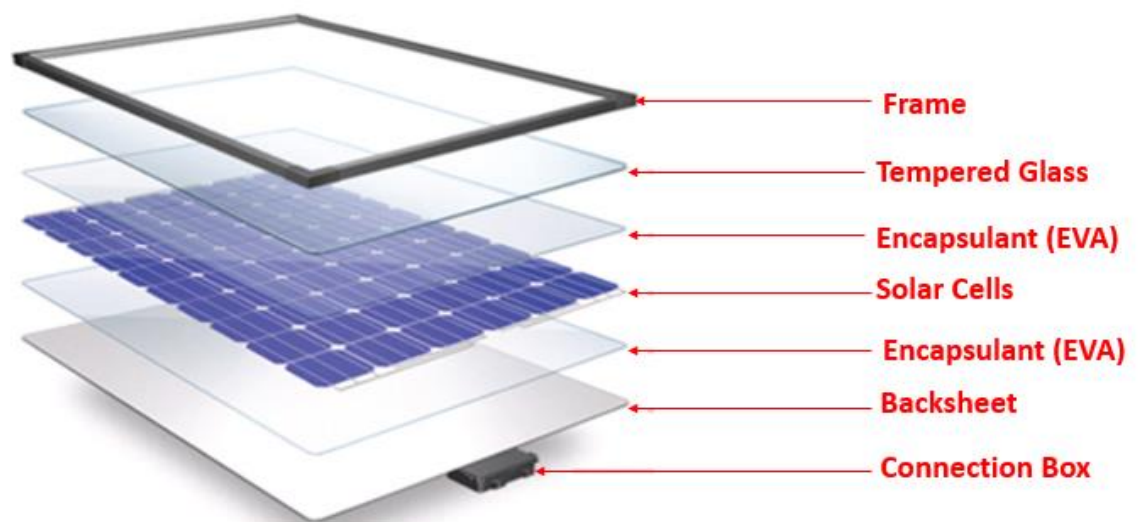
Figure 16. A solar PV module backsheet and its service life challenges *[103]*

36

The front surface of PV modules is encapsulated to ensure the long-term durability of service life of 25 years. Using, for example, tempered, low iron rolled, 3.2 mm thick glass sheets (see Figure 17). This encapsulant glass provides mechanical rigidity, impact resistance, optical transparency, electrical isolation of the solar cell circuit, and outdoor weatherability [104]. An encapsulant should have (i) High optical transmittance, (ii) good adhesion to different PV module materials, (iii) adequate mechanical compliance to accommodate stresses caused by differences in thermal expansion coefficients between the glass and solar cells, and (iv) good electrical insulation properties. PV module delamination, caused by a loss of adhesion between the encapsulant and other PV module layers, is another failure mechanism [104]. Extended UV light exposure degrades polymer encapsulants used in the PV module lamination. To ensure the long-term durability of PV modules with polymer encapsulants, an encapsulant coating should prevent UV light (400 nm) from reaching the encapsulant material by screening out UV light and adding a small amount of the cerium (Ce) to glass [104]. Rejecting infrared (IR) sunlight with wavelengths longer than those used by the solar cells reduces operating temperatures, improves PV module performance, and increases PV module lifespan. No cost-effective method of rejecting infrared heat has been developed [105]. PV module delamination, caused by a loss of adhesion between the encapsulant and other PV module layers, is a failure mechanism that results in a loss of performance due to the optical decoupling of the encapsulant from the solar cells [105].

The effect of encapsulant delamination on the electrical performance of PV modules was evaluated by Nochang et al [106] using a 5-year exposed monocrystalline solar PV module. The electroluminescence analysis was carried out to investigate delamination defects. Electrical mapping was carried out that measured the voltage drop or power loss of every using solar cell Xenon lamp to simulate a line of solar irradiance applied to the PV module. The

experimental setup is shown in Figure 17. The current density was produced at a constant voltage.

The PV module was rotated by a motor and current density was recorded at every rotating angle enabling the current density to be measured at every point of the PV module.
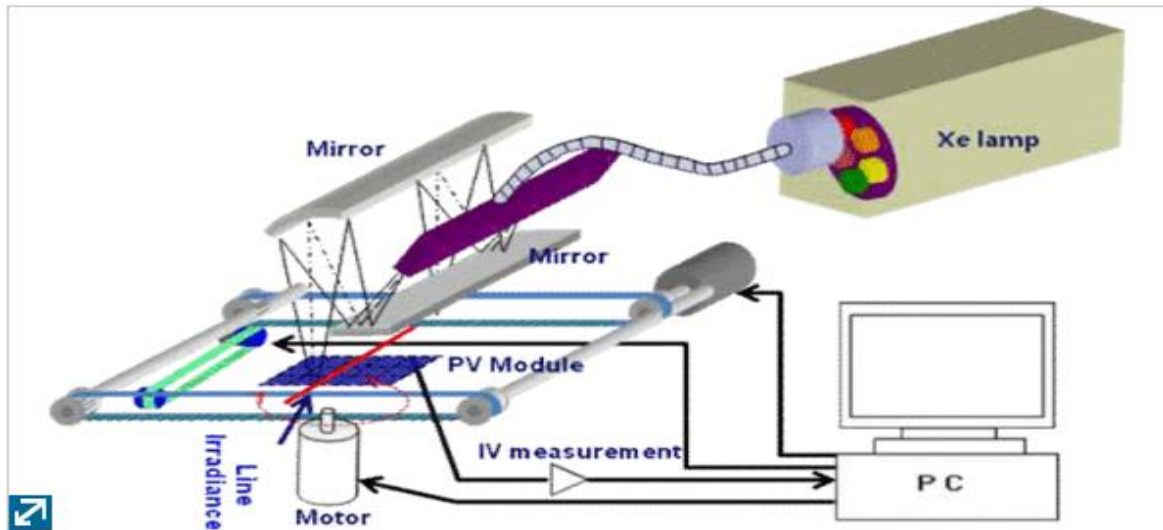
Figure 17. Measurement setup for PV module mapping *[106]*

Their results for physical degradation showed that the main defect was delamination as shown in Figure 18 at the interface between the encapsulant and the front surface of the solar cells. An electrical performance test conducted on the PV module showed about 3.3% less maximum power when compared to the initial value.
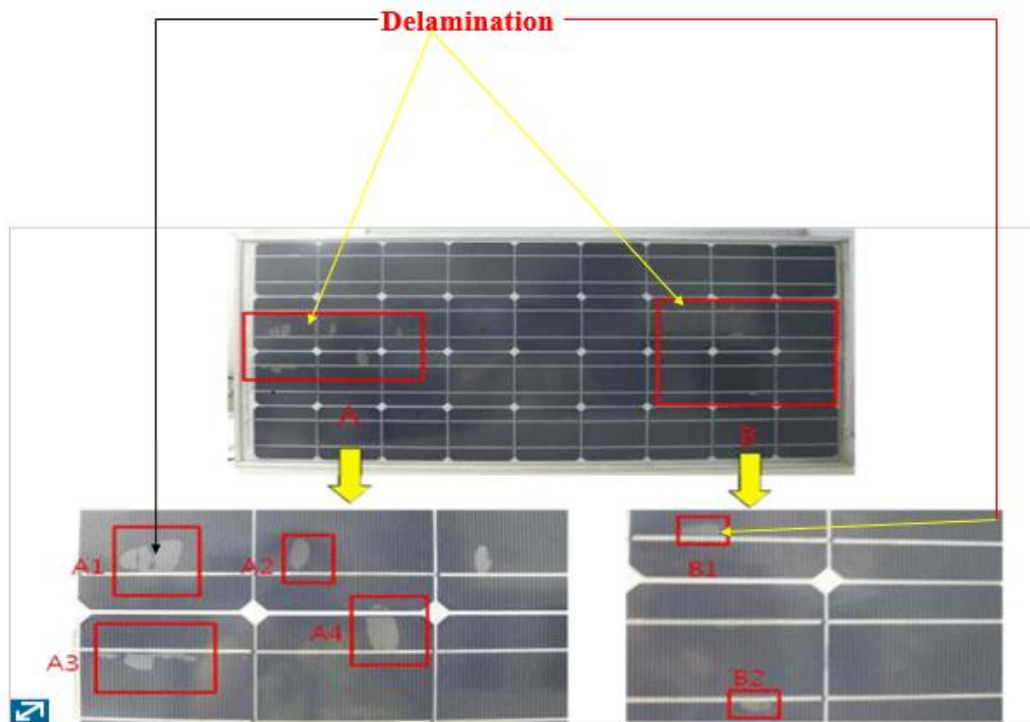
Figure 18. Physical degradation in front of PV module *[106]*

Shioda [107] investigated long-term delamination failures in field-aged PV modules using two different solar PV modules labelled Module A and Module B. The result of the I-V and P-V curves show that the I_{SC} and FF in Module A decreased by 13% and 17% respectively while its initial maximum power decreased by 30% due to large delamination. The I_{SC} and the initial maximum power of Module B decreased by 14% and 13% respectively due to partial

delamination. There was a decrease in I_{SC} due to delamination as illustrated in Figure 19.
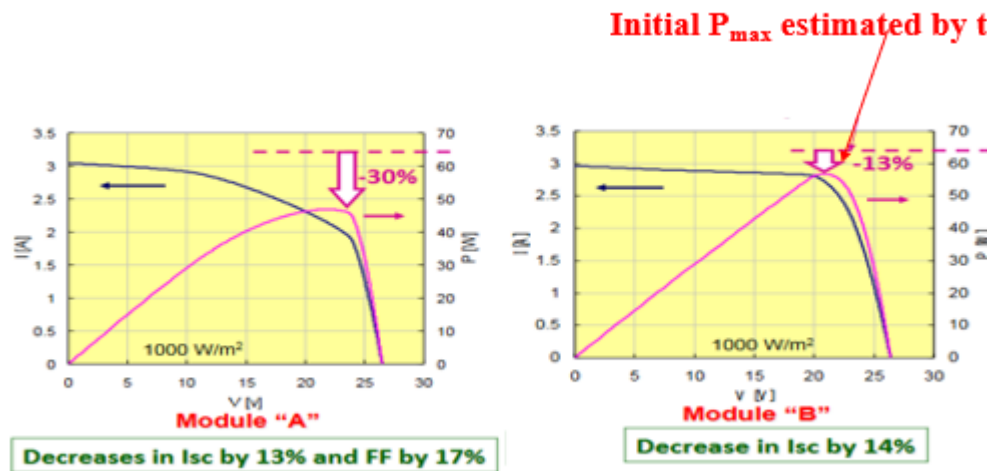
Figure 19. Effect of delamination and EVA discolouration on I-V and P-V curves *[107]*

To find out the relationship between delamination and power reduction: (1) Probes were connected to cut the ribbons located at point C from both ends to isolate or delaminate them from both ends; (2) The whole Module A was put on a solar simulator to obtain the I-V curve for each cell [107] as illustrated in Figure 20:
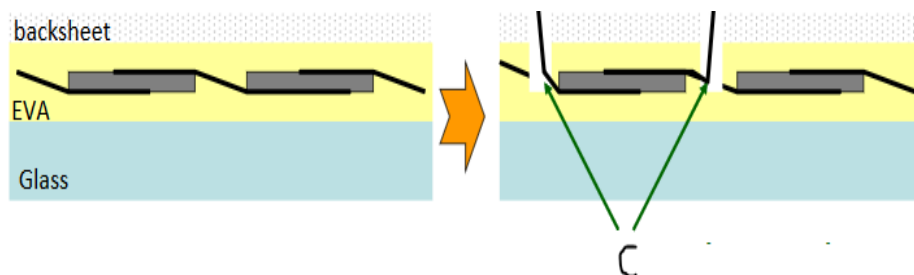
Figure 20. Evaluation of I-V curve in a solar cell *[107]*

Delamination degraded I_{SC} by 43% of its initial value (that is, 43% of 3.5A) and reduced maximum power by the same percentage amount. The solar cell with a partial delamination effect degraded I_{SC} by 13% (that is, 13% of 3.5A) and reduced the maximum power by the same percentage while the solar cell with no delamination had a reduction of I_{SC} and maximum power by 8% caused by discolouration of EVA. Even at that, I_{SC} and maximum power were

still high (almost at the maximum value, 3.5A). Therefore, the effect of delamination affects both I_{SC} and the maximum power, that is, maximum power is dependent on I_{SC}. Thus, delamination leads to a decrease in I_{SC} and maximum power (P_{Max}) as shown in Figures 18-19.

2.2.6 Series Resistance Durability
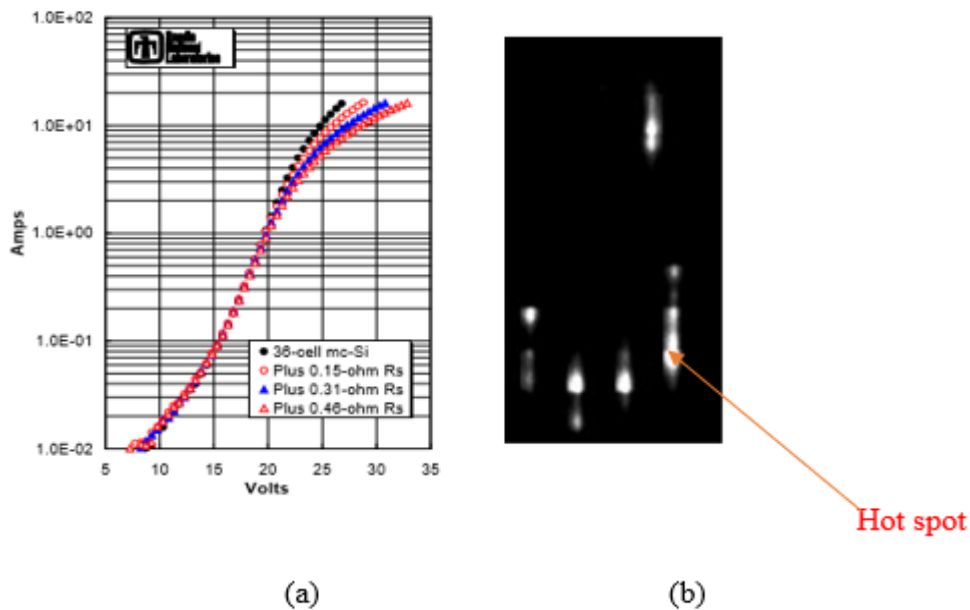
Figure 21. Dark I-V measurements on a typical 36-cell c-Si PV module show the influence of adding increased levels of R_S. (b) Thermal infrared (IR) image of a-Si PV module after about six years in the field, showing localised hot spots at typically resistive solder bond locations.

For this image, the module was in forwarding bias with a continuous current flow of about 10 A *[105]*. In wiring, junction-box terminations, cell-interconnect ribbons, solar cell metallisation, emitter and base regions of solar cells, and solar cell solder bonds, series resistance, R_S, cause voltage losses that limit the overall performance of a photovoltaic system *[105]*. The R_S of the PV module is important to PV module performance, so it is necessary to estimate the variations in R_S under various environmental stresses *[108]*. As a PV system ages, gradual increases in cumulative R_S can result in a 0.5% /yr decrease in output power *[105]*. As

a PV system ages, the mechanical effects of daily thermal cycling in the field result in a gradual increase in R_S *[105].*

Dark current-voltage (I-V) measurement at PV module level is a more direct and sensitive method for measuring increases in R_S [109]. The effects of adding R_S during dark I-V measurements on a typical silicon PV module are shown in Figure 21 (a).

This measurement technique is extremely sensitive to changes in R_S; changes of about 10% can be easily detected. Dark I-V measurements are used in the performance analysis of field-aged PV modules suspected of having R_S issues. Changes in shunt/parallel resistance, $R_P,$ and other cell physical properties are also readily detected in dark I-V measurements [105]. Infrared (IR) wavelength emission imaging provides a convenient non-destructive method for identifying locations in PV modules with high R_S. The method entails connecting a module to a power supply while it is forward-biased, as in a dark I-V measurement. A power supply provides a continuous current through a PV module at roughly twice the nameplate I_{SC}. IR images captured as a PV module heated up using an infrared camera with wavelength sensitivity from 3.6 to 5.0 microns identified solder bonds as a source of increased R_S in some field-aged PV modules. If the solder bonds were typically resistive, they appeared in IR images as localized hot spots. Figure 21 (b) depicts a PV module with resistive solder bonds after approximately 6 years of service. In an IR image, resistive solder bonds appear as localised hot spots [105].

2.2.7 Optical Degradation of Solar Photovoltaic Modules

Optical losses mainly affect the power output generated from a solar cell by reducing the short circuit current, I_{SC}. Optical losses consist of the solar radiation generated from an electron-hole pair which does not allow the solar cells to absorb the solar radiation rather the solar radiation is reflected from the front surface of the solar cells.
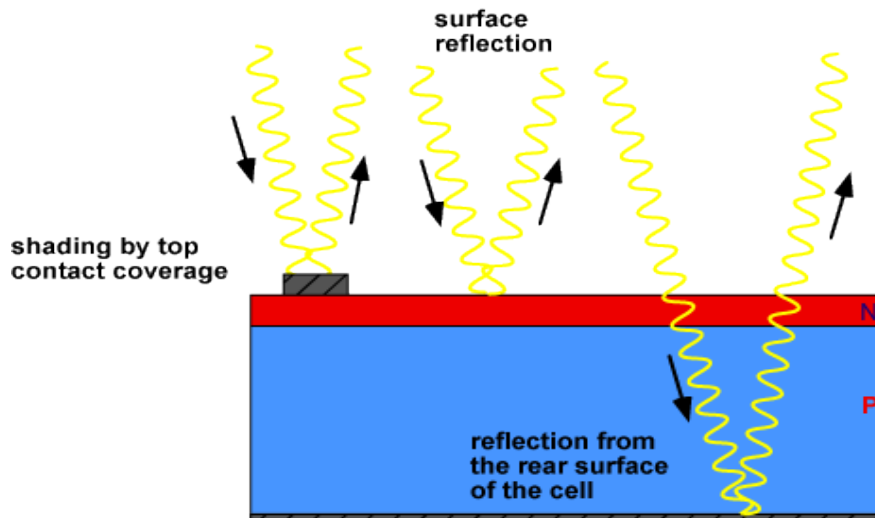
Figure 22. Optical loss in solar PV cells *[110]*

Optical losses in solar PV cells shown in Figure 22 can be reduced by [110]:

i.   To reduce the top contact coverage of a PV cell's surface, shading by top contact coverage is required (see Figure 22). This is done to increase series resistance, R_S and to reduce parasitic resistive losses.

ii. application of anti-reflection coatings on the top surface of a PV cell.

iii. minimising reflection by surface texturing.

iv. a PV cell being thicker to increase absorption of light.

v.   increase the optical path length in a PV cell, by a combination of surface texturing and light trapping.

The solar energy collection probability of PV cells depends on the lifetime of the minority carrier in the base and the surface passivation [111]. Preventing electrons and holes recombining prematurely with one another on the wafer surface and diffusion length (i.e., the average length a carrier moves between generation and recombination) are important considerations.

Electrochemical corrosion of string interconnects of a solar cell due to encapsulant results in the degradation of a PV module [112], [113]. This phenomenon leads to high series resistance (R_S) and low parallel resistance (R_P) in PV modules. Visible PV faults are summarised in Table 10.

Table 10. Visible PV module faults *[92]*, *[85]*

	Power loss	Safety issue	Visualisation
Shorting of module wires and diodes.	<3% of power loss	Fire failure may be caused	
Laminated cell fragment.	<3% of power loss.	Fire failure, electric shock, and physical danger.	
Cell cracks damage 10% of the cell area.	Degradation of power loss which saturates over time.	No effect on safety	
Bubbles or delamination.	Degradation of power loss in steps over time	Electric shock resulting in a major safety problem	
Burn marks on the back sheet.	Degradation of power loss in steps over time.	Failure may cause fire, electric shock, and physical danger.	
Front panel discolouration due to metallic interconnections overheating.	Degradation of power loss in steps over time.	Failure may cause fire, electric shock, and physical danger.	

Multicrystalline Si module delamination.	Degradation of power loss in steps over time.	Failure may cause physical change.	
Thin-film module delamination.	Degradation of power loss in steps over time.	Failure may cause physical change.	
Glass breakage in thin-film modules.	Degradation of power loss in steps over time.	Failure may cause physical danger.	
EVA browning	Degradation of power loss linearly over time.	No effect on safety for slightly browned condition, but as the browning grows faster fire failure may be caused.	
Snail trails	Degradation of power loss linearly over time.	Fire failure may be caused.	
Back sheet delamination	Degradation of power loss linearly over time.	Fire failure may be caused.	

2.2.7 Distinguishing transient performance changes from longer-term degradation

PV module output varies with incident solar irradiance and module temperature. The energy output of a PV system thus depends on weather conditions [114], [115]. It is also affected by shading, rain, and dust [116], [115]. An increase in PV cell temperature can lead to reductions in output and efficiencies. All these output and efficiency variations are transient on a variety of timescales and reversible. Degradation refers to loss of output due to physical degradation or damage to a PV cell, that is not reversible. Degradation will ultimately require replacement of a failed PV cell for the system to return to its initial performance. Degradation is measured by long-term changes in mean efficiency and/or performance ratio long-term as illustrated indicatively in Figure 23. Cell failure can also be observed in perturbation cell failure in current-voltage (I-V) curves for an array.
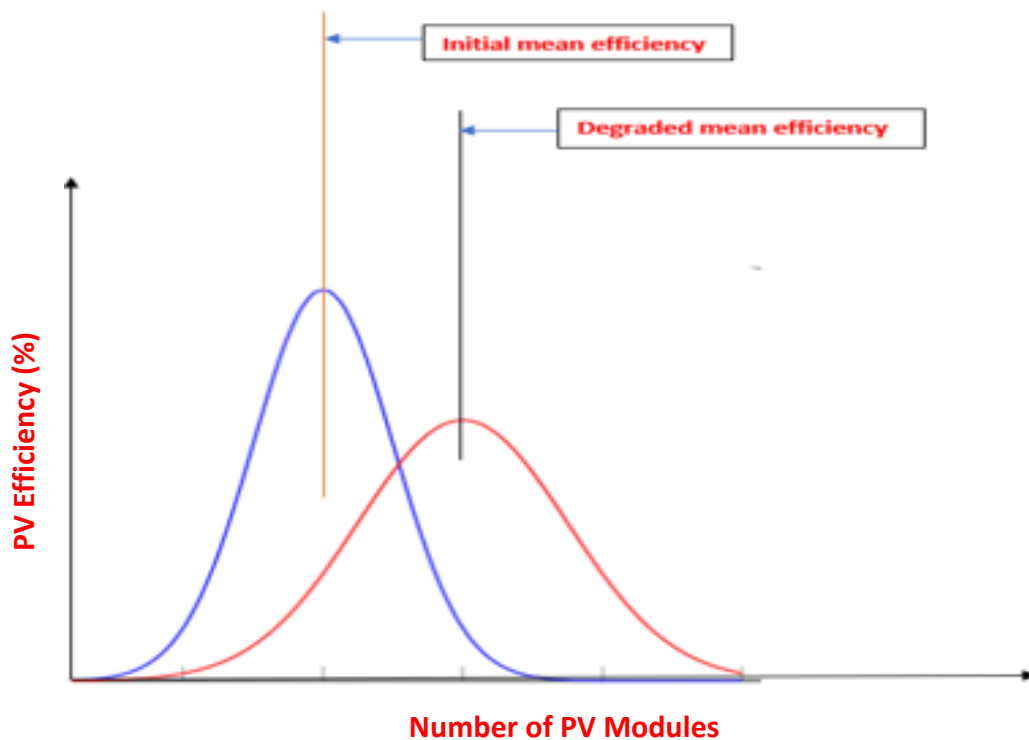
Figure 23. Efficiency degradation of modules in a PV array

Individual module degradation can be attributed to intrinsic property changes in the PV materials caused by external effects such as potential-induced degradation (PID) [117] and light-induced degradation (LID) [118].

As corrosion of interconnections and solder bonds slowly degrades performance [32], it is important to determine degradation rates under outdoor operational conditions rather than indoor testing of isolated modules [32]. One major difficulty in evaluating the degradation rates of PV modules from real operational data is distinguishing system degradation from "measurement degradation" as summarised in Table 11.

Table 11. System degradation and measurement degradation *[32]*

Degradation	**System**	Large fluctuations of the operational data due to uncontrollable external parameters such as weather conditions like solar radiation, rain, cloud movement, wind velocity, and ambient temperature together with unexpected changes of factors external to PV systems such as unexpected shading, inverter problems, and control failures.
	Measurement	Systematic 'degradation' in the measurement of PV module operational performance caused by control sensor drifting with time as a result of electronic ageing of components such as the drifting of irradiance sensors.

Manufacturers usually guarantee PV modules life spans for more than 20 years [32]. Beyond this warranty period, knowing likely degradation behaviour is essential for continual efficient operation and planning maintenance, and repair.

2.2.8   Effect of Soiling on PV System Performance

Soiling is accumulation of dust, combustion products, soot, ash, bird droppings and the growth of mold and moss [119]. Dust particles are defined as particulate matter less than 500 µm in diameter [120]. The most common composition is sand, clay, or eroded limestone. The settlement of dust particles mainly depends on several factors as shown in Table 12. Bird droppings are more opaque than dirt [119] and are not necessarily washed them from the PV module surface by rainfall [121], [122].

Table 12. Factors determining settlement of dirt on a PV array *[123]*, *[124]*, *[125]*

Dust properties	chemical properties, size, shape, weight, biological, and electrostatic properties.
Local environmental conditions	weather conditions, surface finish, tilt angle, humidity, and wind speed.

Solar PV arrays sited in semi-arid and desert regions have a dust layer formed on their surface that hinders the absorption of solar radiation. Within an hour, a desert sandstorm can deposit thick layer of sand that reduces PV efficiency by 70–80% [126]. In such locations, PV arrays need regular, even daily, cleaning. Figure 24 shows various means of cleaning solar PV modules [127].
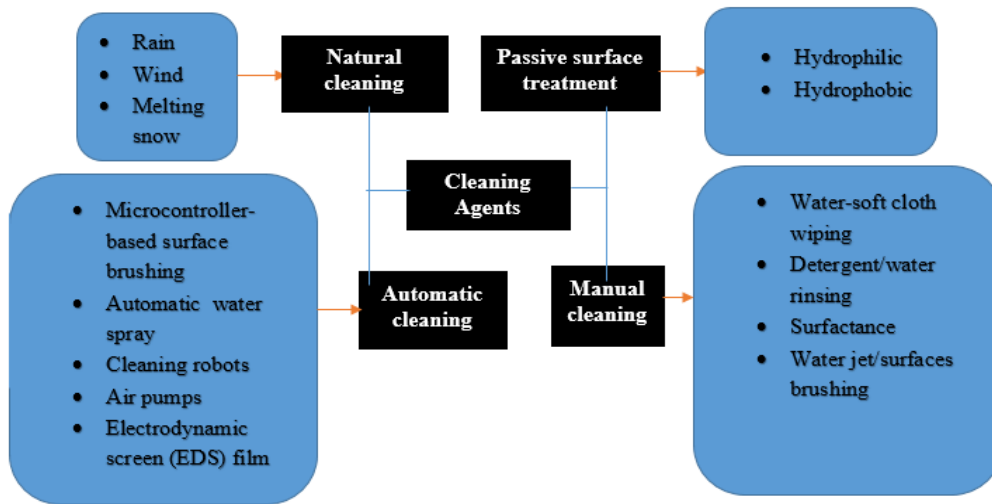
Figure 24. Various means of cleaning solar PV modules *[127]*

Heavy rainfall is an effective way to clean dust particles from PV module surfaces. High relative humidity and low rainfall contribute to the adherence of dust particles on PV module surface by consolidating fine dust particles into lumps of clay. As these become difficult for rainfall to remove this leads to permanent soiling. The accumulation of dust or dirt particles on the surface of the PV module is known as front-surface soiling. Accumulated dirt may partially shade a cell in a module causing it to generate less current than other cells in the string. This partial shading of a cell can lead to irreversible hot-spot damage with eventual module failure [128]. Front-surface soiling can be seen from a visual inspection of a PV module [63]. Soiling causes optical losses both when soiling is homogeneously or non-uniformly distributed. For instance, the average annual change in soiling recorded in I_{SC}, V_{OC}, P_{Max}, and FF was 6.68%, 0.30%, 9.80% and 2.67% respectively [129].

2.2.9   Degradation Rates of Photovoltaic Modules

Annual degradation rates of six crystalline silicon PV modules connected to an electric power grid were studied by Tetsuyuki and Atsushi [130]. Three indicators were used for the annual degradation rates: energy yield, performance ratio, and indoor power. The performance of the module was evaluated both from indoor and outdoor electricity output measurements taken over 3 years. Their results are summarised in Table 13 [130].

Table 13. Annual degradation rates of six crystalline silicon PV modules *[130]*

Indicators	Trends for each of the six modules (%/year)
Energy yield	0.0, -0.4, 0.0, 0.1, 1.5 and 0.5
Outdoor Performance ratio, PR	0.0, -0.4, -0.1, 0.0, 1.4, and 0.5
Indoor maximum power, P_{Max}	0.1, -0.3, 0.2, 0.0, 0.7, and 0.6

The performance of newly installed PV modules has been found to decrease by over 2% because of initial light-induced degradation (LID) [130]. According to Osterwald et al [114], the degradation rate of silicon PV modules is around -0.7% per year of maximum power rating. The power output of an outdoor PV module reduces because of thermal cycling causing cracks to form between solders and metals [131]. Dunlop and Halton [132] studied degradation of PV modules in outdoor conditions over 22 years. They monitored the electrical power outputs of monocrystalline silicon (m-Si), polycrystalline silicon (p-Si), and amorphous silicon (a-Si) modules. They found an 8% to 12% decrease in the maximum power output of the PV modules (P_{Max}) after 20 years of outdoor exposure. Their research showed that about 80% of the reduction was due to corrosion and the remaining 20% was attributed to dust accumulating on the PV modules.

Silvestre et al [133], investigated degradation of thin-film PV modules under long-term outdoor exposure in Spanish continental climatic conditions. Their study examined the degradation of four technologies: Micromorph (thin-film solar cells), copper indium diselenide (CIS) cadmium telluride (CdTe) and hydrogenated amorphous silicon (a-Si:H) under five years of outdoor exposure in Leganés, Spain. The corresponding degradation rates for the four technologies as summarised in Table 14. Their results show that CdTe module was found to have the highest degradation rate (-4.45%/a) while CIS module appears to be the most stable with a degradation rate of -1.04%/a.

Table 14. Degradation rates analyses of four thin-film PV module technologies in Spanish Continental climate conditions *[133]*

Cell type	Micromorph (thin-film solar cells)	CIS	CdTe	a-Si:H
Degradation rate (%/a)	-2.72	-1.04	-4.45	-2.28

An experimental study of degradation modes and their effects on the PV module was conducted after 12 years of field operation [134] and found that degradation led to annual reductions in output power ranging between 2.08% and 5.2%. Short circuit current (I_{sc}) reduced by between 2.75% and 2.84% annually. The open-circuit voltage (V_{oc}) was least affected, with annual reductions ranging between 0.01% and 4.25%.

The long-term performance and degradation analysis of different PV modules under temperate climate in Morocco were investigated by Ameur et al [135]; after six years a-Si degraded faster followed by m-Si and p-Si as summarised in Table 15.

Table 15. Degradation rates analyses of different PV module technologies in Moroccan Temperate climate conditions *[135]*

	Cell type		
	a-Si	m-Si	p-Si
Degradation rate (%/a)	0.9±0.009 and 0.75±0.003	0.53±0.01 and 0.41±0.003	0.36±0.01 and 0.28±0.004

Degradation rate over 10 years of field-exposed residential photovoltaic installations in the UK and Ireland was investigated by Dhimish [136] showed that the lowest PV degradation rates were obtained at Irish PV sites. Higher PV degradation rates were found in England whereas the highest degradation rate was observed in relatively cold areas including Aberdeen and Glasgow in Scotland as summarised in Table 16. The main reason PV systems installed in Aberdeen and Glasgow had the highest degradation rates was frequent hoarfrost and heavy snow affecting these PV systems.

Table 16. Degradation analyses of p-Si PV modules installed in three different locations

	Location		
	Ireland	England	Scotland
Degradation rate (%/a)	-0.4 to -0.6	-0.7 to -0.9	-1.0

2.2.10 Degradation Influences of Photovoltaic Modules

The existence of only one highly-degraded 96 kW_p PV module in a PV system has been found to reduce daily output (Takatoshi et al, [137]) by 19.8 kWh to 18.7 kWh during sunny days, 11.3 kWh to 10.8 kWh during partly cloudy sunny days; and 5.5 kWh to 5.3 kWh during cloudy days.

Pramod et al [138], investigated degradation of m-Si PV modules after 22 years of outdoor exposure. They studied 90 m-Si PV modules installed on the rooftop of the National Institute of Solar Energy (NISE) near New Delhi, India. They carried out a visual inspection, thermal imaging, current-voltage (I-V) characteristic curve analysis and insulation resistance measurement and the calculation of the degradation rate after 22 years of outdoor operation. The mean power reduction rate of 90 PV modules over 22 years was found to be about 1.9% per year at a peak rate of power reduced by 4.1% per year with the minimum rate of power reduction being 0.3% per year. Electrical resistance of insulation measurements of 90 PV modules (both in dry and wet conditions) showed that only two PV modules showed insulation of electrical resistance lower than 400 MΩ in dry conditions. Analysis of electrical parameters indicated that there was a degradation of short circuit current (I_{SC}), from 0.4% to 3.7% per year with a mean value of 1.8% per year. Open-circuit voltage (V_{OC}), ranged from 0.8% to 2.1% per year with a mean value of 1.4% per year, and fill factor (FF), ranged from 0.7% to 2.6% per year with a mean value of 1% per year. Maximum power, P_{max} reduction rate ranges from 0.3% to 4.1% per year with a mean value of 1.9%/year. Reduced power output was mainly due to the degradation of I_{SC}.

2.2.11 Failure Risk Analysis

Severity risk in solar panels is the highest level of severity of damage noticed on the PV panel when there is the subjugation of failure modes such as EVA discolouration, effects of corrosion, hot spot, delamination, bubble, crack in solar cell, bypass diode and potential induced degradation.

Failure modes and effects analysis (FMEA) is a methodology for defining risk of failure (as denoted by a "Risk Priority Number" (RPN)) based on a specification, failure's severity (S), occurrence (O), and detectability (D) [139] for a specific combination of PV system and operating environment conditions [139]. RPN is calculated from (33) [139];

$$RPN = S \times O \times D \tag{33}$$

where:

    S is severity of damage; $\qquad\qquad\qquad\qquad\qquad\quad$ $0 < S < 10$

    O is the probability of occurrence of defect (s) $\qquad\qquad$ $0 < O < 10$

    D is the likelihood that available data can detect failure modes, $\qquad$ $0 < D < 10$

Higher RPN means that defects reduce system performance [140], [141], [142]. Severity rank depends on the degradation rate per year and when that leads to safety issues. It is difficult to assign a severity rank for a particular failure mode, as the degradation of a PV module is an accumulation of many interacting factors [143], [144]. The highest severity rank from 9 to 10 based on safety is insulation resistance failure, as it is a hazard to people [139]. Severity ranks [139] are shown in Table 17.

Table 17. Severity ranking of failure mode *[139]*

Severity	Rank
Degradation rate >1.0%/year with safety hazard probability <90−100>%	10
Degradation rate <0.9–1.0>%/year with safety hazard probability <80–90>%	9
Degradation rate <0.8–0.9>%/year with safety hazard probability <70–80>%	8
Degradation rate <0.7–0.8>%/year with safety hazard probability <60–70>%	7
Degradation rate <0.6–0.7>%/year with safety hazard probability <50–60%> %	6
Degradation rate <0.5–0.6>%/year with safety hazard probability <40–50> %	5
Degradation rate <0.4–0.5>%/year with safety hazard probability <30–40>%	4
Degradation rate <0.3–0.4>%/year with safety hazard probability <20–30>%	3
Degradation rate <0.2–0.3>%/year with safety hazard probability <10–20>%/	2
The degradation rate <0.1–0.2>%/year with no safety hazard	1

2.2.12 Climatic Effects on PV Degradation

In most climate zones, the largest contributor to lower maximum power output (P_{output}) is I_{SC} degradation caused by delamination, discolouration, and cracked solar cells, with a small amount due to light-induced degradation (LID) and soiling [145] [146], [147], [148] [149]. In desert climates, I_{SC} degradation may be accompanied by a small improvement in V_{OC} [146]. In humid conditions, dust accumulated on the front glass can be difficult to remove by wind or rain causing power output to decrease. The effectiveness of cleaning by heavy rain depends on material properties [150]. Importantly, climatic effects alone cause less degradation of fill factor (FF) as this is normally related to corrosion and solder bond breakage [146], [151], [72], [152], [153] whereas EVA browning shows high I_{SC} and low FF degradation. In regions without warm summers, higher FF degradation is observed probably due to cracking of individual solar cells under snow loads [146], [154], [155]. Arid deserts present a harsh environment where PV modules are subjected to significant UV radiation, day-to-night temperature cycles and sand deposition. Desert environments cause discolouration of EVA encapsulant accompanied by delamination and a certain degree of corrosion [67], [156], [157], [72], [158], [159], [160], [161]. Discolouration of EVA is due to formation of benzoic acid and phenol products, which enhance delamination and discolouration [68]. Deterioration of the

solder bonds leads to an increase in series resistance (Rs) [156]. The effects of different climatic conditions are summarised in Table 18.

Table 18. Effects of climatic conditions

Climatic condition	Hot and humid conditions in tropical climates	Degradation of PV modules ensues much faster in comparison to other environmental conditions [162], [163], [164].
	Warm and temperate climate	EVA discolouration, encapsulant delamination and corrosion due to the moisture ingress [150], [165], [147], [148]. and "snail tracks" [166].
	Snow and polar climates	Lower temperatures decelerate thermal degradation modes. Degradation modes are associated with mechanical stresses (such as high snowfall and/or wind stresses) that lead to PV cell cracks, frame breakage or bending, and glass breakage. Frame damages vary depending on the assembly design of the PV modules [167], [168].
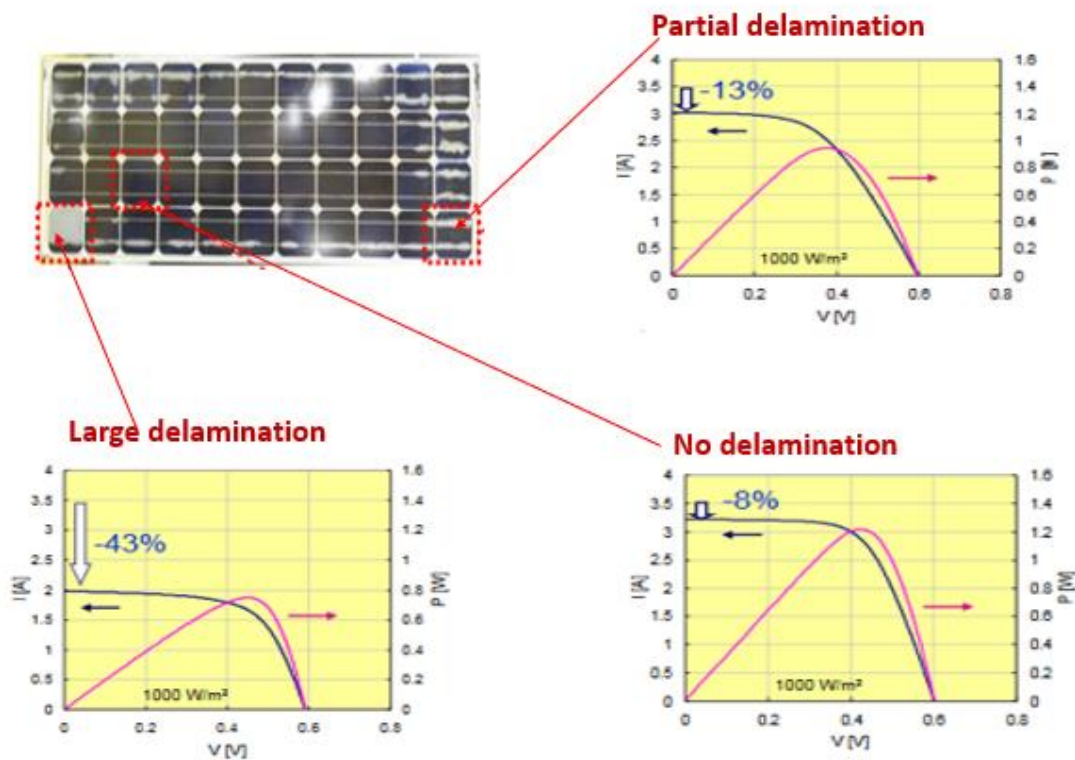
Figure 25. Effect of delamination on I_{SC} and P_{Max} *[107]*
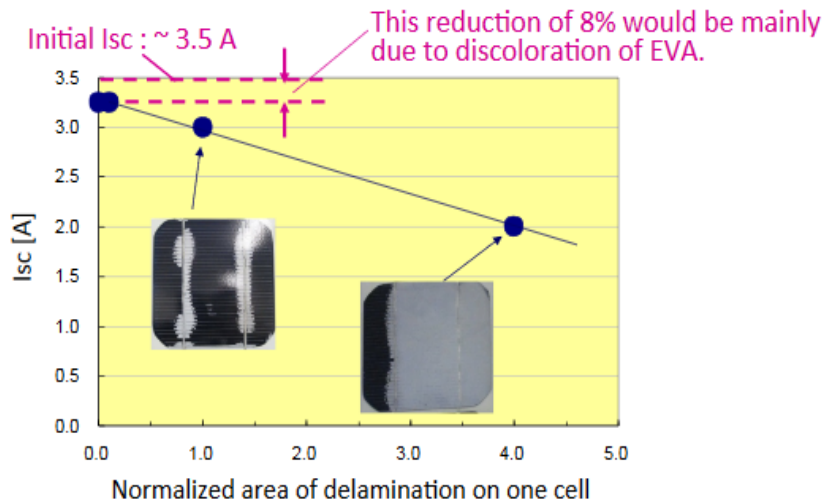
Figure 26. Effect of discolouration of EVA on I_{SC} *[169]*

PV module degradation caused by moisture ingress results in loss of output power generation or complete failure of PV modules [169]. Moisture ingress causes two forms of degradation, namely, corrosion and delamination [170]. Corrosion increases series resistance (R_S) in the PV module leading to power loss. Contact delamination also increases R_S, as the current flow moves further into the heavily-doped Si before being collected by the fingers [169]. Mismatching of solar cells is caused by front surface soiling, encapsulant degradation, anti-reflective (AR) coating deterioration, manufacturing defects, cell cracking, and PV cell partial shading [63]. Mismatched solar cells degrade PV module performance especially when solar cells are connected in series strings. When a defective solar cell in a PV module is generating less electric current than the other cells in a PV module, the latter solar cells act to reverse bias the defective cell. This causes the defective cell to operate in the negative voltage region, becoming a power dissipater [171]. Figure 27 (a) describes how interconnect busbars can assist in preventing a cell from generating less electric current because of the illustrated crack. Thermal stress and hail damage can cause cracking of solar cells. Cracks can also be produced during processing and assembling. The crack in Figure 27 (b) removes a part of the solar cell from its electrical circuit. This will have the effect of a decreased electric current generated by

the solar cell. The same process is observed when a solar cell is partially shaded. Mismatched conditions in PV cells cause cells to heat up. When a mismatched solar cell's temperature exceeds a critical value ($\sim 150°C$), delamination of cell encapsulants may occur [171]. If the high reverse bias exceeds the solar cell's breakdown voltage, a solar cell may be irreversibly damaged by a thermal breakdown. The latter is observed as hot spots on the solar cell that not only lower the efficiency of the PV module, but also influence V_{OC}, I_{SC}, P_{Max}, and FF. When a PV module containing a mismatched solar cell has no integrated bypass diode in its interconnection circuit, a mismatch situation may lead to irreversible hot spot damage. Mismatched cells can be identified by visual inspection, I-V measurements, hot-spot endurance testing, and individual solar cell temperature monitoring when a module is forward-biased [63].
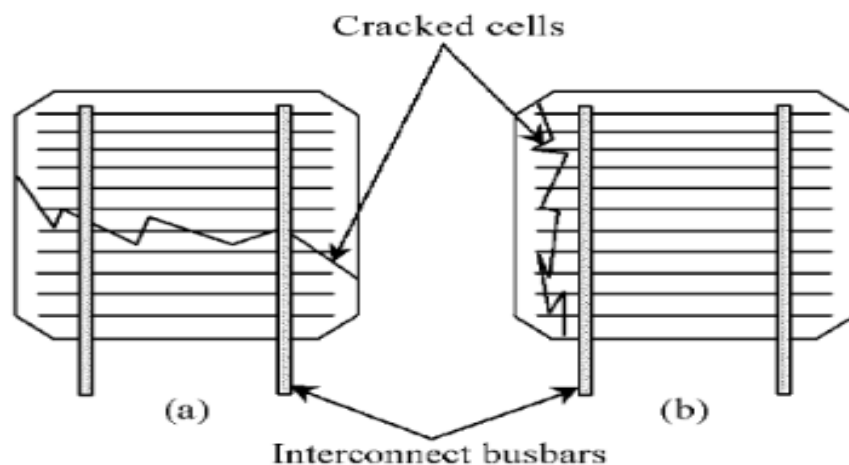
Figure 27. How interconnect busbars can assist in preventing open-circuit failure *[63]*

2.2.13 Evaluation of Solar PV Failure Modes Through Materials Degradation Approach

The reliability and durability of solar PV modules can be analysed by failure modes and degradation mechanisms after long-term outdoor operation [139]. Solar PV module failure arises from partial shading, inverter failure, EVA discolouration, series and shunt resistance, hot spot, corrosion, delamination, bubble, crack in solar PV cell, bypass diode, and potential induced degradation (PID) [139]. Each of these failure modes and their effects are summarised in Table 19.

Table 19. PV failure modes and their defects *[139]*

Failure due to;	Effects
Partial shading	Causes leakage current [172].
Inverter failure	Causes power loss [173].
EVA discolouration	Laboratory exposure has shown that the power output of "brown" PV modules has probably degraded at an average rate of about 1%/year due to a decrease in I_{SC} caused by low transmissivity of solar radiation into a PV cell, thus reducing FF [174], [175], [176].
Series and shunt resistance	Causes a reduction in solar PV cell (for example, a-Si PV) efficiency decreases by about 1% [177].
Hot spot	A decrease in R_{Sh}, resulting I_{SC} decreased [178], [179].
Corrosion	R_S of solar cell/module increases resulting in a performance decrease [180].
Delamination	Destroys the layers of the PV module [181].
Bubble	Bubble formation is a cause of delamination which is known to be one of the major problems linked to PV module reliability and durability [48].
Crack in solar PV cell	Significantly decreases the power as well as the lifespan of PV modules output [182], [183], [184].
Bypass diode	Leakage current may reduce [185].
Potential induced degradation (PID)	PV module degrades by about 42% after nine years of outdoor exposure to negative voltage stress [186].

2.2.14 Diagnosis of Degradation Mechanisms in Photovoltaic Modules

Performance monitoring of PV systems aims to maintain power output from PV systems thus increasing economic viability [187]. To evaluate degradation of PV modules, Parveen and Saurabh [187] calculated output power degradation over three years for amorphous silicon (a-Si), polycrystalline silicon (p-Si), and silicon hetero-junction with an intrinsic thin layer (Si-HIT). The degradation rate for a-Si was lowest at 0.85% per year and was highest for Si-HIT technology at between 0.95% and 2.03% per year. Their results showed good agreement with standard procedure used for performance evaluation.

Ensuring long-term durability of solar photovoltaic (PV) modules requires clustering of different approaches including [187], visual inspection [188], inspection using imaging methods such as infrared (IR) thermography [189], [190], [191], [105], [192], analysis of micro-cracks using electroluminescence [193], [41], or aerial, drone-mounted IR thermography [194], and preventive measures such as water-free cleaning [126].

Glass breakage results in electrical safety issues and performance loss after corrosion ensues due to moisture penetration through cracks. Cracks develop into hot spots, resulting in module overheating. Zaini et al [195] carried out a study on the effects of lightning on a grid-integrated solar PV system with an assumption that lightning strikes a solar PV system at two different points as shown in Figure 28. Lightning strike on a solar PV module results in open-circuit bypass diodes or PV module failure.
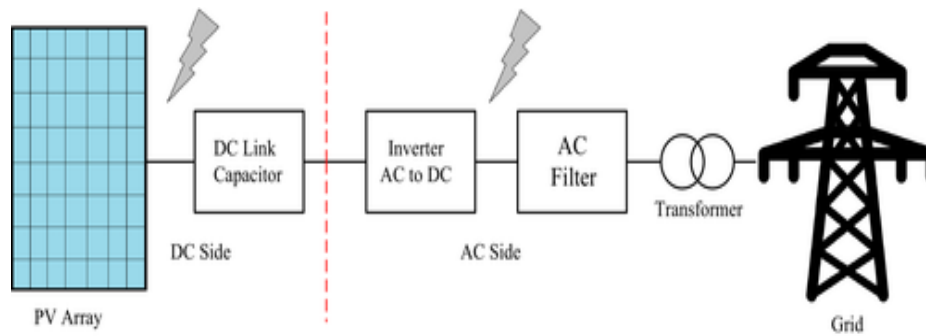
Figure 28. Lightning strikes at different points *[195]*

Most expected failure modes and degradation mechanisms are associated with glass breakage, junction box failure, interconnection faults, and delamination [47]. Kalejs et al [196] noted that inappropriately-designed, or insecurely-closed, junction boxes allow moisture ingress to corrode connections in the junction box, leading to internal discharging. When solder joints meet silver electrodes in a solar PV cell, they dissolve into the Tin-Lead (Pb-Sn) solder electrodes to form an Ag_3Sn compound. Silver leaching develops a crack at the soldered interface because of thermal expansion, resulting in connection breakdown. Delamination occurs because of adhesion contamination or because of environmental factors that ingress humidity, moisture, and corrosion into PV module laminates.

2.2.15 Diagnostic Techniques of Solar Photovoltaic Cells and Modules

Preventive diagnostics detect possible defects before they occur. Spagnolo et al [189], Krenzinger and De Andrade [190], Buerhop et al [191], King et al [105] and Ancuta and Cepisca [192] have used infrared (IR) thermography for inspecting PV-plants. This method is fast, reliable, contact-free, non-destructive, and involves measurements during operating conditions but without clouds and wind [197]. Johnston et al [193], Köntges et al [41] used electroluminescence to find micro-cracks in PV modules.
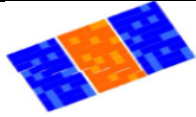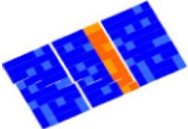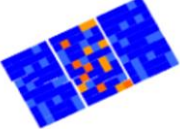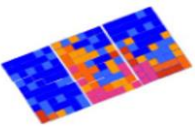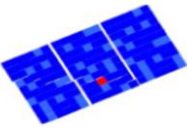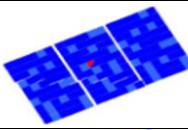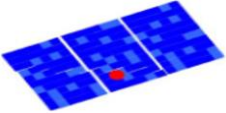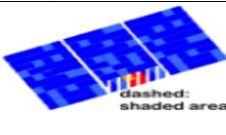
2.2.15.1 Thermography

Detection with a thermal camera uncovers a broad range of defects as shown in Table 20 [198]. A disadvantage is that a thermogram does not make a quantitative assessment [199]. Thermography techniques for PV modules in field conditions are pulse thermography and lock-in thermography [200].

Thermography under steady-state conditions is a non-destructive measuring technique [201]. It can be used as a contactless method for diagnosing some thermal and electrical failures in PV modules. The measurements can be performed during normal operation for both individual PV modules and as a scan of large-scale solar PV systems [201]. Thermography detects temperature differences induced by an external current or by applying light to the PV module. During dark measurements, there is no light applied to a PV module except the external current (I) which is approximate to I_{SC}, supplied in the forward direction [202]. To avoid thermal damage to PV modules (e.g., to thin-film modules), it must be ensured that the I_{SC} of the PV modules is not greater than 30% [200]. Temperatures of PV modules can be measured using an IR camera. Thermography imaging is performed using a portable, uncooled IR camera measuring wavelengths between 8 and 14 μm [203]. Buerhop-Lutz and Scheuerpflug [194] inspected PV-plants using an aerial, drone-mounted infrared thermography system. They carried out their measurement using an unpiloted drone (Multikopter), a lightweight infrared (IR)-camera PI 450 (Optris), a visible camera GoPro, and equipment for navigation. They presented frequently detected failure modes of installed PV modules by focusing on crystalline modules from residential and industrial roofs as well as from solar parks in the field.

Table 20 shows possible failures of PV modules that can be spotted by an IR-Camera [204].

Table 20. The possible failures of PV modules can be spotted by an IR-Camera *[204]*

Observation	Detail	Reason	Electrical characteristics	Power loss	Safety issue
	One PV module in an array appears to be warmer than others.	The PV module is open-circuited, that is, not connected to the system.	The PV module is fully functional.	System failure	No effect on safety
	One row (sub-string) is warmer than the other rows.	Short-circuited (SC) or open sub-string - Bypass diode SC, or - Internal SC.	Sub-strings power loss caused by reduction of V_{OC}.	Constant power loss	May lead to fire
	Single cells are warmer, patchwork patterns.	All bypass diodes are short-circuited (SC) or interconnected connections.	PV module power was reduced to almost zero because of the reduction of V_{OC}.	Constant power loss	No safety effect when external SC, system fire when diodes SC
	Single cells are warmer, lower parts, and close to the frame hotter than the upper and middle parts.	Massive shunts are caused by potential induced degradation (PID) and/or polarisation.	PV module power and FF reduced. Low light performance is more affected than at STC.	Caused by voltage, humidity, and temperature	No effect on safety
	One cell is warmer than the others	-Shadowing effects, - Defect cell, and /or - Delaminated cell	Power decreases are not necessarily permanent (Transverse effect), e.g., shadowing leaf or lichen.	Power loss increases with mechanical load, thermal cycling, and humidity	For extreme conditions May lead to fire
	Part of a cell is warmer	Broken cell and/or Disconnected string interconnect	Drastic power reduction, FF reduction.	Caused by mechanical load and thermal cycling	May lead to fire
	Pointed heating	Partly shadowed by soiling or by a lightning protection rod	Power reduction is dependent on the form and size of shading.	Caused by mechanical load and thermal cycling	May lead to fire
	Sub-string part is remarkably hotter than others when equally shaded	Sub-string with missing or open-circuit bypass diode.	Massive I_{SC} and power reduction when part of this sub-string is shaded.	Transient effect	May lead to fire
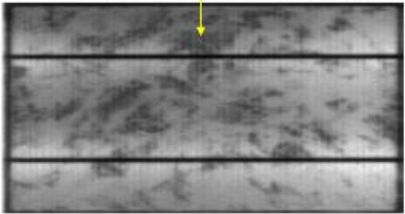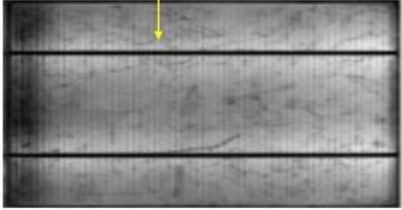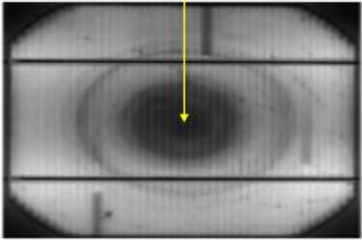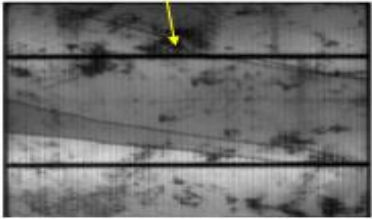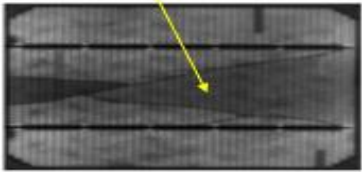
2.2.15.2 Electroluminescence for Crack Detection

Electroluminescence is based on detecting electroluminescence radiation detection emitted by recombined charge carriers during the radiative recombination process. To carry out the diagnostic process, the equipment should be in a place with sufficiently low irradiance such as a dark room and the sensor must be a special sensor that allows detection in the near-infrared area (since the radiation of PV modules has a wavelength of approximately 1 μm) [205]. The PV module is connected to the current source and the current which should not exceed I_{SC} value flows through it. The intensity of the emitted radiation is dependent on this electric current and at the lower electric current level, different defects occur. Places affected by some damage and higher defects are noticed as dark places in the EL images. Such places do not contribute to electricity generation. Therefore, the radiation intensity is then the scale of PV module functionality [206]. Criteria of cracks in PV modules for proper identification as summarised in Tables 21 and 22 [200]:

Table 21. PV module cracks identified by electroluminescence

		Characteristics
Crack Type	Greyline	A solar cell crack appears as a dark grey line in an electroluminescence image. The width and the greyscale should be mainly constant over the whole length of the crack.
	Angle line	A crack orientated at an angle of $\pm 45°$ to roughly $\pm 5°$ to the fingerprint of the solar PV cell would partly run parallel to the fingers of the solar cell so that the crack appears as a wavy step function.
	Defect	Wafers that have been neighbours in the artefact may be found in a PV module. These wafers can be used to check whether a detected dark grey line is a defective structure of the silicon or a cell crack.
	Cell crack	If the electroluminescence intensity changes suddenly at a dark grey line, it is a cell crack. In this case, the crack already reduces the conductivity of the metallisation across the crack.
	Cross crack	It is quite unlikely to find a solar cell crack not starting or ending at the busbar or the edge of the cell except for cross cracks. Cross cracks are quite likely to be found in the middle of the solar cell.

Table 22. PV module failure identification by electroluminescent (EL) diagnostic inspection *[200]*

	Safety	Power loss	Image
Crystal dislocations in a multi-crystalline wafer	No effect on safety	No	 Detection of Micro-crack
Edge wafer failure	No effect on safety	No	 No Micro-crack Detection
Striation rings	No effect on safety	No	 Striation rings
Cracks in the solar cell do not influence the current flow over the crack (no crack resistance)	Safety may not be guaranteed. These cracks reduce the strength of the wafer, causing the wafer to break with substantially less applied force when compared to thicker wafers	No	 Crack Detection
Cracks in solar cell influence the current flow to the cell interconnect ribbon of the cell. However, the cell is still connected.	May cause fire	Yes	 Crack Detection

2.2.15.3   Photoluminescence (PL)

Photoluminescence is utilised for PV cell diagnostics. In contrast with the EL, PL does not require the sample with the contact system, because radiative recombination excitation is stimulated by the strong light force, so the technique can be applied like the control method during the manufacturing process, which can be very important, for instance, during layers deposition. The disadvantage of this technique is the requirement for a special sensor (like EL) and much more complex equipment for radiation excitation [207], [208].

2.2.15.4   Microplasma luminescence

Microplasma luminescence provides information about shorts inside the structure. Unlike EL measurement, a PV module is connected in the reverse direction, with the reverse polarisation not exceeding the cell breakdown voltage [209]. Reverse polarisation in areas affected by some defect causes the occurrence of microplasma. Microplasma shows either noise or light emission. The light emission causes light places in obtained pictures, which means that these pictures are as a matter of fact inverse to the electroluminescent ones [210]. Therefore, the various faults can be identified using the deviation of current-voltage (I-V) characteristics both at the PV cell level and PV Module level can be noticed in Tables 23 and 24.

Table 23. Failure detection in solar PV cells using I-V characteristics *[47]*
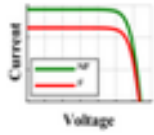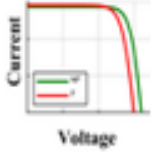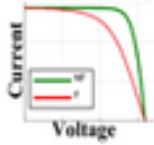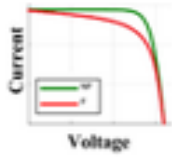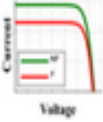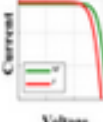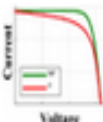
Characteristic	Failure	Broken cell interconnect ribbons	Cracked cells	Short-circuited cells
P_{Max}	Power loss	Degradation of power loss in steps over time	Degradation of power loss in steps over time	Degradation of power loss in steps over time
	Safety issue	Failure may cause fire, electric shock, and physical danger	No effect on safety	No effect on safety
		Failure may cause fire, electric shock, and physical danger	No effect on safety	No effect on safety
I_{SC}		-	No effect on safety	-
V_{OC}		-	-	No effect on safety
R_{OC}		Failure may cause fire, electric shock, and physical danger	-	No effect on safety
R_{SC}		-	-	-

Table 24. Failure detection in solar PV modules using I-V characteristics *[47]*

Characteristic	Failure	Bypass diode (short-circuit)	Delamination		Induced degradation	
			Homogenous	Heterogenous	Potential	Light
P_{max}	Power loss	Degradation of power loss in steps over time	Degradation of power loss which saturates over time	Degradation of power loss which saturates over time	Degradation of power loss linearly over time	Degradation of power loss in steps over time
	Safety issue	Failure may cause fire, electric shock, and physical danger	Failure may cause fire, electric shock, and physical danger	Failure may cause fire, electric shock, and physical danger	No effect on safety	No effect on safety
	-	Failure may cause fire, electric shock, and physical danger	Failure may cause fire, electric shock, and physical danger	Failure may cause fire, electric shock, and physical danger	No effect on safety	No effect on safety
I_{SC}		-	Failure may cause fire, electric shock, and physical danger	Failure may cause fire, electric shock, and physical danger	-	No effect on safety
V_{OC}		Failure may cause fire, electric shock, and physical danger	-	-	No effect on safety	No effect on safety
R_{OC}		-	-	-	-	-
R_{SC}		-	-	-	No effect on safety	-

2.3 The economic impact of solar cell degradation

PV modules, exposed to variable harsh weather conditions for an operational period of more than 30 years, experience maximum stresses leading to the degradation of their materials due to the prevailing climate conditions [211]. The technique of how to resolve the occurring solar cell degradation depends on its impact on power generation and the economy [212]. To investigate the economic impact, it is important to perform cost-based analyses [212]. Therefore, to evaluate the economic impact of solar cell degradation, two main strategies should be adopted [212]:

i. detection of the solar cell degradation mode (DM).

ii. investigation of preventive measures.

To interpret the total economic impact of a technical risk caused by solar cell degradation, the cost priority number (CPN) developed by the H2020 project Solar Bankability was used to support decisions on preventive measures [213]. To evaluate the economic impact of solar cell degradation, reliability, availability and maintainability (RAM) was used which allowed analysis for the investigation of energy generation (losses) of a PV plant [214]. The RAM technique is based on the identification of critical components with significant performance losses to help improve maintenance strategies accordingly [214].

The most significant technical risks related to PV installation projects have been identified and included in a risk matrix organised by components (such as PV modules, inverter, mounting structure, and cabling) [213]. To cover the whole PV value chain, the risk matrix is divided into five categories: product testing/development, PV plant planning/development, transportation/installation, PV plant operation & maintenance, and decommissioning [213]. Cost priority numbers (CPNs) are estimated in €/kWp if a certain time frame is investigated,

or in €/kWp/a as a yearly cost factor and can therefore directly give an estimation of the economic impact of technical risk [212].

The technique that involved the computation of CPN is defined to examine two main economic impacts of solar cell degradation: costs due to downtime (C_{down}) and costs due to repair/substitution (C_{fix}) [212]. For the computation of C_{down}, parameters such as time to detection, time to response and repair time (t_{det}, t_{res}, and t_{rep}) are considered, while for C_{fix}, the cost for detection, labour cost, cost of repair/substitution and cost of transportation (C_{det}, C_{lab}, C_{rep}, and C_{tran}) were included separately [212]. The technique also considers the year of installation, the year of failure and the nominal power (P_{nom}) to be able to run an analysis for various market sections and to evaluate the distribution of failure probability once the available data in the database reach statistical relevance to this type of granularity [212]. The analysis of the economic impact of solar cell degradation showed that high-ranking risks for PV modules are glass breakage, potentially induced degradation (PID), defective backsheet and delamination [215]. Most of these defects were detected by simple visual inspection [215]. For inverter systems, the most significant specific risk is related to the failure of the fan and overheating. If only affected plants are considered, safety-related defects become frequent, for instance, theft of PV modules and fire outbreaks [215].

According to the CPN Technique, costs related to the appearance of specific defects can be split into downtime and fixing [216]:

$$CPN = C_{down} + C_{fix} \qquad (34)$$

i.   Costs due to downtime (C_{down})
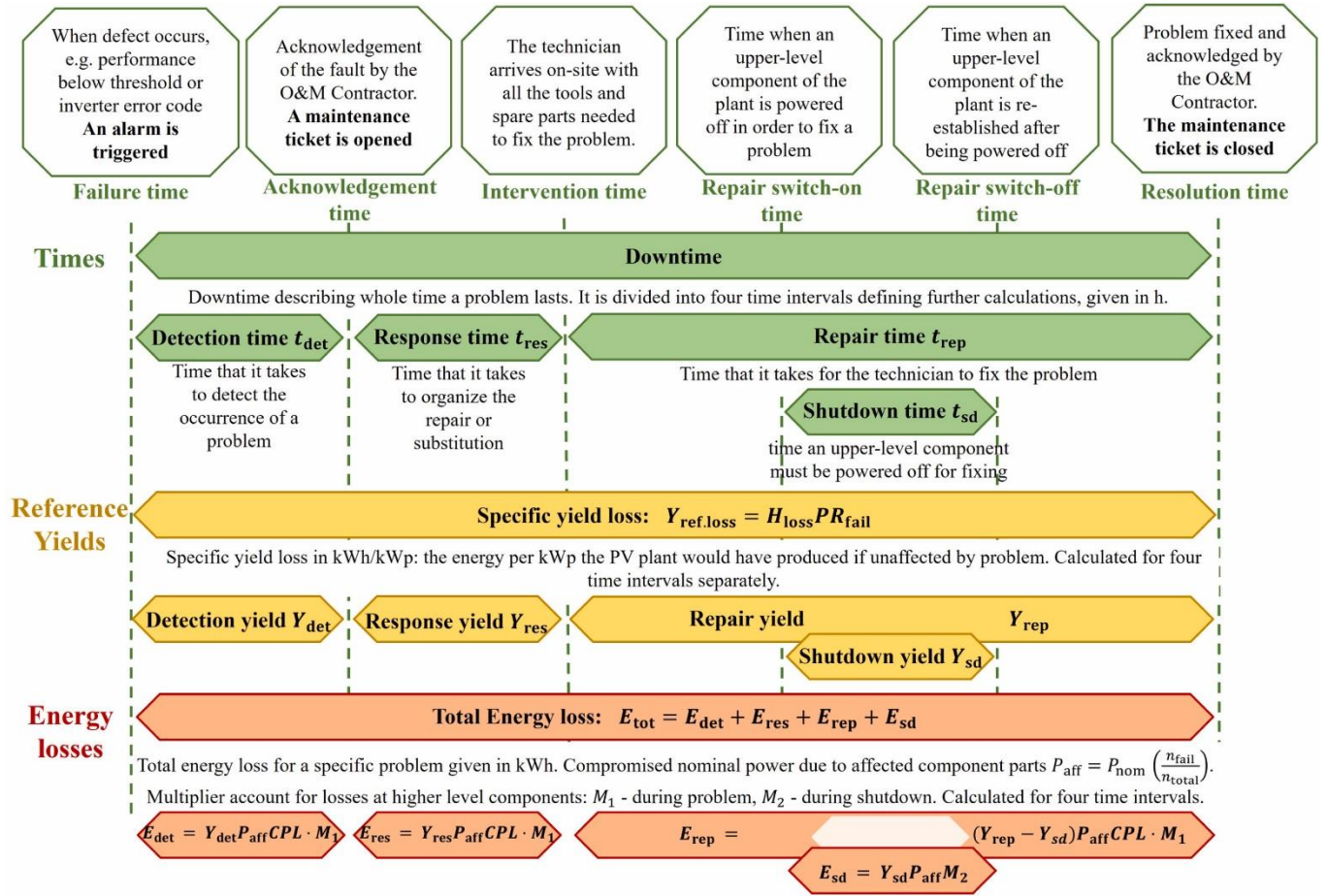
Figure 29. Figure 1: Costs due to downtime computations into four-time intervals with definitions. Times are given in hours, yields in kWh/kWp and energy losses in kWh *[217]*.

The computation is carried out for each specific defect found in the period analysed. The method is shown in Figure 29. For each time interval, the specific yield loss ($y_{ref.loss}$) is examined, which is the energy per kWp that the plant would have generated if unaffected by the defect [217].

$$y_{ref.loss} = H_{loss}.PR_{fail} \qquad (35)$$

H_{loss} is the irradiation incident on the PV plant and PR_{fail} is the performance ratio during the defect. The next step is to compute the energy loss which is normalised by the total number of components affected by a specific defect (n_{fail}) [217]. It is calculated separately for the four

intervals of interest (see Figure 29) and their sum results in the final total energy loss for a specific defect event given in kWh [217]:

$$E_{tot} = E_{det} + E_{res} + E_{rep} + E_{sd} \qquad (36)$$

where:

E_{tot} is the final total energy loss (kWh).

E_{det} is the detection energy (kWh).

E_{res} is the response energy (kWh).

E_{rep} is the repair energy (kWh).

E_{sd} is the shutdown energy (kWh).

Hence, the energy losses for repair and shutdown are considered separately and the possible yield during a shutdown (y_{sd}) is subtracted from the one during repair (y_{rep}). Thus, C_{down} is calculated as [217]:

$$C_{down} = \frac{(E_{tot}.MI)}{P_{norm}} \qquad (37)$$

where MI is the missing income.

Thus, for the calculation of the costs due to downtime, it is significant to consider the MI related to the sale of the electricity in units of €/kWh, for the example given by the feed-in tariff (FIT).

ii.   Costs due to repair/substitution (C_{fix})

Here the first step is to compute the cost of labour due to each specific defect using the repair time (t_{rep}) (in years), the number of technicians deployed, N_{ST} and the internal cost per hour per technician, C_{ST} [217]:

$$C_{lab} = t_{rep}N_{ST}.C_{ST} \qquad (38)$$

where C_{lab} is the labour cost (in €/kW$_p$).

C_{fix} is then computed based on arising costs in units of €/kW$_p$:

$$C_{fix} = \frac{(C_{det}+C_{rep}+C_{tran}+C_{lab})n_{fail}}{P_{norm}} \qquad (39)$$

The CPN technique is applied in three different cases of performance-reducing events in a PV plant such as Cell cracks of type C, short circuit bypass diode and potential induced degradation (PID) detected through electroluminescence inspection with inspection costs of $C_{det} = 1$€/kWp [217].

The CPN value is computed for downtime of one year, the analysis estimates the fixing costs compared to downtime costs (C_{down}) for multiple years and varying feed-in tariffs (FITs) for all cases [217].

2.4 Seasonal Variations on PV Power Output

2.4.1 PV Array Setup

The solar irradiation received by a PV array varies as the position of the sun and shadows change throughout the year [218]. For the arrays examined, the movement of the sun is shown in Figure 30 (a-d) [219]. Hence, the use of sun path diagrams is a very important approach adopted in this research because it is a very useful tool in determining the time of the year, hours of the day and when shading will take place at a particular site [220].

a.

b.

c.

d.
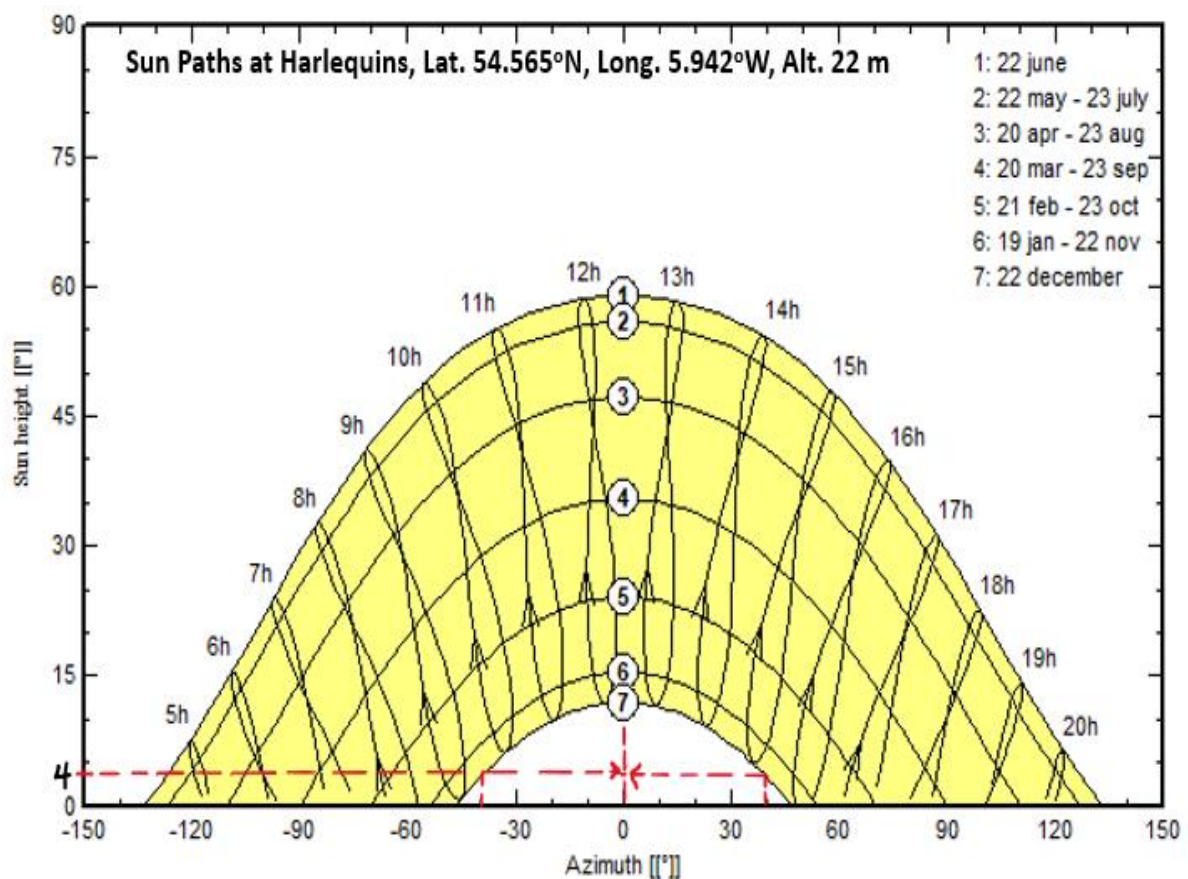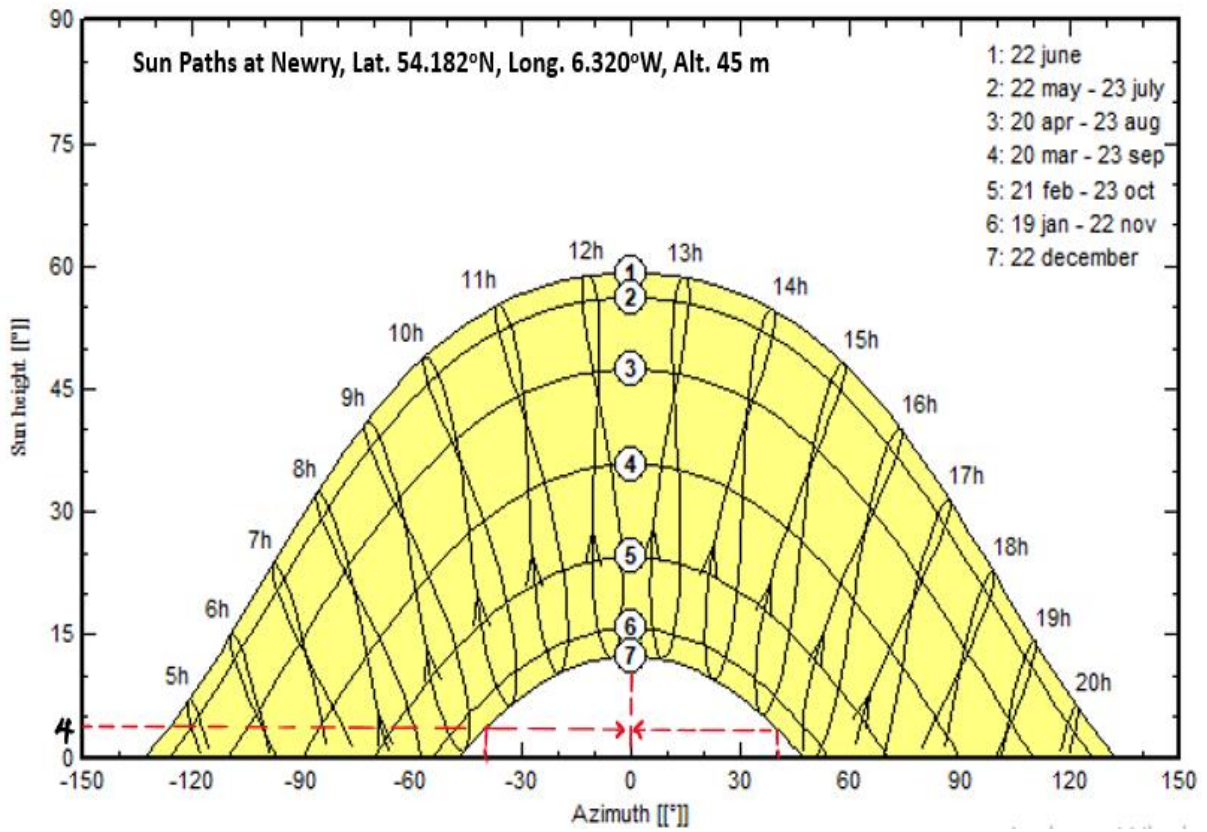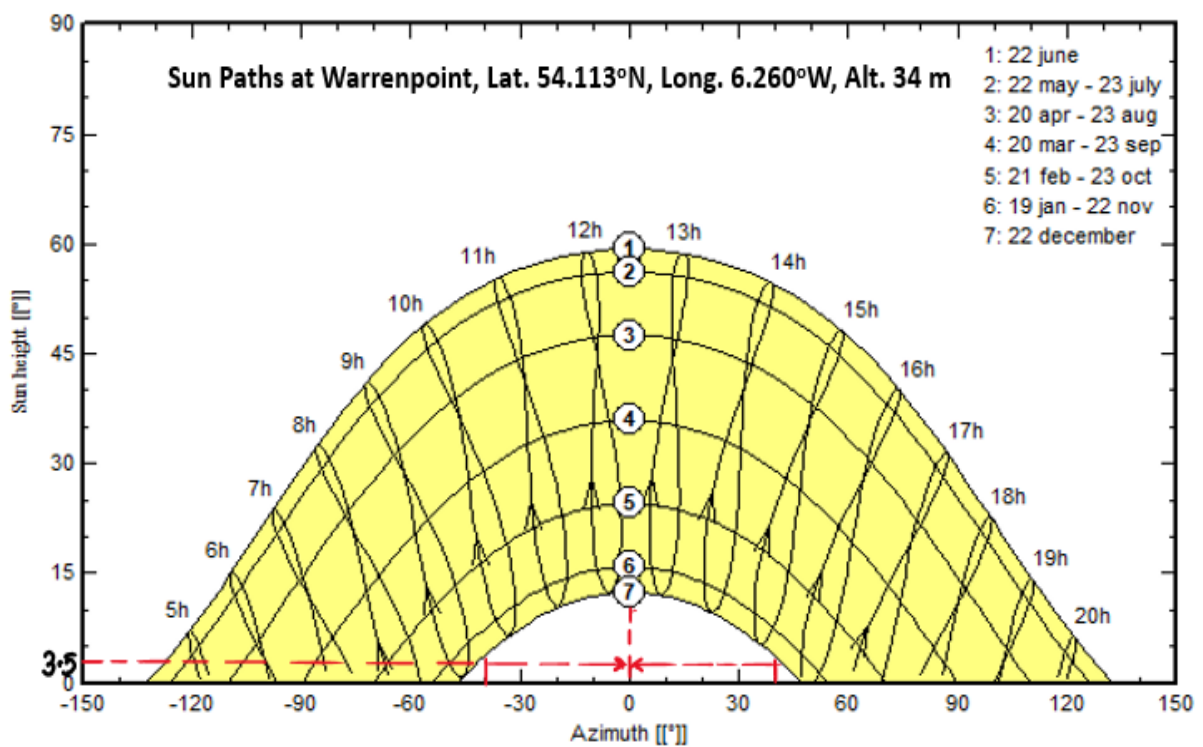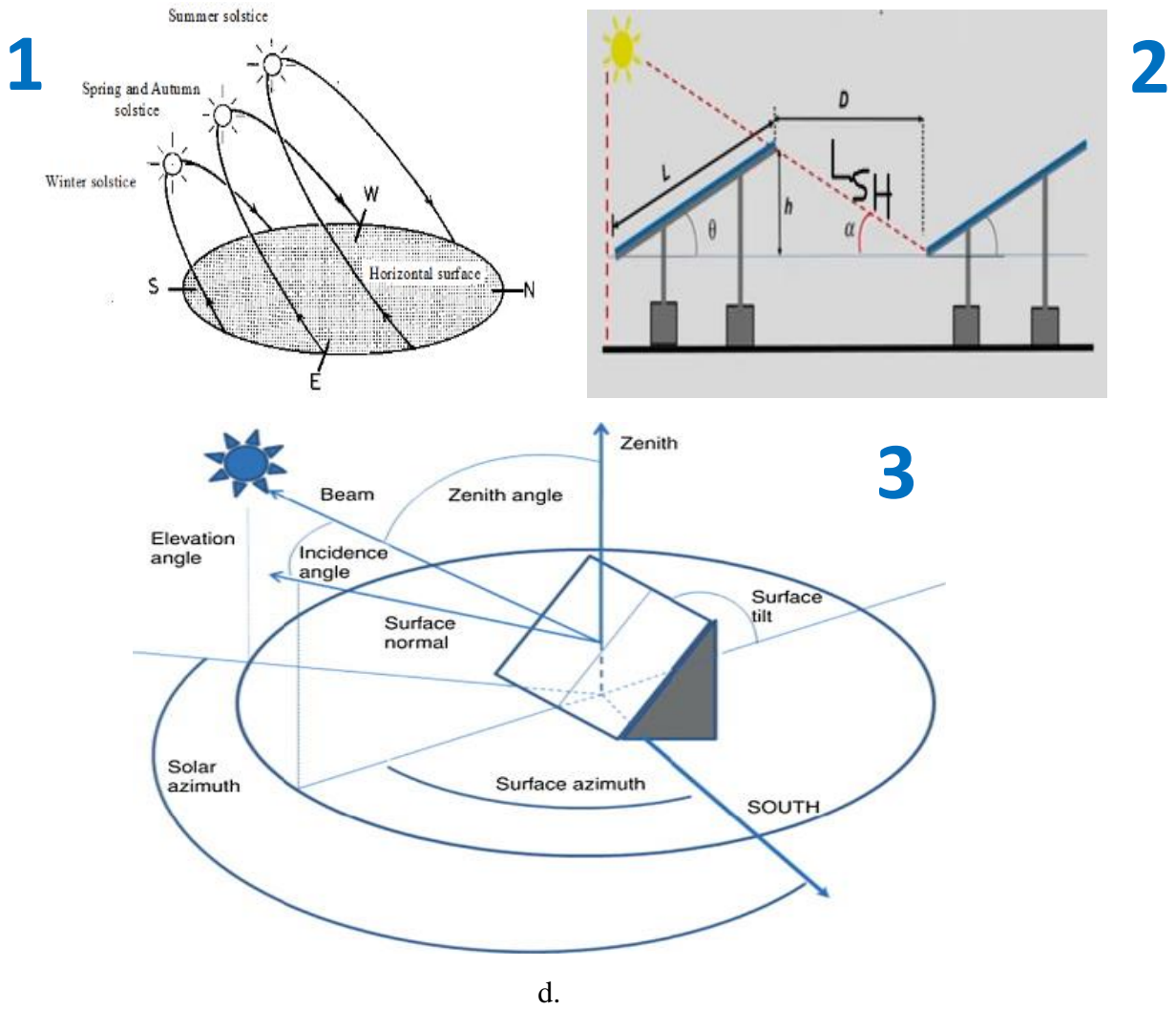
Figure 30 (a-d). Sun path diagrams for the examined arrays *[219], [220]*

The minimum distance is shown in Figure 30 (d) (as labelled in **2**) between two rows of solar

PV modules (i.e., the inter-row distance/spacing) that avoid mutual shading is calculated;

$$L_{SH} = \frac{h \times Cos\ \theta z}{Tan[Sin^{-1}(0.648Cos\emptyset - 0.399Sin\emptyset]} \qquad (40)$$

where $d = L_{SH} \times Cos\ \alpha$ (41)

where:

L_{SH} is the shadow length (mm)

d is the inter-row spacing (mm)

L_{SH} varies from month to month as the angle between the Earth's surface and the incident angle of direct solar radiation varies during the day.

Shadow length is determined by the position of the sun in the sky. Tables 25 – 27 show that the L_{SH} grows in direct proportion to the daylength, so the shorter the daylength, the shorter the shadow length, and vice versa.

2.5 Confirmation of no inter-row module shading

The analysis of the data from the three PV arrays assumes there was no inter-row shading of modules. To check if this was a valid assumption the minimum inter-row spacing to avoid shading of one module row by another was compared with the actual inter-row spacing for all three installations examined.

To calculate the minimum module row spacing across the Harlequins, Newry and Warrenpoint systems, sun path diagrams as shown in Figure 30 were used to find the solar elevation angle (α) and azimuth correction angle (θ_z). The actual values of minimum module inter-row spacing in the three arrays were computed from;

Height, h = Sin (tilt angle) × module width (42)

Shadow length, L_{SH} or Module row spacing $= \frac{h}{Tan\ α}$ (43)

Minimum inter-row spacing, $d_{min} = L_{SH} \times Cos\ \theta_z$ (44)

Height, h is measured in mm.

Table 25. Shading Analysis, Inter-row spacing (d) and Day Length of the ESB Harlequins

site location from 2017 to 2021

Month	Operation days	No. of days, N	δ (°)	α (°)	Cos θz	L_{SH} (mm)	Cos α	d = L_{SH}Cos α (mm)	W_{sr} (°)	DayLength (hrs)
January	31	31	-18.05	17.38	0.3	129	0.95	122.55	63.14	8
February	28	59	-8.67	26.76	0.45	194	0.89	172.66	77.59	10
March	31	90	3.22	38.65	0.63	272	0.78	212.16	95.12	13
April	30	120	14.27	49.7	0.77	332	0.64	212.48	111.51	15
May	31	151	21.77	57.2	0.84	362	0.54	195.48	124.5	17
June	30s	181	23.31	58.74	0.85	367	0.52	190.84	127.11	17
July	31	212	18.55	53.98	0.81	349	0.59	205.91	117.54	16
August	31	243	8.67	44.1	0.69	298	0.72	214.56	101.57	14
September	30	273	-3.22	32.21	0.52	224	0.85	190.4	84.6	11
October	31	304	-14.58	20.85	0.35	151	0.94	141.94	67.73	9
November	30	334	-21.8	13.63	0.23	99	0.97	96.03	55.36	7
December	31	365	-23.2	12.23	0.21	91	0.98	89.18	53.1	7
Average								**170.3491667**		**12**

Table 26. Shading Analysis, Inter-row spacing (d) and Day Length of the ESB Newry site location from 2017 – 2021

Month	Operation days	No. of days, N	δ (°)	α (°)	Cos θz	L_{SH} (mm)	Cos α	ds = L_{SH} Cos α (mm)	w_{sr} (°)	DayLength (hrs)
January	31	31	-18.05	17.77	0.31	249	0.95	236.55	63.16	8
February	28	59	-8.67	27.15	0.46	370	0.89	329.3	77.8	10
March	31	90	3.22	39.04	0.63	506	0.78	394.68	94.47	13
April	30	120	14.27	50.09	0.77	619	0.64	396.16	110.63	15
May	31	151	21.77	57.59	0.84	675	0.54	364.5	124	17
June	30	181	23.31	59.13	0.86	691	0.51	352.41	127	17
July	31	212	18.55	54.37	0.81	651	0.58	377.58	117.71	16
August	31	243	8.67	44.49	0.7	563	0.71	399.73	102	14
September	30	273	-3.22	32.6	0.54	434	0.84	364.56	85.53	11
October	31	304	-14.58	21.24	0.36	289	0.93	268.77	68.88	9
November	30	334	-21.8	14.02	0.24	193	0.97	187.21	56.35	8
December	31	365	-23.2	12.62	0.22	177	0.98	173.46	53.57	7
Average								**320.4091667**		**12**

Table 27. Shading Analysis, Inter-row spacing (d) and Day Length of the ESB Warrenpoint site location from 2017 – 2021

Month	Operation days	No. of days, N	δ (°)	α (°)	Cos θz	L_{SH} (mm)	Cos α	d = L_{SH} Cos α (mm)	w_{sr} (°)	DayLength (hrs)
January	31	31	-17.82	18.07	0.31	176	0.95	167.2	63.63	8
February	28	59	-8.69	27.2	0.46	261	0.89	232.29	77.81	10
March	31	90	3.63	39.52	0.64	363	0.77	279.51	95.03	13
April	30	120	14.62	50.51	0.77	436	0.64	279.04	111.13	15
May	31	151	21.95	57.84	0.85	482	0.53	255.46	123.84	17
June	30	181	23.23	59.12	0.86	487	0.51	248.37	126.38	17
July	31	212	18.21	54.1	0.81	459	0.59	270.81	117.04	16
August	31	243	8.12	44.01	0.69	391	0.72	281.52	101.37	14
September	30	273	-3.83	32.06	0.53	300	0.85	255	84.69	11
October	31	304	-15.09	20.8	0.36	204	0.93	189.72	68.12	9
November	30	334	-22.02	13.87	0.24	136	0.97	131.92	56.02	7
December	31	365	-23.14	12.75	0.22	125	0.98	122.5	53.8	7
Average								**226.1116667**		**12**

For the worst-case scenario of the winter solstice, azimuth correction and solar elevation angles in Harlequins, Newry and Warrenpoint arrays from 9 am to 3 pm shown in Figure 30 are summarised in Table 28.

Table 28. Actual shading analysis of Harlequins, Newry and Warrenpoint arrays

		Calculated				Theoretical minimum spacing (mm)
		Solar elevation angle (α) (°)	Azimuth correction angle (θz) (°)s	Shadow length, L_{SH} (mm)	Actual m inter-row spacing, d_{min} (mm)	
Location	Harlequins	4	40	315	241	170
	Newry	4	41	644	486	320
	Warrenpoint	3.5	41	556	420	226

The actual inter-row spacing for no shade in Harlequins, Newry and Warrenpoint arrays is greater than their theoretical minimum spacing. This means there is no shading of one row of modules by another.

CHAPTER 3

PV ARRAY PERFORMANCE MEASUREMENT AND ANALYSIS

3.1 Site Location and Climate Description

The PV arrays examined in this study were located at Harlequins, Deramore Road, Belfast (5.94°W longitude and 54.57°N latitude), Rampart Road, Newry (6.32°W longitude and 54.18°N latitude) and Upper Dromore Road, Warrenpoint (6.26°W longitude and 54.11°N latitude), Northern Ireland. The specifications of the PV arrays studied are summarised in Table 25.

The start dates of the operation of the Harlequins, Newry and Warrenpoint arrays were 16 September 2015, 24 September 2015, and 28 September 2015 respectively followed by connection on 17 February 2016, 04 December 2015, and 22 February 2016. Across the three sites, data used in this study started from January 01, 2017, to December 31, 2021.

Figure 31 shows the average in-plane solar irradiations and average ambient temperature at these locations.
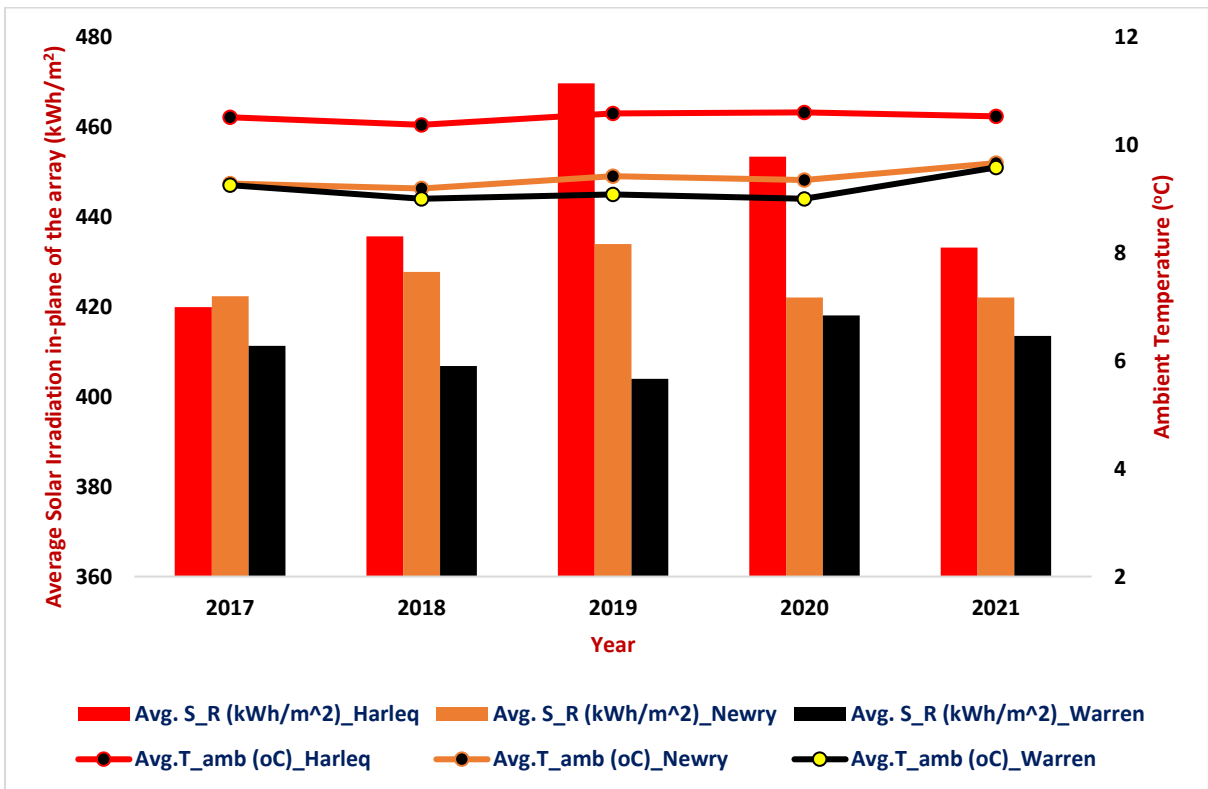
Figure 31. Site location of the examined three PV installations in Northern Ireland including the average in-plane solar irradiations (S_R) and average ambient temperatures (T_{amb}) for the past five years

Table 29.PV System Descriptions

	PV Array Location		
	Harlequins	**Newry**	**Warrenpoint**
Tilt and Azimuth Angles	Azimuth: -162º, Tilt: 12º for PV array 1	Azimuth: -31º, Tilt: 6º for PV array 1	Azimuth: -125º, Tilt: 7º for PV array 1
	Azimuth: 12º, Tilt: 12º for PV array 2	Azimuth: 149º, Tilt: 6º for PV array 2	Azimuth: 55º, Tilt: 7º for PV array 2
Total PV Area	312.36 m^2	311.04 m^2	268.8 m^2
Solar Cell Technology	Polycrystalline silicon (p-Si)	Polycrystalline silicon (p-Si)	Polycrystalline silicon (p-Si)
PV Module Manufacturer	Renesola	Renesola	Renesola
Module Rating	260 W_p at STC	260 W_p at STC	260 W_p at STC
Number of Modules	192	192	192
Installation Type	Rooftop	Rooftop	Rooftop
PV Capacity	49.92 kW$_p$ at STC	49.92 kW$_p$ at STC	49.92 kW$_p$ at STC
Module type (s)	Renesola-JC260M-24/Bbv (260 W)	Renesola-JC260M-24/Bbv (260 W)	Renesola-JC260M-24/Bbv (260 W)
Inverter	Sunny TriPower	Sunny TriPower	Sunny TriPower
Inverter Capacity [AC]	2×20 kW	2×20 kW	2×20 kW

The PV arrays at Harlequins, Newry and Warrenpoint are all installed as fixed-tilt PV as shown in Figure 33 and Figures 34-36. The azimuth and tilt angles of the PV arrays are shown in Figure 32.
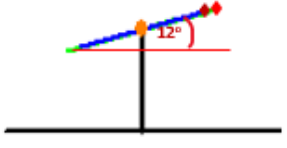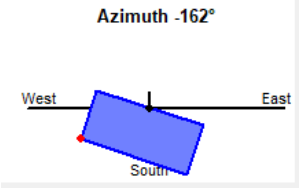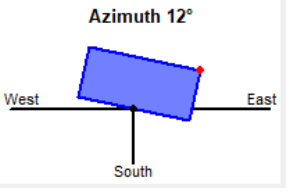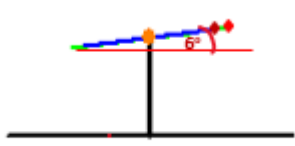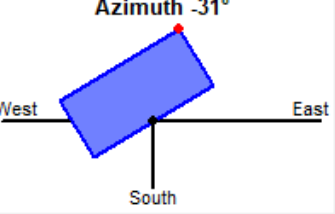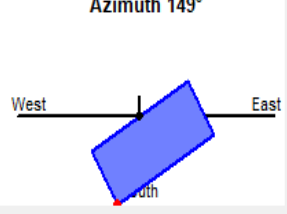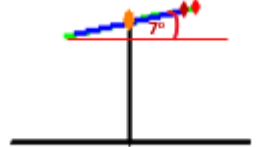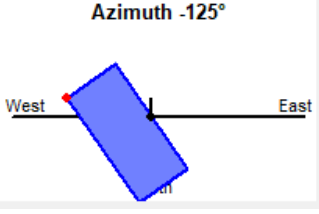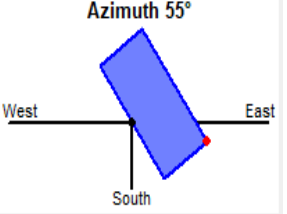
| Tilt | Azimuth | |
	Array 1	Array 2
Harlequins	Azimuth -162°	Azimuth 12°
Newry	Azimuth -31°	Azimuth 149°
Warrenpoint	Azimuth -125°	Azimuth 55°

Figure 32. Tilts and azimuths of Harlequins, Newry and Warrenpoint PV Arrays
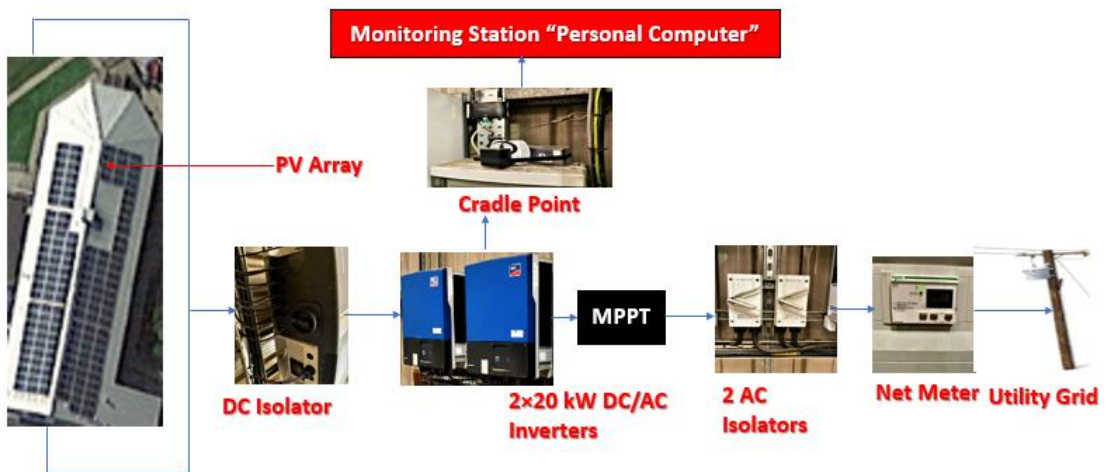
Figure 33. Fixed tilt PV for Harlequins, Newry and Warrenpoint Arrays.

Figure 34. Examined PV arrays installed at Harlequins

Figure 35. Examined PV arrays installed at Newry

Figure 36. Examined PV arrays installed at Warrenpoint

Table 30. Panel Parameters as provided by the Manufacturer

	PV Array		
	Harlequins	**Newry**	**Warrenpoint**
Voltage at maximum power, V_{mp}	30.4 V	30.4 V	30.4 V
Area of a single module, A_{module}	1.63 m²	1.63 m²	1.63 m²
Current maximum power, I_{mp}	8.56 A	8.56 A	8.56 A
Open circuit voltage, V_{OC}	37.6 V	37.6 V	37.6 V
Short-circuit current, I_{SC}	9.09 A	9.09 A	9.09 A
Shunt or parallel resistance, R_{Shunt}	1000 Ω	1000 Ω	1000 Ω
Series resistance, R_{Series}	0.31 Ω	0.31 Ω	0.31 Ω
Derate	77%	77%	77%
Number of cells per module	60	60	60
Nominal operating cell temperature (NOCT)	45ºC	45ºC	45ºC
Temperature coefficient of I_{SC} (α)	0.04%/ºC	0.04%/ºC	0.04%/ºC
Temperature coefficient of power (γ)	-0.4%/ºC	-0.4%/ºC	-0.4%/ºC
Temperature coefficient of voltage	-0.113 v/ºC	-0.113 v/ºC	-0.113 v/ºC
Temperature coefficient of V_{OC} (β)	-0.3%/ºC	-0.3%/ºC	-0.3%/ºC
Maximum system voltage, V_{DC}	1000 V	1000 V	1000 V
Reference irradiance, G_{ref}	**1000 W/m²**		
Reference temperature, T_{ref}	**25ºC**		

Figure 33 shows the interrelationship between principle components. The DC isolator switch is an electrical safety device that manually disconnects the PV panels for maintenance, installations, or repair processes. This is connected in one PV string through the MPPT and to the inverter to ensure that disconnection can be achieved at the ground and roof level of the PV system.

An AC isolator disconnects the inverter from the grid for maintenance, repair, or installation.

A cradle point router sends data back via a 4G internet connection to an online portal where it is analysed remotely using a personal computer. Figures 34-36 show the examined PV arrays installed at Harlequins, Newry and Warrenpoint arrays.

3.2 System Monitoring and Method of Data Acquisition and Assessment

The parameters in Table 31 show the total installations in each location which were recorded at hourly intervals.

Table 31. Parameters measured

			Instrument	Accuracy
Measured parameters	**Ambient conditions**	In-plane solar irradiance	Pyranometers	$\pm$ 0.05 Wm^{-2}
		Ambient temperature	Thermocouple	$\pm$ 1°C
		Wind speed	Anemometer	$\pm$ 0.01 ms^{-1}
		Relative humidity	Hygrometer	$\pm$ 2%
		Air pressure	Barometer	$\pm$ 0.02 Hg
	System conditions	DC energy output	DC energy meter	$\pm$ 0.02 kWh
		DC power output	DC power meter	$\pm$ 0.02 kW
		AC energy output	AC energy meter	$\pm$ 0.02 kWh
		AC power output	AC power meter	$\pm$ 0.02 kW
		PV module temperature	Thermocouple	$\pm$ 1°C

Figure 37 illustrates how these measurements relate to the PV system energy conversion processes.
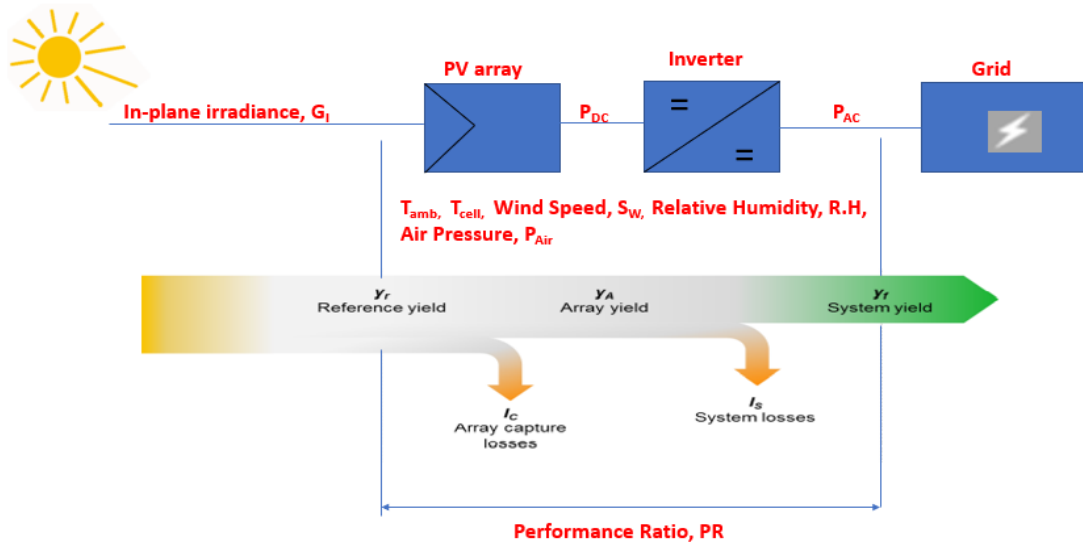
Figure 37. Measured location parameters in Photovoltaic Systems

Figure 38. provides an overview of the overall methodology for PV array performance analysis.
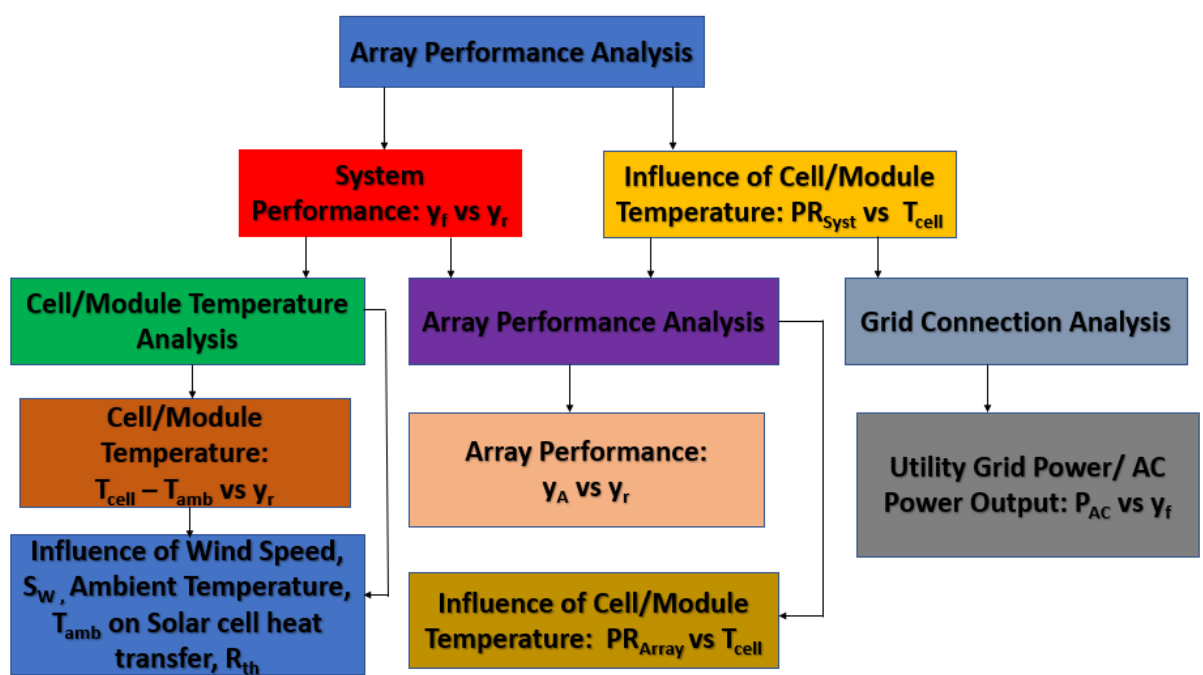
Figure 38. PV Array Performance Analysis Framework

3.3 System and Array Performance Ratios

Figure 39 shows that system yields, y_f are proportional to the reference yields, y_r, with the monthly average system performance ratios ($PR_{avg} = \frac{yf}{yr}$) of the Harlequins, Newry and Warrenpoint PV arrays are 92.6%, 89.7% and 91.2% respectively as determined by the slopes of each of their linear regression lines.
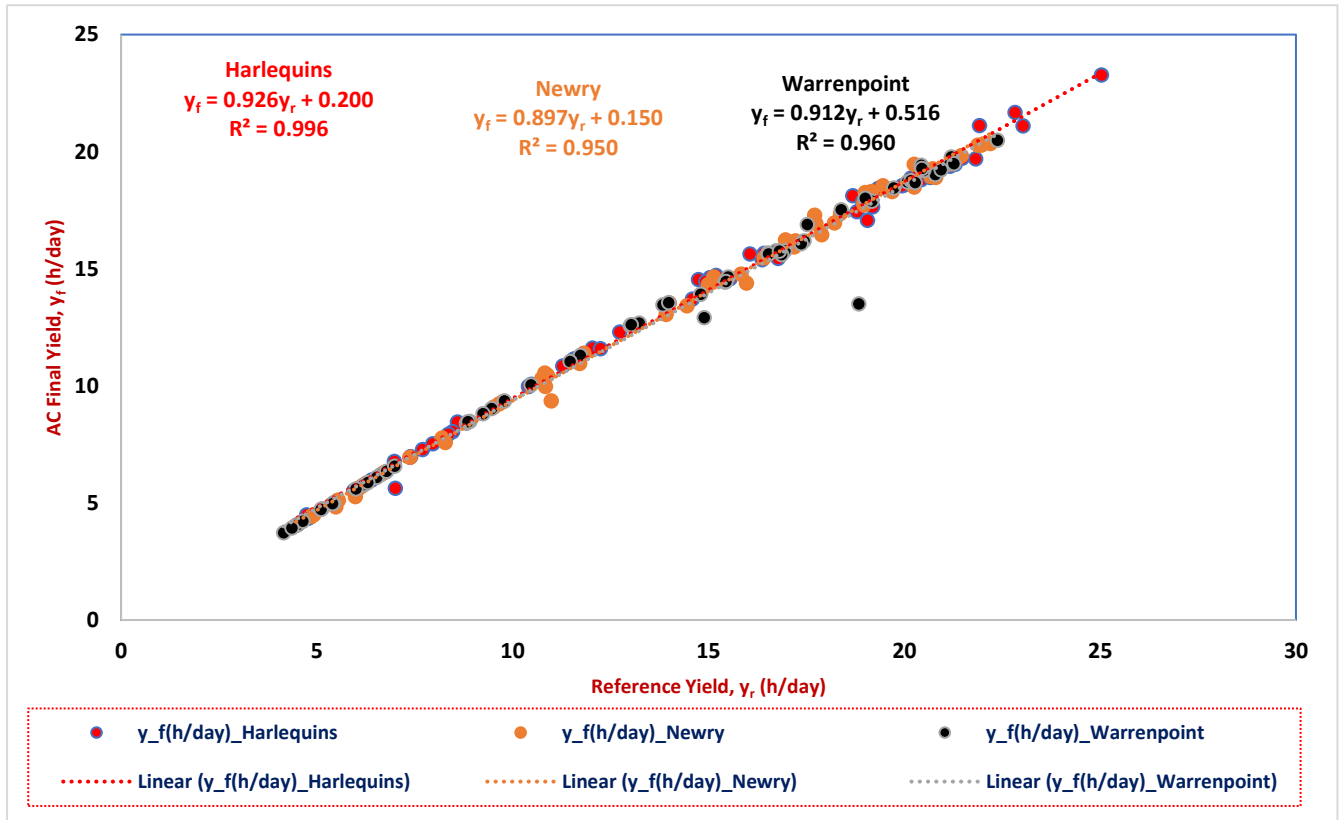
Figure 39. Monthly average system final yield (y_f) versus reference yield (y_r) from hourly data from Harlequins, Newry and Warrenpoint PV arrays from 2017 to 2021

From the plot of DC array yield, y_A versus reference yield, y_r shown in Figure 40, the average array performance ratios ($PR_{avg} = \frac{yA}{yr}$) found from the slope of the regression lines of the Harlequins, Newry and Warrenpoint PV arrays are 94.4%, 91.3% and 93.0% respectively.
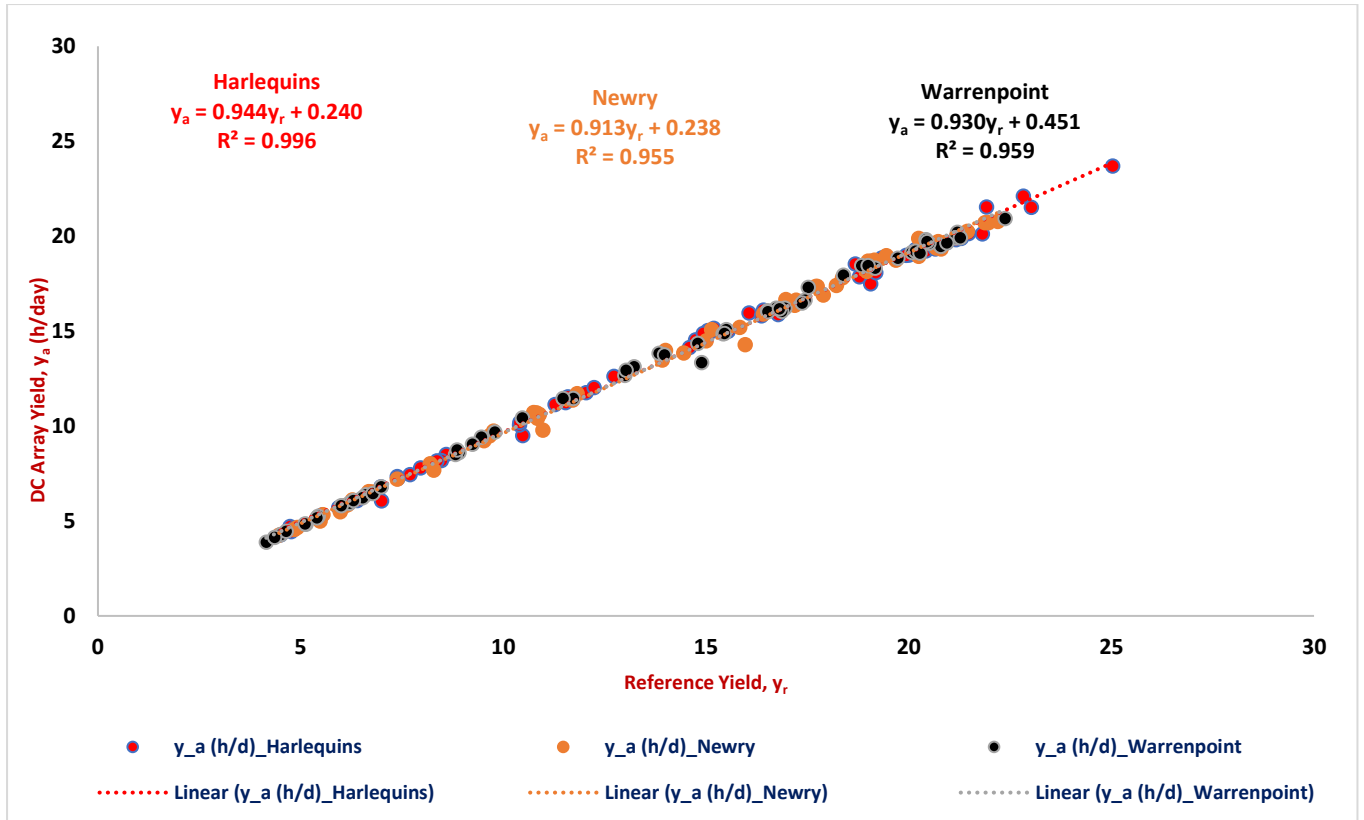
Figure 40. Monthly average DC array yield (y_A) versus reference yield (y_r) from hourly data from Harlequins, Newry and Warrenpoint PV arrays from 2017 to 2021

3.4 Effect of Module Temperature on PV Performance

It can be seen in Figures 41 and 42 that the system and array performance ratios, PR_{Syst} and PR_{Array} across the three arrays decrease as the solar cell temperature decreases due to the amount of solar irradiance received by the PV systems and arrays. For instance, at low solar cell temperatures (ranging from 12°C to 22°C), the PR_{Syst} and PR_{Array} decrease because of low solar irradiance received by the PV systems and arrays which is caused by thermal variations resulting in fluctuations in the ambient temperature of the sites and PR_{Syst} and PR_{array} increase as the solar cell temperature increases (ranging from 30.85°C to 35.69°C) as a result of the PV systems and arrays receiving more solar irradiance (which may be within the range of 400 Wm^{-2} to 500 Wm^{-2}). At above 35.69°C, the PR_{Syst} and PR_{Array} tend to decrease as a result of the generation of more solar irradiance (which may be above 500 Wm^{-2}) as seen in Figures 41 –

42. The slopes of Figure 41 show the effect of PV temperature on the system performance ratio. Figure 42 shows an increase in the PV temperature coefficient of power decreases array performance ratio but in a less consistent manner than the decrease in system performance ratio. In this case, the PV temperature coefficient of power has less effect on array performance ratio when compared to system performance ratio.
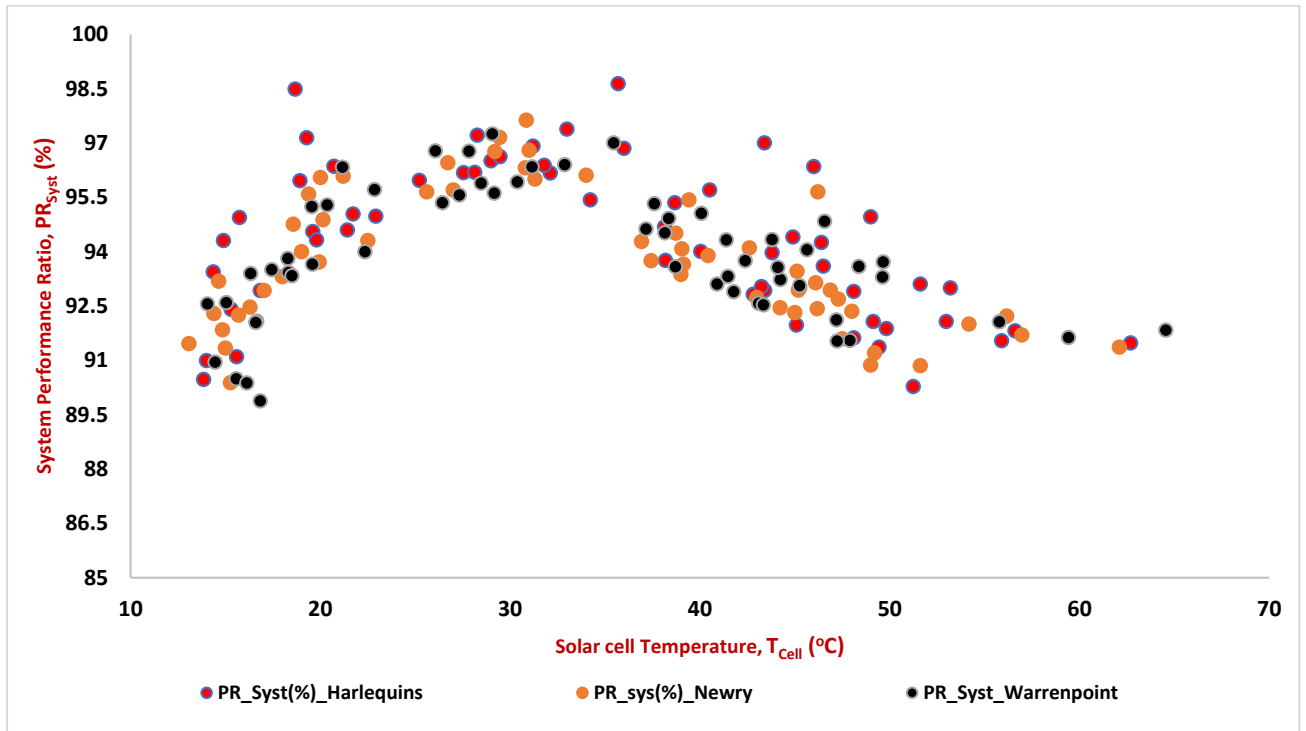
Figure 41.Monthly average System Performance Ratio (PR_{Syst}) versus PV Temperature (T_{Cell}) from hourly data from Harlequins, Newry and Warrenpoint PV arrays from 2017 to 2021
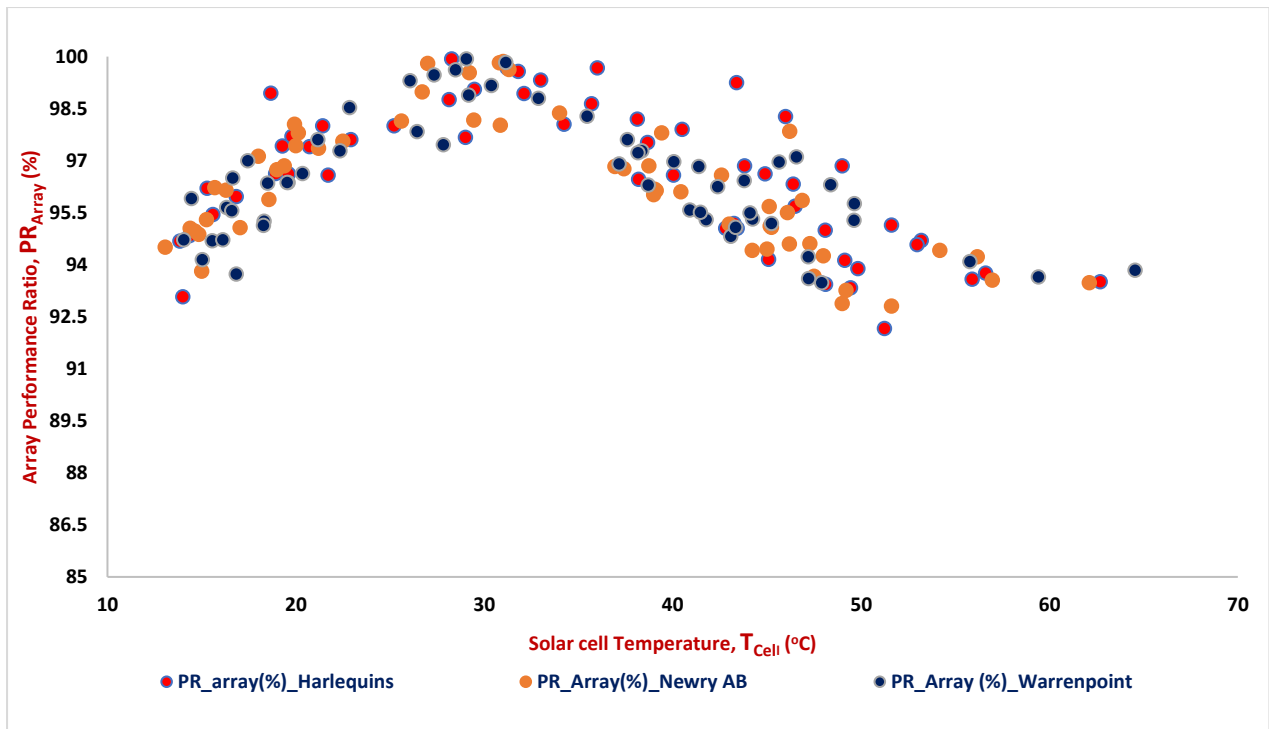
Figure 42. Monthly average Array Performance Ratio (PR_A) versus Solar cell Temperature (T_{Cell}) for hourly data from Harlequins, Newry and Warrenpoint PV arrays from 2017 to 2021

3.5 AC System Loss (L_S) and DC Array Capture Loss (L_C)

Figures 43 (a-c) show monthly average values for the Harlequins, Newry and Warrenpoint PV arrays. AC system losses (L_S) and DC array capture losses (L_C) are due to P_{AC} and P_{DC} as shown in Figure 37. Ls cause the physical dissipation of power in the inverter while L_C causes the dissipation of power in the PV array. Minimum and maximum system losses and capture losses are summarised in Table 32. Increases in Ls and Lc are due to higher PV temperatures [221].

The importance of finding the L_S and L_C in this study is to identify where more dissipation of power is recorded. For instance, more physical dissipation of power is observed in the inverters hence leading to more system losses, L_S while relatively less dissipation of power is noticed in the PV array which thus gave less array capture loss, L_C as shown in Figures 43 (a-c).

Table 32. Maximum and Minimum System and Capture Losses in Harlequins, Newry and

Warrenpoint PV arrays monitored over five years

	Location	Minimum L_S (hour/day)	Maximum L_S (hour/day)	Minimum L_C (hour/day)	Maximum L_C (hour/day)
PV array	Harlequins	0.02 in November 2017, 0.06 in September 2018, 0.1 in December 2019, 0.12 in February 2020 and 0.09 in January 2021	0.58 in October 2017s, 0.43 in August 2018, June 2019, September 2020, May and October 2021	0.04 in December 2017, 0.01 in March 2018, 0.05 in January 2019 and March 2020, and March 2021	1.28 in June 2017, 1.71 in July 2018, 1.57 in September 2019, 1.51 in May 2020 and 1.36 in May 2021
	Newry	0.12 in December 2017, 0.09 in November 2018, 0.07 in March 2019, 0.12 in February 2020 and 0.11 in March 2021	0.43 from March to May 2017, April to May, August 2018, May to July, October 2019, August 2020 and June to August 2021	0.02 in March and October 2017, 0.13 in February 2018, 0.18 in November 2019, 0.07 in March 2020, and 0.04 in October 2021	1.48 in June 2017, 0.56 in April 2018, 1.31 in July 2019, 1.2 in May 2020 and 1.69 in March 2021
	Warrenpoint	0.12 in February 2017, 0.09 in March 2018, 0.08 in January 2019, 0.09 in January 2020, 0.18 in March 2021	0.43 from June to July 2017, May and July 2018, 0.50 in July 2019, 0.43 from March, May and July 2020, 0.43 from April to June and September 2021	0.05 in October 2017, 0.11 in October 2018, 0.01 in March 2019, 0.09 in October 2020 and 0.02 in October 2021	1.55 in March 2017, 1.17 in July 2018, 0.89 in June 2019, 1.00 in June 2020, and 1.35 in June 2021
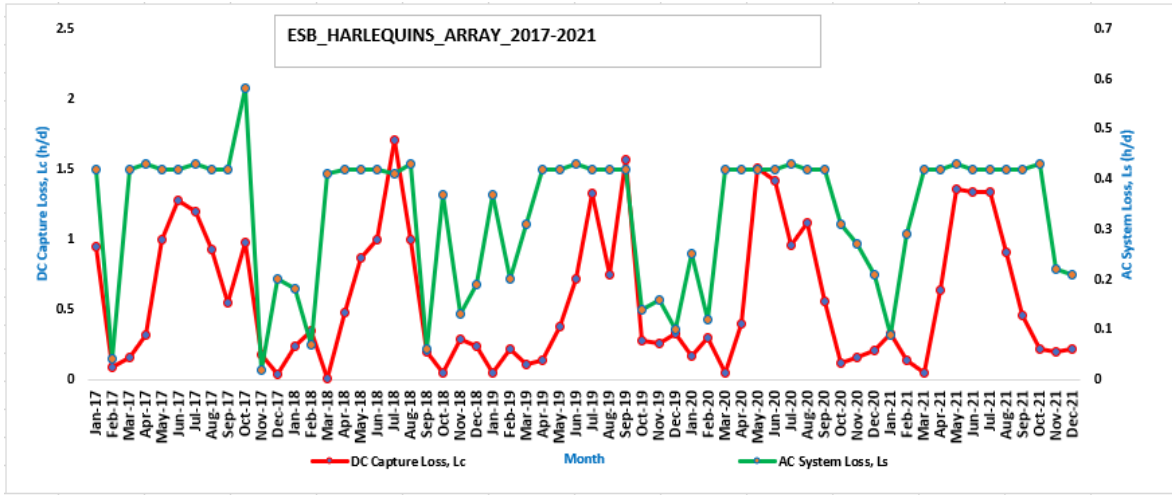
a.
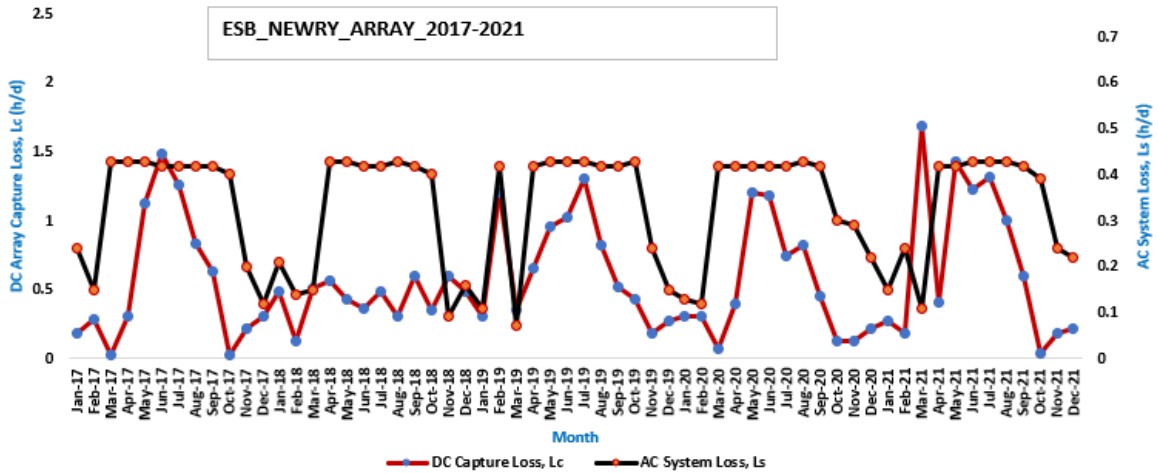
b.
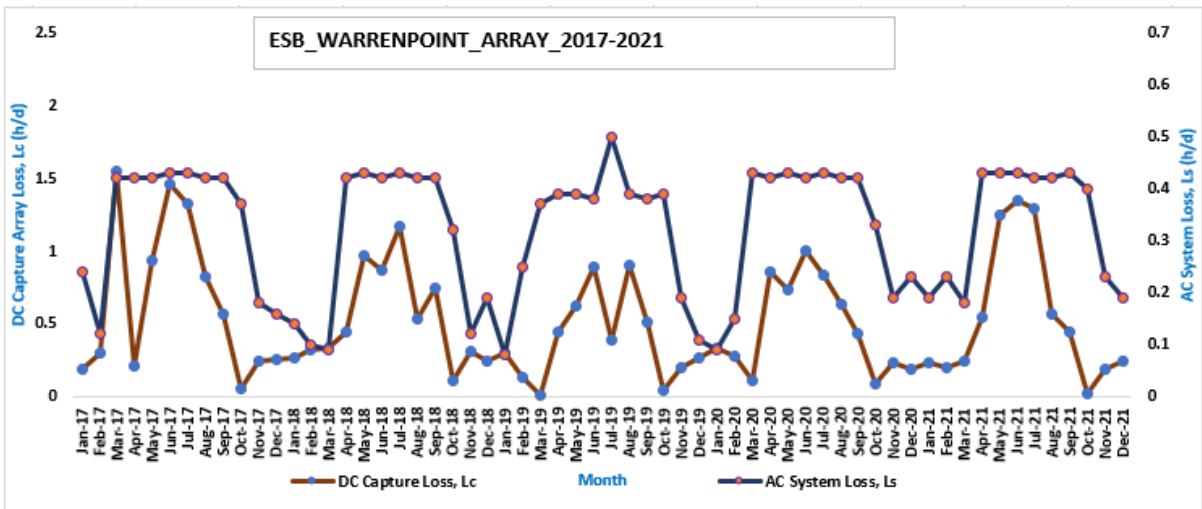
c.

Figures 43 (a-c). Variation of DC capture and AC system energy losses for the three PV arrays from 2017 to 2021

3.6 An Examination of Thermal Resistance for a PV Module

The power output of a PV module depends on the solar irradiation absorbed, and converted by the solar panels [222]. The power output also depends on the module temperature. For instance, an increase in module temperature decreases the power output. An examination of thermal resistance for a PV module is a very significant part of this study. This is because solar irradiance is only partially converted into electricity as one part of the module reaching solar irradiance is reflected from the module's surface and the remaining part continues its way through the front layers of the module until it reaches the active semiconductor layer [222]. If the module is transparent, the transmitted part of the solar irradiation is also present. In this case, reflective losses amounting to 10% of the incoming solar irradiance are noticed to be perpendicular incidence, hence PV temperature is a consequence of the heat balance shown in Figure 44 (a-c) [222], [223]. This means that only one part of the absorbed solar irradiation is converted to electricity, while the rest is converted into heat [222]. Hence, the processes and parameters that determine the heat balance and module temperature are modules reaching irradiance, optical properties of the PV module, PV conversion efficiency, balance of heat flows and electrical characteristics of the load (see Figure 44 (a)) [222].
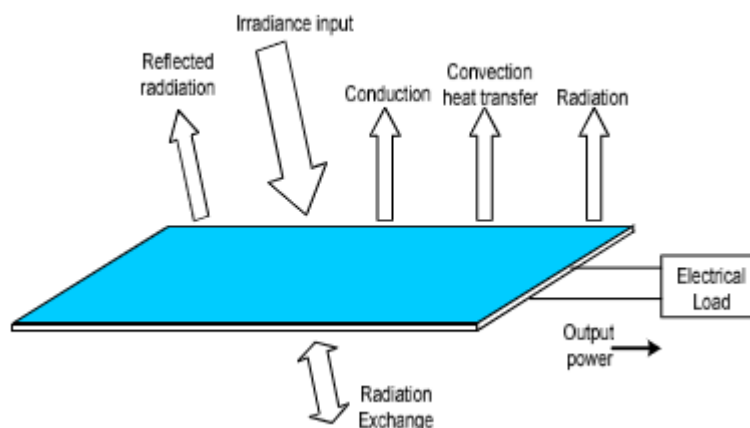
Figure 44 (a). Heat balance of PV System *[222]*
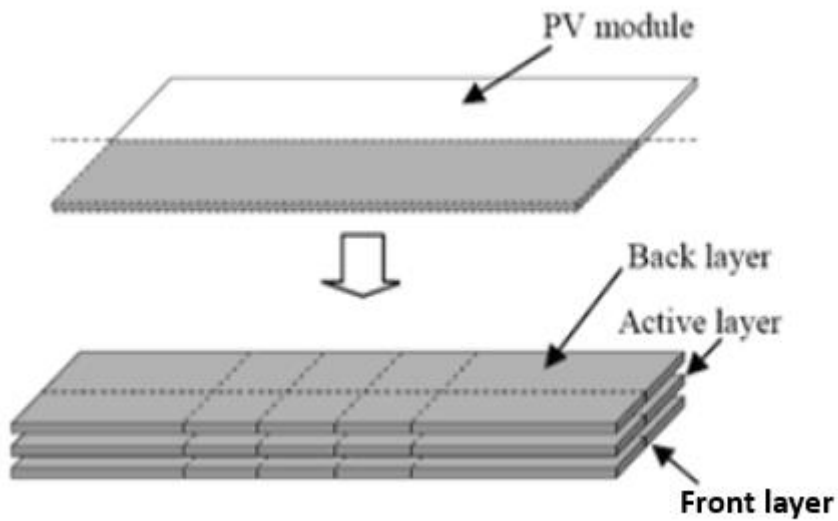
Figure 44 (b). Analysed system of the heat balance of PV System *[222]*
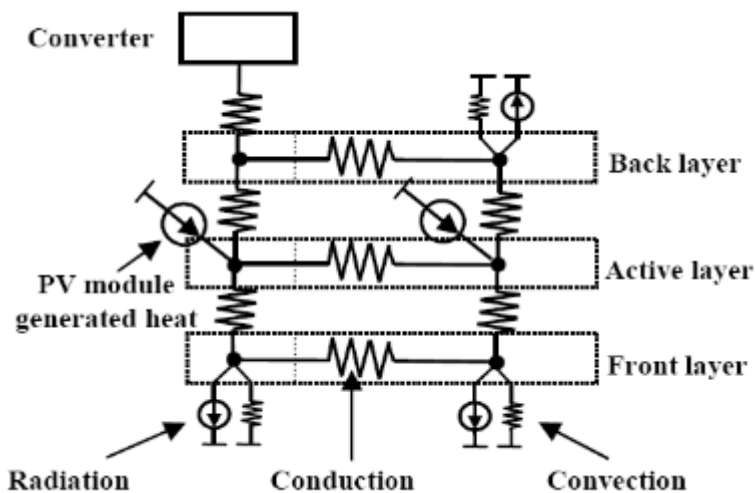
Figure 44 (c). PV module thermal resistor network *[222]*

The absorbed solar irradiance which is not converted into electricity generates heat flow. Thus, the PV module exchanges the heat flow within its environment through conduction, convection and radiation (see Figure 44 (a)) [222]. Finding a single part of the heat flow could be difficult since they depend on the environmental conditions and the way the module is mounted [222]. To prevent the heat flow from the module to the ambient, a converter is used even though it also adds additional heat to the module which changes its temperature distribution, thus,

creating a hotspot on the module surface. The conduction process of the heat flow takes place in the module between the components with different temperatures and also between the module and the converter. The heat generated in the module active layer is conducted through the front and back layers of the module surface (see Figure 44 (b)) [222]. The convection process of the heat flow takes place on the module and converter surface whenever its temperature is higher than the ambient temperature [222].

Hence, the natural convection equation for the horizontal plate applied to the module and converter surfaces using the average surface temperatures is given by [222]:

$$h = C\left(\frac{T_S - T_A}{L}\right) \tag{45}$$

$$L = \frac{W_{mod} H_{mod}}{(W_{mod} + H_{mod})} \tag{46}$$

where

C is a constant value given as 1.32 for the PV module front surface facing upward or 0.59 for the PV module bottom surface facing downward.

h is the heat transfer coefficient which is the function of the surface temperature (^{o}C/mm).

T_S is the surface temperature (^{o}C).

T_A is the ambient temperature (^{o}C)

L is the characteristic length based on the module dimensions (mm).

W_{mod} is the module's width (mm).

H_{mod} is the module's height (mm).

The radiation process of the heat flow also takes place on the module and converter surface and it represents the heat exchange between the module and converter and their environment. The radiation heat flow (Q) on a chosen surface is given by [222]:

$$Q = \sigma A \varepsilon_s \varphi_{sky}(T_s^4 - T_{sky}^4) + \sigma A \varepsilon_s \varphi_{gr}(T_s^4 - T_{gr}^4) \tag{47}$$

where

σ is Stefan-Boltzmann constant (JK^{-1}).

ε is the emissivity of the surface ($Jm^{-2}s^{-1}$).

T_{sky} is the sky temperature (^{o}C).

T_{gr} is the ground temperature (^{o}C).

A is the area of the surface (mm^2).

φ_{sky} and φ_{gr} are called sky and ground view factors which depend on module orientation.

The equivalent thermal resistance, R_{th} ($^{o}CW^{-1}$) is given by;

$$R_{th} = \frac{T_{cell} - T_{amb}}{P_{DC}} \tag{48}$$
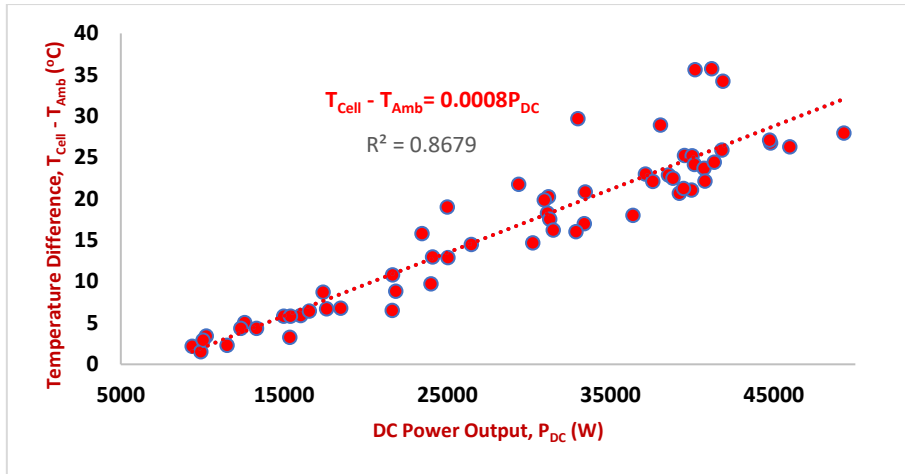
a. Harlequins
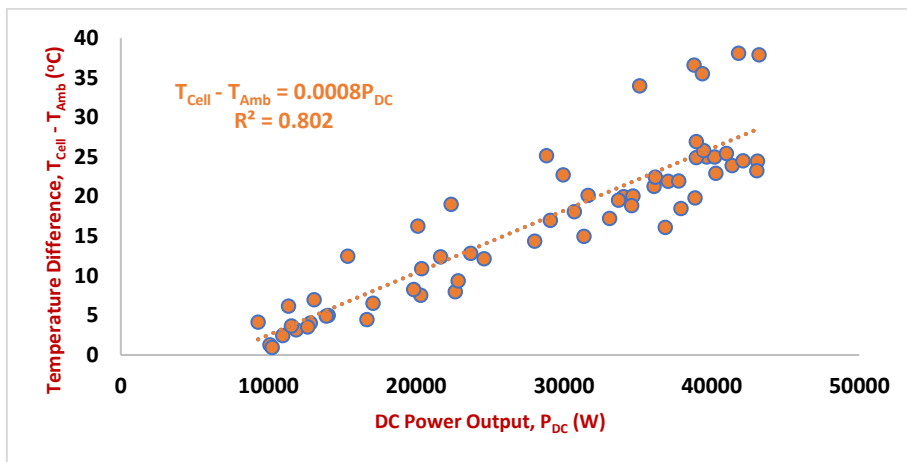
b. Newry
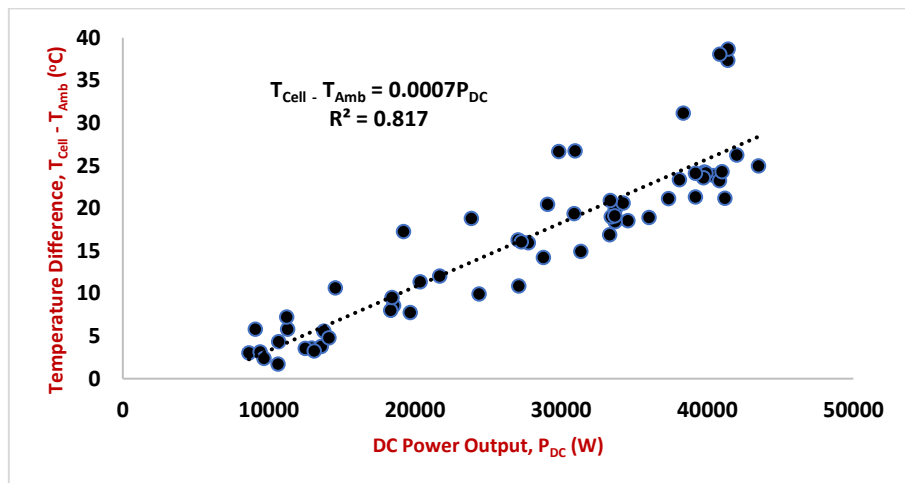
c. Warrenpoint

Figure 45 (a-c). Temperature difference ($T_{cell} - T_{amb}$) versus DC power output (P_{DC}) for

hourly over five periods collected data from PV arrays at Harlequins, Newry and

Warrenpoint locations from 2017-2021

Figures 45 (a-c) show dispersed scatter points. The R_{th} values in the three arrays are very low. As can be seen when they are compared in Figure 46 with values from arrays in Norway [222] and Sydney, Australia [224].

This is unlikely to be due to exceptional cooling but may be caused by detachment of the solar cell temperature sensor from the array's back surface [222]. There was no shading of the PV module on which the solar cell temperature sensor was located. When comparing the slopes of regression lines in Figures 45 (a-c) for the three arrays, the values are consistently close. This is because physically similar PV arrays should have similar R_{th} values [222]. Also, packing factor (PF) computations for the three arrays using equation (24) show similar results of unit value.

Plotting the temperature difference $T_{cell} - T_{amb}$ against DC power output, P_{DC} gives a regression that estimates R_{th}. Figures 45 (a-c) show the plot for the period of 2017 to 2021 for the PV arrays located at Harlequins, Newry and Warrenpoint.

Figures 45 (a-c) also show that as solar cell temperatures increase above ambient levels, DC power output also increases with an increase in solar irradiance. Hence, the temperature difference ($T_{Cell} - T_{amb}$) between the module and ambient shows that both conduction and convective losses are linear with an increase in incident solar irradiance for a given wind speed, provided that the equivalent thermal resistance (R_{th}) and the heat transfer coefficient (h) do not vary strongly with solar cell temperatures.
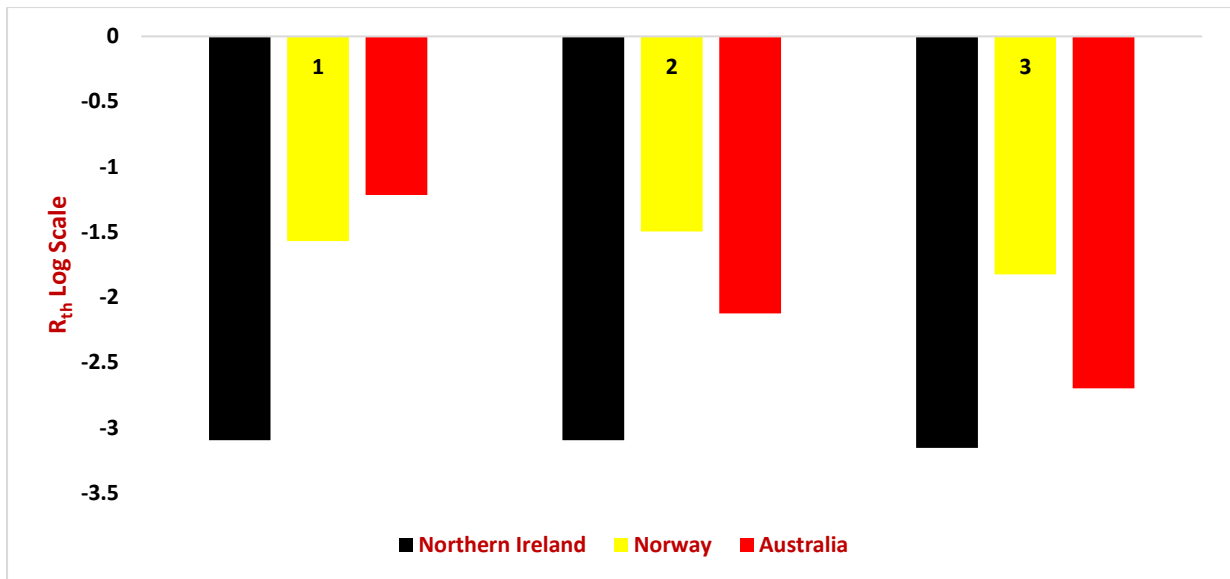
Figure 46. Log scale showing the thermal resistance comparisons of PV arrays installed in Northern Ireland, Norway and Australia.

Thermal equivalent resistance, R_{th} can be influenced by a high or low wind speed, S_W. Figures 47 (a-c) show poor coefficient of determination (R^2) values at Harlequins, Newry and Warrenpoint PV arrays implying no wind speed effect was found on equivalent thermal resistance, R_{th} (as expressed in equation 48) [222].
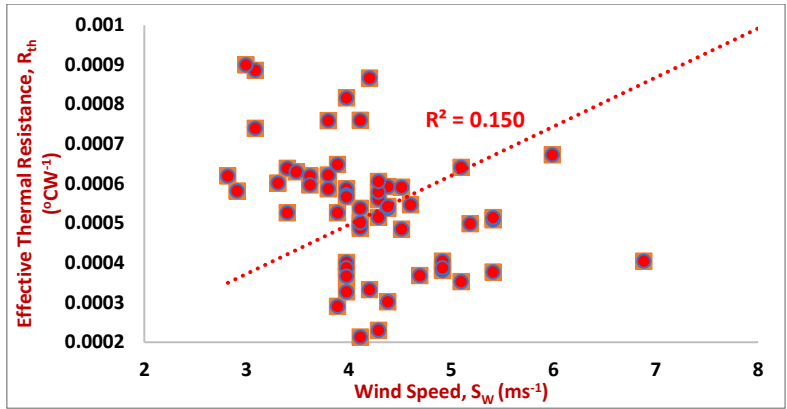
a. Harlequins
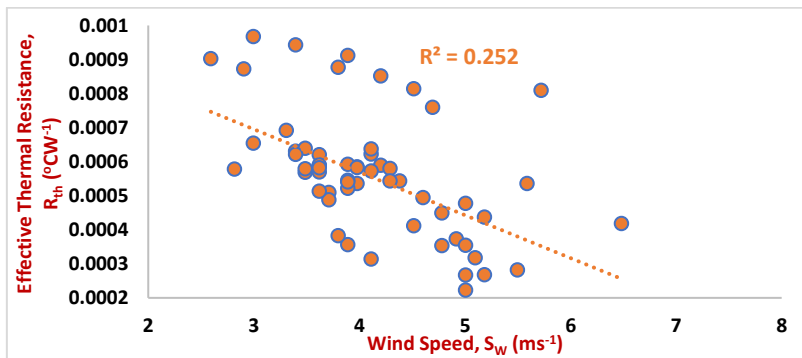
b. Newry
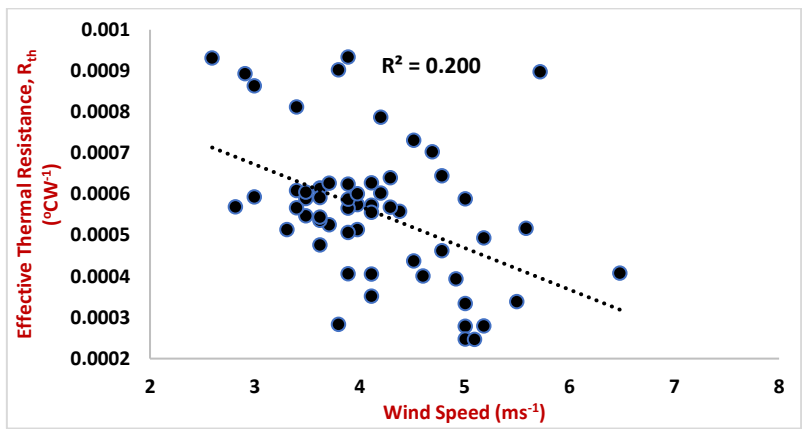
c. Warrenpoint

Figure 47 (a-c). Effective thermal resistance (Rth) versus wind speed (Sw) for hourly

collected data from Harlequins, Newry and Warrenpoint PV arrays from 2017 to 2021.

3.7 Environmental Conditions and PV Array Performance

An increase in wind speed gives higher PV system output [225] but with generally low correlations as shown in Figures 48 (a-f).

a.

b.

c.

d.

e.

f.
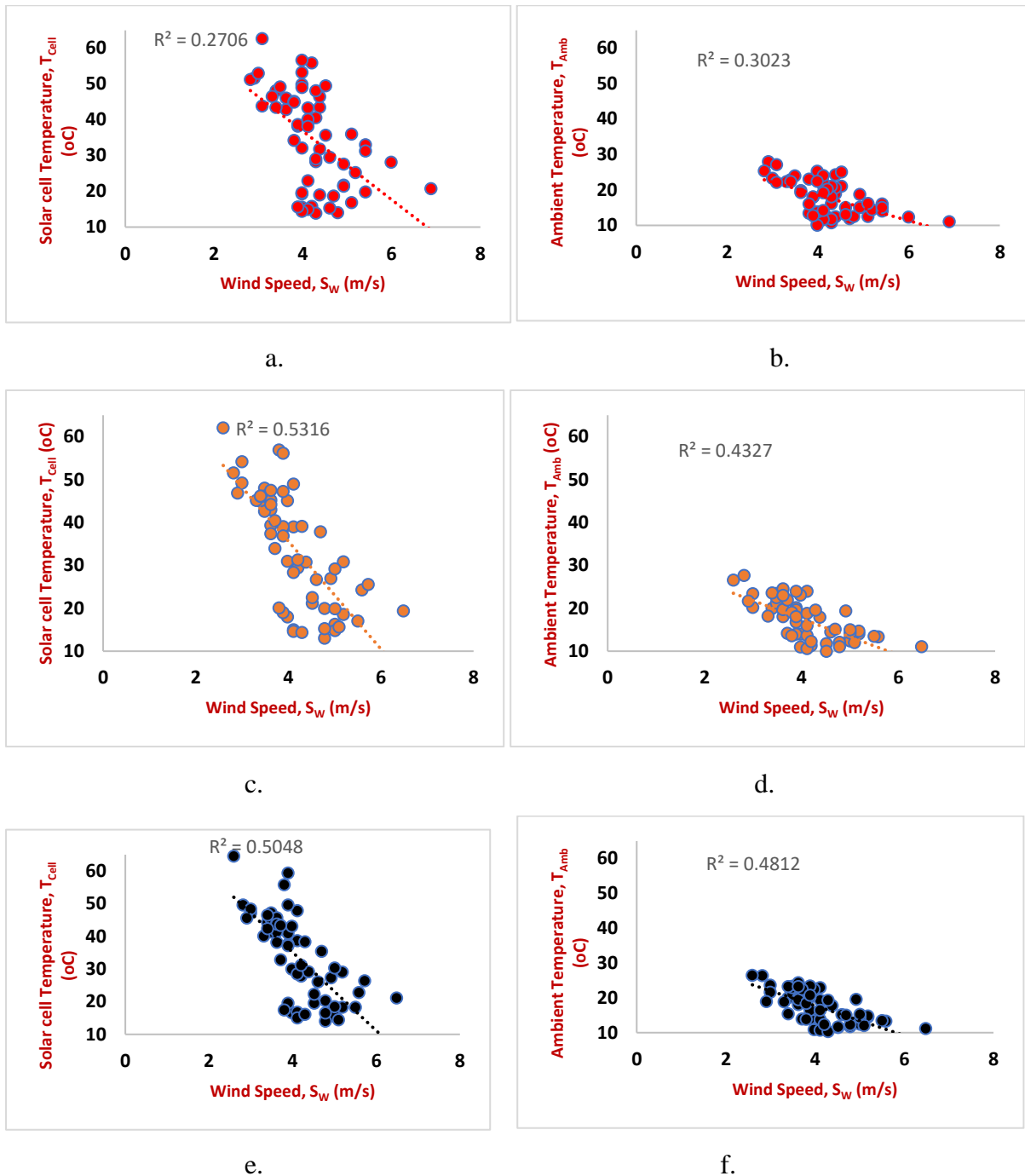
Figure 48. Influence of wind speed, solar cell temperature and ambient temperature on monthly average in (a-b) Harlequins, (c-d) Newry and (e-f) Warrenpoint PV arrays output from 2017-2021

3.8 Air Pressure on the PV System Output

Figures 49 (a-f) shows that air pressure had no effect on AC power output and solar irradiation of the PV system.

a.

b.

c.

d.

e.

f.
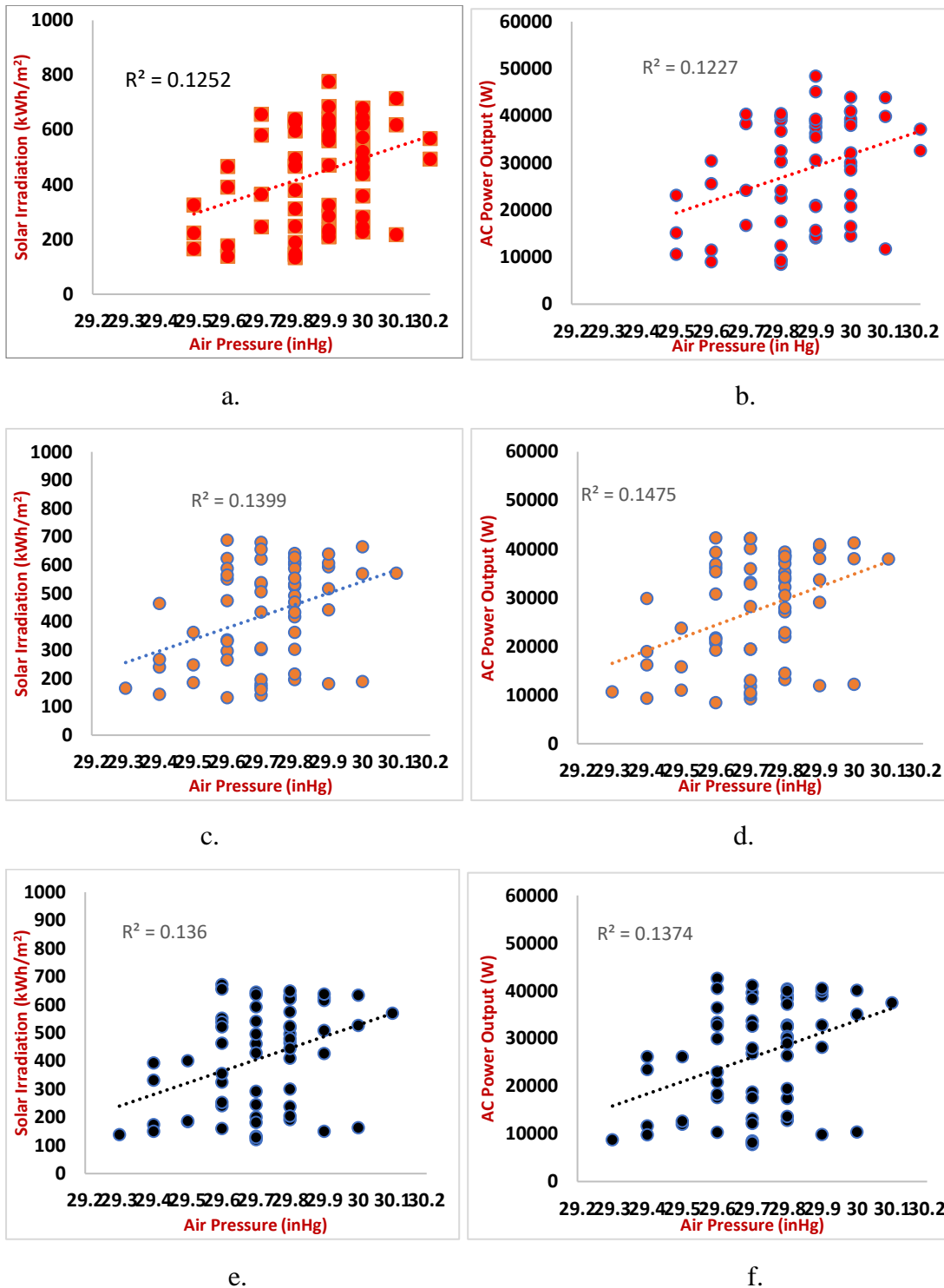
Figure 49. Influence of air pressure and solar irradiation in (a-b) Harlequins, (c-d) Newry and (e-f) Warrenpoint PV arrays output performances from 2017-2021

Humidity is the amount of water vapour in the air. It coincides with clouder conditions. Figure 50 shows that higher solar radiation intensity at the three locations examined coincided with lower relative humidity. Humidity affects PV array performance shown in Figures 51 (a, b and c). Over the five years, the relationship between the relative humidity and AC power output is inversely proportional. Figure 52 shows that whilst output efficiency declines at higher solar radiation intensities, the correlation is poor.
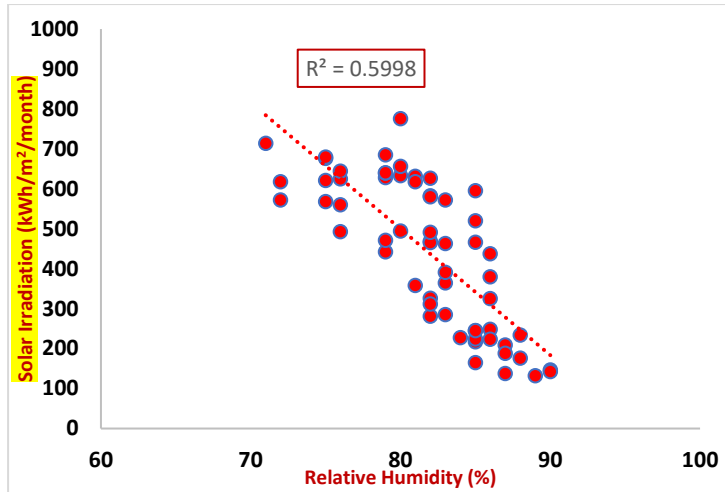
a. Harlequins
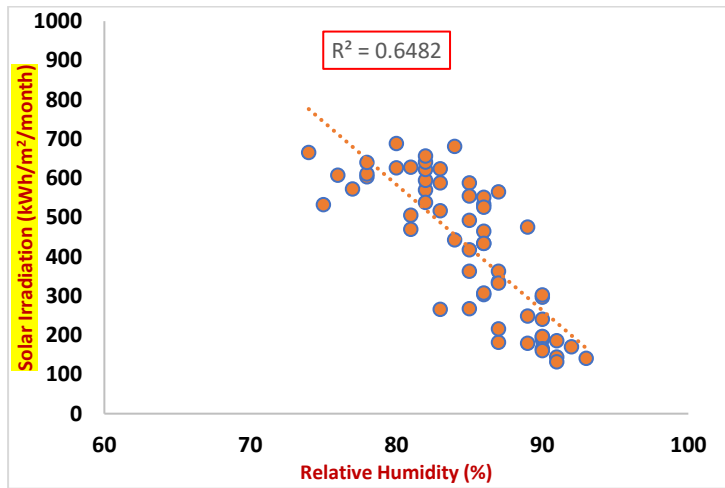
b. Newry
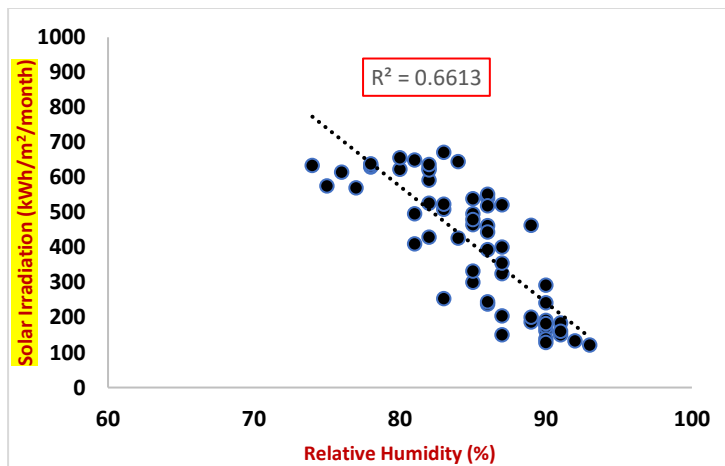
c. Warrenpoint

Figure 50 (a-c). Annual average monthly relative humidity and solar radiation for the sites of the three PV arrays.
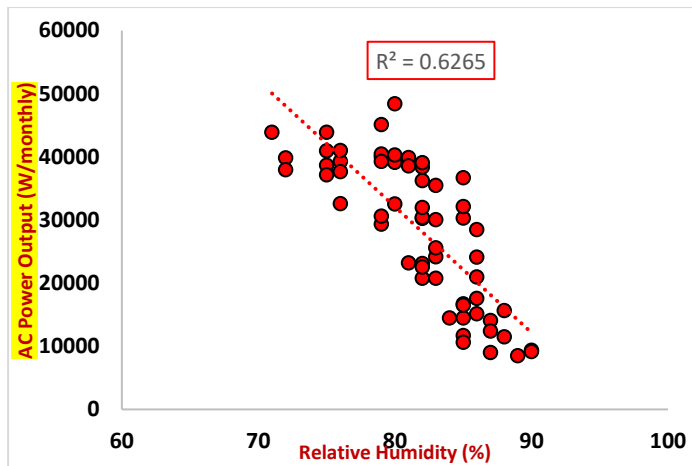
a. Harlequins
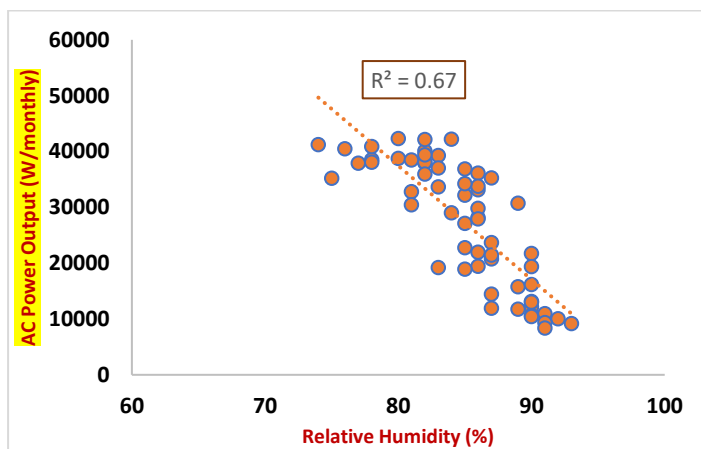
b. Newry
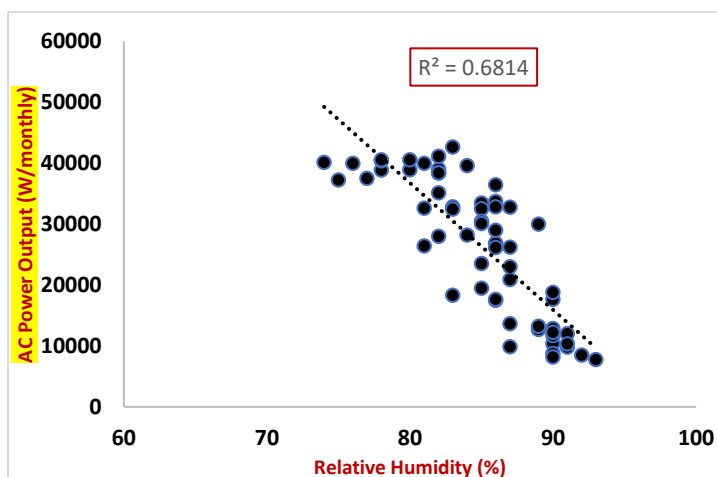
c. Warrenpoint

Figure 51. Influence of relative humidity for PV array in Harlequins, Newry and

Warrenpoint on PV average monthly system output performances from 2017 to 2021
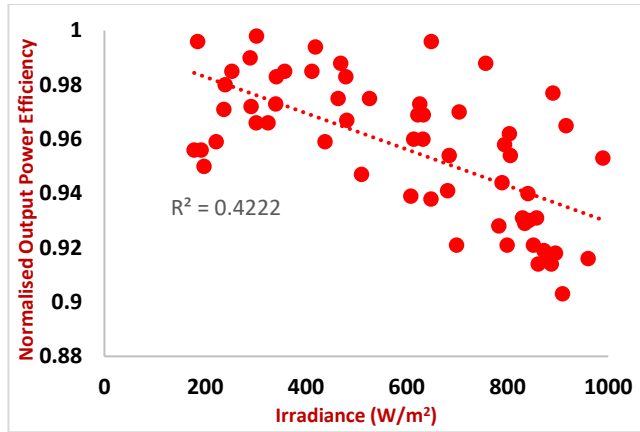
a. Harlequins
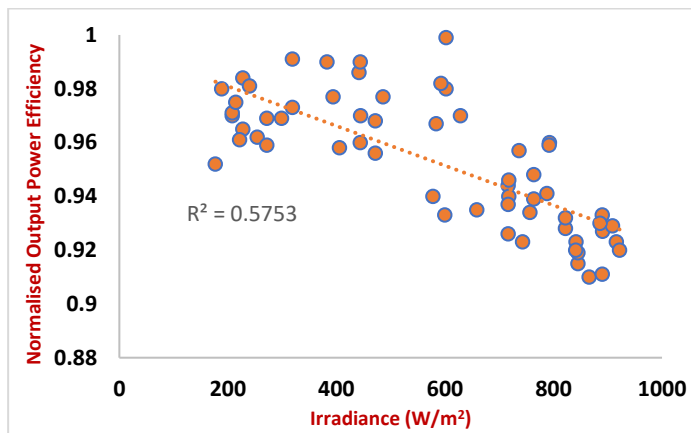
b. Newry
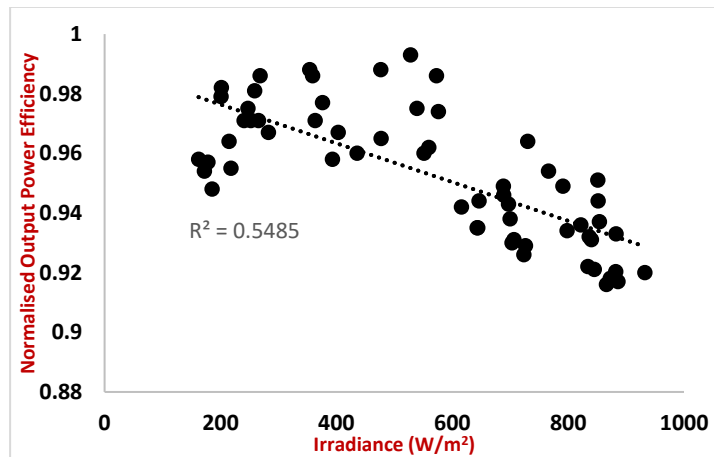
c. Warrenpoint

Figure 52 (a-c). Effect of irradiance on normalised output power efficiencies for the monitored period of five years (2017 – 2021) average monthly hourly data in Harlequins, Newry, and Warrenpoint arrays.

3.9 Effect of Module Temperature on PV Output

Normalised output power efficiency (i.e., a ratio of AC power to DC power rating at standard test conditions compared to plane of array irradiance divided by a reference irradiance) decreased at higher solar cell temperatures as shown in Figures 53 (a,b, and c) and Figure 54 shows that the three arrays have similar performance. This is because as irradiance increases the solar cell temperature increases as illustrated in Figures 55 (a, b, and c) for the three arrays. This show that there is a strong correlation between solar cell temperature and solar irradiance across the three arrays.

As seen in Figures 53 (b-c), Newry and Warrenpoint arrays show relatively higher correlation coefficients than the Harlequins array. This is because Newry and Warrenpoint are sited almost at the same location as illustrated in the location map shown in Figure 31.
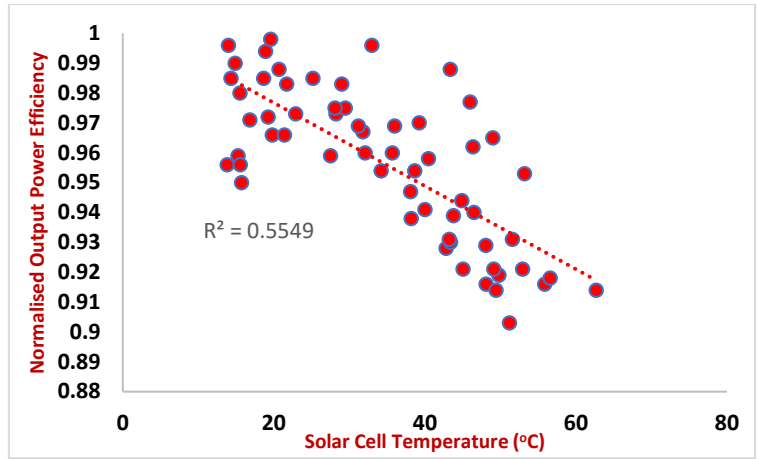
a. Harlequins
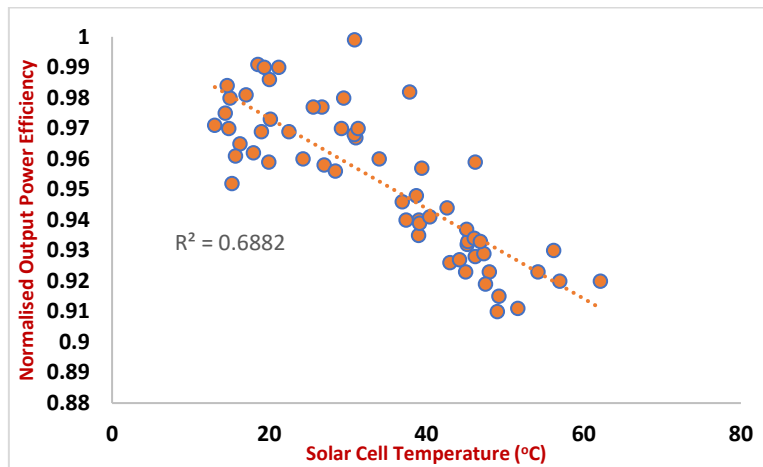
b. Newry
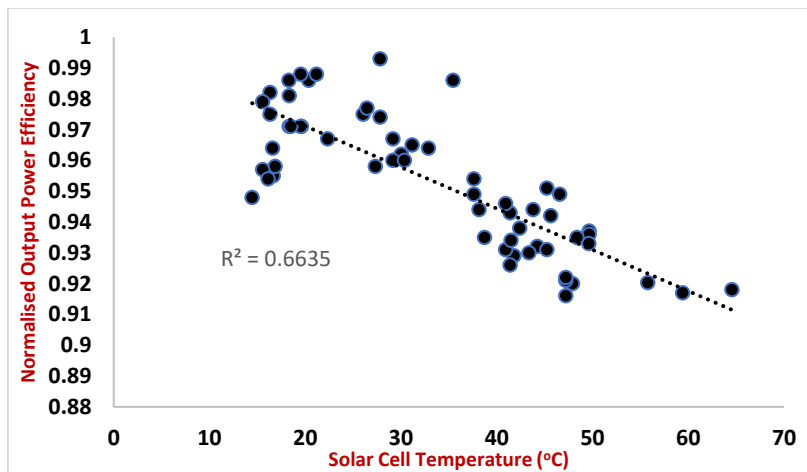
c. Warrenpoint

Figure 53 (a-c). Effect of solar cell temperature on normalised output power efficiencies for the monitored period of five years (2017 – 2021) average monthly hourly data in Harlequins, Newry, and Warrenpoint arrays.
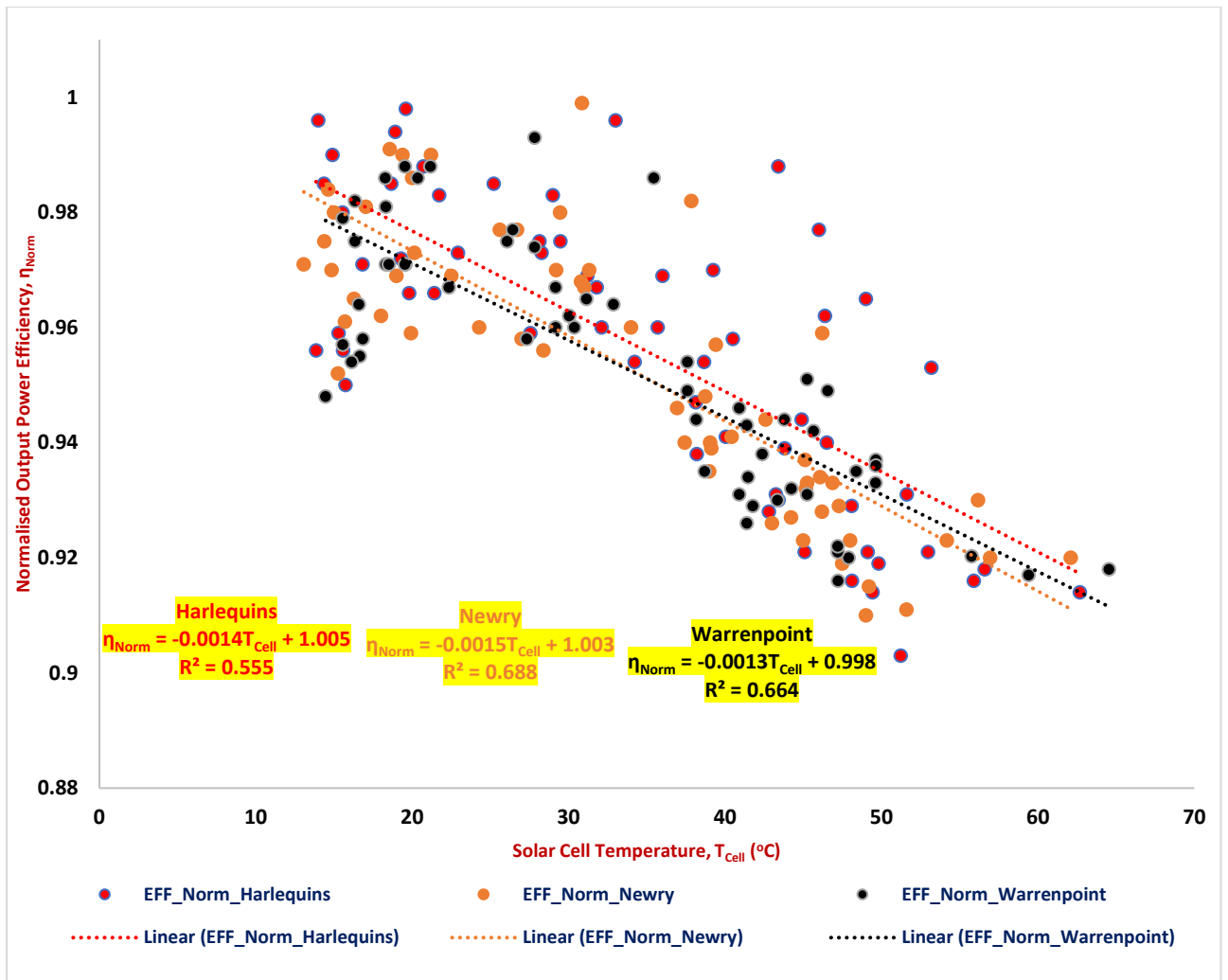
Figure 54. Overlaid illustration of similar performances at Harlequins, Newry and

Warrenpoint arrays
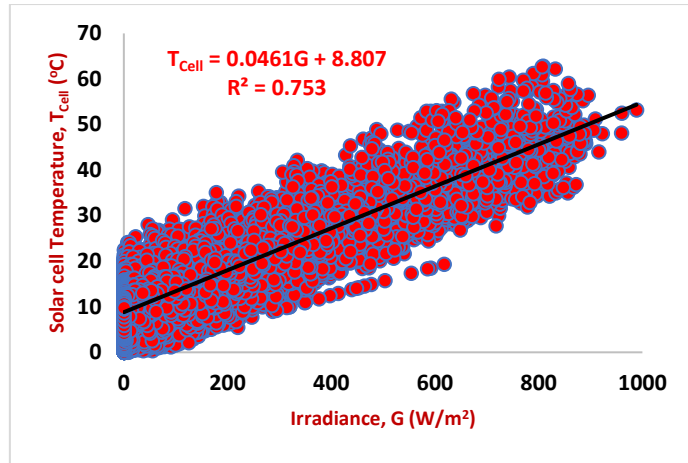
a.
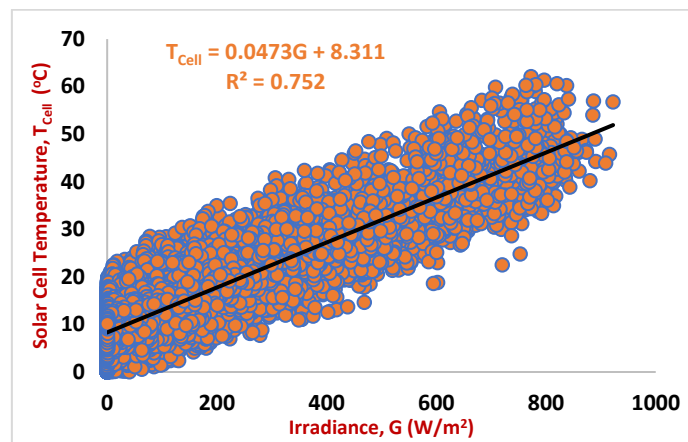
b.
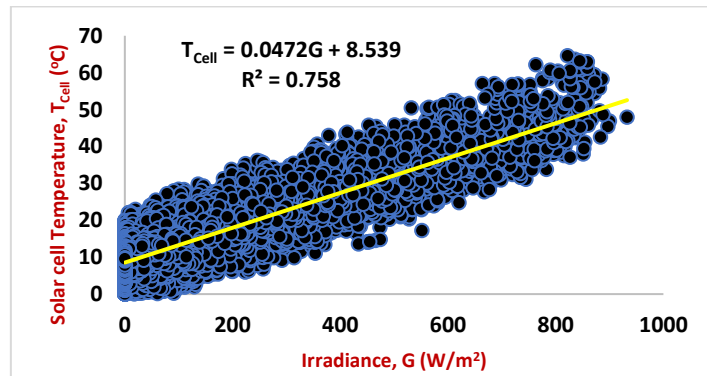
c.

Figure 55 (a-c). Solar cell temperature versus irradiance for the monitored period of five

years (2017 – 2021) average hourly data in Harlequins, Newry, and Warrenpoint arrays.

Figures 56 (a-c) show the effect of solar cell temperature and irradiance on the conversion

efficiency and fill factor (FF) for the Harlequins, Newry and Warrenpoint arrays. From Figures

56 (a-c), the fill factor of the solar cells decreases with an increase in solar cell temperature and a decrease in solar cell temperature results in a higher fill factor value. FF increases at irradiance less than 500 W/m^2 and decreases at irradiance greater than 500 W/m^2 [226]. Efficiency increases logarithmically for irradiance less than 400 W/m^2 and it neither decreases nor increases for irradiance higher than 400 W/m^2 [226]. Although high solar cell temperatures above ambient levels increase DC power output with an increase in solar irradiance (see Figure 55 (a-c), this decrease the FF and conversion efficiency of the PV system. Hence, at a low solar cell temperature and low solar irradiance, the FF and efficiency increase due to low ambient temperature.

FF is an indicator in finding the quality of PV panels. The typical FF values range between 60% and 70% [227]. For instance, the graphs of fill factors (FF) in Figures 56 (a-c) show that the PV panels performed well firstly in the range above 70% (at a low solar cell temperature) and later below 70% (at a high solar cell temperature) across the three arrays monitored for five years. The least recorded FF values in Harlequins, Newry and Warrenpoint arrays across the five years are 61.3%, 64.89% and 66.03% respectively. Hence, there is a poor correlation between system efficiency, fill factor, solar cell temperature and irradiance across the three arrays for five years.
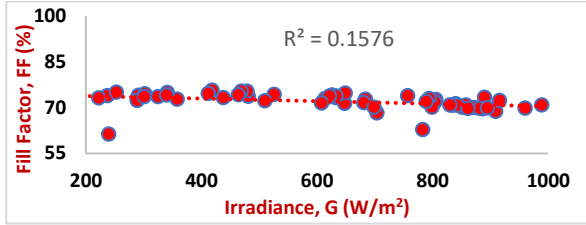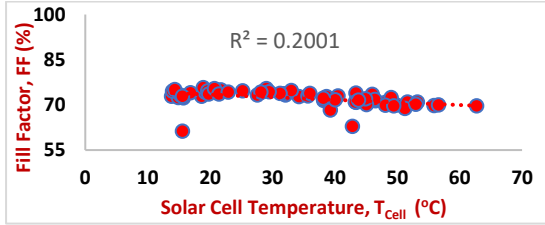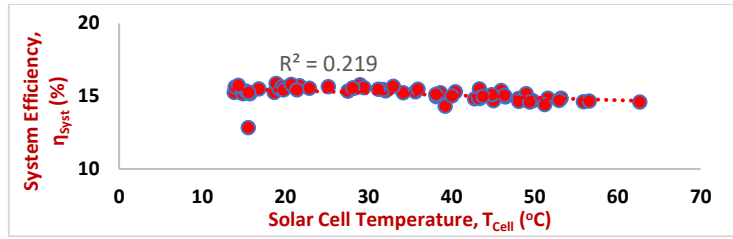
a. Harlequins arrays
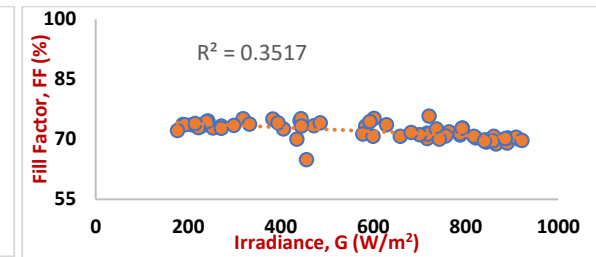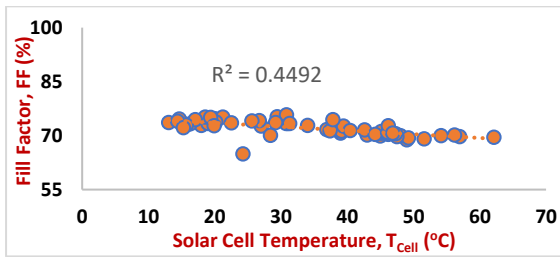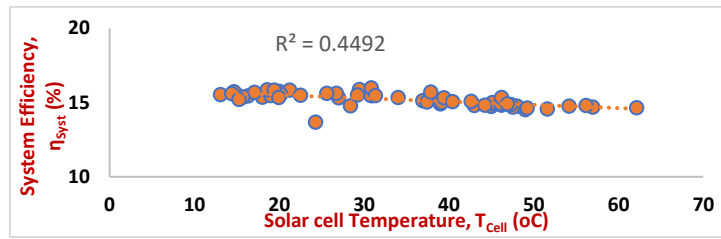
b. Newry array
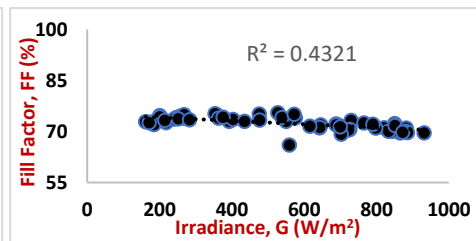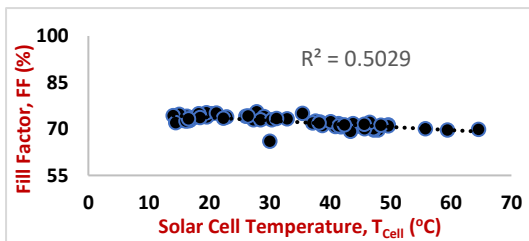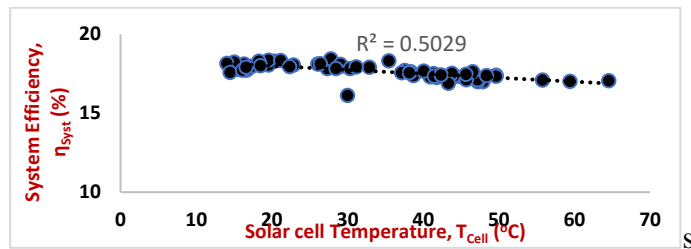
c. Warrenpoint array

Figure 56 (a-c). Effect of solar cell temperature, irradiance, conversion efficiency, and fill factor on PV system performance output in Harlequins, Newry and Warrenpoint arrays.

From Figures 57 (a-f), it can be observed that maximum power output from a module decreases as solar cell temperature and irradiance increase and this lowers conversion efficiency as seen in Figures 56 (a-c). This is because as the solar irradiance exceeds 500 Wm^{-2} [226], the maximum power output decreases thereby reducing the conversion efficiency of the PV system. Hence, high solar irradiance does not necessarily lead to the PV panel operating efficiently. Although an irradiance increase does increase the maximum power output, this is counterbalanced by higher solar cell temperature reducing fill factor. Hence, solar cell temperature can be critical to forecasting energy generation. This behaviour of fill factor and conversion efficiency with solar cell temperature agrees with the results of Fesharaki et al [228], Amelia et al [227], and Tobnaghi et al [229]. Thus, the irradiance and solar cell temperature do not correlate with the maximum power output.
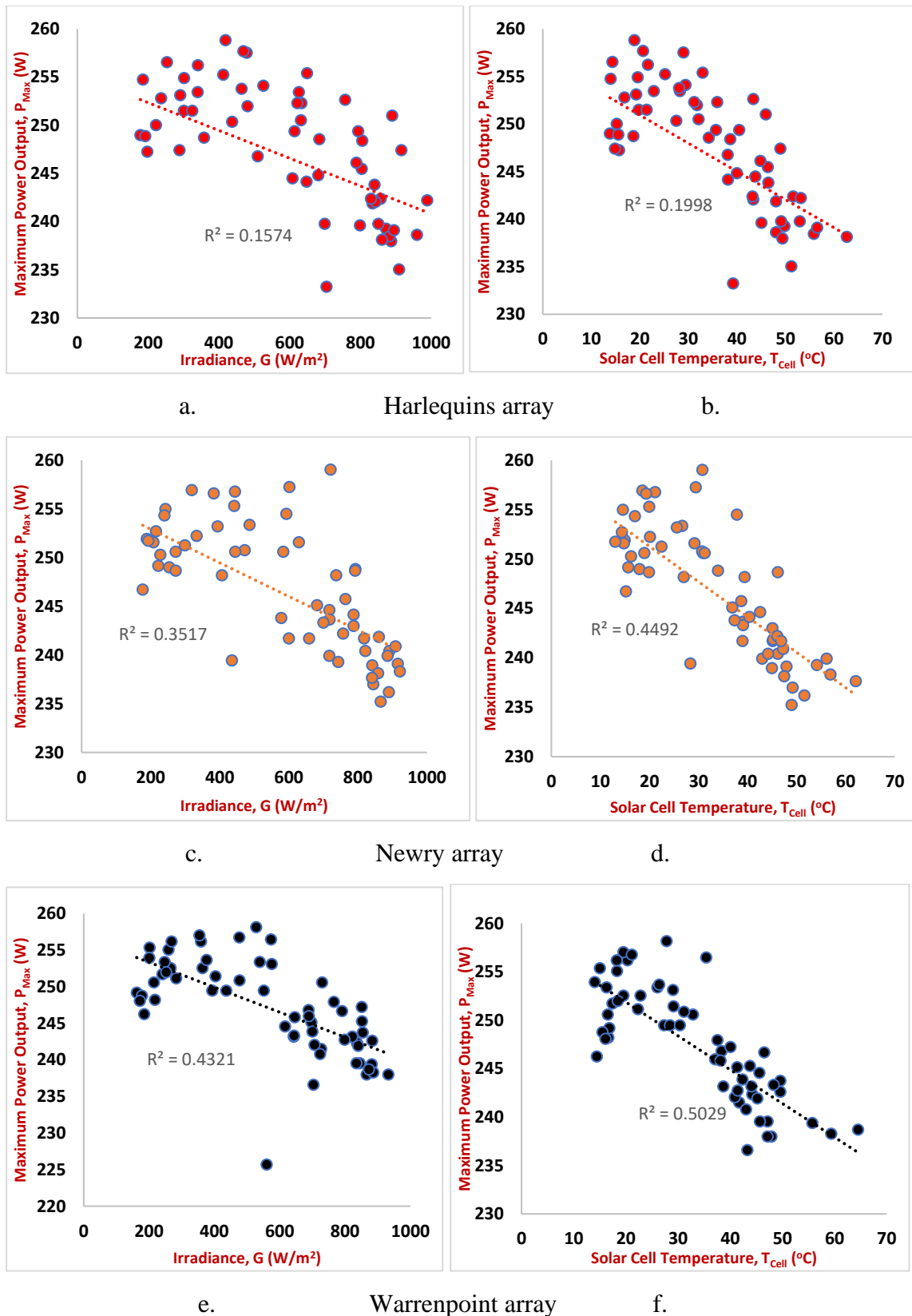
Figure 57 (a-f). Effect of maximum power output, irradiance, and solar cell temperature on PV system performance output in Harlequins, Newry and Warrenpoint arrays.

To carry out the power losses in Harlequins, Newry and Warrenpoint arrays, the reference parameters such as maximum output power, (P_{MaxR} = 260 W), reference temperature (T_R = 25°C) and temperature coefficient of maximum output power (γ = -0.4%/^{o}C) were used as shown in Table 33.

Table 33.Average Power losses recorded in Harlequins, Newry and Warrenpoint Arrays for the five-year monitored period.

Location											
Harlequins				Newry				Warrenpoint			
T_{Cell} (^{o}C)	T_{Loss} (%) = (T_{Cell} − T_R)γ	P_{Loss} (W) = P_{MaxR} × T_{Loss}	P_{Max} (W) = P_{MaxR} - P_{Loss}	T_{Cell} (^{o}C)	T_{Loss} (%) = (T_{Cell} − T_R)γ	P_{Loss} (W) = P_{MaxR} × T_{Loss}	P_{Max} (W) = P_{MaxR} - P_{Loss}	T_{Cell} (^{o}C)	T_{Loss} (%) = (T_{Cell} − T_R)γ	P_{Loss} (W) = P_{MaxR} × T_{Loss}	P_{Max} (W) = P_{MaxR} - P_{Loss}
62.69	-15.08	39.21	220.79	62.11	-14.84	38.59	221.41	64.55	-15.82	41.13	218.87

Table 33 shows the Harlequins, Newry and Warrenpoint arrays lose 15.08%, 14.84% and 15.82% in the power output when the solar cells reach 62.69^{o}C, 62.11^{o}C and 64.55^{o}C respectively. This brought power losses in Harlequins, Newry and Warrenpoint arrays to 39.21 W, 38.59 W and 41.13 W which shows that the maximum power output the Harlequins, Newry and Warrenpoint arrays operate at 62.69^{o}C, 62.11^{o}C and 64.55^{o}C are 220.79 W, 221.41 W and 218.87 W respectively.

The AC output power as a function of irradiance and variation of solar cell temperature are shown in Figures 58 (a-c) and 59 (a-c). Figures 58 (a-c) show that AC power output increased as the solar irradiance increased which is shown by strong coefficients of determination (R^2) values while in Figures 59 (a-c) it can be observed that AC power output decreased as cell

temperature increased lowering conversion efficiency as seen in Figures 56 (a-c). This is shown by poor coefficients of determination (R^2) values with AC power output.
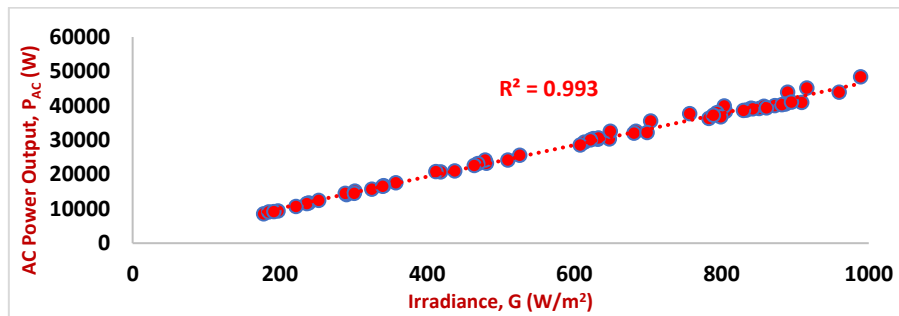
a. Harlequins
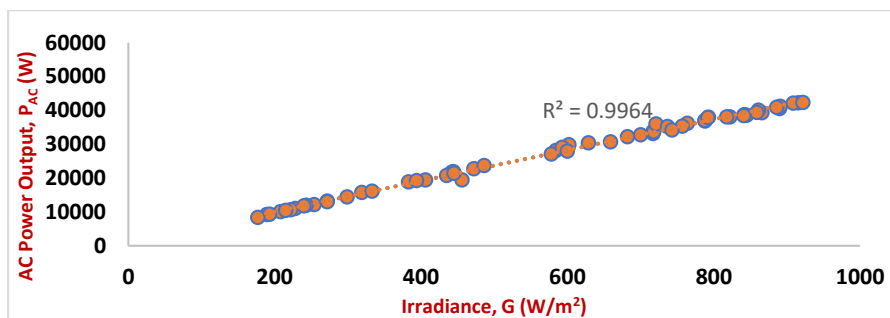
b. Newry
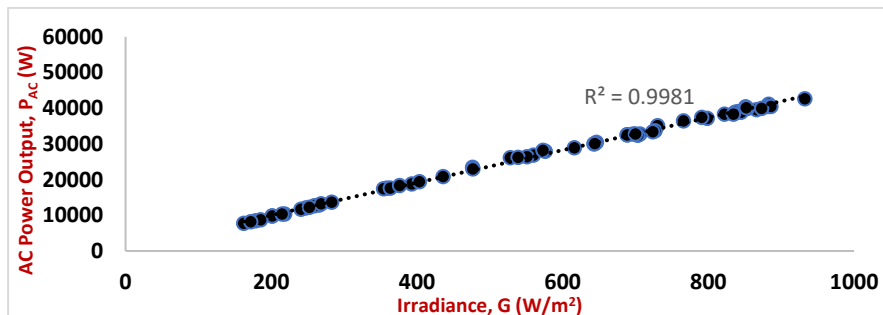
c. Warrenpoint

Figure 58 (a-c). Effect of Irradiance on AC output power in Harlequins, Newry and Warrenpoint arrays monitored over five years period
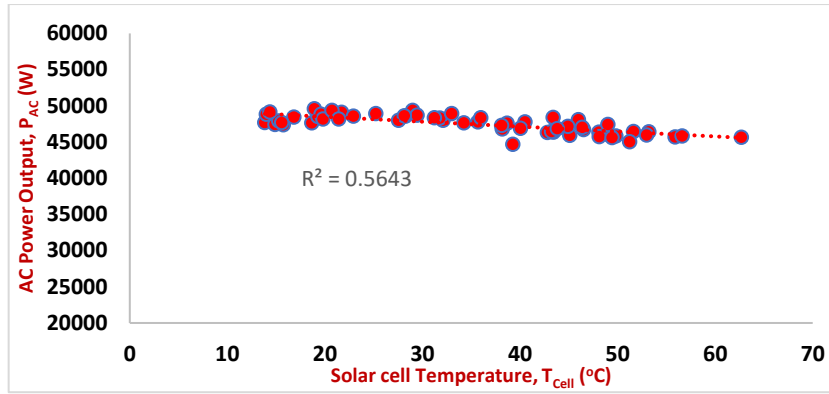
a. Harlequins
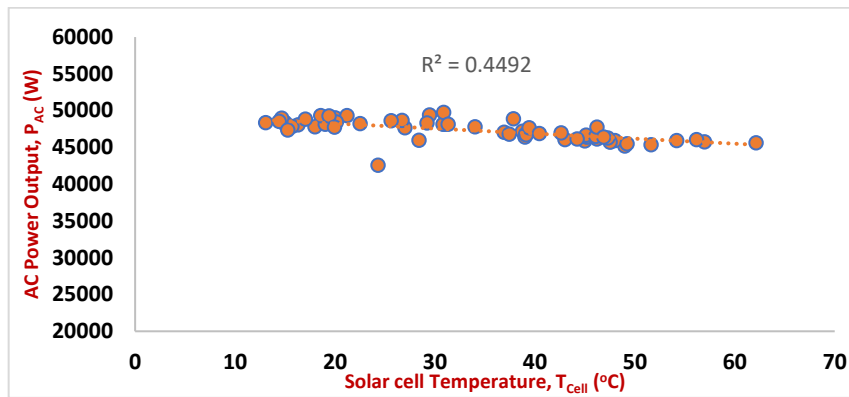
b. Newry
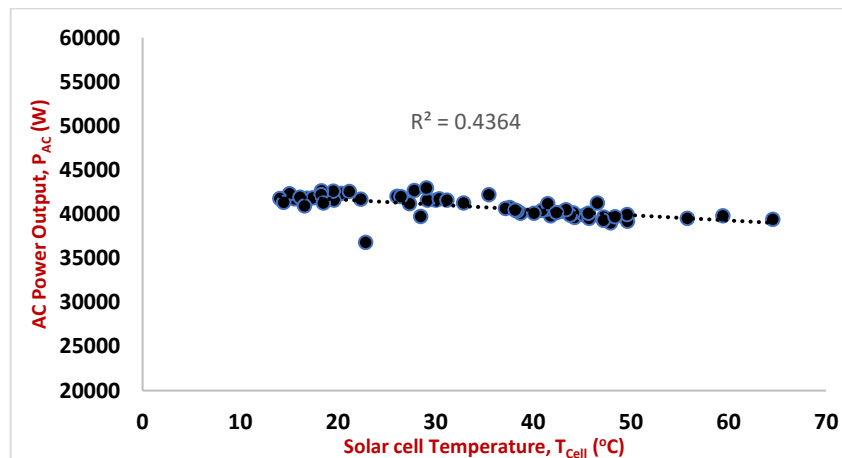
c. Warrenpoint

Figure 59 (a-c). Effect of variation solar cell temperature on AC output power in Harlequins,

Newry and Warrenpoint arrays monitored over five years period.

3.10 Inverter Performance

The relationship between DC output (inverter input power) from PV modules and AC output from the inverter in Figure 60, shows almost a perfect correlation between inverter input power and inverter output power across the three arrays. For instance, the Harlequins array shows a perfect correlation which shows that there is no form of shading recorded on the site.
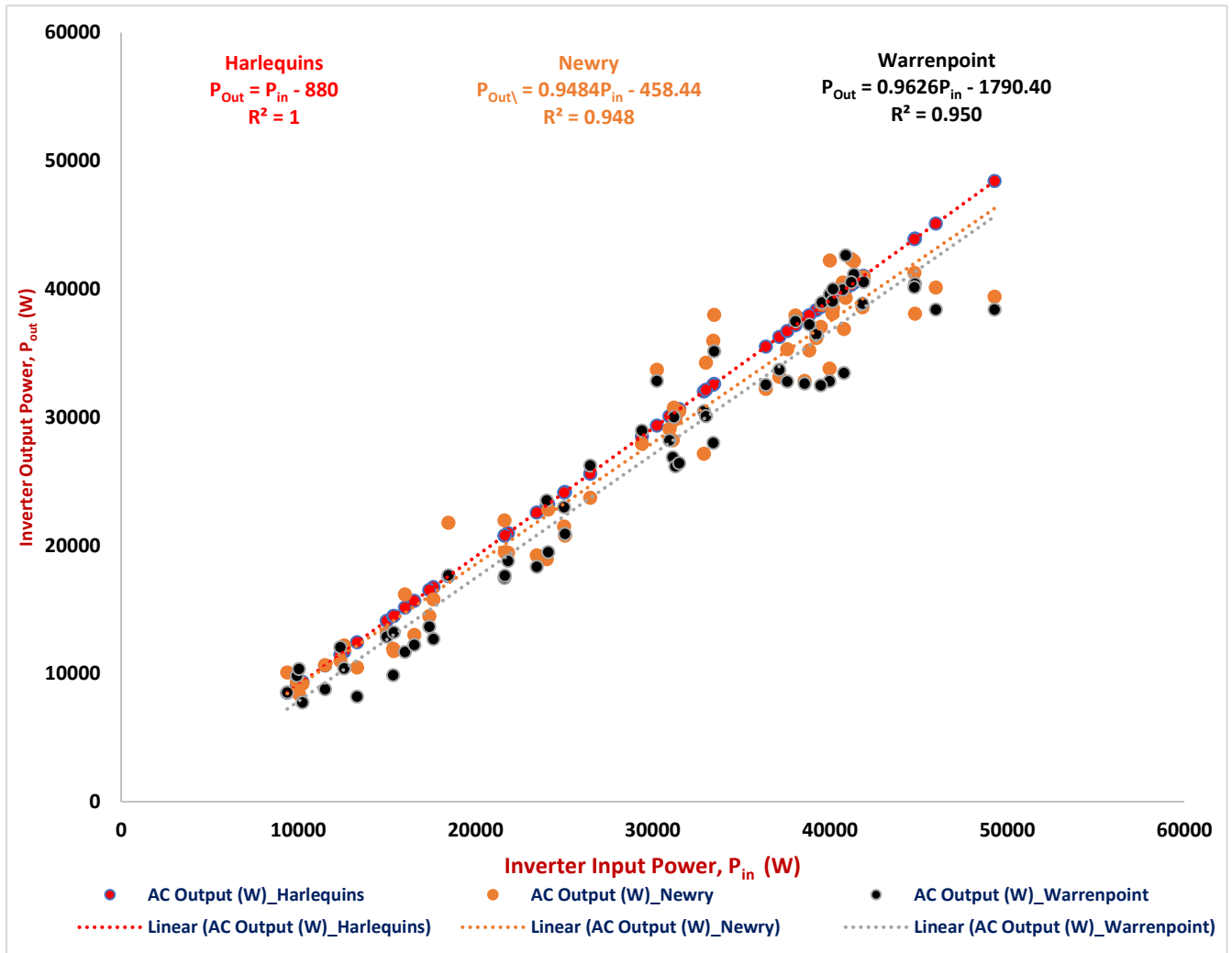
Figure 60. Relationship between input power and output power of the inverter

Figures 61 (a-c) indicate that maximum inverter efficiency strongly depends on ambient temperature and DC power output. For instance, for the Harlequins system, inverter efficiency reaches its maximum value of 98.21% at a DC power output of 48,416 W when the ambient temperature is at 25.26^{o}C (see Figure 61 (a)) and shows a drop of 1.79% when the temperature increases from 25.26^{o}C to 32.00^{o}C under the same standard solar irradiance of (1000 W/m^2) and this is seen by a straight line. At Newry, maximum inverter efficiency is recorded at 97.96% at a DC power output of 43,057 W when the ambient temperature is 23.50^{o}C (see Figure 61 (b)). It shows an efficiency drop of 2.04% when the ambient temperature increases from 23.50^{o}C to 27.70^{o}C while at Warrenpoint, maximum inverter efficiency is 98.06% at a DC power output of 41, 202 W when the ambient temperature is 18.90^{o}C (see Figure 61 (c)). It shows a drop of 1.94% when ambient temperature increases from 18.90^{o}C to 26.40^{o}C. Therefore, the loss encountered during conversion is due to higher ambient temperatures.
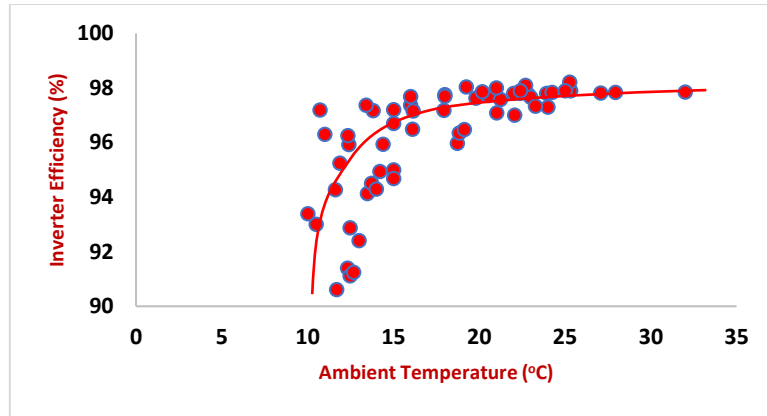
a.   Harlequins
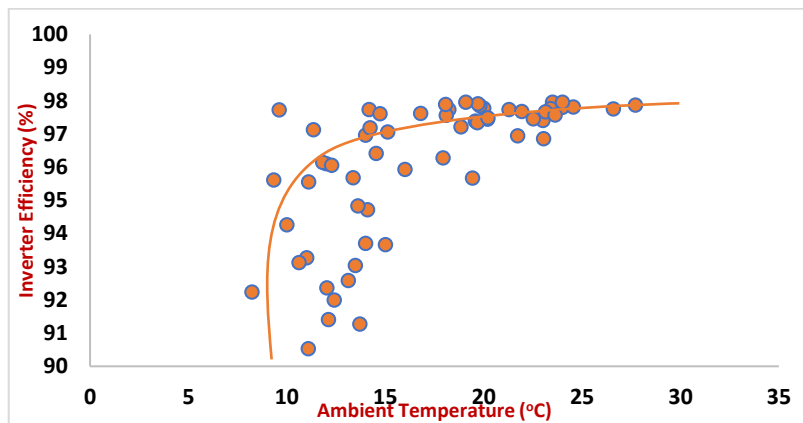
b.   Newry
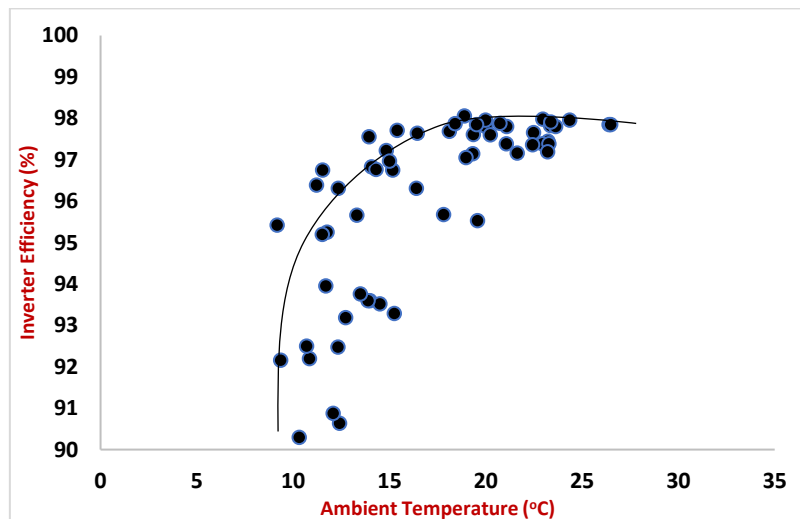
c.   Warrenpoint

Figure 61 (a-c). The monthly average relationship between inverter efficiency and ambient temperature monitored over five years period

125

Figure 62 shows the variation of inverter efficiency with the inverter output power. There is an increase in inverter efficiency when inverter output power increased. For instance, in the Harlequins system, the maximum inverter efficiency is 98.21% at an inverter output power of 48,400 W, and the Newry system has its maximum inverter efficiency recorded as 97.96% at an inverter output power of 42,200 W while the maximum inverter efficiency observed in Warrenpoint system is 97.98% at an inverter output power of 42,600 W.
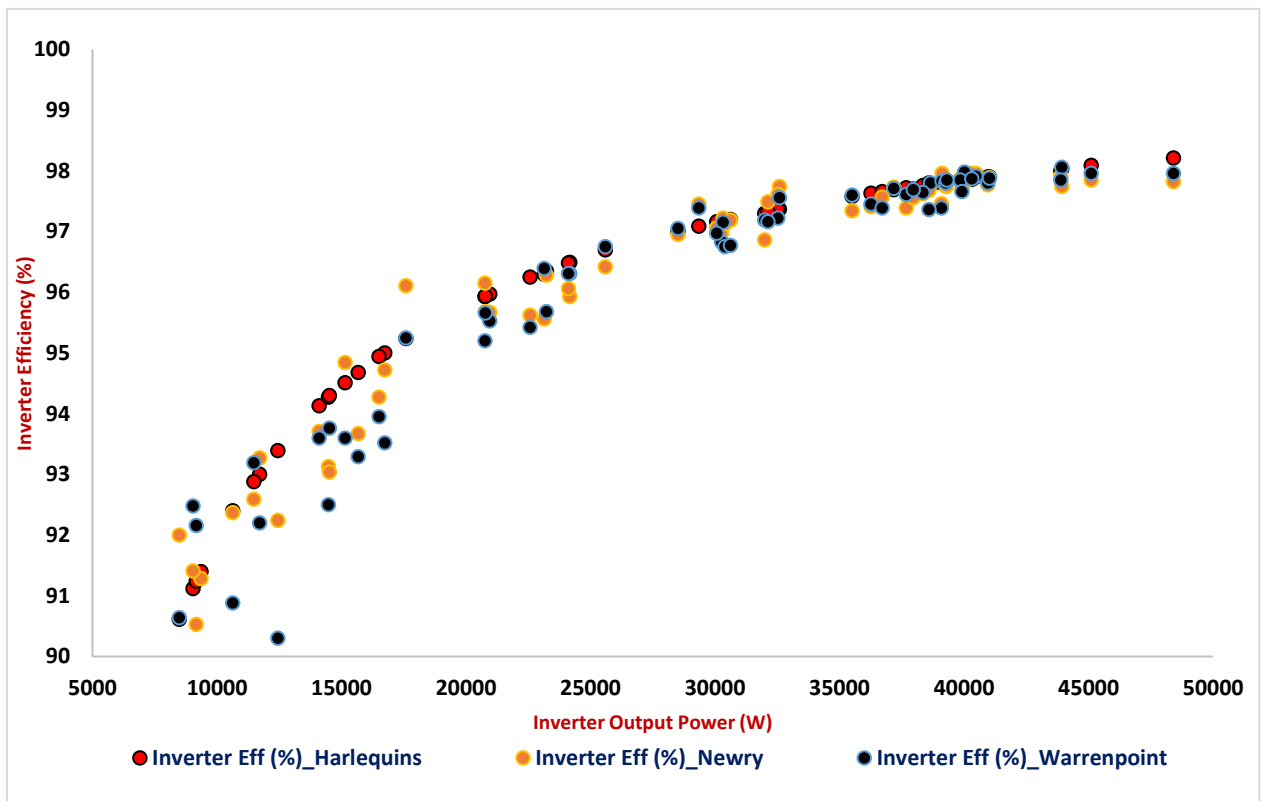
Figure 62. Monthly average inverter efficiency versus inverter output power monitored over five years period

When an inverter converts DC from the PV system to AC, energy is lost due to increasing ambient temperatures, loss in cables, PV modules, inverter and DC power output level. The output or AC energy (E_{AC}) is thus not the same as the DC energy (E_{DC}). Such inverter percentage conversion losses or inverter failures [173] can cause large fluctuations in the PV system's performance ratios. Figures 63 (a-c) show that the inverter percentage conversion loss decreases exponentially with the inverter output power. The losses encountered during the conversion processes are due to increased ambient temperatures as shown in Figures 63 (a-c). In the Harlequins system, the maximum conversion efficiency was recorded as 98.21%, this means that due to the increase in ambient temperature from 25.26^{o}C to 32.00^{o}C, a percentage conversion loss of 1.79% ensues (see Figure 63 (a)), at the Newry system, the maximum conversion efficiency was recorded as 97.96% and its percentage conversion loss was 2.04% due to increase in ambient temperature from 23.50^{o}C to 27.70^{o}C (see Figure 63 (b)) while the maximum conversion efficiency in Warrenpoint system is 98.06% and its percentage conversion loss is 1.94% due to increase in ambient temperature from 18.90^{o}C to 26.40^{o}C (see Figure 63 (c)).
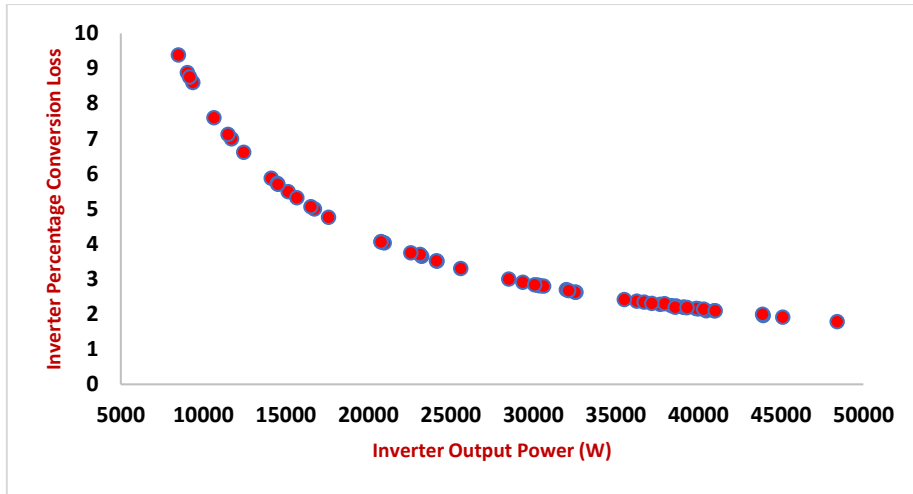
a. Harlequins
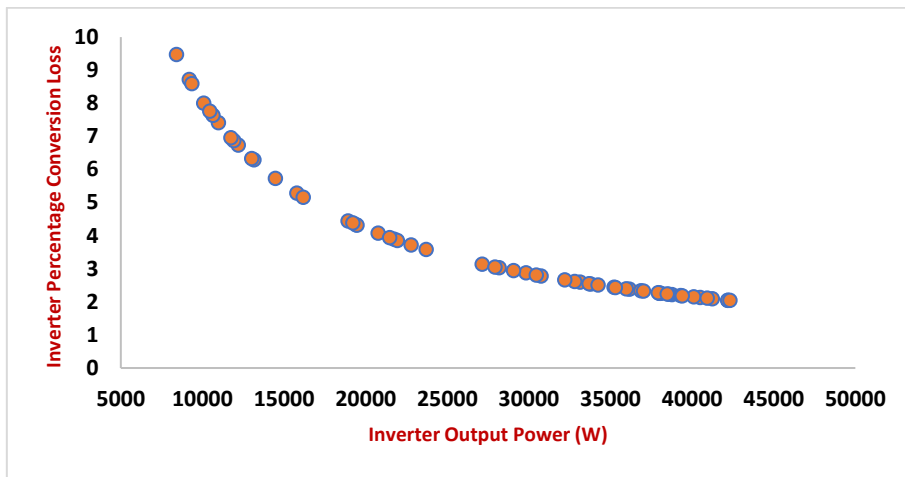
b. Newry
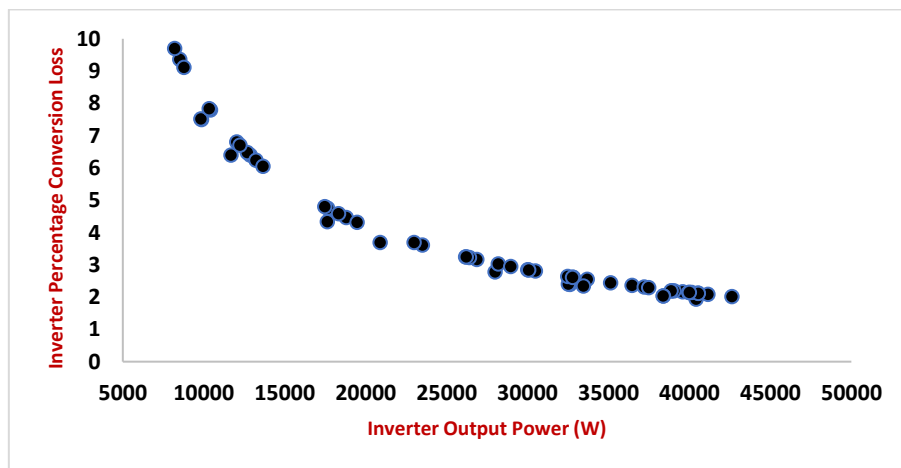
c. Warrenpoint

Figure 63 (a-c). Monthly average inverter percentage conversion loss versus inverter output power monitored over five years period

3.11 Energy Output and Efficiency

Figures 64 (a-c) illustrate the monthly energy DC array output, energy AC system output, DC array efficiencies, and AC system efficiencies of Harlequins, Newry and Warrenpoint systems from 2017 to 2021. The annual average of DC and AC energy generations from the PV array and the PV system from 2017 to 2021 in the three systems is shown in Table 34. In Table 34, as the DC and AC energy generations increase, the efficiencies of the PV array and PV system also increase. Figures 64 (a-b) and Table 34 show that the Harlequins and Newry systems generated more energy output across the five years than the Warrenpoint system (see Figure 64 (c)). This is because the Harlequins and Newry systems received more solar irradiation than the Warrenpoint system by 7.69% and 3.62% respectively. The higher array and system efficiencies recorded in Warrenpoint is as a result of its area of PV array (totalling 268.8 m^2).

Table 34. Annual average energy DC array output, energy AC system output, the efficiency of PV array and efficiency of the AC system at the sites considered.

Location													
		Harlequins				Newry				Warrenpoint			
		E_{DC} (kWh)	E_{AC} (kWh)	η_{PV} (%)	η_{Sys} (%)	E_{DC} (kWh)	E_{AC} (kWh)	η_{PV} (%)	η_{Sys} (%)	E_{DC} (kWh)	E_{AC} (kWh)	η_{PV} (%)	η_{Sys} (%)
Year	2017	20202	19559	15.52	14.90	20488	19845	15.81	15.17	19783	19141	18.27	17.47
	2018	21223	20581	15.87	15.25	20855	20213	15.90	15.28	19906	19263	18.54	17.76
	2019	22984	22341	15.91	15.32	20938	20296	15.69	15.08	19696	19112	18.45	17.74
	2020	21986	21342	15.74	15.18	20586	19941	15.92	15.30	20432	19788	18.41	17.69
	2021	20928	20285	15.72	15.12	20430	19788	15.85	15.20	20088	19445	18.40	17.63
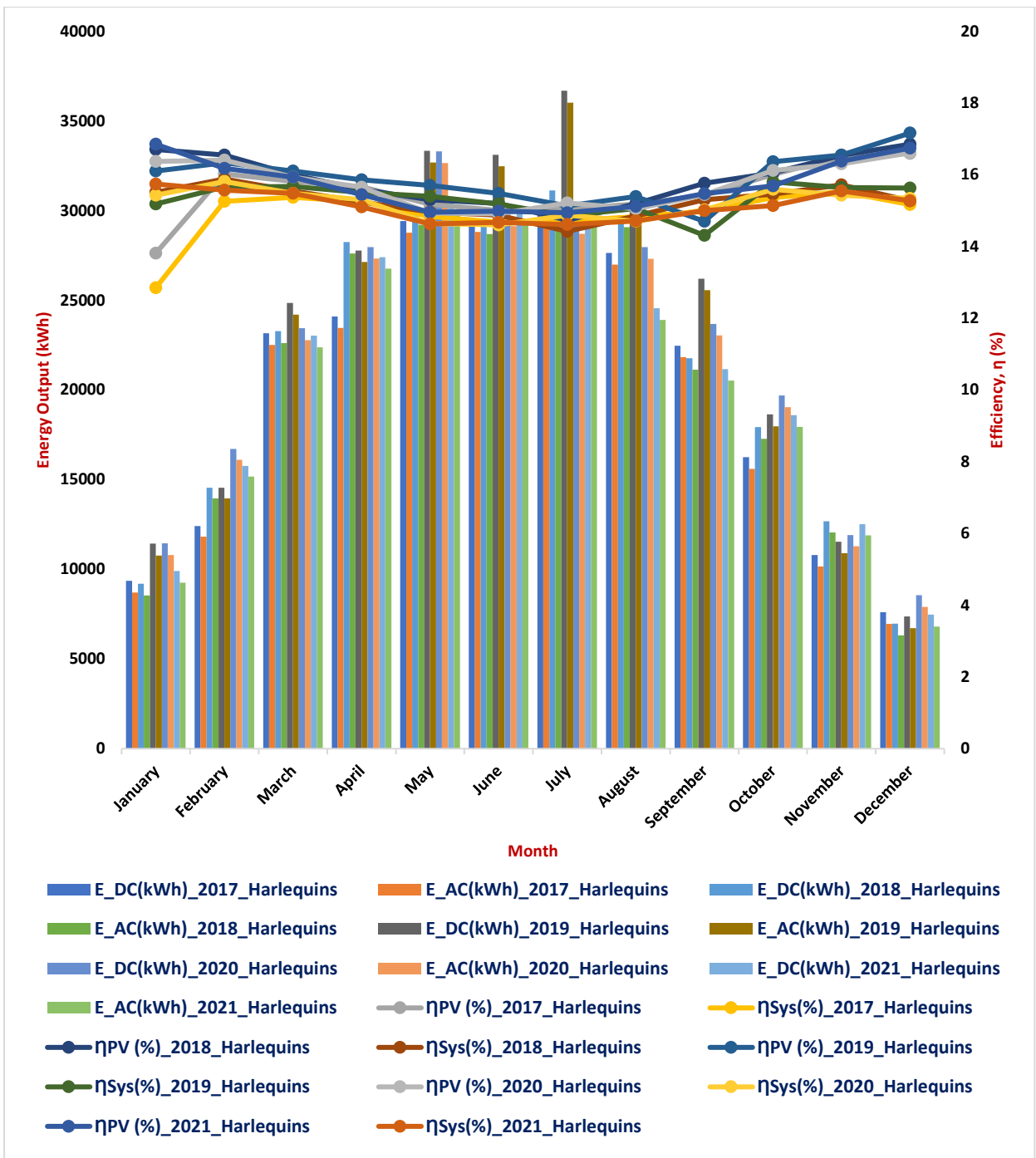
a. Harlequins
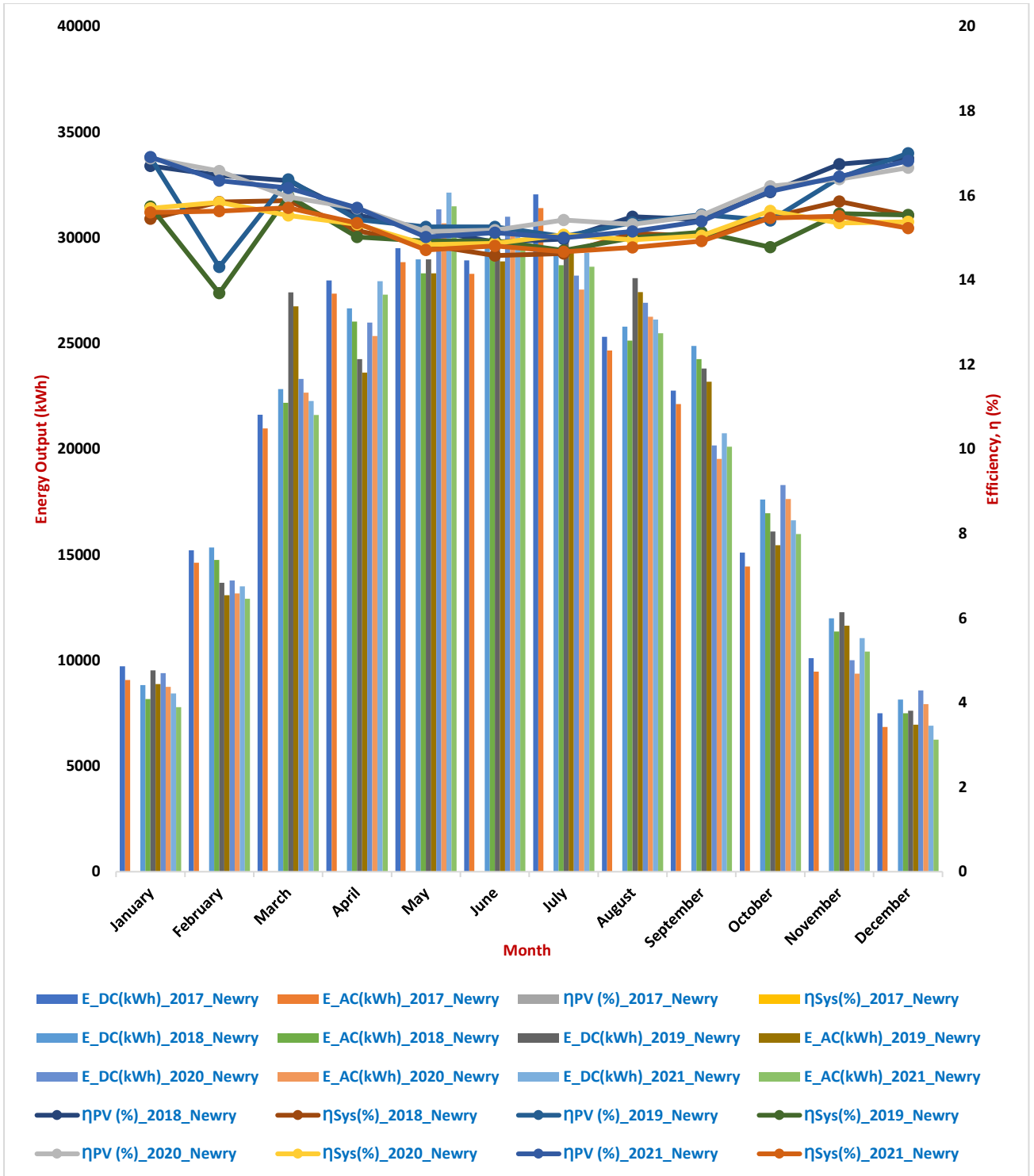
b. Newry
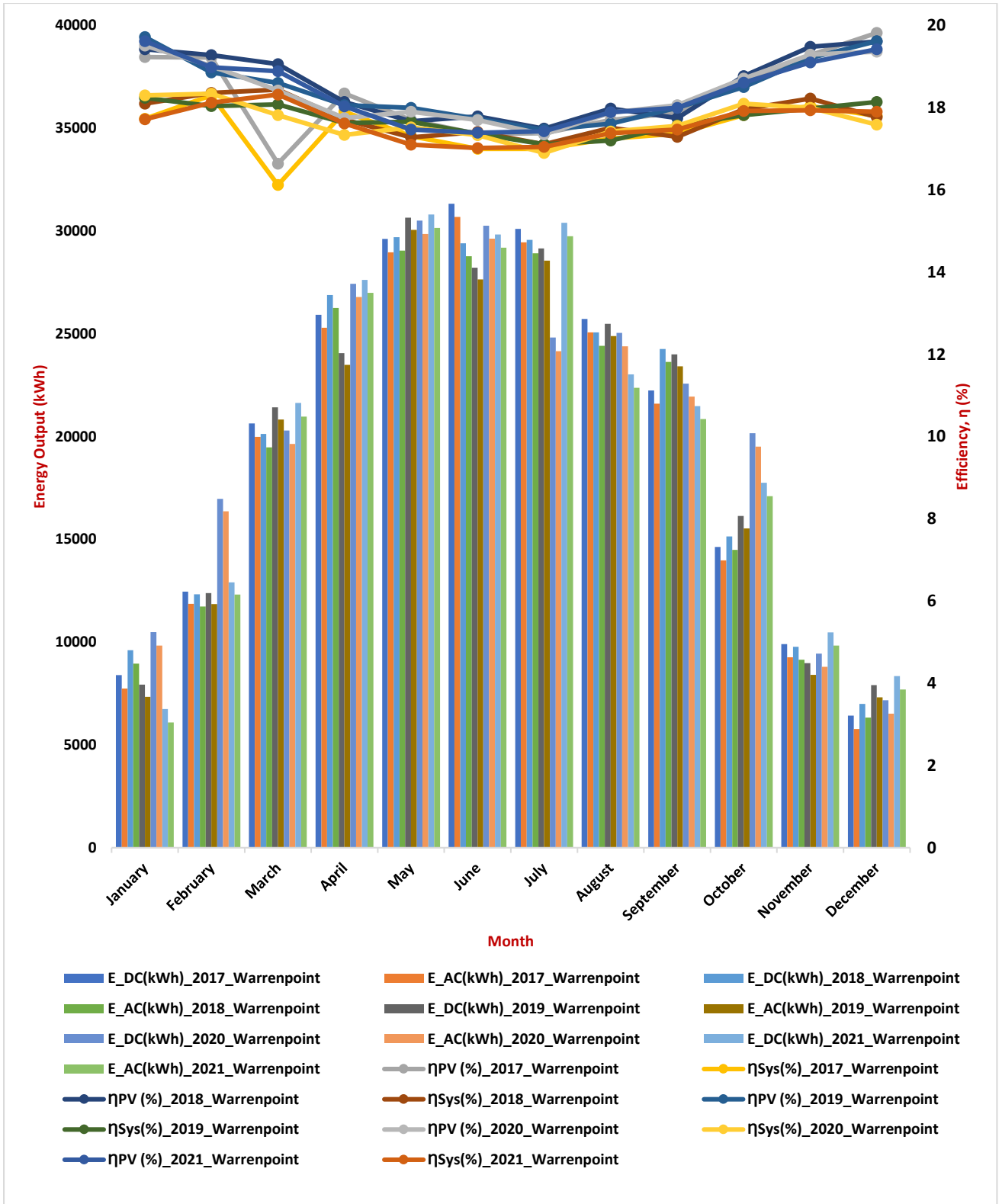
c. Warrenpoint

Figure 64 Monthly average DC array output, AC energy output and efficiencies for (a). ESB Harlequins, (b) ESB Newry, and (c) ESB Warrenpoint Systems monitored over five years period.

Winter and Autumn have shorter days thus lower power output is generated as shown in Appendices 1 (c-d) (Harlequins array), Appendices 2 (c-d) (Newry array) and Appendices 3 (c-d) (Warrenpoint array). The winter season generates the least power output (see Appendices 1 (d), 2 (d) and 3 (d)). In the winter and autumn season, solar panels work more efficiently because of lower ambient temperature.

Harlequins, Newry and Warrenpoint arrays noticed cloudy weather conditions in the autumn and winter seasons (see Appendices 1 (c-d), Appendices 2 (c-d) and Appendices 3 (c-d)) which show low solar irradiation than the spring and summer seasons. PV systems in autumn and winter generate less power output because of stormy, cloudy, or overcast weather conditions. Harlequins, Newry and Warrenpoint arrays in Appendices 1 (a-d), Appendices 2 (a-d) and Appendices 3 (a-d) show the influence of weather conditions on PV power output. For instance, the Harlequins array in spring season shows that March 2017 – May 2017 and March 2021 – May 2021 are faced with weather variabilities (scattered cloud and sunny conditions) and March 2018 – May 2020 shows clear and sunny conditions while in summer season heavy cloudy condition is noticed in July 2017 and June 2017, June 2020 – August 2021 witnessed variable weather conditions while June 2018 – August 2019 witnessed clear and sunny conditions. Newry and Warrenpoint arrays show that in spring, the weather variability is noticed in March 2017 – May 2017 and March 2021 – May 2021 while in summer the heavy cloudy condition is noticed in July 2017 and June 2020 – August 2021 shows weather variability. Therefore, July witnessed low power output generation which may be because of overcast, cloud conditions, wind speed, and/or dust.

The time between sunrise and sunset is calculated using equations 49 to 53.

$$\text{Day Length} = \frac{2}{15^o} \text{Cos}^{-1}[-\text{Tan } \delta . \text{Tan } \emptyset] \quad \text{or Day Length} = \frac{2}{15^o} \omega_{sr} \qquad (49)$$

$$\delta = 23.5 \text{Sin } [\frac{360}{365}(284+N)] \qquad (50)$$

$\alpha = 90^{\circ} + \emptyset - \delta$ (51)

$\alpha = \text{Sin}^{-1}[\text{Sin}\emptyset.\text{Sin }\delta + \text{Cos}\emptyset.\text{Cos }\delta.\text{Cos }\omega]$ (52)

$\omega_{sr} = \text{Cos}^{-1}(-\text{Tan }\delta.\text{Tan }\emptyset) = \omega_{ss}$ (53)

where:

δ: Declination angle ($^{\circ}$).

α: Sun elevation angle ($^{\circ}$).

N: Number of days.

$\theta z = 90^{\circ}$ or $\frac{\pi}{2}$ is the zenith angle.

h: Altitude (for Harlequins array (22m), Newry array (45m) and Warrenpoint array (34m)).

L_{SH}: Shadow length (m).

ω_{sr}: Hour angle of sunrise ($^{\circ}$).

ω_{ss}: Hour angle of sunset ($^{\circ}$).

$\emptyset$: Latitude (for Harlequins site (54.57°N), Newry site (54.18°N) and Warrenpoint site (54.11°N)).

Sunshine hours as reported by meteorological services are less than the theoretical daylength as they are calculated from the duration of time solar radiation intensity has a particular value.

Harlequins, Newry and Warrenpoint arrays receive an average of 2.18 hours, 2.51 hours, and 2.34 hours of peak sunlight (i.e., one hour in which the intensity of solar irradiance reaches an average of 1,000 W/m^2) per day, which increases in an average of 3.85 hours, 4.18 hours and 3.01 hours in the summer and drops in an average of 0.50 hour, 0.74 hour, and 0.61 hour in the winter. Appendices 1 (a), 2 (a) and 3 (a) show that from the beginning and end of the spring

(that is March-May) when there is a low ambient temperature, low solar irradiance and more daylength, the efficiency of the solar panels increases at 1 pm and 2 pm which results in high power output despite the sun's limited elevation in these months. Appendices 1 (b), 2 (b) and 3 (b)s showed that in summer, as the daylength decreases the power output is noticed to decrease because of nearness to shorter daylength. From August (late summer), September to November (beginning and ending of autumn) there is a gradual reduction in power output because of a reduction in solar irradiance, daylength and more overcast. The same low power output is noticed at the beginning of winter (December) but partly increased in January and February due to nearness to daylength.

3.2 Conclusion

For three large-scale roof-mounted photovoltaic (PV) systems over five years, AC final yield, reference yield, DC array yield, DC array performance ratio, AC system performance ratio, PV module and system efficiencies were determined.

Table 33 shows that the Harlequins, Newry and Warrenpoint arrays lose 15.08%, 14.84% and 15.82% in the power output when the solar cells reach 62.69°C, 62.11°C and 64.55°C respectively, thus showing the maximum power output the Harlequins, Newry and Warrenpoint arrays operates are 220.79 W, 221.41 W and 218.87 W respectively.

As solar cell temperatures increased the efficiency of the inverter system decreased due to an increase in solar irradiances closer to the rated capacity of the module. Also, the maximum inverter efficiency strongly depends on ambient temperature and DC power output.

Increases in solar cell temperature increase AC system losses (Ls) and DC array capture losses (Lc). Increases in ambient temperature decreased inverter efficiency. For instance, for the Harlequins system, inverter efficiency shows a drop of 1.79% when the ambient temperature increases from 25.26°C to 32.00°C under the same standard solar irradiance of (1000 W/m^2). At Newry, it shows an efficiency drop of 2.04% when the ambient temperature increases from 23.50°C to 27.70°C while at Warrenpoint, it shows a drop of 1.94% when the ambient temperature increases from 18.90°C to 26.40°C

Relative humidity was found to strongly correlate with solar radiation intensity. In particular, climate prevailing at the PV array locations, higher humidity is synonymous with lower atmospheric transmittance due to higher atmospheric moisture content and cloud cover. This work corroborates the results of Brito et al [230] who also found a relationship between global solar radiation and radiation air humidity and Furlan et al [231] who demonstrated that the diffuse fraction of solar radiation increased with humidity.

The average system and array performance ratios for Harlequins, Newry and Warrenpoint show that they are proportional to the reference yields with strong correlations. For instance, the average system performance ratios recorded in Harlequins, Newry and Warrenpoint were 92.6%, 89.7% and 91.2% respectively while the average array performance ratios recorded in Harlequins, Newry and Warrenpoint were 94.4%, 91.3% and 93.0% respectively. Hence, the performance of the array shows there was no shading in the site locations. Fill factor (FF) is an indicator of finding the quality of PV arrays. The typical FF values range between 60% and 70% [227]. The PV arrays performed well firstly in the range above 70% (at a low solar cell temperature) and later below 70% (at a high solar cell temperature) across the three arrays monitored for five years. The least recorded FF values in Harlequins, Newry and Warrenpoint arrays across the five years are 61.3%, 64.89% and 66.03% respectively.

CHAPTER 4

DISAGGREGATING LONG-TERM PERFORMANCE DEGRADATION FROM TRANSIENT PERFORMANCE CHANGES

4.1 Assumptions

To carry out the measured performance degradation analysis, the following assumptions were made [232]:

1. PV degradation rates in the three arrays: Harlequins, Newry and Warrenpoint examined are linear because all the modules studied are operating in the flat part of their respective "bathtub" rates-of-failure curves.

2. the dominant parameter representing transient behaviour is cell temperature and solar irradiance. This is because PV systems performance parameters such as system efficiency and power output depend linearly on cell temperature and irradiance. Solar irradiance that is above 500 Wm^{-2} can cause the cell temperature to increase, thus, decreasing the efficiency and output power of the PV system [226], [227]. Hence, an increase in cell temperature will decrease the system efficiency and power output while a decrease in cell temperature will increase both efficiency and power output.

3. soiling is transient as there was regular surface cleaning from rain.

4.2 Temperature-Corrected Performance Ratio (PR$_{corr}$)

The performance ratio (PR) for solar photovoltaic installations normalises system output to installed capacity and available solar irradiance at the installation site, PR allows comparison of the performance of systems with different installed capacities in different geographical locations [233].

Weather-uncorrected performance ratio (PR$_{uncorr}$) is calculated using equation (54):

$$PR_{uncorr} = \frac{\sum P_{AC\_t}}{\sum_t [P_{STC}(\frac{G_{POA}}{G_{STC}})]} \times 100\% \qquad (54)$$

PR may be corrected for temperature [234], [235] by introducing a temperature correction to calculate a "temperature-corrected" PR_{corr};

$$PR_{corr} = \frac{\sum P_{AC\_t}}{\sum_t [P_{STC}(\frac{G_{POA}}{G_{STC}})(1-\frac{\beta}{100}(T_{cell\_avg}-T_{cell}))]} \qquad (55)$$

$$T_{cell\_avg} = \frac{\sum (G_{POA} \times T_{cell\_i})}{\sum G_{PAO\_i}} \qquad (56)$$

where;

P_{AC} is the measured AC electrical generation (W).

$P_{PV,rated}$ or P_{STC} is the installed PV module capacity (in this case 49920 W_p).

G_{POA} is the measured solar radiation intensity on the plane of array irradiance (W/m^2).

t is the data collection period.

G_{STC} is the irradiance at standard test conditions (1000 W/m^2).

T_{cell_avg} is the average annual PV cell temperature (^{o}C) shown in Table 35.

T_{cell} is the instantaneous PV cell temperature (^{o}C).

β is the Temperature coefficient of PV array power (-0.4%/^{o}C).

Average cell temperatures for 2021 across the three locations were noticed to be considerably higher than in 2017 to 2020 because of intense solar radiation brought by a heatwave in that year.

Table 35. Average annual PV cell temperatures for Harlequins, Newry and Warrenpoint Systems

Year	Harlequins	Newry	Warrenpoint
	Average cell Temperature, Tc_{ell_avg} (°C)	Average cell Temperature, Tc_{ell_avg} (°C)	Average cell Temperature, Tc_{ell_avg} (°C)
2017	37.87	37.21	37.09
2018	38.37	38.14	37.70
2019	39.95	37.14	36.09
2020	38.06	36.50	36.79
2021	39.98	39.76	39.68

Figures 65 (a-c) and Figures 66 (a-c) show seasonal variations in the performance ratios for the Harlequins, Newry and Warrenpoint PV arrays and systems from 2017 to 2021 data.

Weather-uncorrected performance ratios calculated using equation (54) show high seasonality with low values during warmer months and higher values during colder months [236]. Temperature-corrected PR calculated using equation (55) show introduction of the temperature correction reduces the seasonal performance ratio variation.
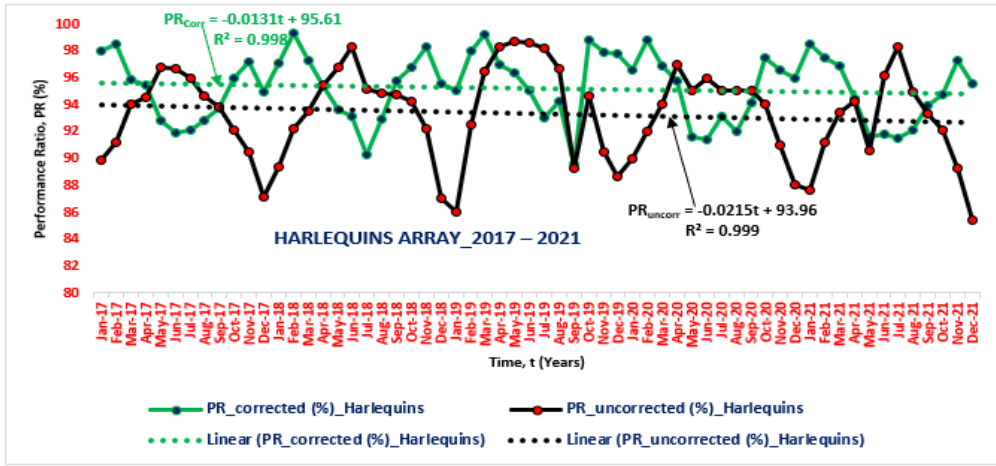
a.
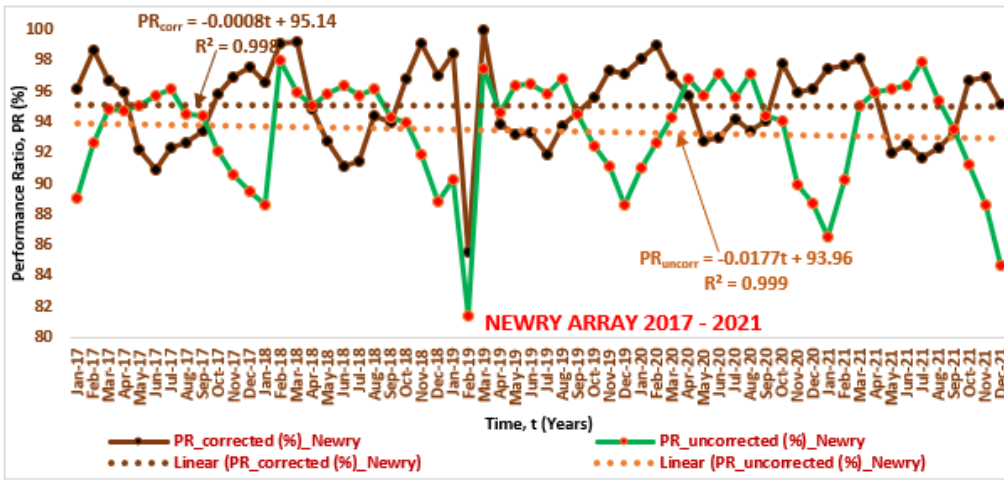
b.
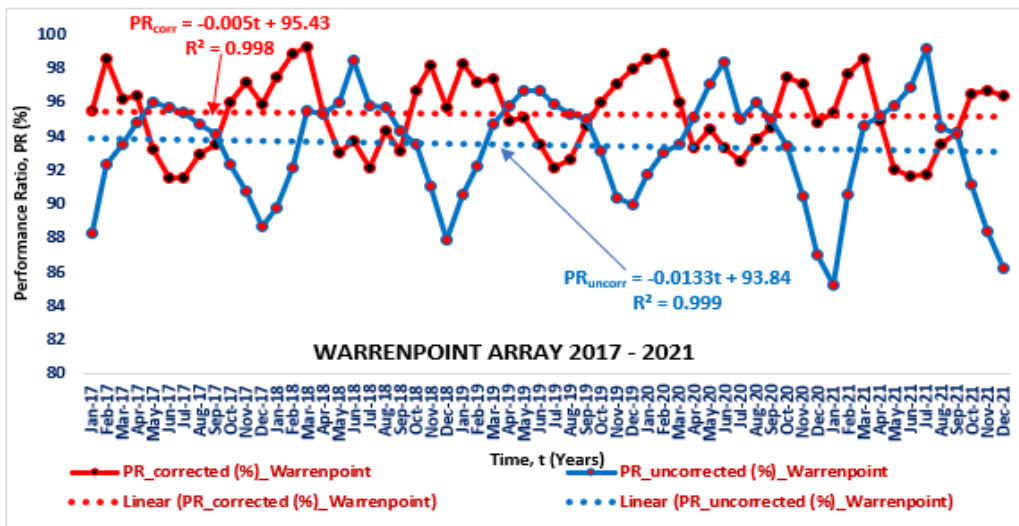
c.

Figure 65 (a-c). Weather-uncorrected and temperature-corrected PR for three arrays from 2017 to 2021

141
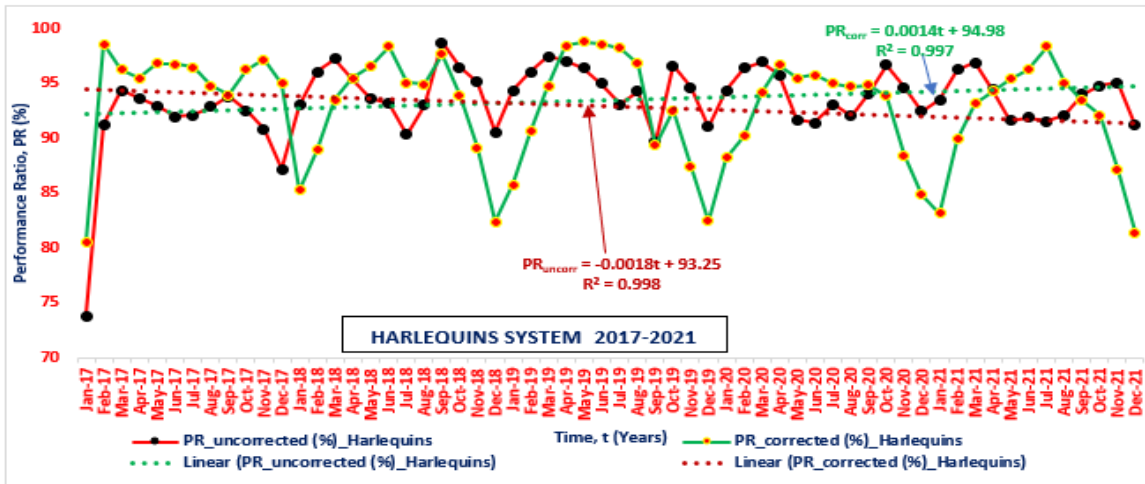
a.
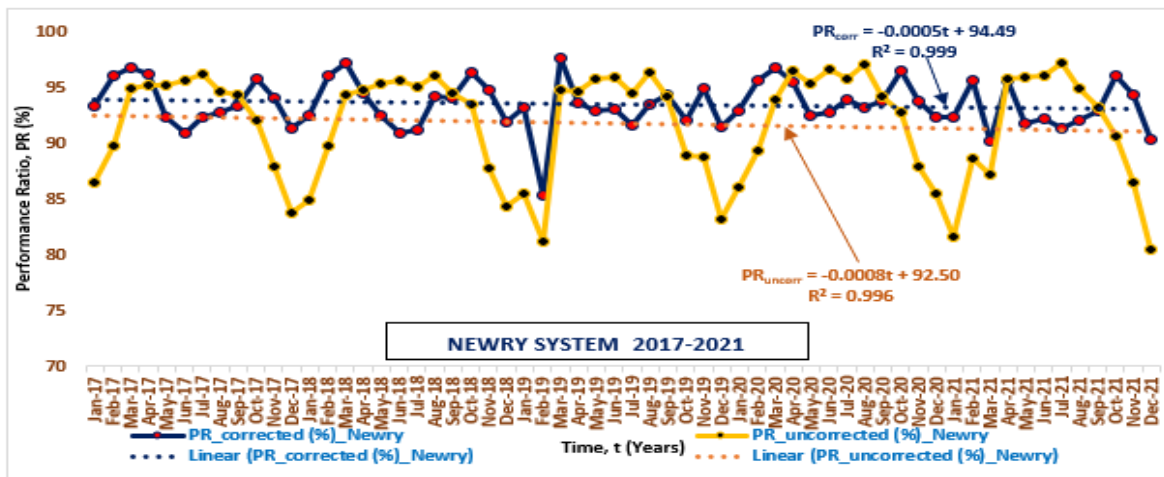
b.
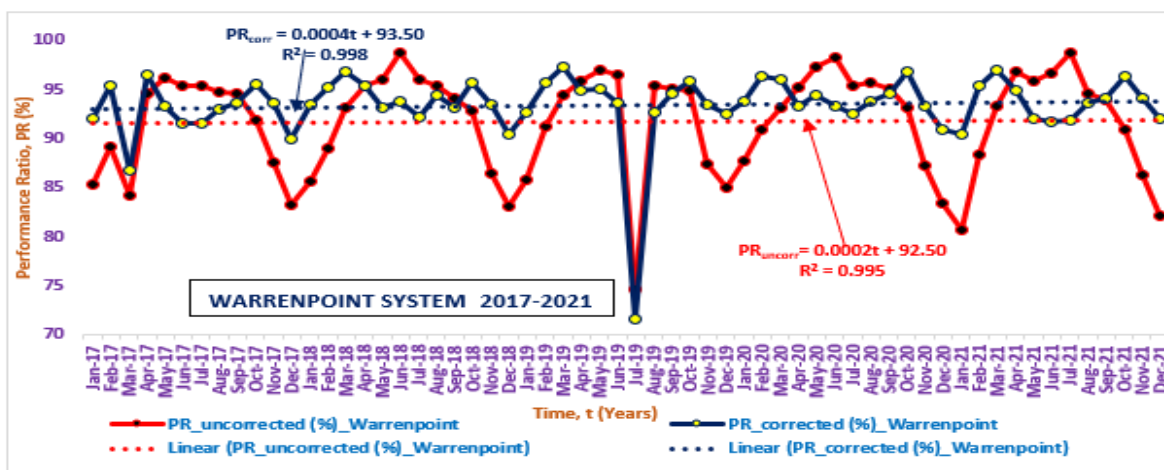
c.

Figure 66 (a-c). Weather-uncorrected and temperature-corrected PR for three systems from 2017 to 2021

142

The regression model for different elapsed periods from 2017 to 2021 across the three PV arrays and systems as shown in Figures 67 (a-c) and Figures 68 (a-c) shows the graphs of coefficient of determination (R^2) versus cumulative periods of evaluation for both weather-uncorrected and temperature-corrected R^2. The periods of evaluation were conducted semi-annually and it can be seen from Figures 67 (a-c) and Figures 68 (a-c) that temperature-corrected R^2 shows more performance than the weather-uncorrected R^2. Hence, using temperature-corrected performance ratios, long-term (in this case those seen after five-years operation) performance degradation trends become evident with high confidence after six months for one PV array and within three years for the two other arrays. If lower statistical confidence in trends is acceptable, long-term degradation rates can be identified within one year of operation for all PV arrays examined. This means that the temperature-correction has reduced the variation in seasonal performance ratio.
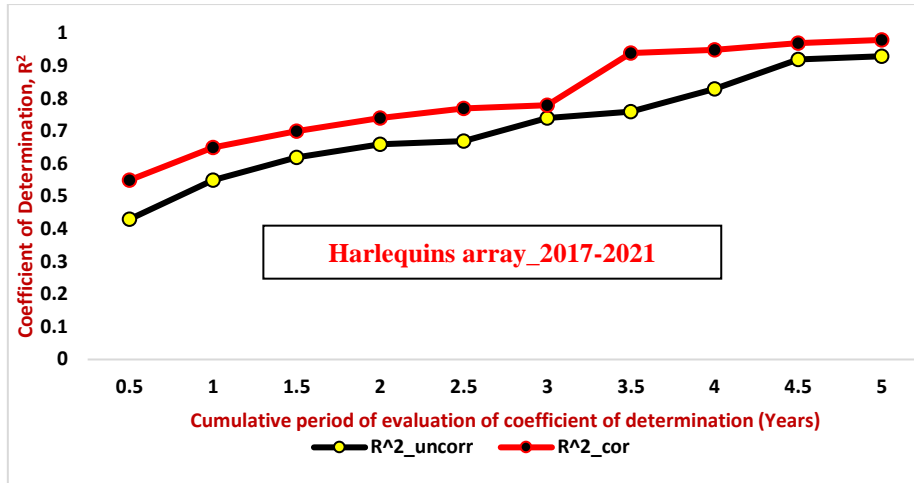
a.
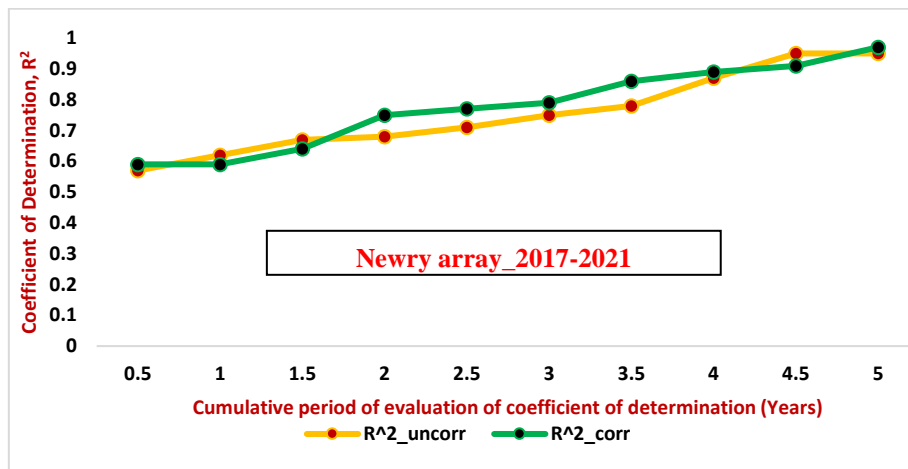
b.
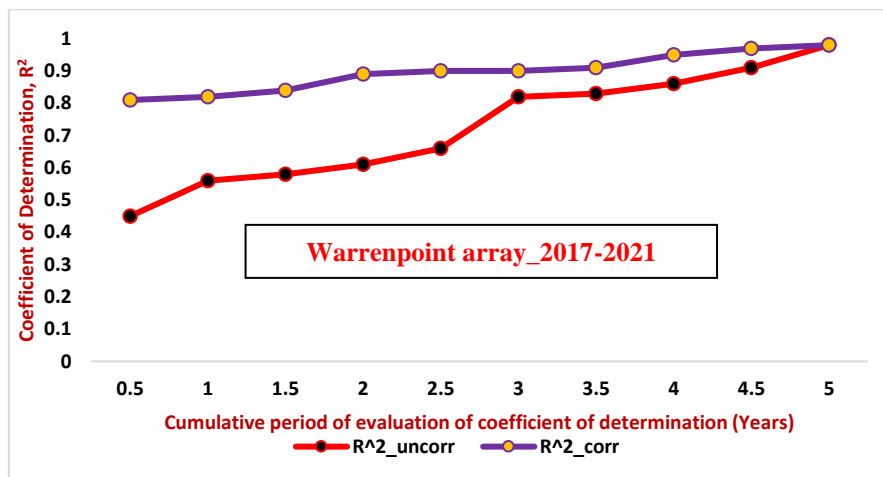
c.

Figure 67 (a-c). Influence of temperature-correction in reducing seasonal performance ratio variation in Harlequins, Newry and Warrenpoint arrays monitored over five years period.
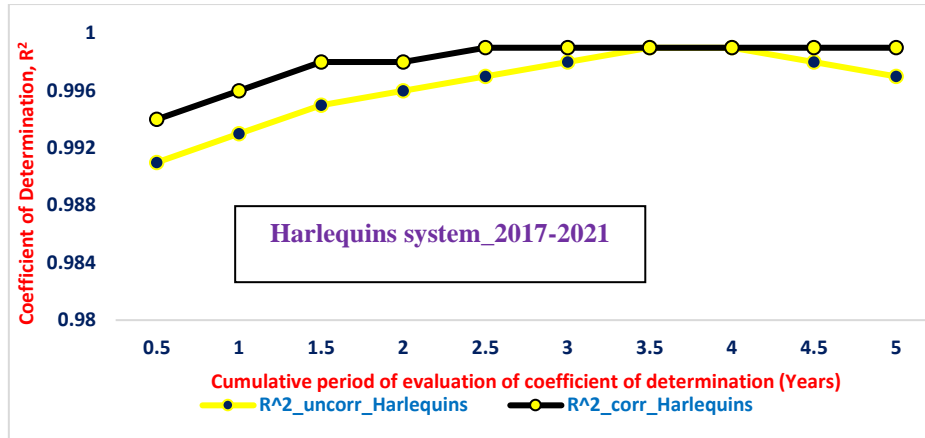
a.
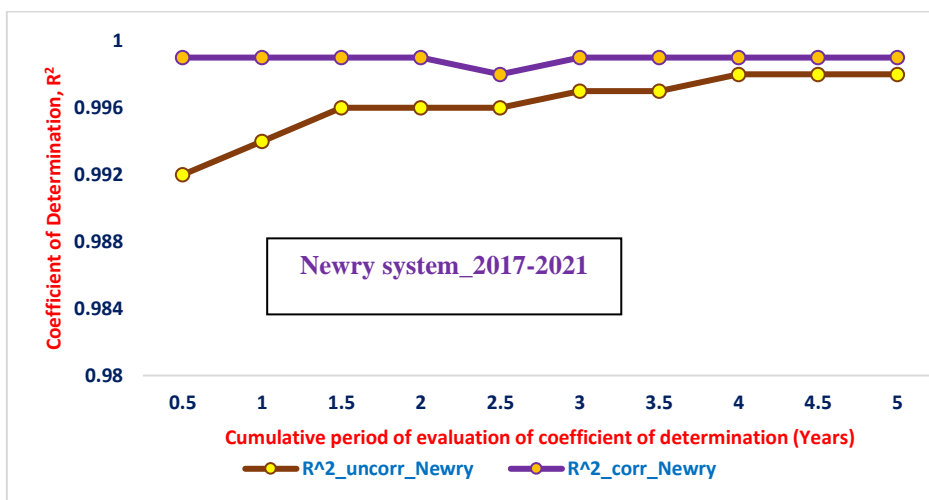
b.
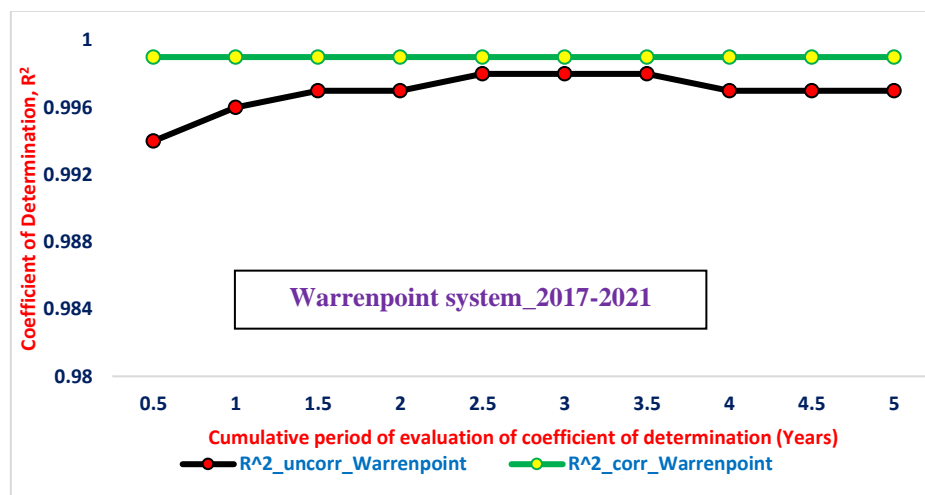
c.

Figure 68 (a-c). Influence of temperature-correction in reducing seasonal performance ratio variation in Harlequins, Newry and Warrenpoint systems monitored over five years period.
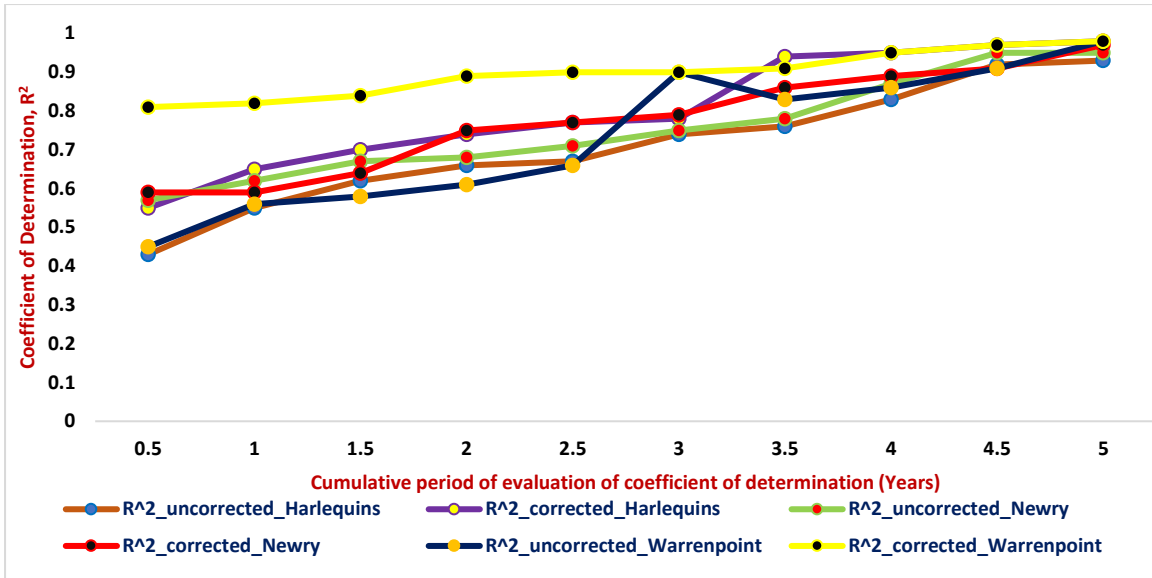
Figure 69. Elapsed time to reach a 0.810 coefficient of determination (R2) on the long-term PV array degradation trend.
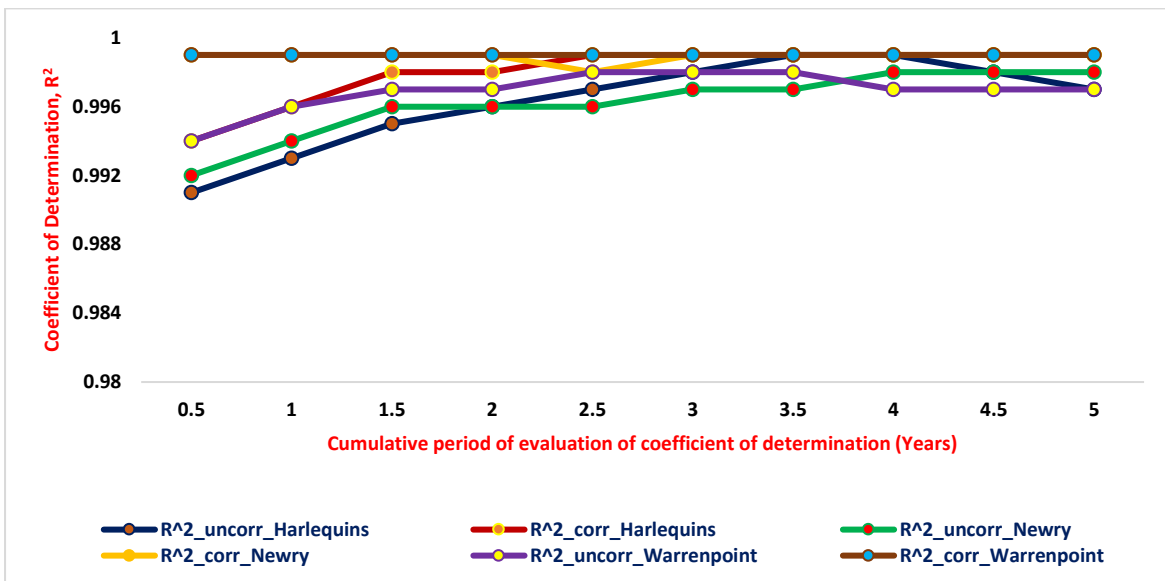
Figure 70. Elapsed time to reach a 0.999 coefficient of determination (R2) on the long-term PV system degradation trend.

Data that shows a high coefficient of determination (R^2) to a linear trend would indicate that the trend line could be reliably extrapolated. A coefficient of determination (R^2) of 0.810 and 0.999 is chosen as values indicative of a strongly correlating data set.

In Figures 69 and 70, the improvements in coefficients of determination (R^2) for PR are calculated over different cumulative elapsed times (shown in Figures 67 and 68) are shown together. As can be seen, the temperature-corrected PR values reach the 0.810 and 0.999 coefficients of determination (R^2) after cumulative degradation trends evaluation periods of between 6 months (for the Warrenpoint PV array and system) to approximately 3 years for the Harlequins and Newry PV arrays and systems. "Weather-uncorrected" PR values require longer elapsed accumulative evaluation periods (approximately 4 years) to reach 0.810 and 0.999 coefficients of determination on their long-term degradation trends.

This result indicates that long-term degradation trends become evident sooner using temperature-corrected PR values.

4.3 Performance loss rate of PV system

Relative performance loss rate and absolute performance loss rate are two alternative ways of computing the rate of performance loss [237]. Relative performance loss rate, PLR_{rel} is defined as;

$$PLR_{rel} = (\beta_1 \frac{t}{\beta_o}) \times 100 \qquad (57)$$

Where;

β_1 is the gradient and β_o is the y-intercept of the linear trend line for PLR.

t is a scaling parameter that converts the time scale at which power or performance ratio (PR) is observed to a yearly scale, as PLR (%/a) is per year (12 months).

Absolute performance loss rate PLR_{abs} is given by

$$PLR_{abs} = (\beta_1 \times t) \qquad (58)$$

Absolute PLR in equation (58) is independent of the initial yield. A fitting parameter βo must be also given [238]. The unit of PLR_{abs} is metric/annum (/a).

147

To investigate long-term degradation, annual average five-year relative performance loss rates (PLR_{rel}), absolute relative loss rates (PLR_{abs}) and the non-linear trends were fitted to simple linear best-fit lines. The weather-uncorrected and temperature-corrected annual monthly relative and absolute performance loss rates from Harlequins, Newry and Warrenpoint arrays and systems from 2017 to 2021, the gradient (β_1) and the y-intercept (β_o) of each year across the three arrays and systems were found using the time series (Yt) linear regression model (59) [236]:

$$Y_t = \beta_1 t + \beta_o \qquad\qquad (59)$$

An annual aggregated gradient (β_1) of the linear fit, divided by the y-intercept (β_o) gives the final linear relative performance loss rate (PLR_{rel}) of the PV systems at Harlequins, Newry and Warrenpoint. The annual aggregated gradient (β_1) of the linear function multiplied by the yearly scale (12 months) gives the final linear absolute performance loss rates (PLR_{abs}) (see Equation 58).

The y-intercept (β_o) shows PR values for the five-year weather-uncorrected and temperature-corrected values for the Harlequins array (93.96% and 95.61%) and system (93.25% and 94.98%), Newry array (93.96% and 95.14%) and system (92.50% and 94.49%) and Warrenpoint array (93.84% and 95.43%) and system (92.50% and 93.50%) are almost constant.

The relative performance loss rates (PLR_{rel}) and absolute performance loss rates (PLR_{abs}) for the Harlequins, Newry and Warrenpoint arrays and systems as shown in Figures 71 – 72 are summarised in Tables 36 – 39.

Where Arr. is the PV array and Sys. Is the PV system.

Table 36. Temperature-correction for relative performance loss rates (PLR$_{rel}$) for Harlequins, Newry and Warrenpoint arrays and systems

Harlequins		Observation	Newry		Observation	Warrenpoint		Observation
Arr. PLR$_{rel}$ (%/a)	Sys. PLR$_{rel}$ (%/a)	This means that PLR$_{rel}$ of the Harlequins array shows that solar panel generation will increase at the annual rate by -0.27%/a which shows an improvement while PLR$_{rel}$ of the Harlequins system shows that PV system generation will decrease at the annual rate of 0.018%/a.	Array PLR$_{rel}$ (%/a)	Sys. PLR$_{rel}$ (%/a)	There are improvements in both the Newry array and system. For this reason, both the PLR$_{rel}$ for the Newry array and system shows that they will both increase at the annual rates by -0.23%/a and -0.00635%/a respectively.	Arr. PLR$_{rel}$ (%/a)	Sys. PLR$_{rel}$ (%/a)	The PLR$_{rel}$ in Warrenpoint array shows that there is an improvement in the array. This means that solar panel generation will increase at an annual rate of -0.17%/a while the PLR$_{rel}$ in the Warrenpoint system shows that PV system generation will decrease at the annual rate of 0.00514%/a.
-0.27	0.018		-0.23	-0.00635		-0.17	0.00514	

Table 37. Temperature-correction for absolute performance loss rates (PLR$_{abs}$) for Harlequins, Newry and Warrenpoint arrays and systems

Harlequins		Observation	Newry		Observation	Warrenpoint		Observation
Arr. PLR$_{abs}$ (/a)	Sys. PLR$_{abs}$ (/a)	The PLR$_{abs}$ of the Harlequins array show that solar panel generation will increase at the annual rate of -0.26/a which shows an improvement while the PLR$_{abs}$ of the Harlequins system shows that PV system generation will decrease at the annual rate of 0.017/a.	Arr. PLR$_{abs}$ (/a)	Sys. PLR$_{abs}$ (/a)	Both the Newry array and system show improvements. This means that their PLR$_{abs}$ will increase at the annual rates by -0.21/a and -0.006/a respectively.	Arr. PLR$_{abs}$ (/a)	Sys. PLR$_{abs}$ (/a)	Warrenpoint array shows a PLR$_{abs}$ improvement while the Warrenpoint system shows a decrease in PLR abs. This shows that solar panel generation will increase at an annual rate of -0.16/a while the Warrenpoint system shows that PV system generation will decrease at an annual rate of 0.0048/a.
-0.26	0.017		-0.21	-0.006		-0.16	0.0048	

Table 38. Weather-uncorrected relative performance loss rates (PLR_rel) for Harlequins, Newry and Warrenpoint arrays and systems

Harlequins		Observation	Newry		Observation	Warrenpoint		Observation
Arr. PLR_rel (%/a)	Sys. PLR_rel (%/a)	Both the Harlequins array and system showed an improvement at their PLR_rel. This shows that solar panel and PV generations will increase at annual rates of -0.16%/a and -0.023%/a respectively. This will be difficult to predict any PLR_rel in the PV array and system due to the seasonal variation effect noticed in weather-uncorrected relative performance loss rates. To resolve this, the weather-uncorrected PLR_rel are normalised with the average cell temperature.	Array PLR_rel (%/a)	Sys. PLR_rel (%/a)	There are improvements in the Newry array and system. For this reason, their PLR_rel shows that both the Newry array and system will increase at the annual rates by -0.01%/a and -0.00104%/a respectively. Just like the Harlequins array and system, it will be difficult to predict any PLR_rel in the PV array and system due to the seasonal variation effect noticed in weather-uncorrected relative performance loss rates. To resolve this, the weather-uncorrected PLR_rel are normalised with the average cell temperature.	Arr. PLR_rel (%/a)	Sys. PLR_rel (%/a)	There is an improvement in the Warrenpoint array and a decrease in the Warrenpoint system. This shows that solar panel generation will increase at an annual rate by -0.063%/a while the Warrenpoint system shows that PV system generation will decrease at the annual rate of 0.00259%/a.
-0.16	-0.023		-0.01	-0.00104		-0.063	0.00259	

Table 39. Weather-uncorrected absolute performance loss rates (PLR_abs) for Harlequins, Newry and Warrenpoint arrays and systems

Harlequins		Observation	Newry		Observation	Warrenpoint		Observation
Arr. PLR_abs (/a)	Sys. PLR_abs (/a)	Both the Harlequins array and system show improvements in PLR_abs. This show that solar panel and PV generations will increase at annual rates of -0.15/a and -0.022/a. Just like PLR_rel in the Harlequins array and system, it will be difficult to predict any PLR_rel in the PV array and system due to the seasonal variation effect noticed in weather-uncorrected relative performance loss rates. To resolve this, the weather-uncorrected PLR_rel are normalised with the average cell temperature.	Arr. PLR_abs (/a)	Sys. PLR_abs (/a)	There are improvements in both the Newry array and system. This means that their PLR_abs show that both the Newry array and system will increase at the annual rates by -0.0096/a and -0.0096/a respectively. Just like the Newry array and system, it will be difficult to predict any PLR_rel in the PV array and system due to the seasonal variation effect noticed in weather-uncorrected relative performance loss rates. To resolve this, the weather-uncorrected PLR_rel are normalised with the average cell temperature.	Arr. PLR_abs (/a)	Sys. PLR_abs (/a)	Performance improvement is noticed in the Warrenpoint array and there is a decrease in performance in the Warrenpoint system. This means that solar panel generation will increase at an annual rate of -0.06/a while the Warrenpoint system shows that PV system generation will decrease at the annual rate of 0.0024/a.
-0.15	-0.022		-0.0096	-0.0096		-0.06	0.0024	

Figure 71. Five-year monitored data showing performance loss rates from 2017 to 2021 at Harlequins, Newry and Warrenpoint arrays
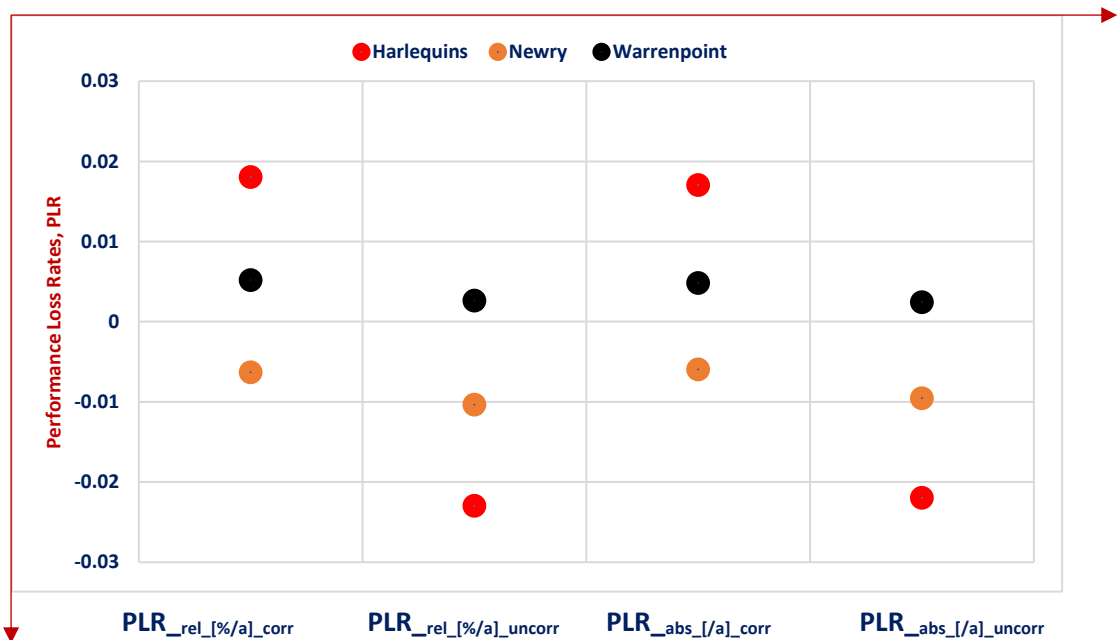
Figure 72. Five-year monitored data showing performance loss rates from 2017 to 2021 at Harlequins, Newry and Warrenpoint systems.

From Figures 71 and 72, the performance loss rates differ in the three PV arrays and PV systems because of differences in their meteorological conditions (such as the ambient temperature, relative humidity, wind speed and air pressure) and system conditions (solar cell temperature, and solar radiation).

Figures 73 and 75 (a-b) show the analyses of the annual relative performance loss rate (PLR_{rel}) and absolute performance loss rate (PLR_{abs}) of Harlequins, Newry and Warrenpoint arrays and systems for five years. The system losses seen are a result of solar cell temperature losses, DC/AC inverter efficiencies conversion losses, and solar radiation reflection losses.

Figures 74 (a-b) and 76 (a-b) shows the difference between the temperature-corrected and weather-uncorrected relative and absolute performance losses which are computed using (60) and (61):

$$D_{PLRcorr} = PLR_{rel.corr} - PLR_{abs.corr} \qquad (60)$$
$$D_{PLRuncorr} = PLR_{rel.uncorr} - PLR_{abs.uncorr} \qquad (61)$$

where;

$D_{PLRcorr}$ and $D_{PLRuncorr}$ are differences in temperature-corrected and weather-uncorrected performance loss rates in arrays and systems (in per annum).

$PLR_{rel.corr}$ and $PLR_{rel.uncorr}$ are relative temperature-corrected and weather-uncorrected performance loss rates in arrays and systems.

$PLR_{abs.corr}$ and $PLR_{abs.uncorr}$ are absolute temperature-corrected and weather-uncorrected performance loss rates in arrays and systems.
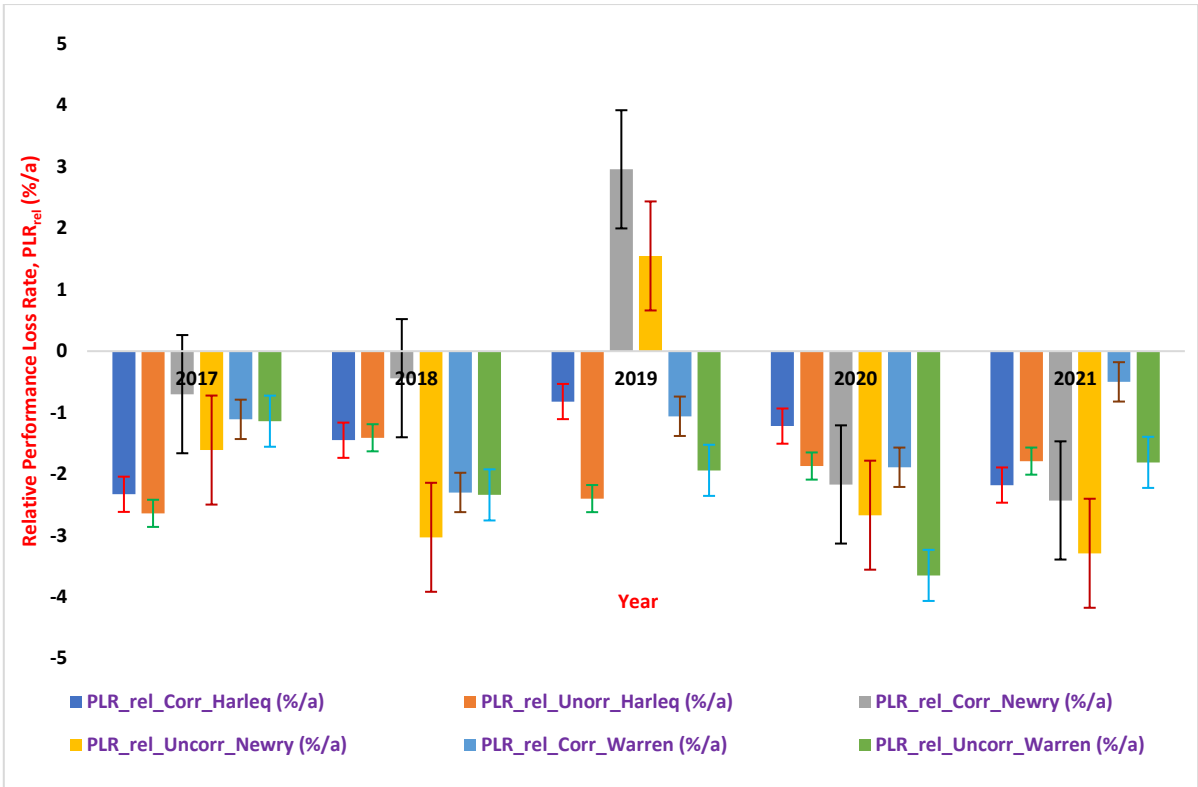
a.
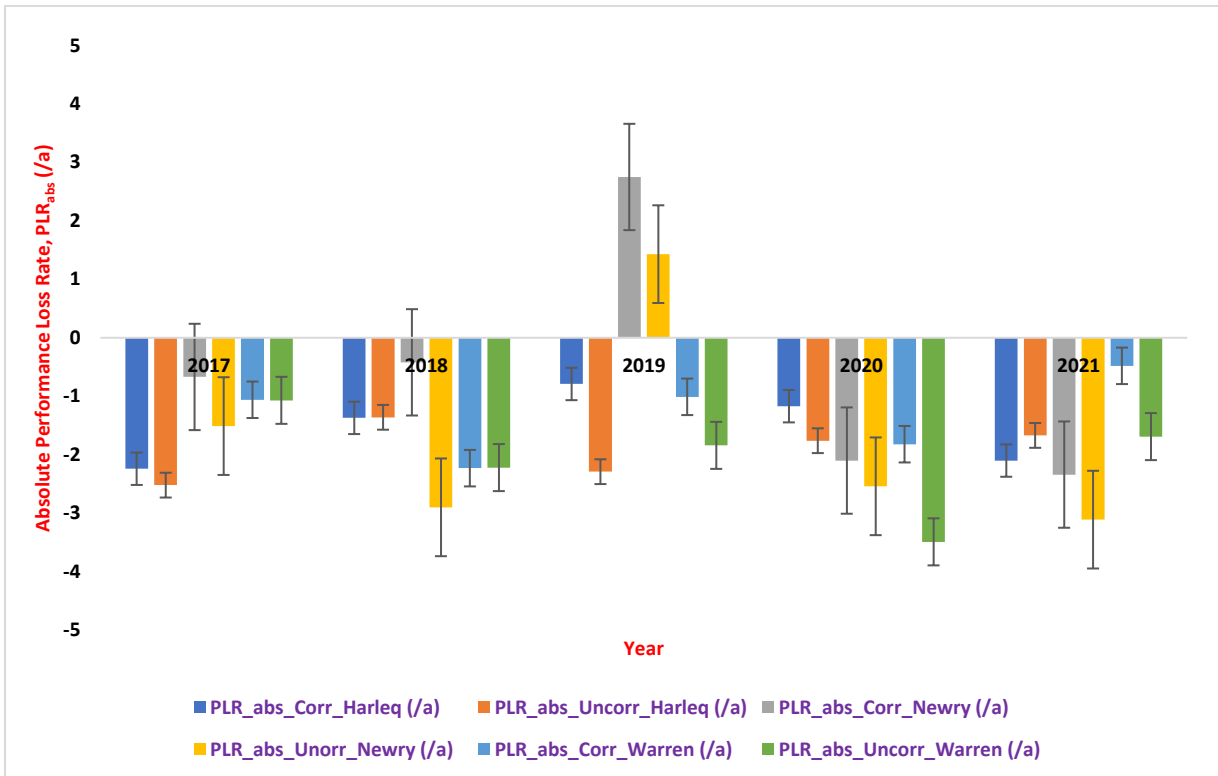
b.

Figure 73. Relative performance loss rate (PLRrel) and (b) Absolute performance loss rate

(PLRabs) for Harlequins, Newry and Warrenpoint arrays from 2017 to 2021.
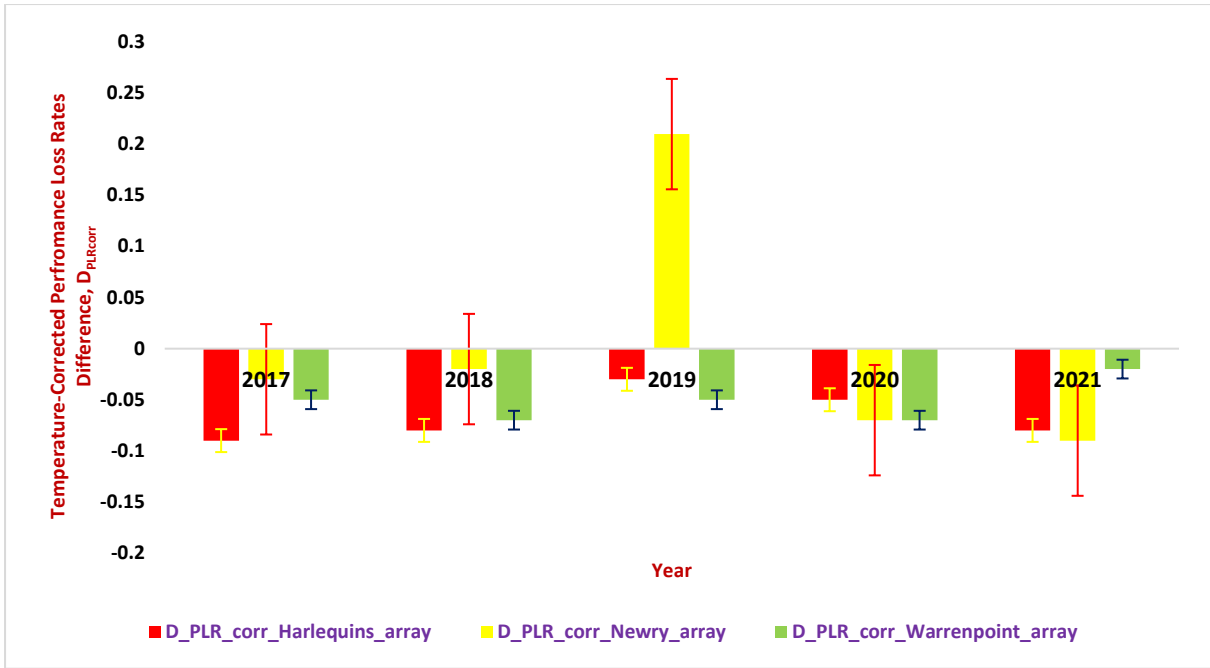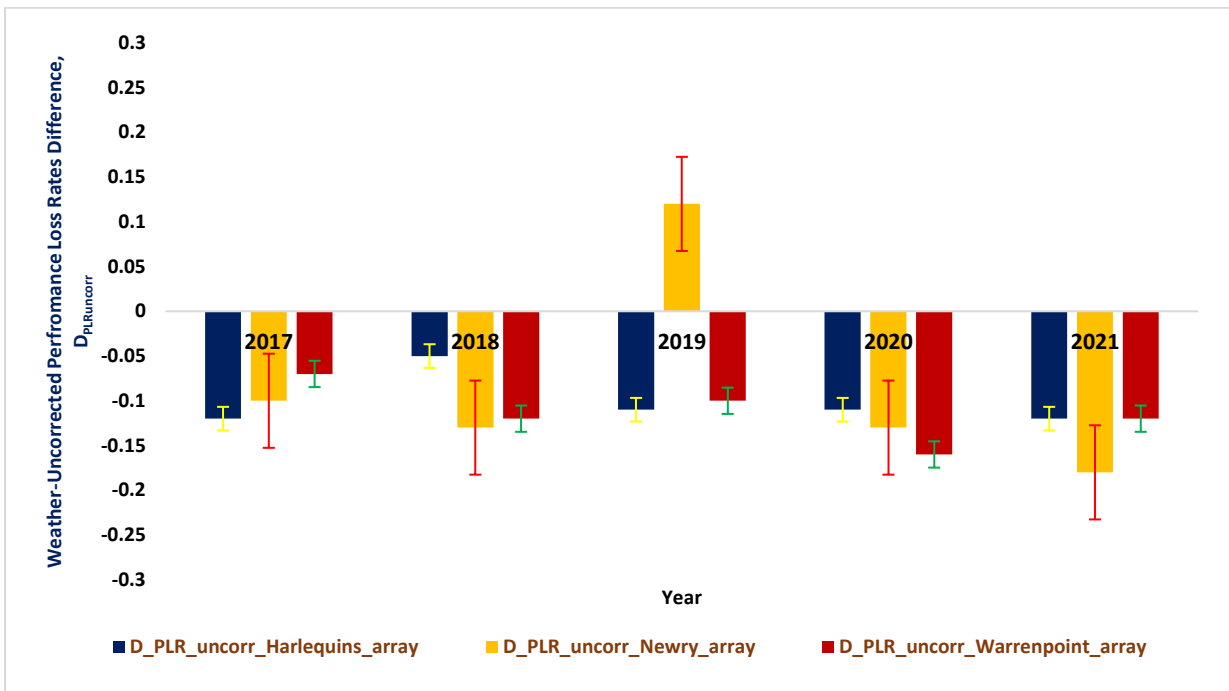
Figure 74. Difference in (a) temperature-correction (b) uncorrected performance loss rates between relative and absolute performance loss rates in Harlequins, Newry and Warrenpoint arrays from 2017 to 2021.
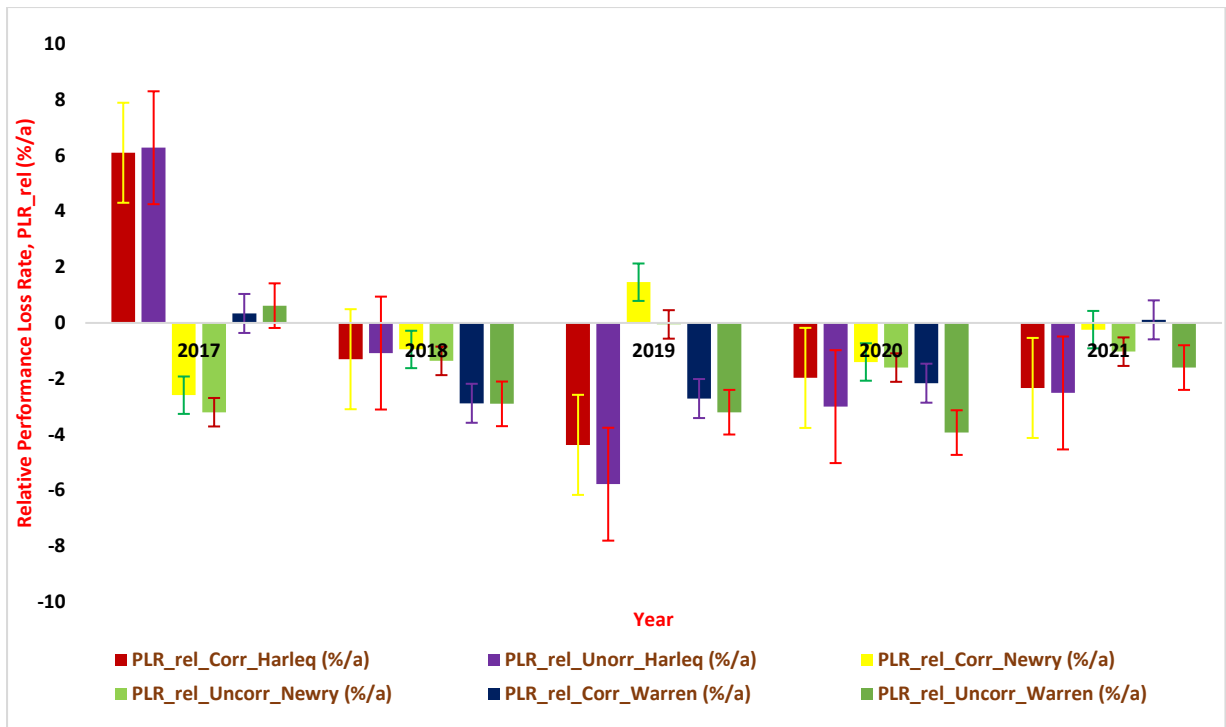
a.
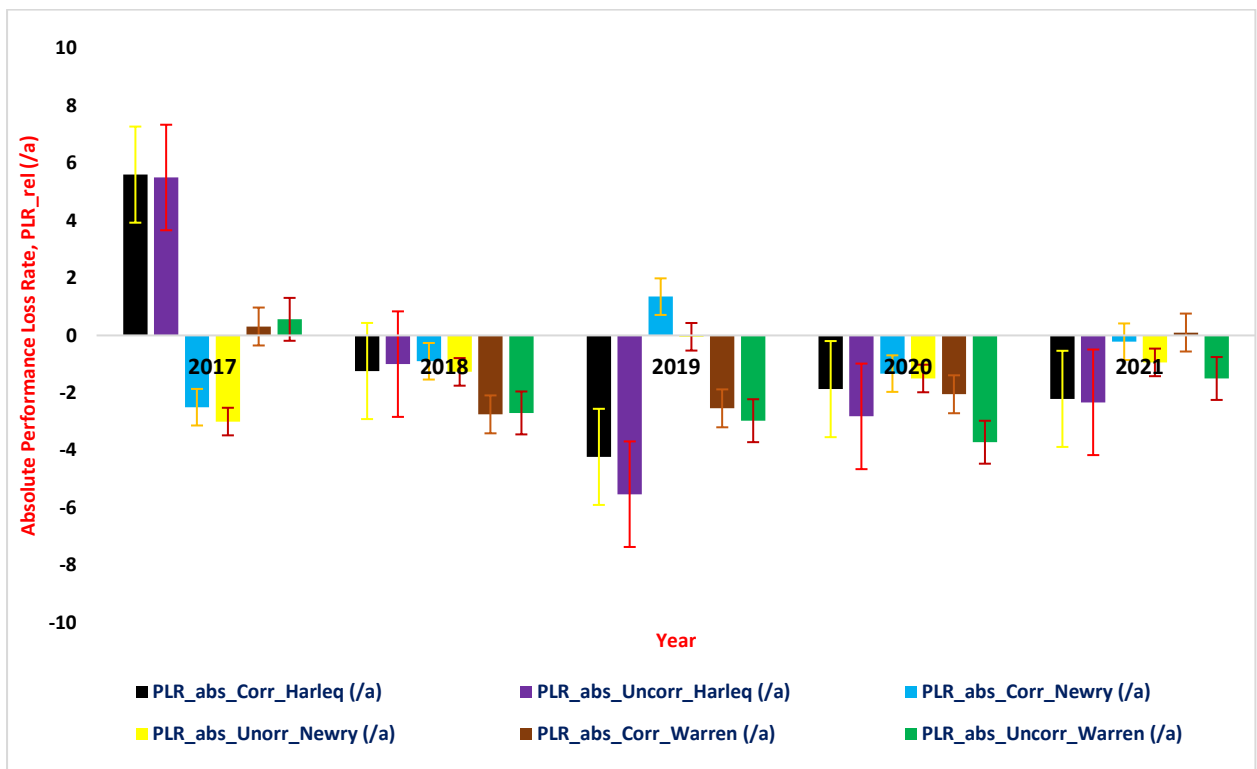
b.

Figure 75. Relative performance loss rate (PLR$_{rel}$) and (b) Absolute performance loss rate (PLR$_{abs}$) for Harlequins, Newry and Warrenpoint systems from 2017 to 2021.
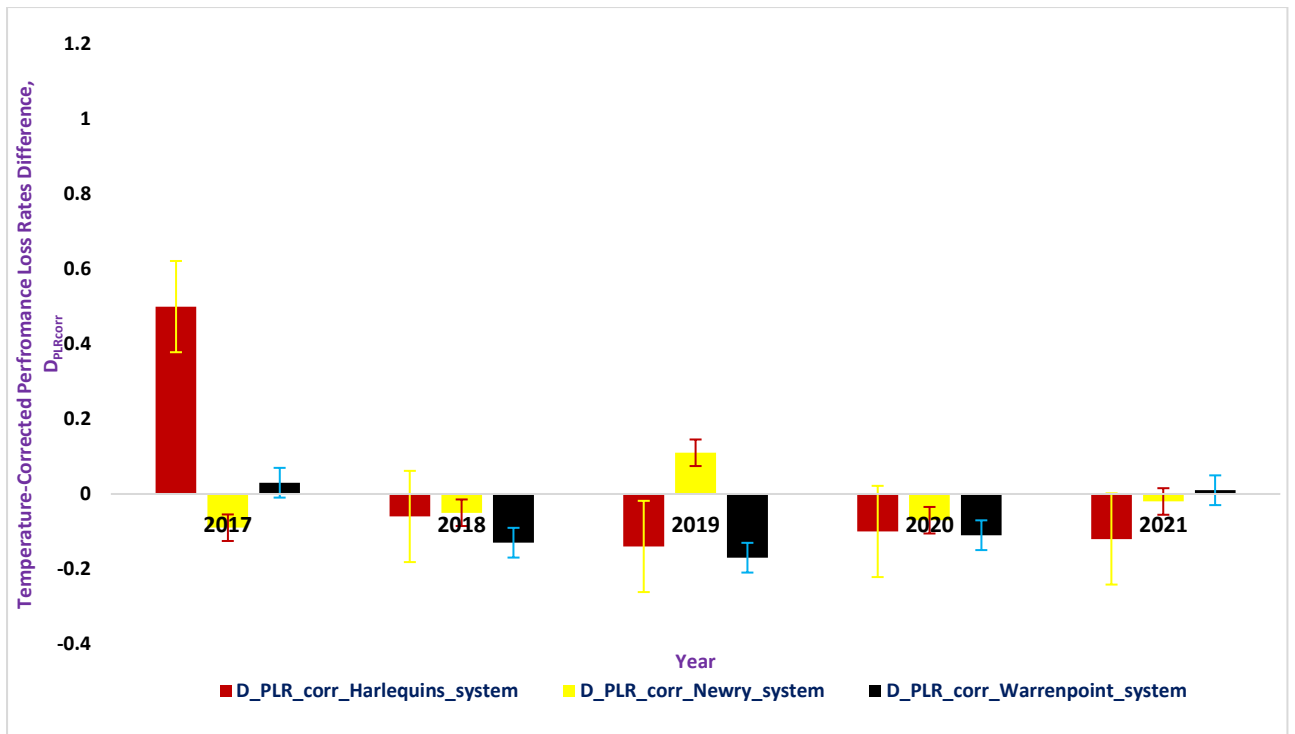
a.
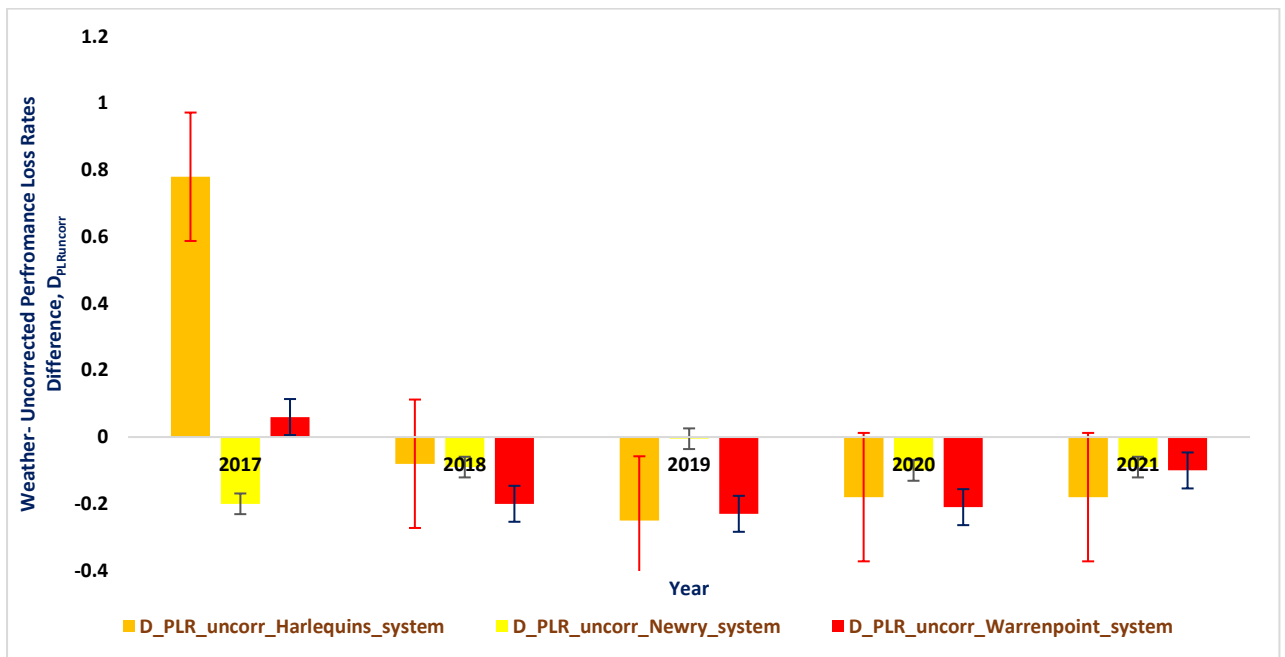
b.

Figure 76. Difference in (a) temperature-correction (b) uncorrected performance loss rates between relative and absolute performance loss rates in Harlequins, Newry and Warrenpoint systems from 2017 to 2021.

AC output energy loss due to PLR_{rel} and PLR_{abs} for temperature-corrected and weather-uncorrected PR in Harlequins, Newry and Warrenpoint sites are summarised in Tables 40-43.

Table 40. AC energy output loss and PLR_{rel} for temperature-corrected PR in Harlequins, Newry and Warrenpoint arrays

	Harlequins			Newry			Warrenpoint		
Year	PLR_{rel} [%/a]	E_{total} [kWh]	E_{Loss} [kWh/a]	PLR_{rel} [%/a]	E_{total} [kWh]	E_{Loss} [kWh/a]	PLR_{rel} [%/a]	E_{total} [kWh]	E_{Loss} [kWh/a]
2017	-2.64	234710.60	-6196.36	-1.61	238140	-3834.05	-1.13	229688	-2595.47
2018	-1.41	246968.92	-3482.26	-3.03	242552	-7349.33	-2.34	231161	-5409.17
2019	-2.40	268097.00	-6434.33	1.55	243548	3775.00	-1.94	229342	-4449.23
2020	-1.87	256102.00	-4789.11	-2.67	239297	-6389.23	-3.65	237452	-8667.00
2021	-1.79	243417.00	-4357.16	-3.30	237455	-7836.02	-1.81	233342	-4223.49

Table 41. AC energy output loss and PLR_{rel} for weather-uncorrected PR in Harlequins, Newry and Warrenpoint arrays

	Harlequins			Newry			Warrenpoint		
Year	PLR_{rel} [%/a]	E_{total} [kWh]	E_{Loss} [kWh/a]	PLR_{rel} [%/a]	E_{total} [kWh]	E_{Loss} [kWh/a]	PLR_{rel} [%/a]	E_{total} [kWh]	E_{Loss} [kWh/a]
2017	-2.33	234710.60	-5468.76	-0.70	238140	-1667.00	-1.11	229688	-2549.54
2018	-1.50	246968.92	-3704.53	-0.44	242552	-1067.23	-2.31	231161	-5339.82
2019	-0.82	268097.00	-2198.40	2.96	243548	7209.02	-1.06	229342	-2431.03
2020	-1.22	256102.00	-3124.44	-2.17	239297	-5192.74	-1.90	237452	-4511.59
2021	-2.18	243417.00	-5306.49	-2.43	237455	-5770.16	-0.50	233342	-1166.71

Table 42. AC energy output loss and PLR_{abs} for temperature-corrected PR in Harlequins, Newry and Warrenpoint arrays

	Harlequins			Newry			Warrenpoint		
Year	PLR_{abs} [/a]	E_{total} [kWh]	E_{Loss} [kWh/a]	PLR_{abs} [/a]	E_{total} [kWh]	E_{Loss} [kWh/a]	PLR_{abs} [/a]	E_{total} [kWh]	E_{Loss} [kWh/a]
2017	-2.49	234710.6	-5844.29	-1.52	238140	-3619.73	-1.05	229688	-2411.72
2018	-1.35	246968.92	-3334.08	-2.90	242552	-7034.01	-2.22	231161	-5131.77
2019	-2.29	268097.00	-6139.42	1.43	243548	3482.74	-1.84	229342	-4219.89
2020	-1.76	256102.00	-4507.40	-2.54	239297	-6078.14	-3.49	237452	-8287.07
2021	-1.67	243417.00	-4065.06	-3.11	237455	-7384.85	-1.70	233342	-3966.81

Table 43. AC energy output and PLR_{abs} for weather-uncorrected PR in Harlequins, Newry and Warrenpoint arrays

	Harlequins			Newry			Warrenpoint		
Year	PLR_{abs} [/a]	E_{total} [kWh]	E_{Loss} [kWh/a]	PLR_{abs} [/a]	E_{total} [kWh]	E_{Loss} [kWh/a]	PLR_{abs} [/a]	E_{total} [kWh]	E_{Loss} [kWh/a]
2017	-2.24	234710.6	-5257.52	-0.67	238140	-1595.54	-1.06	229688	-2434.69
2018	-1.37	246968.92	-3383.47	-0.42	242552	-1018.72	-2.24	231161	-5178.00
2019	-0.79	268097.00	-2118.0	2.75	243548	6697.57	-1.01	229342	-2316.35
2020	-1.16	256102.00	-2970.78	-2.10	239297	-5025.24	-1.83	237452	-4345.37
2021	-2.08	243417.00	-5063.07	-2.34	237455	-5556.45	-0.48	233342	-1120.04

To normalise relative and absolute temperature-corrected performance loss rate, PLR$_{corr}$ from weather-uncorrected performance loss rate, PLR$_{uncorr}$ the average cell temperatures as shown in Table 35 for each PV array installed at Harlequins, Newry and Warrenpoint are used. Hence the PLR$_{corr}$ for PLR$_{rel}$ and PLR$_{abs}$ are normalised using equations (62) and (63).

$$\text{PLR}_{corr\_rel} = \frac{\text{PLR}_{uncorr\_rel}}{1 - \frac{\delta}{100}(\text{Tcell}_{avg})} \tag{62}$$

$$\text{PLR}_{corr\_abs} = \frac{\text{PLR}_{uncorr\_abs}}{1 - \frac{\delta}{100}(\text{Tcell}_{avg})} \tag{63}$$

Figures 77-78 show the graphs of temperature-corrected relative performance loss rates, PLR$_{corr.rel}$ and temperature-corrected absolute performance loss rates, PLR$_{corr.abs}$ across the three arrays and systems. The standard deviation error bars in these Figures are overlapped because of the closeness of their standard deviation values as shown in Tables 44 to 45.

Table 44. Relative and Absolute average and standard deviation values of temperature-corrected performance loss rates in arrays.

Harlequins				Newry				Warrenpoint			
μ_{rel}	σ_{rel}	μ_{abs}	σ_{abs}	μ_{rel}	σ_{rel}	μ_{abs}	σ_{abs}	μ_{rel}	σ_{rel}	μ_{abs}	σ_{abs}
-1.75	0.44	-1.66	0.41	-1.00	2.17	-1.99	0.66	-1.89	0.81	-1.79	0.79

Table 45. Relative and Absolute average and standard deviation values of temperature-corrected performance loss rates in systems.

Harlequins				Newry				Warrenpoint			
μ_{rel}	σ_{rel}	μ_{abs}	σ_{abs}	μ_{rel}	σ_{rel}	μ_{abs}	σ_{abs}	μ_{rel}	σ_{rel}	μ_{abs}	σ_{abs}
-1.04	3.91	-1.06	3.57	-1.26	1.00	-1.17	0.94	-1.91	1.56	-1.79	1.46

where μ_{rel} and μ_{abs} are relative and absolute averages of the temperature-corrected performance loss rates while σ_{rel} and σ_{abs} are relative and absolute standard deviations of the temperature-corrected performance loss rates.
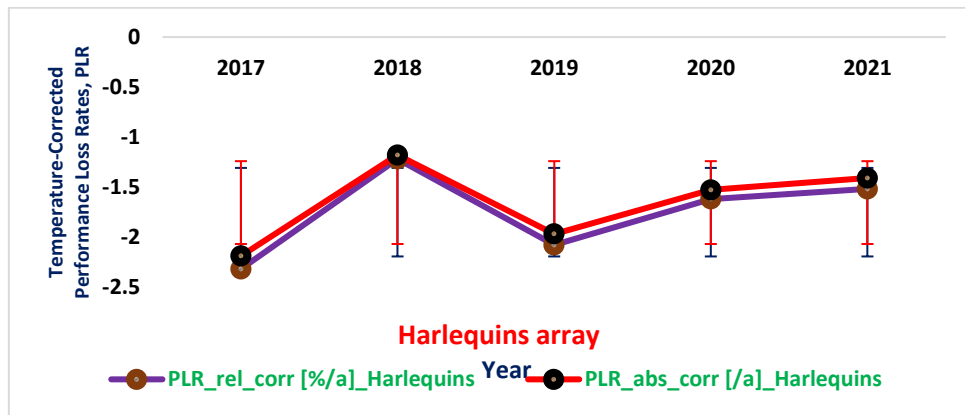
a.
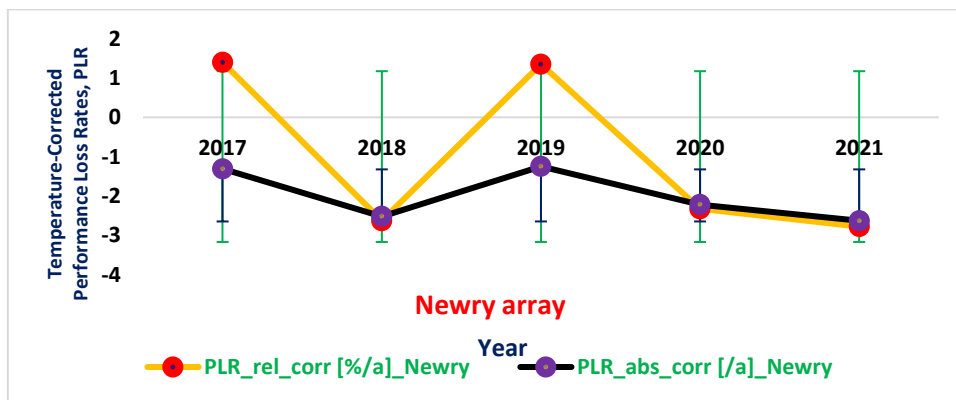
b.
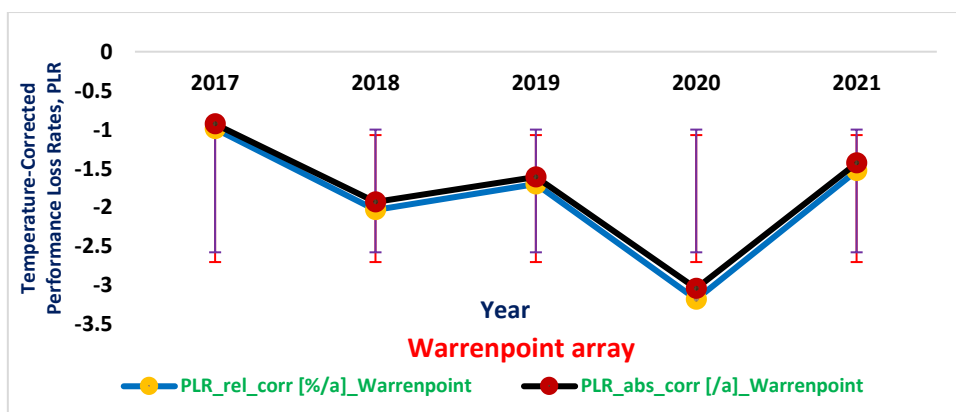
c.

Figure 77 (a-c). Standard deviation error bars show the overlap between relative and absolute temperature-corrected performance loss rates of PV arrays monitored for five years period.
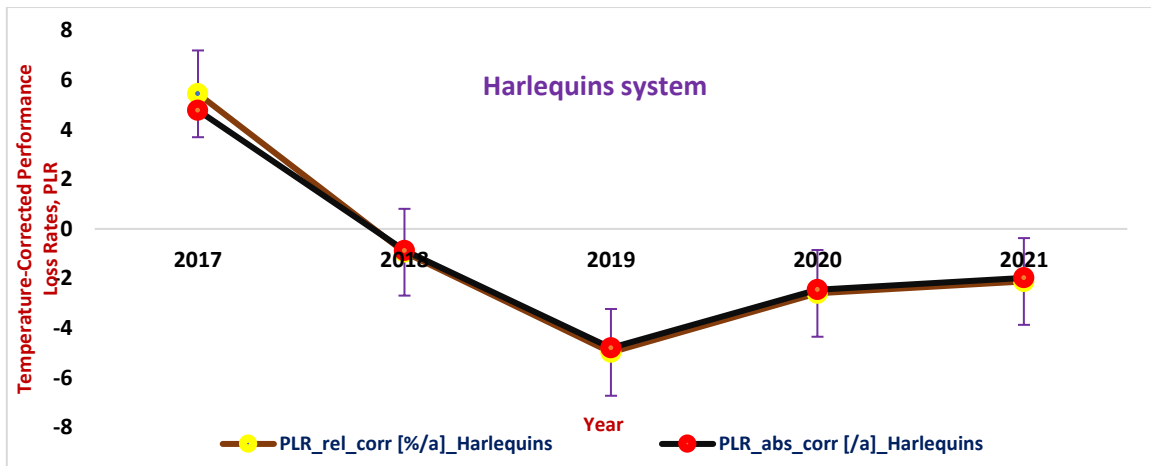
a.
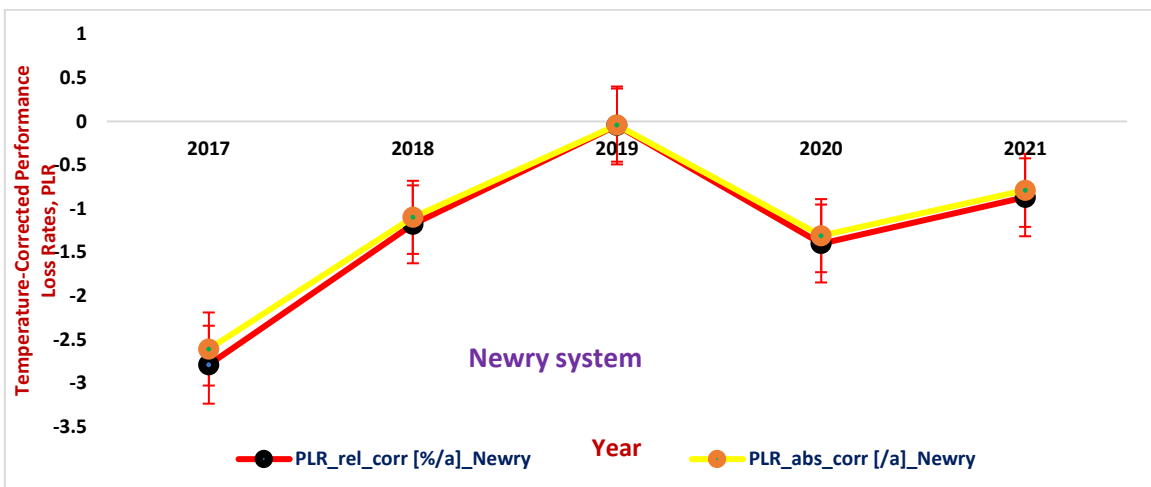
b.
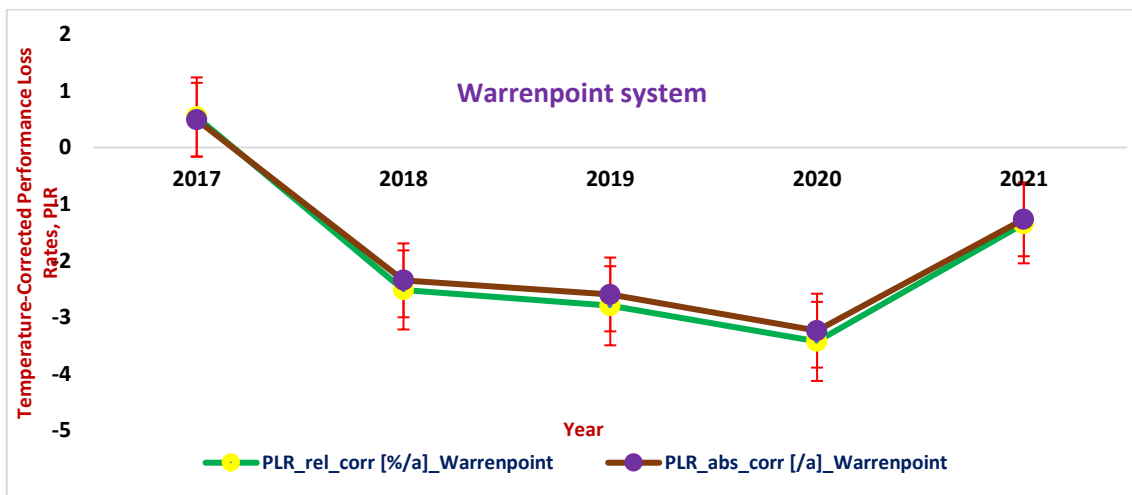
c.

Figure 78 (a-c). Standard deviation error bars show the overlap between relative and absolute temperature-corrected performance loss rates of PV systems monitored for five years period.

The test of significance for relative and absolute temperature-corrected performance loss rates across the three sites is computed using equation (64).

$$t_{cal} = \frac{\sum d_i}{\sqrt{\frac{n(\sum di^2)-(\sum di)^2}{DF}}} \qquad (64)$$

where $di = PLR_{abs\_corr} - PLR_{rel\_corr}$ (65)

n = 5 is the number of monitored data points

DF = n – 1 is the degree of freedom.

t_{cal} is the calculated t-value.

$PLR_{abs.corr}$ is the absolute weather-corrected performance loss rate.

$PLR_{rel.corr}$ is the relative weather-corrected performance loss rate.

Calculated t-values, t_{cal} for Harlequins and Warrenpoint arrays for temperature-corrected performance loss rates are greater than the critical values, $t_{critical}$ ($t_{cal} > t_{critical}$) at 0.05, 0.10 and 0.01 levels of significance and Newry array t_{cal} value is less than the critical value, $t_{critical}$ ($t_{cal} < t_{critical}$) at 0.05, 0.10 and 0.01 levels of significance while t_{cal} for Harlequins system for temperature-corrected performance loss rates is less than the critical values, $t_{critical}$ ($t_{cal} < t_{critical}$) at 0.05, 0.10 and 0.01 levels of significance. This is shown in the t-distribution statistical table in Table 41. Warrenpoint and Newry systems are significant at 0.05 and 0.10 because $t_{cal} > t_{critical}$ while they are not significant at 0.01 because $t_{cal} < t_{critical}$. This means that the difference, d_i between the PLR_{abs_corr} and PLR_{rel_corr} for Harlequins array, Warrenpoint array and Newry system are all significant at 0.05, 0.10 and 0.01 because $t_{cal} > t_{critical}$ while Harlequins system and Newry array are not significant because $t_{cal} < t_{critical}$ and Warrenpoint system is only significant at 0.05, 0.10   using equation (64).

Table 46. Test of Significance for the temperature-corrected performance loss rates in Harlequins, Newry and Warrenpoint Arrays and Systems

$t_{critical}$ at level of significance, α	t_{cal} **for Harlequins**		t_{cal} **for Newry**		t_{cal} **for Warrenpoint**	
	Array	**System**	**Array**	**System**	**Array**	**System**
$\alpha_{0.05} = 2.13$	6.24	-0.15	-1.45	3.10	7.65	2.51
$\alpha_{0.10} = 1.53$	6.24	-0.15	-1.45	3.10	7.65	2.51
$\alpha_{0.01} = 3.74$	6.24	-0.15	-1.45	3.10	7.65	2.51

4.4 Conclusion

PV system output varies because of system design, site location, weather conditions and time of day. "Weather-uncorrected PR" shows high seasonality with low PR values during warmer periods and higher values during colder periods. This is because PR is affected by the module and ambient temperature. To quantify and correct this variation, the weather-uncorrected performance ratio was normalised using the average annual cell temperature (T_{cell_avg}) to give temperature-corrected performance ratios (PRs).

A five-year performance loss rates investigation indicates that Warrenpoint and Newry arrays show more improvement in performance with a temperature-corrected relative performance loss rate of -0.17%/a and -0.23%/a respectively followed by Harlequins array (-0.27%/a). This show that generation from solar panels will increase at the annual rates of -0.17%/a, -0.23%/a, and -0.27%/a respectively. Harlequins and Warrenpoint systems recorded more decrease in performance with temperature-corrected relative performance loss rates recorded as 0.018%/a and 5.14×10^{-3} %/a respectively showing an annual decrease in PV system generation at Harlequins and Warrenpoint systems by 0.018%/a and 5.14×10^{-3} %/a respectively while in temperature-corrected Newry system, a -6.35×10^{-3} %/a implies that generation from a PV system will increase at a rate of -6.35×10^{-3} %/a.

For weather-uncorrected relative and absolute performance loss rates, seasonal variation effects were noticed in the three arrays and systems as there were fluctuations in performance improvement. This shows the importance of temperature-correction to distinguish individual longer-term behaviour of PV arrays and systems.

When comparing the results of the relative and absolute performance loss rates from the three arrays and systems (see Tables 36 – 39), their results were very close. Hence, the performance loss rate computations for PV arrays and PV systems can be done using either relative performance loss rates (PLR$_{rel}$) or absolute performance loss rates (PLR$_{abs}$).

Long-term degradation that will be seen after 5 years of generation becomes apparent much sooner. Using temperature-corrected PR, for one particular installation, 0.810 and 0.999 coefficient of determination in monthly average PR data to the long-term degradation trend becomes apparent only six months. For all three installations examined the long-term trends in the degradation of temperature-corrected PR were apparent within three years. The usual 0.810 and 0.999 coefficients of determination criteria for evidence of long-term behaviour in data becoming statistically relevant sets a high certainty that long-term trends are truly evident. Obviously when a lower coefficient of determination value is used as a criterion then the long-term trends are established sooner but with less confidence.

CHAPTER 5

CONCLUSIONS AND RECOMMENDATIONS

5.1 Conclusions

Performance monitoring of PV systems aims at maintaining a useful power output for longer thus giving both (i) enhancing the environmental sustainability of the PV electricity produced as a greater amount is produced for the same energy and greenhouse gases embodied in the PV array and (ii) continue to produce electricity at the cost of operation and maintenance after a time has been reached when the initial capital cost has returned by the value of electricity produced.

Weather-uncorrected performance ratio (PR_{uncorr}) shows high seasonality with low values during the warmer months and higher values during the colder months. To correct this seasonal variability, temperature-corrected PRs were calculated. A correction to PR was performed using the measured annual average cell temperature (T_{cell_avg}). The introduction of the temperature-correction and normalisation with the annual average cell temperature (T_{cell_avg}) reduced the seasonal variation in PR compared to the weather-uncorrected PR.

To investigate long-term degradation, the annual average five-year relative performance loss rates (PLR_{rel}) and absolute relative loss rates (PLR_{abs}) of Harlequins, Newry and Warrenpoint arrays were calculated.

The y-intercept (β_o) of the function indicates that the PR values for the five-year weather-uncorrected and weather-corrected performance ratio values for all three PV arrays studied were almost constant. PLR_{rel} and PLR_{abs} showed that the Warrenpoint PV array showed more improvement in performance than the Harlequins and Newry arrays. For weather-uncorrected relative and absolute performance loss rates, seasonal variation effects were noticed in the three arrays and systems as there were fluctuations in performance improvement. This shows the

importance of temperature-correction to distinguish individual longer-term behaviour of PV arrays and systems.

To examine short-term performance variations, the monthly weather-uncorrected and temperature-corrected relative and absolute performance loss rates from Harlequins, Newry and Warrenpoint arrays and systems from 2017 to 2021, the gradient (β_1) and the y-intercept (β_o) of weather-uncorrected and temperature-corrected performance ratios of each year across the three arrays and systems were carried out using the time series (Yt) linear regression model equation.

Regarding the PLR_{rel} and PLR_{abs} trends, there were significant array improvements from 2017 to 2018 and from 2020 to 2021 in the three arrays except that in 2019, there was a decrease in performance for the Newry array. The system losses were a result of high solar cell temperature, DC/AC inverter efficiencies conversion losses, and solar radiation reflection losses [239].

When the solar radiation in a site location increases, the ambient temperature also increases reducing PV efficiency. An increase in relative humidity is seen at lower solar irradiation due to solar energy transmission through the atmosphere has been attenuated by moisture. A particularly strong correlation of solar radiation with relative humidity was found in the climate in which these PV arrays were located.

The relative and absolute performance loss rates results of this study in the three PV arrays correspond with the result of Dhimish [136] which according to his results showed that the lowest PV degradation rates were obtained at the Irish PV sites.

Degradation trends evident from five years of data (indication of longer-term degradation) have been clearly demonstrated to be apparent in PV array and PV system performance data sooner than five years. A linear coefficient of determination on temperature-corrected PR trends of

0.810 and 0.999 was found after between 6 months and three years. If a lower coefficient of determination is predicted, long-term degradation trends become evident sooner but obviously with less confidence. For the three installations examined the time for long-term performance degradation trends to be evidenced by trends with different levels of confidence (as predicted by coefficients of determination) is shown in Figures 69-70. If the lower coefficient of determination trends are acceptable, then degradation trends have been shown to be evident within one year. This has implications for use of short-term real-time performance degradation measurement becoming a possible competing option to accelerated testing.

The impact of solar cell degradation affects both the energy generation and the overall economic performance of photovoltaic systems. Therefore, when the PV module degrades:

- less energy is generated over a module life.

- the installation is less economically viable as more cost is being incurred for operation, maintenance and repair.

- manufacturers and/or installers incur more costs to satisfy performance guarantees.

- inspection and maintenance costs are higher.

- It becomes more difficult to provide inherently resilient electricity generation.

5.2 Recommendations for Further Research

It is recommended that further research investigates the following:

I.   Further refinement of the weather-corrected performance loss rates to take account of balance-of-systems component behaviours (including that of inverters).

II.   Detailed comparison of accelerated lifetime testing for PV Modules with short and long-term monitoring.

III.   Further work is to readily distinguish between different PV module failures from degradation.

IV.   Investigation of very long-term degradation rates of PV plants using multi-annual datasets from multiple different plant locations.

REFERENCES

[1]   H. Xuan and P. Minh, "Mathematical modelling of photovoltaic cell/module/arrays with tags in Matlab/Simulink.," *Environmental Systems Research, a SpringerOpen Journal,* vol. 4, p. 24, 2015.

[2]   D. King, W. Boyson and J. Kratochvill, "Photovoltaic Array Performance Model," Sandia National Laboratories, Albuquerque, New Mexico, 2004.

[3]   F. Lindholm , J. Fossum and E. Burgess, "Application of the superposition principle to solar-cell analysis," *IEEE Transactions on Electron Devices,* vol. 26, no. 03, pp. 165 - 171, 1979.

[4]   G. Adhyaksa, L. Veldhuizen, Y. Kuang and S. Brittman, "Carrier diffusion lengths in hybrid perovskites: Processing, Composition, Aging, and Surface Passivation Effects," *Chem. Mater., ACS Publications,* vol. 28, pp. 5259-5263, 2016.

[5]   A. Augusto, S. Herasimenka , R. King , S. Bowden and G. Honsberg , "Analysis of the recombination mechanisms of a silicon solar cell with low band-gap voltage offset.," *Applied Physics,* vol. 121, pp. 205704-1 to 205704-6, 2017.

[6]   J. Haschke, D. Amkreutz, L. Korte, F. Ruske and B. Rech, "Towards wafer quality crystalline silicon thin-film solar cells on glass.," *Solar Energy Materials and Solar Cells,* vol. 128, pp. 190-197, 2014.

[7]   R. Sinton and A. Cuevas , "Contactless determination of current-voltage characteristics and minority-carrier lifetimes in semi-conductors from quasi-steady-state photoconductance data.," *Applied Physics Letters,* vol. 69, pp. 2510-2512, 1996.

[8]   R. Sinton, A. Cuevas and M. Stuckings, "Quasi-steady-state photoconductance, a new method for solar cell material and device characterization," in *Conference Record of the Twenty Fifth IEEE Photovoltaic Specialists Conference*, Washington, DC, USA, 1996.

[9]   D. Bartesaghi, I. Perez, J. Kniepert , S. Roland , M. Turbiez , D. Neher and L. Koster , "Competition between recombination and extraction of free charges determines the fill factor of organic solar cells.," pp. 1-10, 2015.

[10]   V. Fesharaki , M. Dehghani and J. Fesharaki , "The Effect of Temperature on Photovoltaic Cell Efficiency," in *Proceedings of the 1st International Conference on Emerging Trends in Energy Conservation*, ETEC Tehran, Tehran, Iran., 2011.

[11]   E. Van Dyk , E. Meyer , F. Vorster and A. Leitch , "Long-term monitoring of photovoltaic devices," *Renew Energy,* vol. 25 , p. 183-197, 2002.

[12]   G. Spagnuolo, G. Petrone, B. Lehman, C. Ramos Paja, Y. Zhao and M. Orozco Gutierrez , "Control of photovoltaic arrays: dynamical reconfiguration for fighting mismatched conditions and meeting load requests," *IEEE Ind Electron Mag.,* vol. 9, p. 62-76 , 2015.

[13]   G. Stapleton and S. Neill , Grid-connected Solar Electric Systems: The Earthscan Expert Handbook for Planning, Design, and Installation, New York, NY: Routledge: Taylor and Francis Group , 2012, pp. 115-145.

[14]   J. Duffie and W. Beckman , Solar Engineering of Thermal Processes., Wiley, New York, 1991, p. 913.

[15] J. Mondol, Y. Yohanis and B. Norton, "The effect of low insolation conditions and inverter oversizing on the long performance of a grid-connected photovoltaic system.," *Prog. Photovolt. Res. Appl,* vol. 15, pp. 353-368, 2007.

[16] C. Buttay, J. Rashid, C. M. Johnson, F. Udrea, G. Amaratunga, P. Ireland and R. K. Malhan, "Compact Inverter Designed for High-Temperature Operation," in *IEEE Power Electronics Specialists Conference*, Orlando, FL, USA, 2007.

[17] F. Vignola and F. Mavromatakis, "Performance of PV Inverters," in *American Solar Energy Society*, Proc. of the 37th ASES, Oregon, USA, 2008.

[18] A. Desai, T. Joshi, I. Mukhopadhyay and A. Ray, "Effect of Temperature on Conversion Efficiency of Single-Phase Solar PV Inverter," in *IEEE 48th Photovoltaic Specialists Conference (PVSC)*, Fort Lauderdale, FL, USA, 2021.

[19] K. Chumpolrat, V. Sangsuwan, N. Udomdachanut, S. Kittisontirak, S. Songtrai, P. Chinnavornrungsee, A. Limmanee, J. Sritharathikhun and K. Sriprapha, "Effect of Ambient Temperature on Performance of Grid-Connected Inverter Installed in Thailand," *International Journal of Photoenergy,* vol. 2014, pp. 1-6, 2014.

[20] N. Ketjoy , W. Chamsa-ard and P. Mensin, "Analysis of factors affecting efficiency of inverters: Case study grid-connected PV systems in lower northern region of Thailand," *Energy Reports,* vol. 7, pp. 3857-3868, 2021.

[21] D. Bagnall and M. Boreland, "Photovoltaic technologies," *Energy Policy,* vol. 36, pp. 4390-4396, 2008.

[22] R. Agarwal and H. Garg , "Study of a photovoltaic thermal system-thermosyphonic solar water heater combined with solar cells.," *Energy Convers,* vol. 35, pp. 605-620, 1994.

[23]   E. Skoplaki and J. Palyvos , "On the temperature dependence of photovoltaic module electrical performance: A review of efficiency/power correlations.," *Solar Energy,* vol. 83, pp. 614-624., 2009.

[24]   R. Kumar and M. Rosen, "A critical review of photovoltaic thermal solar collectors for air heating.," *Applied Energy,* vol. 88, pp. 3603-3614, 2011.

[25]   L. Ayompe, A. Duffy, S. McCormack and M. Conlon, "Measured performance of a 1.72 kW rooftop grid connected photovoltaic system in Ireland," *Energy Conversion and Management,* vol. 52, pp. 816-825, 2011.

[26]   E. Kymakis , S. Kalykakis and T. Papazoglou , "Performance analysis of a grid-connected photovoltaic park on the island of Crete," *Energy conversion and management,* vol. 50, pp. 433-438, 2009.

[27]   C. Sidi, M. Ndiaye , M. Bah , A. Mbodji , A. Ndiaye and P. Ndiaye , "Performance analysis of the first large-scale (15 MWp) grid-connected photovoltaic plant in Mauritania," *Energy Conversion and Management,* vol. 119, pp. 411-421, 2016.

[28]   D. Okello, F. Vorster and van Dyk E.E, "Analysis of measured and simulated performance data of a 3.2 kWp grid-connected PV system in Port Elizabeth, South Africa.," *Energy Conversion and Management,* vol. 100, pp. 10-15, 2015.

[29]   M. Nallapaneni, M. Rohit, P. Ruth and M. Mathew, "Performance analysis of 100 kWp grid-connected Si-poly photovoltaic system using PVsyst simulation tool.," *Energy Procedia,* vol. 117, pp. 180-189, 2017.

[30]   A. Leon , J. Arne , H. Salah , A. Giovanna , M. Abdulrahman , B. Ahmed , B. Erich , B. Adil , K. Wepie , B. Klaus and B. Christof , "Photovoltaic system performance

monitoring guidelines for measurement, data exchange and analysis.," International Electrotechnical Commission, Geneva, Switzerland, 1998.

[31] T. Dierauf, A. Growitz , S. Kurtz , J. Cruz , E. Riley and C. Hansen , "Weather-Corrected Performance Ratio," National Renewable Energy Laboratory, NREL, United States, 2013.

[32] X. Li, "Degradation analysis of photovoltaic modules based on operational data: effects of seasonal pattern and sensor drift.," in *IOP Conf. Series: Earth and Environmental Science.*, Beijing, China, 2016.

[33] F. Allen and P. David, "Photovoltaic Module Weather Durability & Reliability Testing," Solar Energy Competence Center Atlas Material Testing Technology LLC,, Chicago, US, 2012.

[34] P. Tchakoua, R. Wamkeue, M. Ouhrouche, F. Slaoui-Hasnaoui , T. Tameghe and G. Ekemb , "Wind turbine condition monitoring: state-of-the-art review, new trends, and future challenges.," *Energies,* vol. 7, p. 2595-2630, 2014.

[35] C. Ferrara and D. Philipp, "Why do PV modules fail?," *Energy Procedia.,* vol. 15, p. 379-387, 2012.

[36] J. Wohlgemuth, "Reliability of PV Systems, Reliability of Photovoltaic Cells, Modules, Components, and Systems.," in *Proc. of SPIE*, San Diego, California, United States, 2008.

[37] P. A. Basore , "Understanding Manufacturing Cost Influence on Future Trends in Silicon Photovoltaics," *IEEE Journals of Photovoltaics,* vol. 4, no. 6, pp. 1477 - 1482, 2014.

[38] X. Zhengpeng , M. Timothy and G. Armin , "PV module durability testing under high voltage biased damp-heat conditions," *Energy Procedia,* vol. 8, pp. 384-389, 2011.

[39] Z. Allen, "PV Durability and Reliability Issues," Atlas Material Testing, Renewable Energy World, Dallas, Texas, 2009.

[40] J. Kuitche , R. Pan and G. Tamizhmani , "Investigation of dominant figures modes for field-aged c-Si modules in desert climatic conditions," *IEEE J. Photovolt.,* vol. 4, pp. 814-826 , 2014.

[41] M. Köntges, I. Kunze , V. Naumann , S. Richter , C. Hagendorf and J. Berghold , "Snail tracks, worm marks and cell cracks. Photovoltaic power systems programme," IEA international energy agency, Fraunhofer, Germany, 2008.

[42] T. Tsoutsos , Z. Gkouskos and S. Tournaki , "Catalogue of common failures and improper practices on PV installations and maintenance," PVTRIN WP2_D2.6_catalogue of common failures and improper practices on PV installations and maintenance_ver 1, EPIA, 2011.

[43] D. Jordan, T. Silverman, J. Wohlgemuth, S. Kurtz and K. VanSant , "Photovoltaic failure and degradation modes," *Prog. Photovolt. Res. Appl,* vol. 25, pp. 318-326, 2017.

[44] D. Degraaff , R. Lacerda , Z. Campeau and S. Corp , "Degradation mechanisms in Si module technologies observed in the field; statistics., their analysis and statistics," SunPower Corporation, Colorado, 2011.

[45] F. Freire , S. Melcher , C. Hochgraf , S. Kurinec and G. Clark, "Degradation analysis of an operating PV module on a Farm Sanctuary.," *J Renew Sustain Energy,* vol. 10, pp. 013505-1 to 013505-13, 2018.

[46] K. Bothe and J. Schmidt , "Electronically activated boron-oxygen-related recombination centers in crystalline silicon," *Appl Phys.,* vol. 99, pp. 013701-1 to 013701-11, 2006.

[47] H. Ahteshamul, V. Kurukuru, A. Mohammed, K. Irshad and A. Zainul , "Fault diagnosis of photovoltaic modules," *Energy Science and Engineering,* vol. 7, pp. 622-644, 2019.

[48] M. Köntges , S. Kajari-Schröder , I. Kunze and U. Jahn , "Crack statistic of crystalline silicon photovoltaic modules," in *26th European Photovoltaic Solar Energy Conference and Exhibition*, Emmerthal, Germany, 2011.

[49] L. Yixian and A. Tay , "Stress analysis of silicon wafer-based photovoltaic modules under IEC 61215 mechanical load test.," *Energy Procedia,* vol. 33, p. 265-271, 2013.

[50] L. Neumaier , G. Pinter , M. Erceg , L. Neumaier, G. Pinter, M. Erceg, A. Omazic, G. Oreski, M. Halwachs, G. Eder and C. Hirschi, "Relation between degradation of polymeric components in crystalline silicon PV module and climatic conditions: A literature review," *Journal of Solar Energy Materials and Solar cells,* vol. 192, pp. 123-133, 2019.

[51] D. Wu , J. Zhu , T. Betts and R. Gottschalg , "Degradation of interfacial adhesion strength within photovoltaic mini-modules during damp-heat exposure," *Prog. Photovolt.: Res. Appl.,* vol. 22, pp. 796-809, 2014.

[52] T. Felder, H. Hu, W. Gambogi, K. Choudhury, S. MacMaster , L. Garreau-Iles and J. Trout , "Field study and analysis of backsheet degradation in 450MW+ PV installations," in *Proceedings of the 4th Atlas/NIST Workshop on Photovoltaic Materials Durability*, Gaithersburg, Maryland, USA, 2017.

[53] T. Dan , T. Joe , M. Thomas , Q. Michael and Z. Kenneth , "Accelerated Aging Testing and Reliability in Photovoltaics, Energy Efficiency and Renewable Energy," Solar Energy Technologies Program, 2007.

[54] T. Dan, T. Joe , M. Thomas , Q. Michael , S. Kurtz and C. Osterwald , "U.S. Department of Energy, Accelerated Aging Testing and Reliability in Photovoltaics Workshop II," Solar Energy Technologies Programme, 2008.

[55] S. Kurtz , "Photovoltaic Module Reliability Workshop 2011," National Renewable Energy Laboratory, Oak Ridge, 2013.

[56] M. Vandebroek, Thermal fracture of glass, Antwerp, Belgium: Ghent University, Faculty of Engineering and Architecture ; University of Antwerp. Faculty of Science, Ghent, 2014.

[57] W. Shin, S. Whan Ko, H. Song, Y. Chul Ju, H. Hwang and G. Kang, "Origin of Bypass Diode Fault in c-Si Photovoltaic Modules: Leakage Current under High Surrounding Temperature," *Energies,* vol. 11, no. 9, p. 2416, 2018.

[58] M. Khalil and P. Soulatiantork, "Reliability assessment of PV inverters," in *14th IMEKO TC10 Workshop Technical Diagnostics, New Perspectives in Measurements, Tools and Techniques for system's reliability, maintainability and safety*, Milan, Italy, 2016.

[59] O. Segbefia, A. Imenes and T. Sætre, "Moisture ingress in photovoltaic modules: A review," *Solar Energy,* vol. 224, pp. 889-906, 2021.

[60] W. Gambogi, J. Kopchick, T. Felder, S. MacMaster, A. Bradley, B. Hamzavy, E. Kathmann, K. Stika, T. Trout , L. Garreau-Iles and T. Sample , "Backsheet and Module Durability and Performance and Comparison of Accelerated Testing to Long Term fielded Modules," in *28th European Photovoltaic Solar Energy Conference and Exhibition*, Paris, France., 2013.

[61] J. Wohlgemuth and W. Herrmann, "Hot spot tests for crystalline silicon modules," in *Conference Record of the 31st IEEE Photovoltaic Specialists Conference*, Lake Buena Vista, FL, USA, 2005.

[62] M. Kempe, "Ultraviolet Light Test and Evaluation methods for Encapsulants of Photovoltaic Modules," *Sol. Energy Mater. Sol. Cells,* vol. 94, pp. 246-253, 2010.

[63] L. Edson and E. Eugene , "Assessing the Reliability and Degradation of Photovoltaic Module Performance Parameters," *IEEE Transactions on Reliability,* vol. 53, pp. 83-92, 2004.

[64] F. Pern and A. Czanderna, "EVA degradation mechanisms simulations those in PV modules," in *Proceedings of the AIP Conference, National Renewable Energy Laboratory*, Golden, Colorado, USA, 1992.

[65] F. Pern , A. Czanderna , K. Emery and R. Dhere, "Weathering degradation of EVA encapsulant and the effect of its yellowing on solar cell efficiency," in *Proceedings of the 22nd IEEE PV Specialists Conference*, Las Vegas, NV, USA, 1991.

[66] F. Pern, "Spectroscopic, scanning laser OBIC and characterizations of browned EVA solar cells," in *Proceedings of the 25th IEEE PV Specialists Conference*, Washington, DC, USA, 1996.

[67] A. Czanderna and F. Pern , "Encapsulation of PV modules using ethylene-vinyl acetate copolymer as a pottant: a critical review.," *Sol. Energy Mater. Sol. Cells,* vol. 43, pp. 101-181, 1996.

[68] A. Jentsch , K. Eichhorn and B. Voit, "Influence of typical stabilizers on the ageing behavior of EVA foils for photovoltaic applications during artificial UV-weathering," *Polym. Test,* vol. 44, pp. 242-247, 2015.

[69] A. Isarankura Na and J. Wootthikanokkhan, "Investigation of the photo-degradation behaviours of an ethylene/vinyl acetate copolymer solar cell encapsulant and effects of antioxidants on the photo-stability of the material," *J. Appl. Polym. Sci.,* vol. 107, pp. 3853-3863, 2008.

[70] O. Hasan and A. Arif , "Performance and life prediction model for photovoltaic modules: effect of encapsulant constitutive behaviour," *Sol. Energy Mater. Sol. Cells,* vol. 122, pp. 75-87, 2014.

[71] A. Gxasheka , E. Van Dyk and E. Meyer, "Evaluation of performance parameters of PV modules deployed outdoors," *Renew. Energy,* vol. 30, pp. 611-620, 2005.

[72] E. Kaplani, "Detection of degradation effects in field-aged c-Si solar cells through IR thermography and digital image processing," *Int. J. Photoenergy,* vol. 1, pp. 1-11, 2012.

[73] G. Griffini and S. Turri , "Polymeric materials for long-term durability of photovoltaic systems," *J. Appl. Polym. Sci.,* vol. 133, no. 11, p. 43080, 2016.

[74] Z. Xia , J. Wohlgemuth and D. Cunningham , "A lifetime prediction of PV encapsulant and backsheet via time temperature superposition principle," in *Proceedings of the 34th IEEE Photovoltaic Specialists Conference (PVSC)*, Philadelphia, Pennsylvania, USA, 2009.

[75] G. Ehrenstein and S. Pongratz , "Resistance and Stability of Polymers.," Hanser Publishers, Munich, 2013.

[76] H. Zweifel, Macromolecular Systems - Materials Approach: Stabilization of Polymeric Materials, Springer, 1998, pp. 41- 44.

[77] A. Beinert , C. Peike , I. Dürr , M. Kempe and K. Weiß , "The influence of the additive composition on the photochemical degradation of EVA," in *Proceedings of the 29th European Photovoltaic Solar Energy Conference and Exhibition*, Amsterdam, Netherlands, 2014.

[78] . I. TÜV Rheinland, "Performance, Operation and Reliability of Photovoltaic Systems," Fraunhofer Institute for Solar Energy Systems ISE, Freiburg, Germany, 2013.

[79] J. Wohlgemuth, P. Hacke, N. Bosco, D. Miller, M. Kempe and S. Kurtz , "Assessing the causes of encapsulant delamination in PV modules," in *Proceedings of the 2016 IEEE 43rd Photovoltaic Specialists Conference (PVSC)*, Portland, Oregon, 2016.

[80] G. Neelkanth, "Reliability of PV modules and balance-of-system components," in *Proceedings of the 31st IEEE Photovoltaic Specialist Conference*, Lake Buena Vista, FL, USA, 2005.

[81] E. Wang , H. Yang, J. Yen , S. Chi and C. Wang , "Failure modes evaluation of PV module via materials degradation approach," *Energy Procedia,* vol. 33, pp. 256-264, 2013.

[82] S. Meyer , S. Timmel , U. Braun and C. Hagendorf , "Polymer foil additives trigger the formation of snail trails in photovoltaic modules," *Energy Procedia,* vol. 55, pp. 494-497, 2014.

[83] P. Peng, A. Hu, W. Zheng, P. Su, D. He, K. Oakes, A. Fu, R. Han , S. Lee , J. Tang and Y. Zhou , "Microscopy study of snail trail phenomenon on photovoltaic modules," *RSC Adv.,* vol. 2, pp. 11359-11365, 2012.

[84] I. Duerr , J. Bierbaum , J. Metzger , J. Richter and D. Philipp , "Silver grid finger corrosion on snail track affected 5PV6 modules – investigation on degradation products and mechanisms," *Energy Procedia,* vol. 98, pp. 74-85, 2016.

[85] S. Meyer, S. Richter, S. Timmel, M. Glaser, M. Werner, S. Swatek and C. Hagendorf , "Snail trails: root cause analysis and test procedures," *Energy Procedia,* vol. 38, p. 498-505, 2013.

[86] M. Köntges, G. Oreski, P. Hacke, K. Weiss, G. Razongles, M. Paggi, D. Parlevliet, T. Tanahashi , R. French and T. Rheinland, "Assessment of Photovoltaic Module Failures in the Field," INTERNATIONAL ENERGY AGENCY, 2017.

[87] M. López-Escalante, L. Caballero, F. Martín, M. Gabás, A. Cuevas and J. Ramos-Barrado , "Polyolefin as PID-resistant encapsulant material in 5PV6 modules," *Sol. Energy Mater. Sol. Cells,* vol. 144, pp. 691-699, 2016.

[88] U. Itoh, M. Yoshida, H. Tokuhisa, K. Takeuchi and Y. Takemura , "Solder joint failure modes in the conventional crystalline Si module," *Energy Procedia,* vol. 55, p. 464-468, 2014.

[89] G. Kleiss , J. Kirchner and K. Reichart , "Quality and reliability – sometimes the customer wants more," SolarWorld, NREL PV Modules Reliability Workshop, Bonn, Germany, 2015.

[90] D. Wu, D. Montiel-Chicharro, T. Betts, R. Gottschalg and J. Zhu, "Realistic adhesion test for photovoltaic modules qualification," *IEEE J Photovolt,* vol. 8, p. 218-223, 2017.

[91] A. Delahoy , K. Jansen and A. Delahoy , "A laboratory technique for the evaluation of electrochemical transparent conductive oxide delamination from glass substrates," *Thin Solid Films,* vol. 423, p. 152-160, 2016.

[92] D. Veldman, I. Bennett , B. Brockholz and P. De Jong , "Non-destructive testing of crystalline silicon photovoltaic back-contact modules," in *37th IEEE Photovoltaic Specialists Conference*, Seattle, WA, USA, 2011.

[93] A. Ibrahim, "Non-destructive testing of a monocrystalline silicon solar cell : magnetic field – electrical properties correlation," *SpringerLink,* vol. 11, pp. 22439-2443, 2017.

[94] J. Tang , C. Ju and R. Lv , "The performance of double glass photovoltaic modules under composite test conditions," *Energy Procedia,* vol. 130, p. 87-93, 2017.

[95] M. Dhimish , V. Holmes , B. Mehrdadi and M. Dales , "The impact of cracks on photovoltaic power performance," *J Sci Adv Mater Devices,* vol. 2, p. 199-209., 2017.

[96] S. Kajari-Schröder , I. Kunze and M. Köntges , "Criticality of cracks in PV modules," *Energy Procedia,* vol. 27, p. 658-663, 2012.

[97] A. Fairbrother , M. Boyd and Y. Lyu , "Differential degradation patterns of photovoltaic backsheets at the array level," *Sol Energy.,* vol. 163, p. 62-69, 2018.

[98] S. Mohammed , B. Boumediene and B. Miloud , "Assessment of PV modules degradation based on performances and visual inspection in Algerian Sahara," *Int J Renew Energy Res.,* vol. 6, p. 106-116, 2016.

[99] H. Hoehne , J. Berghold and S. Pingel , "Potential induced degradation of solar cells and panels," in *35th IEEE PVSC*, Honolulu, HI, USA, 2010.

[100] M. D. Kempe, G. J. Jorgensen, K. M. Terwilliger, T. J. McMahon, C. E. Kennedy and T. T. Borek, "Ethylene-Vinyl Acetate Potential Problems for Photovoltaic Packaging.," in *IEEE 4th World Conference on Photovoltaic Energy Conversion (WCPEC-4)*, Waikoloa, Hawaii, USA, 2006.

[101] M. Chang, C. Chen, C. H. Hsueh, E. Yen, K. L. Ho, H. P. Chuang, C. Y. Lee and H. Chen, "The Reliability Investigation of PV Junction Box based on 1GW Worldwide Field Database.," in *42nd IEEE Photovoltaic Specialists Conference*, New Orleans, USA, 2015.

[102] M. Humood, A. Beheshti and A. A. Polycarpou, "Surface reliability of annealed and tempered solar protective glasses: Indentation and scratch behaviour.," *Solar Energy,* vol. 142, pp. 13-25, 2017.

[103] S. N. Bureau, "Backsheets and EVA: Enduring PV Production Behind the Scene," *Saur Energy International Magazine,* Wednesday July 2017.

[104] D. King , M. Quintana , J. Kratochvil , D. Ellibee and B. Hansen , "Photovoltaic Module Performance and Durability Following Long-Term Field Exposure.," *Progress in Photovoltaic,* vol. 8, pp. 241-256, 2000.

[105] D. King , J. Kratochvil , M. Quintana and T. McMahon , "Applications for infrared imaging equipment in a photovoltaic cell, module, and system testing.," in *Proceedings of the Twenty-Eighth IEEE Photovoltaic Specialists Conference*, Anchorage, AK, USA, 2000.

[106] P. Nochang , H. Changwoon , H. Wonsik and K. Donghwan , "The effect of encapsulant delamination on electrical performance of PV module," in *37th IEEE Photovoltaic Specialists Conference*, Seattle, WA, USA, 2011.

[107] T. Shioda, "Delamination failures in long-term field-aged PV modules from point of view of encapsulant. NREL PV Module Reliability Workshop," in *Proceedings of the PV Module Reliability Workshop,*, Marriott Denver West, USA., 2013.

[108] K. Rahul , A. Shivani , S. Ivan , K. Sunit and K. Bikash , "Study on long-term reliability of photovoltaic modules and analysis of power degradation using accelerated aging tests and electroluminescence technique.," *Energy Procedia,* vol. 8, pp. 396-401, 2011.

[109] D. King and J. Hansen , "Dark current-voltage measurements on photovoltaic modules as a diagnostic or manufacturing tool," in *Proceedings of the 25th IEEE PV Specialists Conference*, Anaheim, CA, USA, 1997.

[110] C. Zhou, J. Yan, R. Dong and B. Jin, "Technologies to reduce the optical losses of silicon solar cells," *Advanced Materials Research,* Vols. 953-954, pp. 91-94, 2014.

[111] M. Hermie , F. Granek , O. Schultz and S. Glunz, "Analsing the effects of front-surface fields on back-junction silicon solar cells using the charge collection-probability and the reciprocity theorem.," *Applied Physics,* vol. 103, pp. 054507-1 to 054507-7, 2008.

[112] L. Cristaldi , M. Faifer and M. Lazzaroni , "Failure modes analysis and diagnostic architecture for photovoltaic plants," in *13th IMEKO TC10 Workshop on Technical Diagnostics. Advanced measurement tools in technical diagnostics for systems' reliability and safety*, Warsaw, Poland, 2014.

[113] L. Cristaldi, M. Faifer, M. Lazzaroni, M. Khalil, M. Catelani and L. Ciani , "Diagnostic architecture: a procedure based on the analysis of the failure causes applied to photovoltaic plants," *Measurement,* vol. 67, p. 99-107, 2015.

[114] C. Osterwald , A. Anderberg , S. Rummel and L. Ottoson , "Degradation analysis of weathered crystalline-silicon PV modules," in *Proc. 29th IEEE Photovolt. Spec. Conf.*, New Orleans, Louisiana, USA., 2002.

[115] G. Tiwari , R. Mishra and S. Solanki , "Photovoltaic modules and their applications: A review on thermal modelling," *Applied Energy,* vol. 88, pp. 2287-2304, 2011.

[116] E. Dunlop and D. Halton, "The performance of crystalline silicon photovoltaic solar modules after 22 years of continuous outdoor exposure," *Prog Photovoltaics.,* vol. 14, pp. 53-64, 2006.

[117] S. Pingel , O. Frank , M. Winkler , S. Daryan and T. Geipel , "Potential induced degradation of solar cells and panels.," in *Proc. 35th IEEE Photovolt. Spec. Conf.*, Honolulu, HI, USA., 2010.

[118] B. Sopori, P. Basnyat, S. Shet, V. Mehta, J. Binns and R. Appel, "Understanding light-induced degradation of c-Si solar cells," in *J Proc. IEEE Photovolt. Spec. Conf*, Austin, TX, USA, 2012.

[119] A. Akram, "A New Method to Reduce Soiling Effect on Performance of a Solar PV Module.," *International Journal of Advanced Research and Innovation,* vol. 3, pp. 601-606, 2015.

[120] T. Sarver , A. Al-Quaraghuli and L. Kazmerski , "A comprehensive review of the impact of dust on the use of solar energy: History, investigations, results, literature, and

mitigation approaches," *Renewable and Sustainable Energy Reviews,* vol. 22, pp. 698-733, 2013.

[121] S. Gibson, "Don't Hire a Cleaning Crew to Wash Your Solar Panels. Paying to have photovoltaic panels cleaned will cost more than the extra energy is worth," *Green Building Advisor,* 01 August 2013.

[122] R. Appels, B. Muthirayan, A. Beerten, R. Paesen, J. Driesen and J. Poortmans , "The effect of dust deposition on photovoltaic modules," in *38th IEEE Photovoltaic Specialists Conference (PVSC)*, Austin, TX, USA, 2012.

[123] M. Mani and R. Pillai , "Impact of dust on solar photovoltaic (PV) performance: Research status, challenges, and recommendations.," *Renewable and Sustainable Energy Reviews,* vol. 14, pp. 3124-3131, 2010.

[124] J. Kaldellis and A. Kokala , "Simulation of the dust effect on the energy performance of photovoltaic generators based on experimental measurements," *Energy,* vol. 36 , pp. 5154-61, 2011.

[125] S. Mekhilefa , R. Saidurb and M. Kamalisavestani , "Effect of dust, humidity, and air velocity on efficiency of photovoltaic cells," *Renew Sustain Energy Rev,* vol. 16 , pp. 2920-2925, 2012.

[126] R. Annie , E. Ryan and K. Malay , "Water Free Cleaning Solution: Environmental Durability of Electrodynamic Screen (EDS) Films in Water-Free Cleaning of Solar Collectors," in *IEEE 46th Photovoltaic Specialists Conference (PVSC)*, Chicago, IL, USA , 2019.

[127] M. Aidara , M. Ndiyae , A. Mbaye , M. Sylla and P. Ndiaye , "Study of the Performance of a system for dry cleaning dust deposited on the surface of solar photovoltaic panels," *International Journal of Physical Sciences,* vol. 13 , pp. 16-23, 2018.

[128] J. Mazer, Solar Cells: An Introduction to Crystalline Photovoltaic Technology, Kluwer Academic Publishers, 1996 .

[129] J. Lopez-Garcia , A. Pozza and T. Sample , "Long-term soiling silicon PV modules in a moderate subtropical climate," *Solar Energy,* vol. 130 , pp. 174-183, 2016.

[130] I. Tetsuyuki and M. Atsushi , "Annual degradation rates of recent crystalline silicon photovoltaic modules," *Progress in Photovoltaics: Research and Applications,* vol. 25 , pp. 953-967, 2017.

[131] P. Nochang , J. Jaeseong and H. Changwoon , "Estimation of the degradation rate of multi-crystalline silicon photovoltaic module under thermal cycling stress," *Microelectronics Reliability,* vol. 54, pp. 1562-1566 , 2014.

[132] E. Dunlop and D. Halton , "The performance of crystalline silicon photovoltaic solar modules after 22 years of continuous outdoor exposure," *Prog Photovoltaics,* vol. 14 , p. 53–64, 2006.

[133] S. Silvestre, S. Kichou , L. Gulielminotti, G. Nofuentes and M. Alonso, "Degradation analysis of thin film photovoltaic modules under outdoor long term exposure in Spanish continental climate conditions," *Solar Energy,* vol. 139, pp. 599-607, 2016.

[134] M. Saadsaoud , A. Ahmeda , Z. Er and Z. Rouabah , "Experimental study of degradation modes and their effects on reliability of photovoltaic modules after 12 years of field

operation in the steppe region," *Journal of Acta Physica Polonica A.,* vol. 132 , pp. 3-11, 2017.

[135] A. Ameur , A. Berrada, A. Bouaichi and K. Loudiyi, "Long-term performance and degradation analysis of different PV modules under temperate climate," *Renewable Energy,* vol. 188, pp. 37-51, 2022.

[136] M. Dhimish, "Performance Ratio and Degradation Rate Analysis of 10-Year Field Exposed Residential Photovoltaic Installations in the UK and Ireland," *Clean Technologies,* vol. 2, no. 2, pp. 170-183, 2020.

[137] H. Takatoshi , N. Tomoya , T. Tadashi and I. Yoshitaka , "Influence of degradation in units of PV modules on electric power output of PV system.," *Journal of International council on Electrical Engineering,* vol. 8 , p. 118–126, 2018.

[138] R. Pramod , G. Tiwari , O. Sastry, B. Birinchi and S. Vikrant , "Degradation of mono-crystalline photovoltaic modules after 22 years of outdoor exposure in the composite climate of India," *Journal of Solar Energy,* vol. 135, pp. 786-795 , 2016.

[139] R. Pramod, M. Maria, M. Nallapaneni, O. Sastry and G. Tiwari , "Risk priority number for understanding the severity of photovoltaic failure modes and their impacts on performance degradation," *Case Studies in Thermal Engineering,* vol. 16 , pp. 1-11, 2019.

[140] M. Moorthy and G. Tamizhmani , "Automation of risk priority number calculation of photovoltaic modules," in *IEEE 43rd Photovoltaic Specialists Conference (PVSC)*, Portland, OR, USA, , 2016.

[141] S. Tatapudi, P. Sundarajan, C. Libby, J. Kuitche and G. Tamizhmani , "Risk priority number for PV module defects: influence of climatic condition," in *Proceedings of SPIE - The International Society for Optical Engineering*, San Diego, USA , 2018.

[142] S. Tatapudi , J. Kuitche and G. Tamizhmani , "A novel climate specific-field accelerated testing of PV modules.," in *New Concepts in Solar and Thermal Radiation Conversion and Reliability, International Society for Optics and Photonics*, San Diego, USA , 2018.

[143] S. Chattopadhyay, R. Dubey, V. Kuthanazhi, J. John, A. Kottantharayil, B. Arora, K. Narasimhan, V. Kuber, J. Vasi, A. Kumar and O. Sastry , "Visual degradation in field-aged crystalline silicon PV modules in India and correlation With electrical degradation," *IEEE J. Photovolt,* vol. 4 , pp. 1470-1476, 2014.

[144] S. Kumar , S. Roy and R. Gupta , "Comparison of reliability tests by characterization of degradation in photovoltaic modules," *MOJ Sol. Photoenergy Syst.,* vol. 1, pp. 21-25 , 2017.

[145] M. Quintana and D. King , "Commonly observed degradation in field-aged photovoltaic modules," in *Proceedings of the 29th IEEE Photovoltaic Specialists Conference*, New Orleans, USA , 2002.

[146] D. Jordan , J. Wohlgemuth and S. Kurtz , "Technology and climate trends in PV module degradation," in *Proceedings of the 27th European Photovoltaic Solar Energy Conference and Exhibition*, Frankfurt, Germany , 2012.

[147] R. Smith , D. Jordan and S. Kurtz , "Outdoor PV module degradation of current-voltage parameters: preprint," in *Proceedings of the World Renewable Energy Forum*, Denver, Colorado , 2012.

[148] T. Sakamoto, "Field test results on the stability of crystalline silicon photovoltaic modules manufactured in the 1990s," in *Proceedings of the 3rd World Conference on Photovoltaic Energy Conversion,*, Osaka, Japan , 2003.

[149] J. Lindroos and H. Savin , "Review of light-induced degradation in crystalline silicon solar cells," *Sol. Energy Mater. Sol. Cells,* vol. 147 , pp. 115-126, 2016.

[150] E. Urrejola, J. Antonanzas, P. Ayala, M. Salgado, G. Ramírez-Sagner , C. Cortés , A. Pino and R. Escobar , "Effect of soiling and sunlight exposure on the performance ratio of photovoltaic technologies in Santiago, Chile," *Energy Convers. Manag.,* vol. 114, pp. 338-347 , 2016.

[151] A. Skoczek , T. Sample and E. Dunlop , "The results of performance measurements of field-aged crystalline silicon photovoltaic modules," *Prog. Photovolt: Res. Appl,* vol. 17, pp. 227-240 , 2009.

[152] N. Umachandran , J. Kuitche and G. TamizhMani , "Statistical methods to determine dominant degradation modes of fielded PV modules," in *Proceedings of the 42nd IEEE Photovoltaic Specialist Conference (PVSC)*, New Orleans, USA , 2015.

[153] D. Quansah , M. Adaramola , G. Takyi and I. Edwin , "Reliability and degradation of Solar PV modules case study of 19-year-old polycrystalline modules in Ghana," *MDPI Technologies,* vol. 5 , pp. 1-18, 2017.

[154] N. Bogdanski, W. Herrmann , F. Reil , M. Köhl , K. Weiss and M. Heck , "PV reliability (cluster II): results of a German four-year joint project: Part II, results of three years module weathering in four different climates," in *Proceedings of the 25th European Photovoltaic Energy Conversion*, Valencia, Spain , 2010.

[155] J. Arp and B. Jaeckel , "Long-term statistics on micro cracks and their impact on performance," in *Proceedings of the 31st European Photovoltaic Solar Energy Conference and Exhibition*, Hamburg, Germany , 2015.

[156] K. Yedidi, S. Tatapudi, J. Mallineni, B. Knisely, K. Kutiche and G. TamizhMani , "Failure and degradation modes and rates of PV modules in a hot-dry climate: results after 16 years of field exposure," in *Proceedings of the IEEE 40th Photovoltaic Specialist Conference (PVSC)*, Denver, CO, USA, 2014 .

[157] A. Suleske, "Performance Degradation of Grid-Tied Photovoltaic Modules in a Desert Climatic Condition (Master thesis)," in *Electrical Engineering/Alternative Energy*, Arizona State University, USA, 2010 .

[158] F. Bandou, A. Hadj Arab, M. Belkaid, P. Logerais, O. Riou and A. Charki , "Evaluation performance of photovoltaic modules after a long-time operation in Saharan environment," *Int. J. Hydrog. Energy,* vol. 40 , pp. 13839-13848, 2015.

[159] Y. Tang, B. Raghuraman, J. Kuitche, G. TamizhMani, C. Backus and C. Osterwald , "An evaluation of 27+ years old photovoltaic modules operated in a hot-dessert climatic conditions," in *in: 2006 IEEE Proceedings of the 4th World Conference on Photovoltaic Energy Conversion*, Waikoloa Hawai, USA , 2006.

[160] M. Chicca and G. TamizhMani , "Nondestructive techniques to determine degradation modes: Experimentation with 18 years old photovoltaic modules," in *IEEE Proceedings of the 42nd Photovoltaic Specialists Conference (PVSC)*, New Orleans, USA , 2015.

[161] A. Bouraiou, M. Hamouda, A. Chaker, M. Mostefaoui, S. Lachtar, M. Sadok, N. Boutasseta, M. Othmani and A. Issam , "Analysis and evaluation of the impact of climatic

conditions on the photovoltaic modules performance in the desert environment," *Energy Convers. Manag.,* vol. 106, pp. 1345-1355 , 2015.

[162] P. Hülsmann, C. Peike, M. Blüml, P. Schmid, K. Weiß and M. Köhl, "Impact of Permeation Properties and Backsheet-Encapsulant Interactions on the Reliability of PV Modules," *International Scholarly Research Network (ISRN), Renewable Energy,* vol. 2012 , pp. 1-5, 2012.

[163] B. Ottersböck , G. Oreski and G. Pinter , "Correlation study of damp heat and pressure cooker testing on backsheets," *J. Appl. Polym. Sci.,* vol. 133 , p. 44230, 2016.

[164] M. Knausz, G. Oreski, G. Eder, Y. Voronko, B. Duscher, T. Koch , G. Pinter and K. Berger , "Degradation of photovoltaic backsheets: comparison of the ageing induced changes on module and component level," *J. Appl. Polym. Sci.,* vol. 132 , pp. 1-8, 2015.

[165] M. Kottek, J. Grieser, C. Beck , B. Rudolf and F. Rubel, "World Map of the Köppen-Geiger climate classification updated," *metz,* vol. 15 , p. 259–263, 2006.

[166] N. Allen , M. Edge , M. Mohammadian and K. Jones , "Physicochemical aspects of the environmental degradation of poly (ethylene terephthalate)," *Polym. Degrad. Stab,* vol. 43 , pp. 229-237, 1994.

[167] M. Köntges, S. Altmann, T. Heimberg, U. Jahn and K. Berger, "Mean degradation rates in PV systems for various kinds of PV module failures," in *Proceedings of the 32nd European Photovoltaic Solar Energy Conference and Exhibition*, Munich, Germany , 2016.

[168] S. Chattopadhyay, R. Dubey, V. Kuthanazhi, J. John, C. Solanki, A. Kottantharayil, B. Arora, K. Narasimhan , J. Vasi , B. Bora , Y. Singh and O. Sastry , "All India Survey of

Photovoltaic Module Degradation. Survey methodology and statistics," in *IEEE 42nd Photovoltaic Specialist Conference (PVSC)*, New Orleans, LA, USA , 2015.

[169] A. Reza , V. Raghu and A. Muhammad , "Physics-Based computational modeling of moisture ingress in solar modules: Location-specific corrosion and delamination.," in *IEEE 43rd Photovoltaic Specialists Conference*, Portland, OR, USA , 2016.

[170] P. Ndiaye, V. Sambou, A. Ndiaye, A. Charki, A. Kobi and C. Kébé, "Degradations of silicon photovoltaic modules: A literature review," *Sol. Energy,* vol. 96 , pp. 140-151, 2013.

[171] W. Hermann , W. Wiesner and W. Vaaen , "Hot spot investigation on PV modules-new concepts for test standard and consequences for module design with respect to bypass diodes," in *Proceedings of the 26th IEEE PV Specialists Conference*, Anaheim, CA, USA, 1997 .

[172] Y. Chaibi, M. Malvoni, A. Chouder, M. Boussetta and M. Salhi , "Simple and efficient approach to detect and diagnose electrical faults and partial shading in photovoltaic systems," *Energy Convers. Manag.,* vol. 196, pp. 330-343 , 2019.

[173] P. Hacke, S. Lokanath, P. Williams, A. Vasan, P. Sochor, G. Tamizhamni , H. Shinohara and S. Kurtz , "A status review of photovoltaic power conversion equipment reliability, safety, and quality assurance protocols," *Renew. Sustain. Energy Rev.,* vol. 82 , pp. 1097-1112, 2018.

[174] U. Weber, R. Eiden, C. Strubel, T. Soegding, M. Heiss, P. Zachmann, K. Nattermann, H. Englemann, A. Dethlefsen and N. Lenck , "Acetic acid production, migration, and

corrosion effect in ethylene –vinylacetate EVA based PV modules," in *27th European Photovoltaic Solar Energy Conference and Exhibition*, Frankfurt, Germany, 2012 .

[175] M. Kempe , T. Moricone , M. Kilkenny and J. Zhang , "Accelerated stress testing of hydrocarbon-based encapsulants for medium concentration CPV applications," in *34th IEEE Photovoltaic Specialists Conference, Photovoltaic Specialists Conference (PVSC)*, Philadelphia, PA, USA , 2009.

[176] A. Sinha , O. Sastry and R. Gupta , "Nondestructive characterization of encapsulant discoloration effects in crystalline-silicon PV modules," *Sol. Energy Mater. Sol. Cells,* vol. 155, pp. 234-242 , 2016.

[177] M. Fortes, E. Comesana, J. Rodriguez, P. Otero and A. Garcia-Loureiro , "Impact of series and shunt resistances in amorphous silicon thin-film solar cells," *Sol. Energy,* Vols. 114-123 , p. 100, 2014.

[178] G. Tamizhmani and J. Kuitche , "Accelerated lifetime testing of photovoltaic modules. Photovoltaic Reliability Laboratory," Photovoltaic Reliability Laboratory, Arizona State University, USA , 2014.

[179] P. Rajput, Shyam, V. Tomar, G. Tiwari, O. Sastry and T. Bhatti , "A thermal model for N series-connected glass/cell/polymer sheet and glass/cell/glass crystalline silicon photovoltaic modules with hot solar cells connected in series and its thermal losses in real outdoor condition," *Renew. Energy,* vol. 126 , pp. 370-386, 2018.

[180] D. Carlson, R. Romero, F. Willing, D. Meakin, L. Gonzalez , R. Murphy , H. Moutinho and M. Al-Jassim , "Corrosion effects in thin-film photovoltaic modules," *Prog. Photovolt. Res. Appl.,* vol. 11, pp. 377-386 , 2003.

[181] S. Mau , T. Krametz, W. Jahna and H. Fechner, "Quality testing for PV modules according to standard and performance control for supporting manufacturing," in *19th EUPVSEC, 7-11 June* , Pairs, France, 2004.

[182] J. Wendet , M. Träger , M. Mette , A. Pfennig and B. Jäckel , "The link between mechanical stress induced by soldering and micro damages in Silicon solar cells.," in *24th European Photovoltaic Solar Energy Conference*, Hamburg, Germany, , 2009.

[183] F. Reil, J. Althus , W. Vaaben , W. Herrman and K. Strohkendl , "The effect of transportation impacts and dynamic load tests on the mechanical and electrical behaviour of crystalline PV modules," in *25th European Photovoltaic Solar Energy Conference and Exhibition/5th World Conference on Photovoltaic Energy Conversion*, Valencia, Spain , 2010.

[184] B. Claudia , G. Mariacristina and P. Marco , "Fatigue crack growth in Silicon solar cells and hysteretic behaviour of busbars," *Sol. Energy Mater. Sol. Cells,* vol. 181 , pp. 21-29, 2018.

[185] J. Delgado-Sanchez, E. Sanchez-Cortezon, C. Lopez-Lopez , R. Aninat and M. Alba , "Failure mode and effect analysis of a large-scale thin-film CIGS photovoltaic module," *Eng. Fail. Anal.,* vol. 76 , pp. 55-60, 2017.

[186] M. Islam , M. Hasanuzzaman and R. Abd , "Investigation of the potential induced degradation of on-site aged polycrystalline PV modules operating in Malaysia," *Measurement,* vol. 119, pp. 283-294 , 2018.

[187] B. Parveen and B. Saurabh , "Clustering-based computation of degradation rate for photovoltaic systems," *Journal of Renewable and Sustainable Energy,* vol. 11 , pp. 014701-1 to 014701-9, 2019.

[188] A. David , A. Muyiwa , T. Gabriel and A. Isaac , "Reliability and degradation of solar PV modules-case study of 19-year-old polycrystalline modules in Ghana," *Technologies,* vol. 5 , no. 2, p. 22, 2017.

[189] G. Spagnolo, P. Del Vecchio, G. Makary, D. Papalillo and A. Martocchia , "A review of IR thermography applied to PV systems. Proceedings of the Environment and Electrical Engineering (EEEIC)," in *11th International Conference on Environment and Electrical Engineering*, Venice, Italy , 2012.

[190] A. Krenzinger and A. De Andrade, "Accurate outdoor glass thermographic thermometry applied to solar energy devices," *Journal of Solar Energy,* vol. 81 , pp. 1025-1034, 2007.

[191] C. Buerhop , D. Schlegel , M. Niess and C. Vodermayer , "Quality Control of PV-Modules in the Field Using Infrared-Thermography," in *Proceedings of the 26th PVSEC*, Hamburg, Germany , 2011.

[192] F. Ancuta and C. Cepisca , "Fault analysis possibilities for PV panels," in *Proceedings of the Proceedings of the 3rd International Youth Conference on Energetics (IYCE)*, Leiria, Portugal , 2011.

[193] S. Johnston , N. Call , B. Phan and R. Ahrenkiel , "Applications of imaging techniques for solar cell characterization," in *Proceedings of the 34th IEEE, Photovoltaic Specialists Conference (PVSC)*, Philadelphia, Pennsylvania, USA , 2009.

[194] C. Buerhop-Lutz and H. Scheuerpflug , "Inspecting PV-plants using aerial, drone-mounted infrared thermography system," in *Proc. 3rd South African Solar Energy Conference*, Pretoria, South Africa , 2015.

[195] N. Zaini, M. Ab-Kadir and M. Izadi , "On the effect of lightning on a solar photovoltaic system," in *33rd Int. Conf. Light. Prot. ICLP*, Estoril, Portugal , 2016.

[196] K. Juris, "Junction box wiring and connector durability issues in photovoltaic modules," in *Proceedings of SPIE -The International Society for Optical Engineering*, San Diego, California, USA , 2014.

[197] O. Breitenstein , J. Rakotoniaina and M. Al Rifai, "Quantitative evaluation of shunts in solar cells by lock-in thermography," *Prog. Photovolt: Res. Appl.,* vol. 11 , pp. 515-526, 2003.

[198] J. Tsanakas , L. Ha and C. Buerhop , "Faults and infrared thermographic diagnosis in operating c-Si photovoltaic modules: a review of research and future challenges," *Renew Sustain Energy Rev.,* vol. 62 , p. 695-709, 2016.

[199] N. Avdelidis , D. Almond , A. Dobbinson and B. Hawtin , "Pulsed thermography: philosophy, qualitative and quantitative analysis on aircraft materials and applications. Thermal NDT," *Journal Insight,* vol. 48 , p. 286-289, 2016.

[200] M. Köntges, S. Kurtz, U. Jahn, A. Berger, K. Kato, T. Friesen , H. Liu and M. Iseghem, Performance and Reliability of Photovoltaic Systems Subtask: Review of failures of photovoltaic Modules., Berlin, Germany : International Energy Agency (IEA) photovoltaic power systems programme, 2014.

[201] R. Tscharner , K. Rao and A. Shah , "Evaluation of Photovoltaic Panels with IR-Thermography," in *Proc. SPIE 0520, Thermosense VII: Thermal Infrared Sensing for Diagnostics and Control*, Cambridge, United States , 1985.

[202] U. Hoyer , A. Burkert , R. Auer and C. Buerhop-Lutz , "Analysis of PV Modules by Electroluminescence and IR Thermography," in *Proc. 24th EUPVSEC*, Hamburg, Germany , 2009.

[203] S. Zamini , R. Ebner , G. Újvári and B. Kubicek , "Non-destructive techniques for quality control of photovoltaic modules: Electroluminescence imaging and infrared thermography," *Photovoltaics International,* vol. 15 , pp. 126-135, 2012.

[204] C. Buerhop, U. Jahn, U. Hoyer, B. Lerche and S. Wittmann, "Überprüfung der Qualität von Photovoltaik-Modulen mittels Infrarot-Aufnahmen.," BAYERISCHES ZENTRUM FÜR ANGEWANDTE ENERGIEFORSCHUNG E.V. Abteilung Thermosensorik und Photovoltaik. ZAE BAYERN., 2007 .

[205] J. Haunschild, M. Glatthaar , M. Kasemann , S. Rein and E. Weber , "Fast series resistance imaging for silicon solar cells using electroluminescence," *Phys Status Solidi Rapid Res Lett.,* vol. 3, p. 227-229 , 2009.

[206] J. Hofierka and J. Kaňuk , "Assessment of photovoltaic potential in urban areas using open-source solar radiation tools," *Renew Energy.,* vol. 34 , p. 2206-2214, 2009.

[207] L. Lenchyshyn , M. Thewalt and J. Sturm , "High quantum efficiency photoluminescence from localized excitons in Si1-xGex," *Appl Phys Lett.,* vol. 60 , p. 3174-3176, 1992.

[208] M. Currie, J. Mapel, T. Heidel, S. Goffri and M. Baldo, "High-Efficiency Organic Solar Concentrators for Photovoltaics," *Science .,* vol. 321, no. 5886 , pp. 226-228, 2007.

[209] J. Vanek, P. Koktavy, K. Kubickova, P. Sadovsky and M. Raska, "Usage of microplasma signal noise for solar cells diagnostic," in *Proc. SPIE 6600 Noise Fluctuations Circ. Dev.,*, Florence, Italy , 2007.

[210] J. Bauer , J. Wagner and A. Lotnyk , "Hot spots in multi-crystalline silicon solar cells: avalanche breakdown due to etching pits," *Phys Status Solidi Rapid Res Lett.,* vol. 3 , p. 40-42, 2009.

[211] G. C. Eder, Y. Voronko, S. Dimitriadis, K. Knobl, G. Ujvari and K. A. Berger, "Climate-specific accelerated ageing tests and evaluation of ageing-induced electrical, physical, and chemical changes," *Prog Photovolt, Res Appl,* vol. 27, no. 11, pp. 934-949, 2019.

[212] L. Koester, S. Lindig, A. Louwen and A. Astigarraga, "Review of photoltaic module degradation, field inspection techniques and techno-economic assessment," *Renewable and Sustainable Energy Reviews,* vol. 165, pp. 1-15, 2022.

[213] D. Yang and L. Liu, "Solar Project Financing, Bankability, and Resource Assessment.," in *Sustainable Energy Solutions for Remote Areas in the Tropics*, Springer Charm, 2020, pp. 179-211.

[214] A. Sayed , M. El-Shimy , M. El-Metwally and M. Elshahed, "Reliability, availability and maintainability of analysis of grid-connected solar photovoltaic systems," *Energies,* vol. 12, no. 17, p. 1213, 2019.

[215] D. Moser , M. Del Buono , W. Bresciani, , E. Veronese, U. Jahn and M. Herz, "Technical Risks in PV Projects: Solar Bankability Project," EURAC Institute for Renewable Energy , 2016.

[216] "Identification of technical risks in the photovoltaic value chain and quantification of the economic impact," *Prog Photovolt Res Appl,* vol. 25, no. 7, pp. 592-604, 2017.

[217] P. Chiantore and W. Hemetsberger, Operation & maintenance best practice guidelines version 4.0, SolarPower Europe, 2019.

[218] A. Jaafer, "Design and Construction of a Tracking Device for Solar Electrical Systems," *The Journal of Scientific and Engineering Research,* vol. 5 , no. 7, pp. 225-236, 2018.

[219] N. Barsoum, "Fabrication of Dual-Axis Solar Tracking Controller Project," *Intelligent Control and Automation,* vol. 2 , no. 2, pp. 57-68, 2011.

[220] S. Kalogirou, "Environmental Characteristics: Sun Path Diagram," *Processes and Systems,* vol. 2, pp. 51-123, 2014.

[221] A. Ghoname and N. Hidekazu , "Techno-Economic Performance Analysis of a 40.1 kWp Grid-Connected Photovoltaic (GCPV) System after Eight Years of Energy Generation: A Case Study for Tochigi, Japan.," *Journal of Sustainability,* vol. 13 , p. 7680, 2021.

[222] K. Sayed, M. Abdel-Salam, M. Ahmed and A. Ahmed, "Electro-Thermal Modelling of Solar Photovoltaic Arrays," in *International Mechanical Engineering Congress and Exposition (IMECE2011-62541),* Denver, Colorado, USA, 2011.

[223] F. Mazda, Power Electronics Handbook, Newnes, Australia: Antony Rowe Ltd, Eastbourne, 2003.

[224] S. Odeh, "Thermal Performance of Dwellings with Rooftop PV Panels and PV/Thermal Collectors," *Energies,* vol. 1879, no. 11 , pp. 1-14, 2018.

[225] D. Goossens and K. Van , "Aeolian dust deposition on photovoltaic solar cells: the effects of wind velocity and airborne dust concentration on cell performance," *Solar Energy,* vol. 66, no. 4, pp. 277-289 , 1999.

[226] M. Cheggar, A. Hamzaoui, A. Namoda, P. Petit, M. Aillerie and A. Herguth , "Effect of Illumination Intensity on Solar Cells Parameters," *Energy Procedia,* vol. 36 , pp. 722-729, 2013.

[227] A. Amelia, Y. Irwan, W. Leow, M. Irwanto, I. Safwati and M. Zhafarina, "Investigation of the Effect of Temperature on Photovoltaic (PV) Panel Output Performance," *International Journal on Advanced Science Engineering Information Technology,* vol. 6 , pp. 682-688, 2016.

[228] V. Fesharaki, M. Dehghani and J. Fesharaki, "The Effect of Temperature on Photovoltaic Cell Efficiency," in *Proceedings of the 1st International Conference on Emerging Trends in Energy Conservation*, Tehran , 2011.

[229] D. Tobnaghi , R. Madatov and D. Naderi , "The effect of temperature on electrical parameters of solar cells," *International Journal of Advanced Research in Electrical, Electronics and Instrumentation Engineering,* vol. 2 , pp. 6404-07, 2013.

[230] A. Brito, H. Araújo and G. Zebende, "Detrended Multiple Cross Correlation Coeffcient applied to solar radiation, air temperature and relative humidity," *Nature Scientif Reports,* vol. 9 , no. 19764, 2019.

[231] C. Furlan, A. de Oliveira, J. Soares, G. Codato and J. Escobedo, "The role of clouds in improving the regression model for hourly values of diffuse solar radiation," *Applied Energy,* pp. 0306-2619 , 2011.

[232] M. Theristis, A. Livera , C. Birk Jones, G. Makrides, G. Georghiou and J. Stein, "Nonlinear Photovoltaic Degradation Rates: Modeling and Comparison Against Conventional Methods," *IEEE Journal of Photovoltaics,* vol. 10, no. 4, pp. 1112-1118, 2020.

[233] D. Quansah and M. Adaramola, "Assessment of early degradation and performance loss in five co-located solar photovoltaic module technologies installed in Ghana using performance ratio time-series regression," *Renewable Energy,* vol. 131, pp. 900-910 , 2019.

[234] S. Kurtz , J. Luis Becerra Cruz , E. Riley and C. Hansen , "Weather-Corrected Performance Ratio," National Renewable Energy Laboratory Technical Report, NREL/TP-5200-57991., Oak Ridge, USA , 2013.

[235] D. Jordan, C. Deline, S. Kurtz, G. Kimball and M. Anderson , "Robust PV Degradation Methodology and Application," *IEEE Journal of Photovoltaics,* vol. 8 , pp. 525-531, 2018.

[236] R. French, L. Bruckman, D. Moser, S. Lindig, M. Van Iseghem, B. Müller, J. Stein, M. Richter, M. Herz, W. Sark and F. Baumgartner, "Assessment of Performance Loss Rate of PV Systems," International Energy Agency, Fraunhofer ISE, Germany , 2021.

[237] S. Lindig , I. Kaaya , K. Weiβ , D. Moser and M. Topic , "Review of statistical and analytical degradation models for photovoltaic modules and systems as well as related improvements," *IEEE Journal of Photovoltaics,* vol. 8, pp. 1773-1786 , 2018.

[238] P. Ingenhoven , G. Belluardo and D. Moser , "Comparison of statistical and deterministic smoothing methods to reduce the uncertainty of performance loss rates estimates," *IEEE Journal of Photovoltaics,* vol. 8 , pp. 224-232, 2018.

[239] M. Tur, I. Colak and R. Bayindir, "Effect of Faults in Solar Panels on Production Rate and Efficiency," in *International Conference on Smart Grid (icSmartGrid)*, Nagasaki, Japan, 2018.
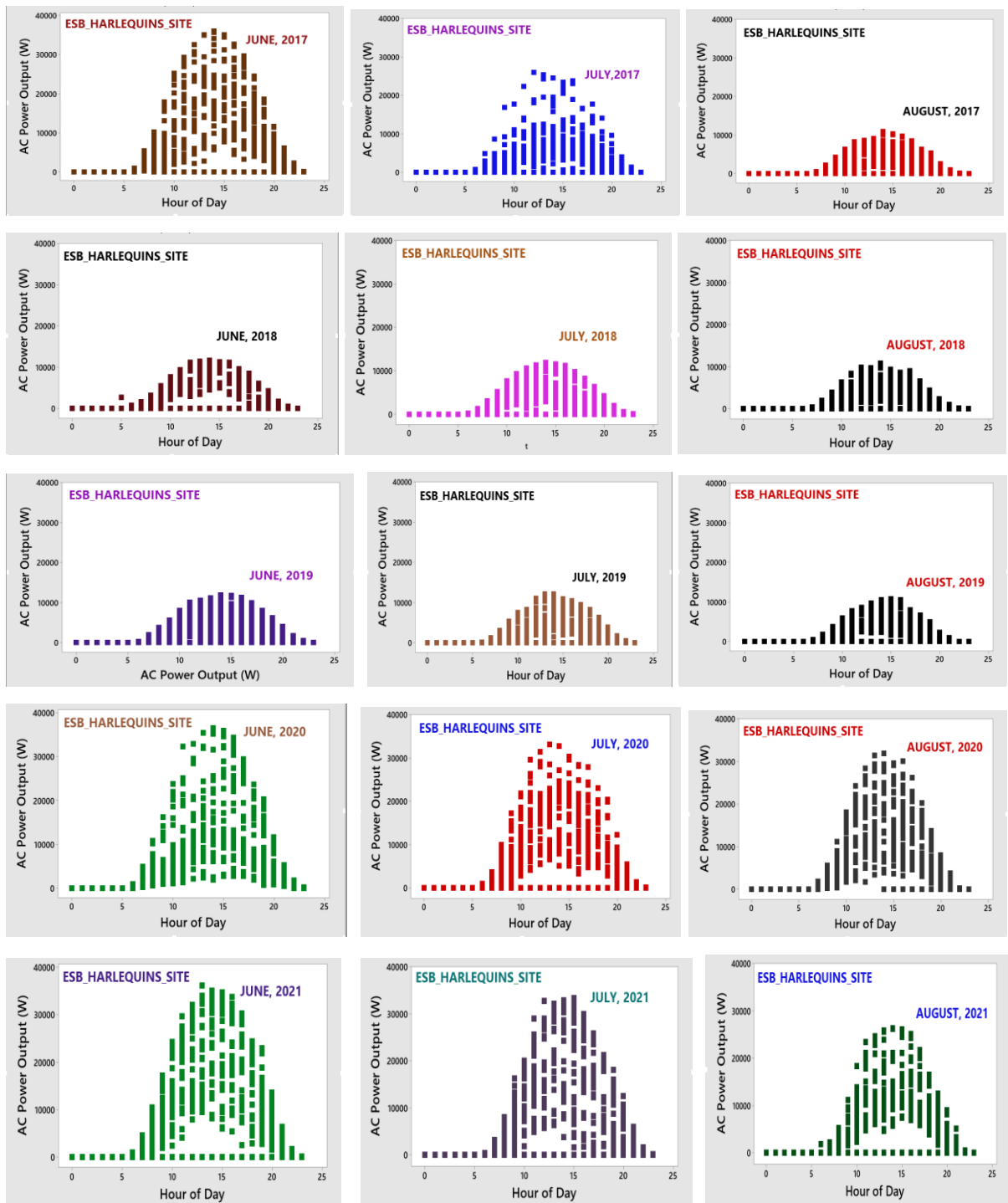
APPENDICES

Appendix 1: Effect of seasonal variation in PV power out at Harlequins

Appendix 1 (a): AC power output profiles in the spring season at Harlequins from 2017 – 2021
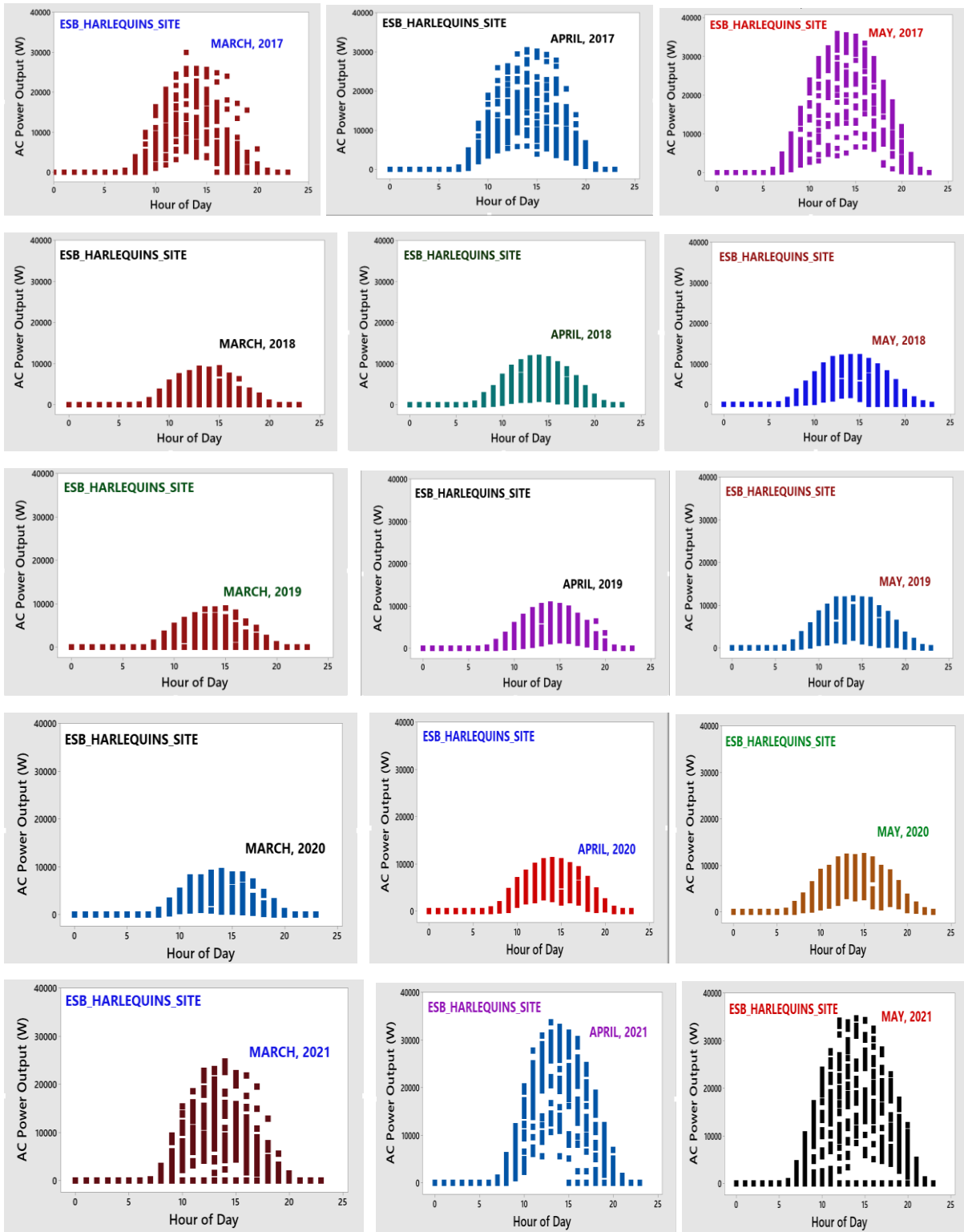
Appendix 1 (b): AC power output profiles in the summer season at Harlequins from 2017 – 2021

Appendix 1 (c): AC power output profiles in the autumn season at Harlequins from 2017 – 2021.
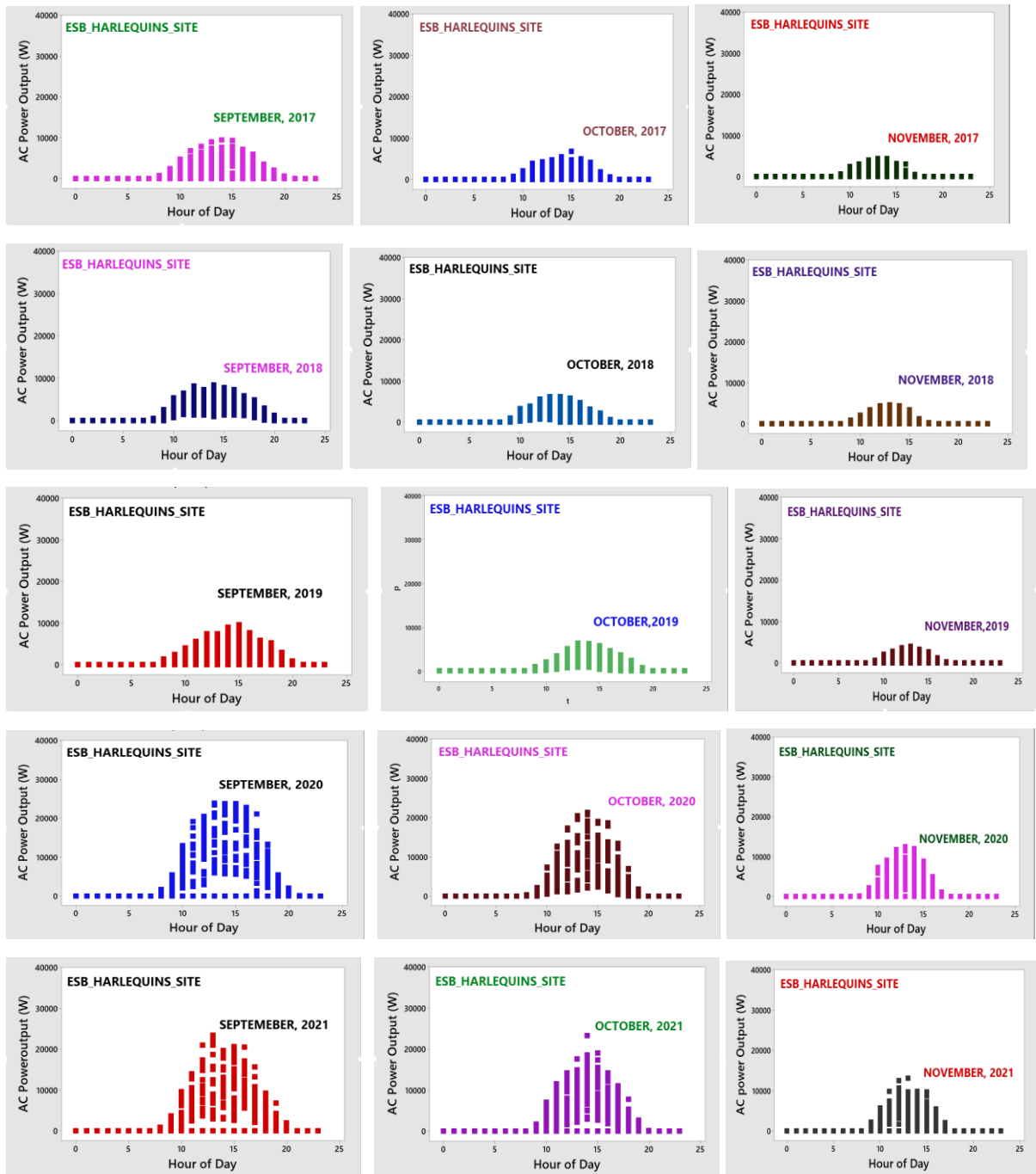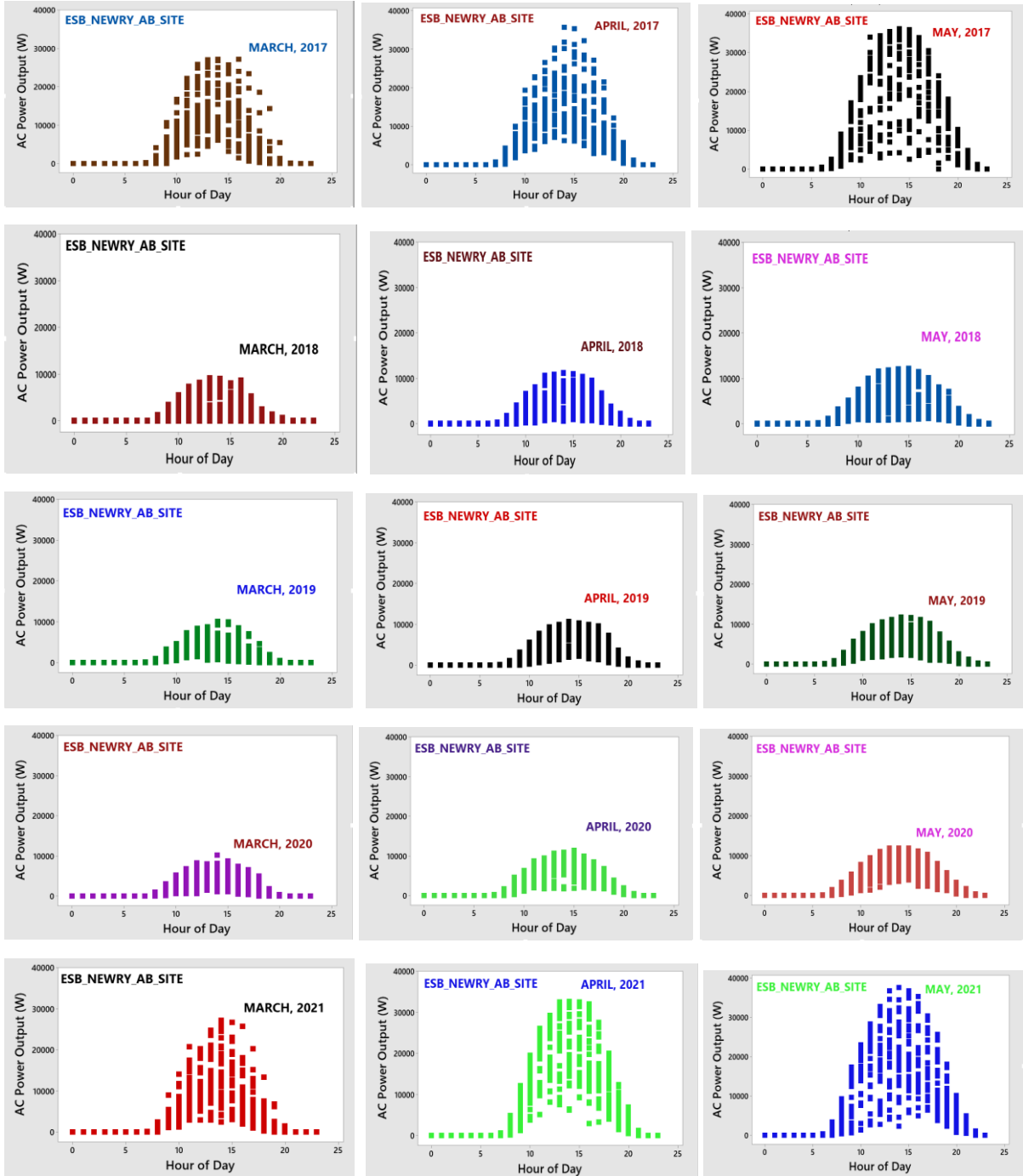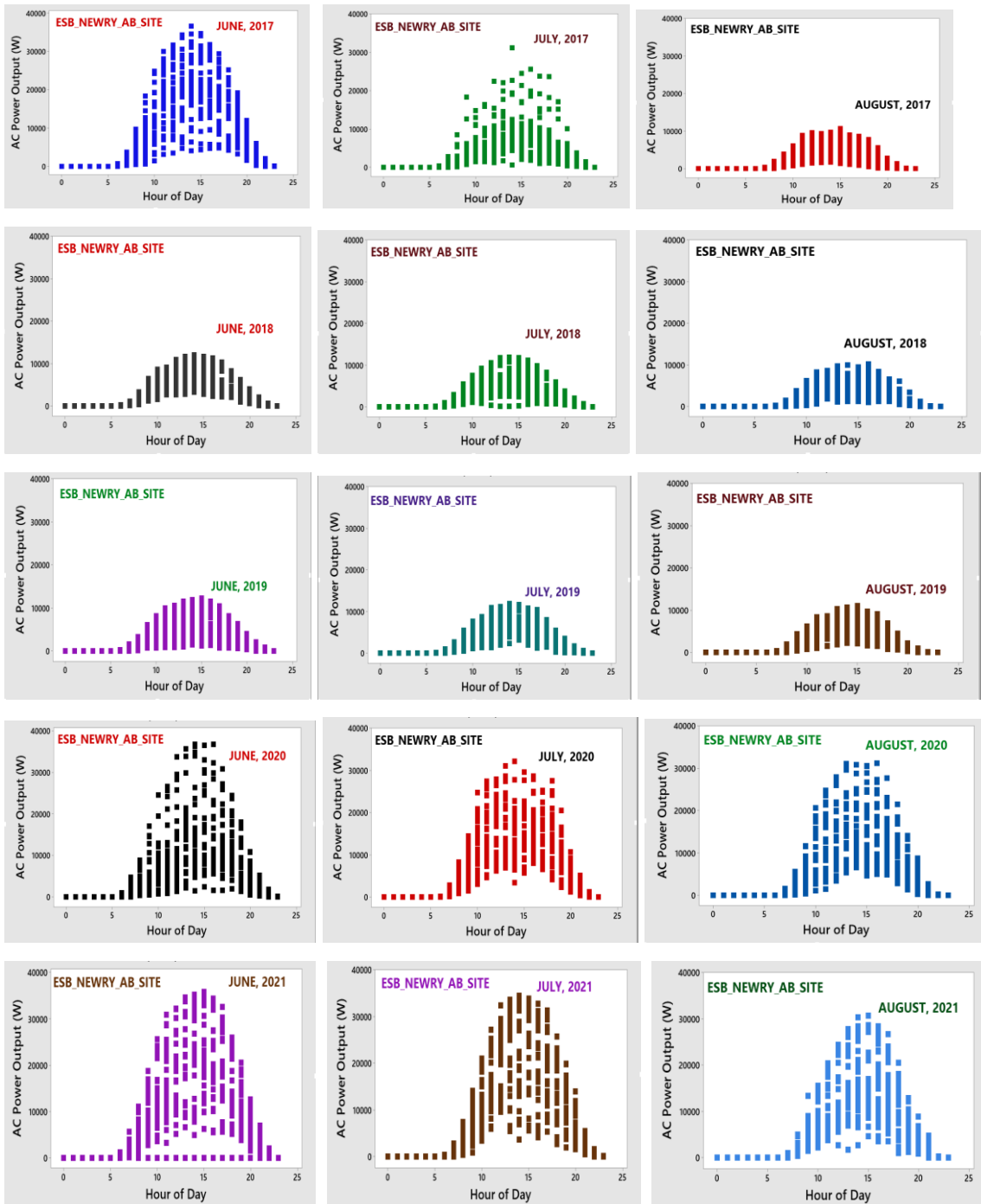
Appendix 1 (d): AC power output profiles in the winter season at Harlequins from 2017 – 2021.
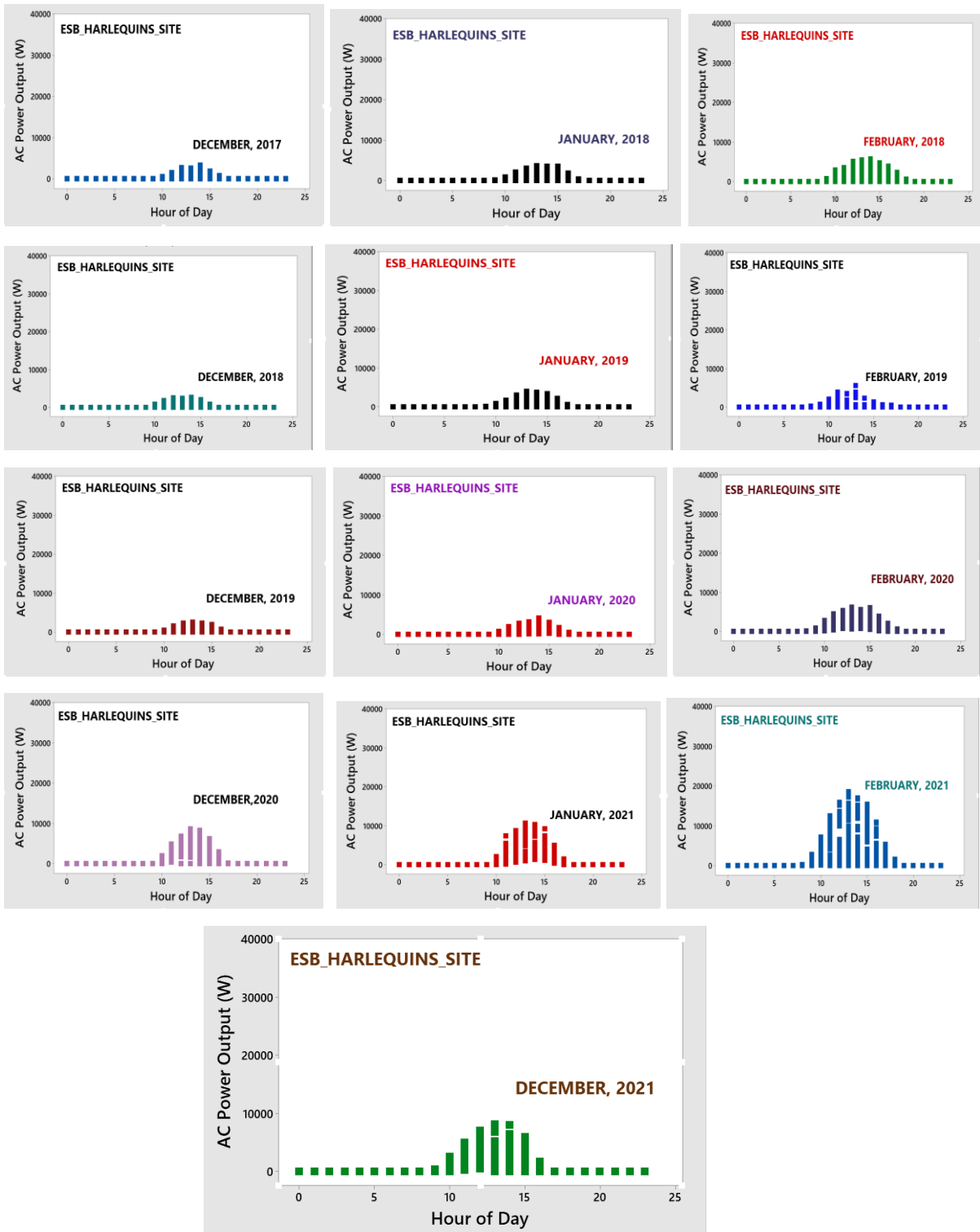
Appendix 2: Effect of seasonal variation in PV power out at Newry

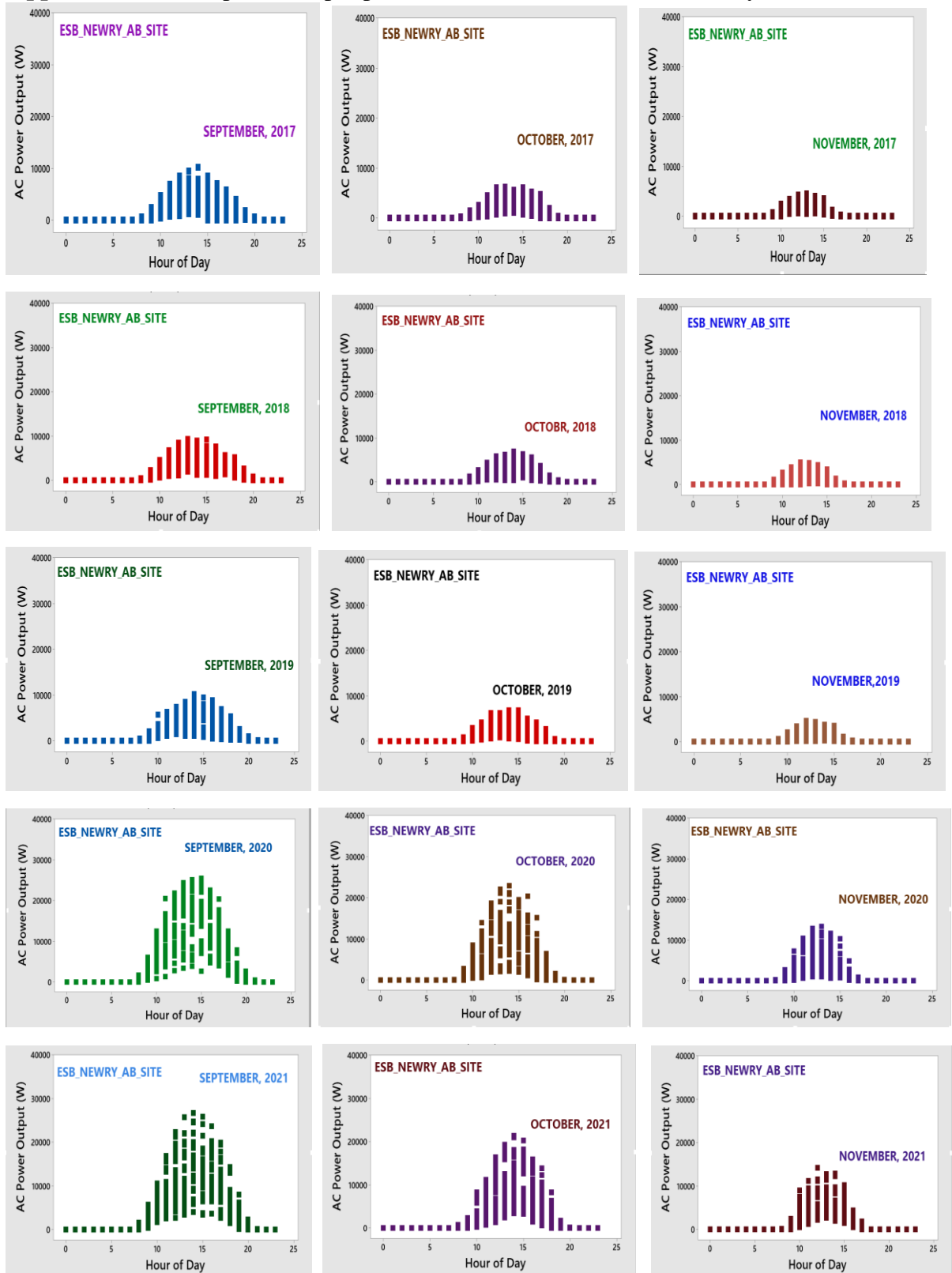**Appendix 2 (a):** AC power output profiles in the spring season at Newry from 2017 – 2021.
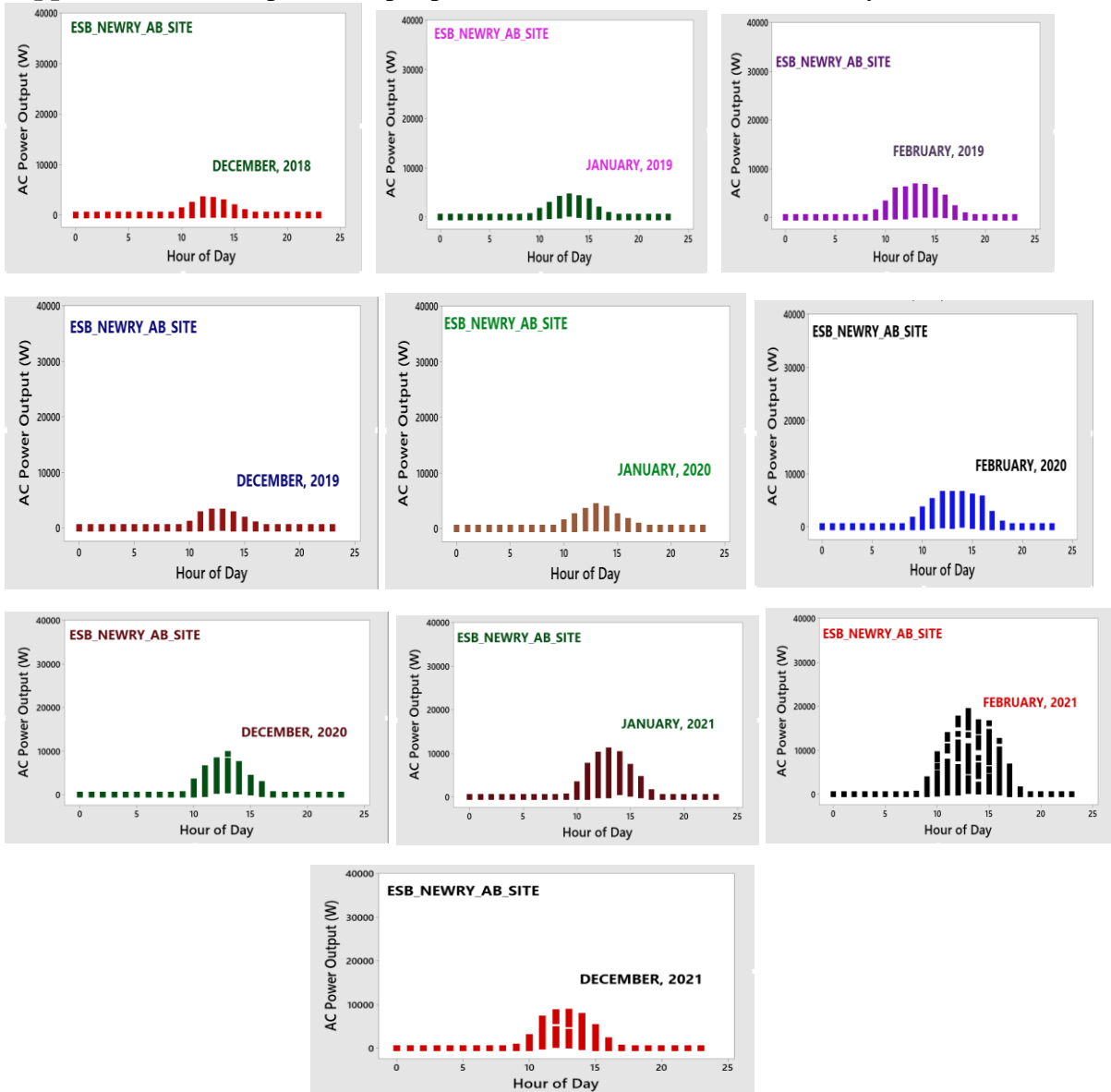

s

Appendix 2 (b): AC power output profiles in the summer season at Newry from 2017 – 2021.

Appendix 2 (c): AC power output profiles in the autumn season at Newry from 2017 – 2021.
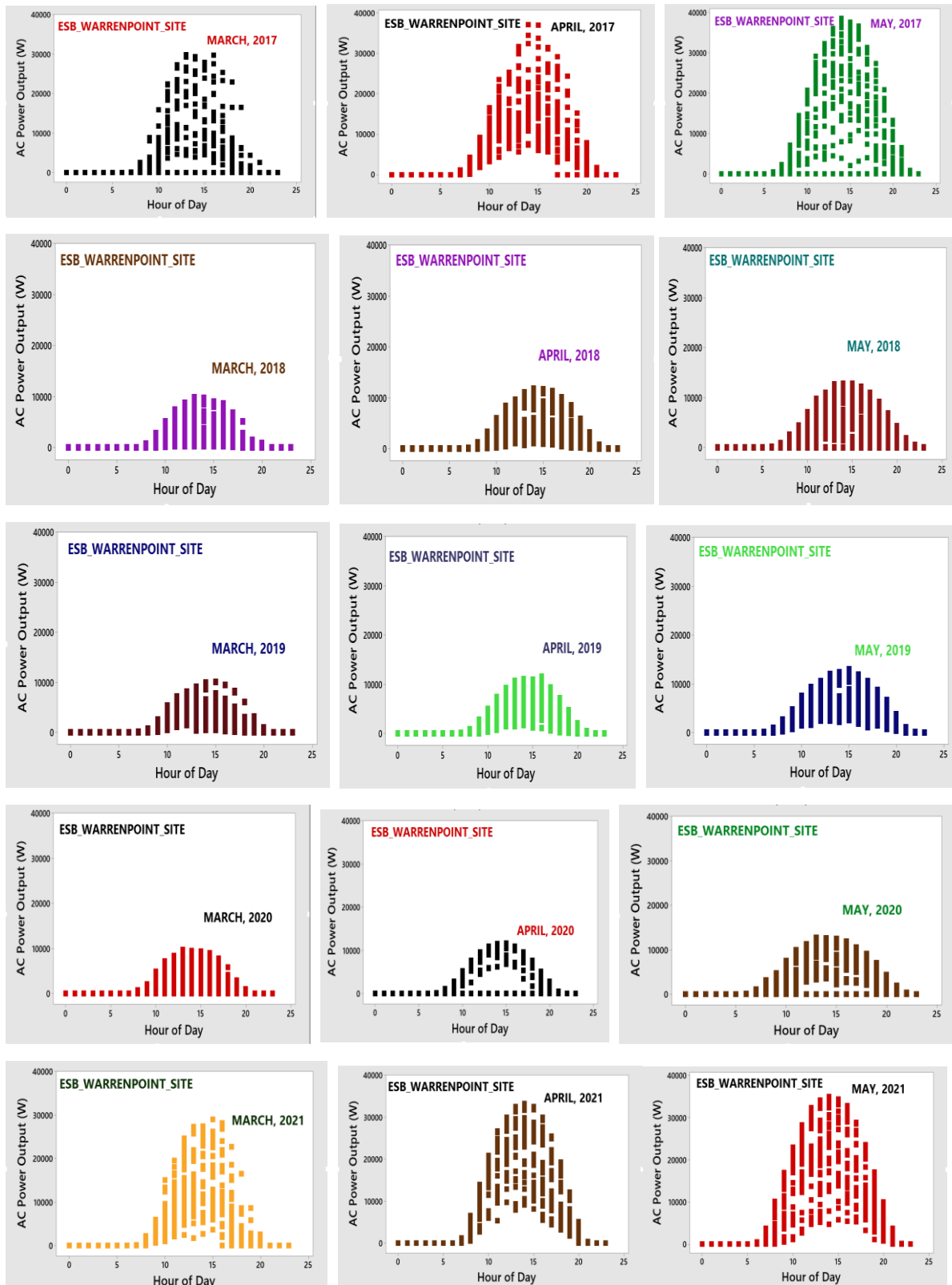
Appendix 2 (d): AC power output profiles in the winter season at Newry from 2017 – 2021.
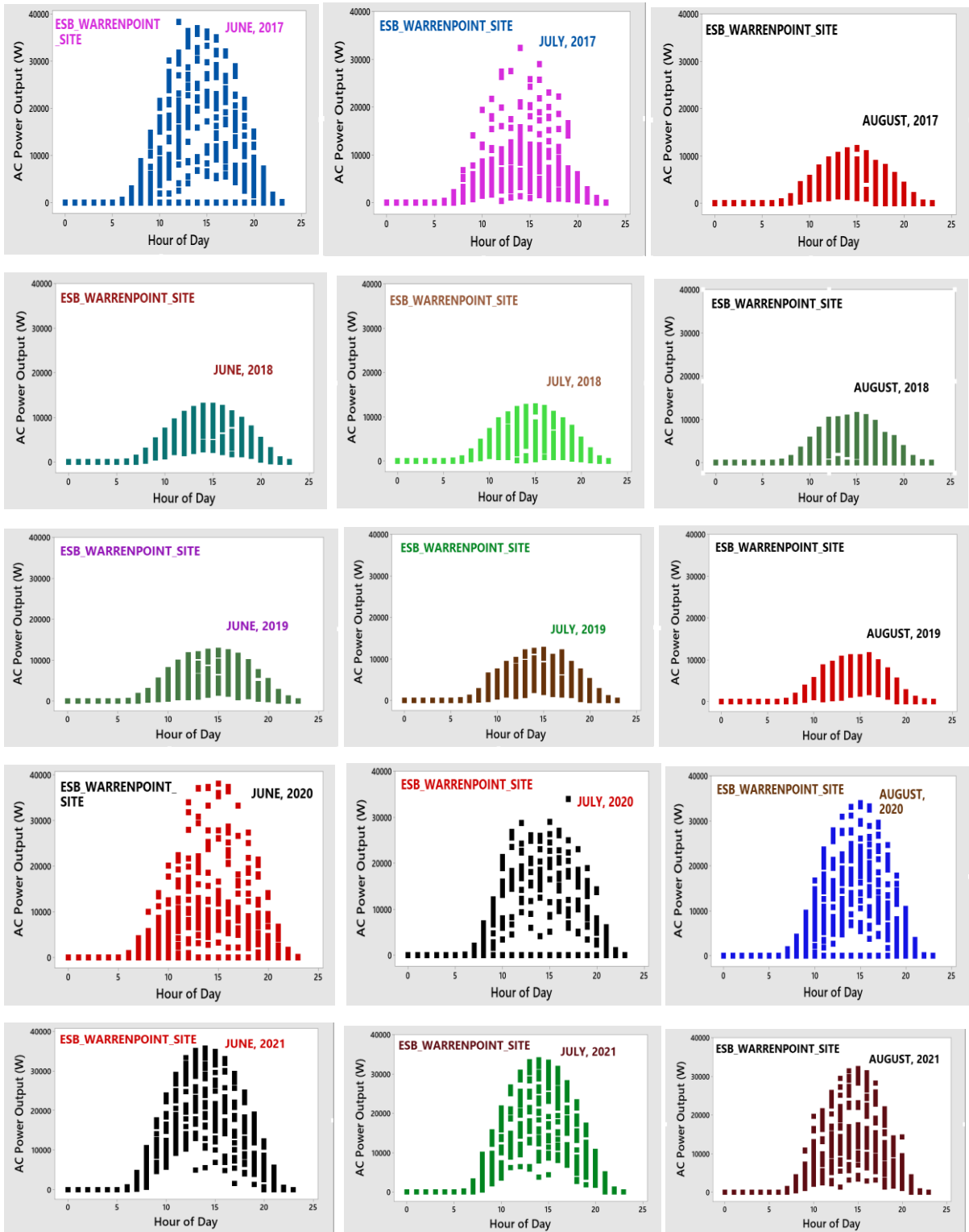
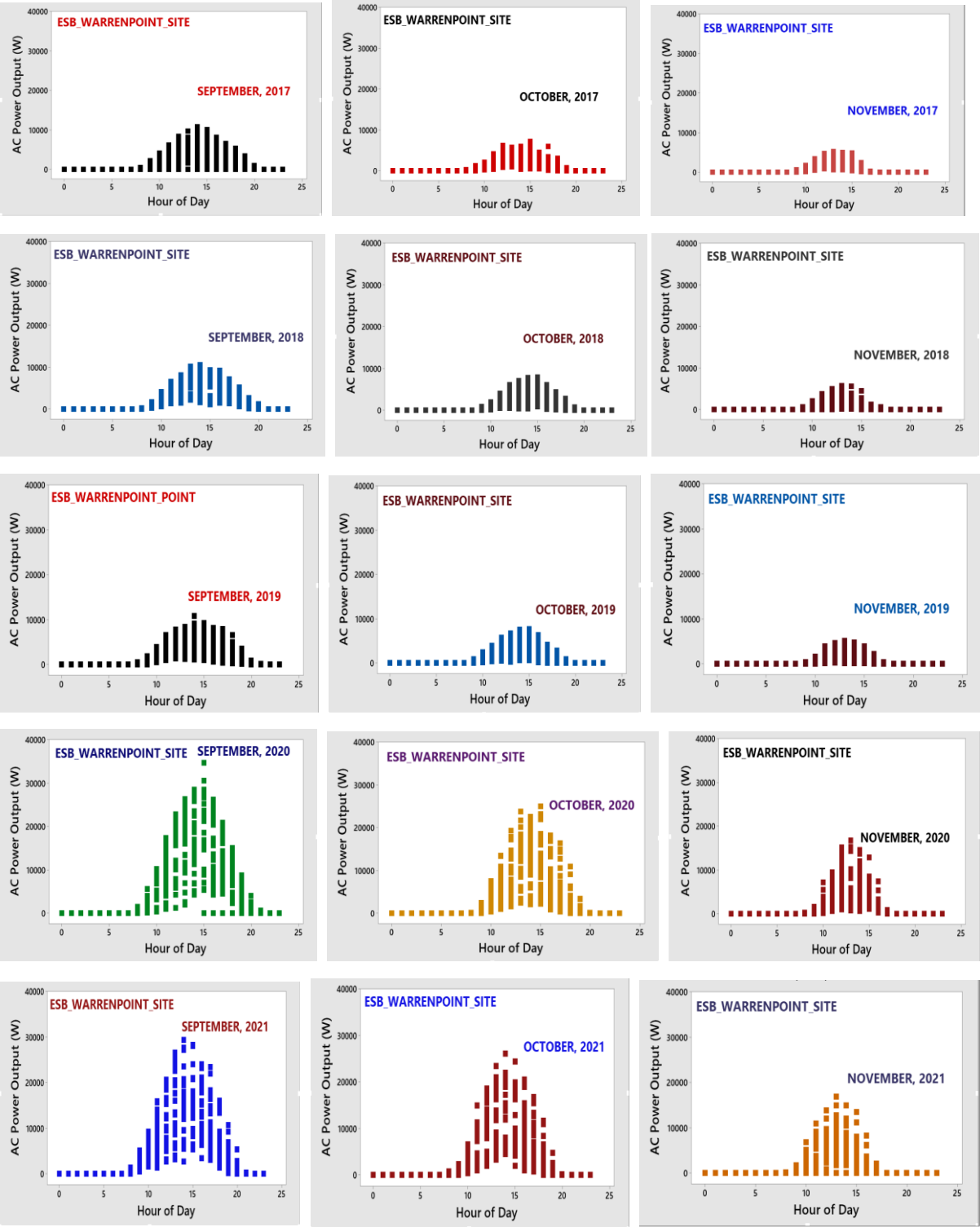# Appendix 3: Effect of seasonal variation in PV power out at Warrenpoint

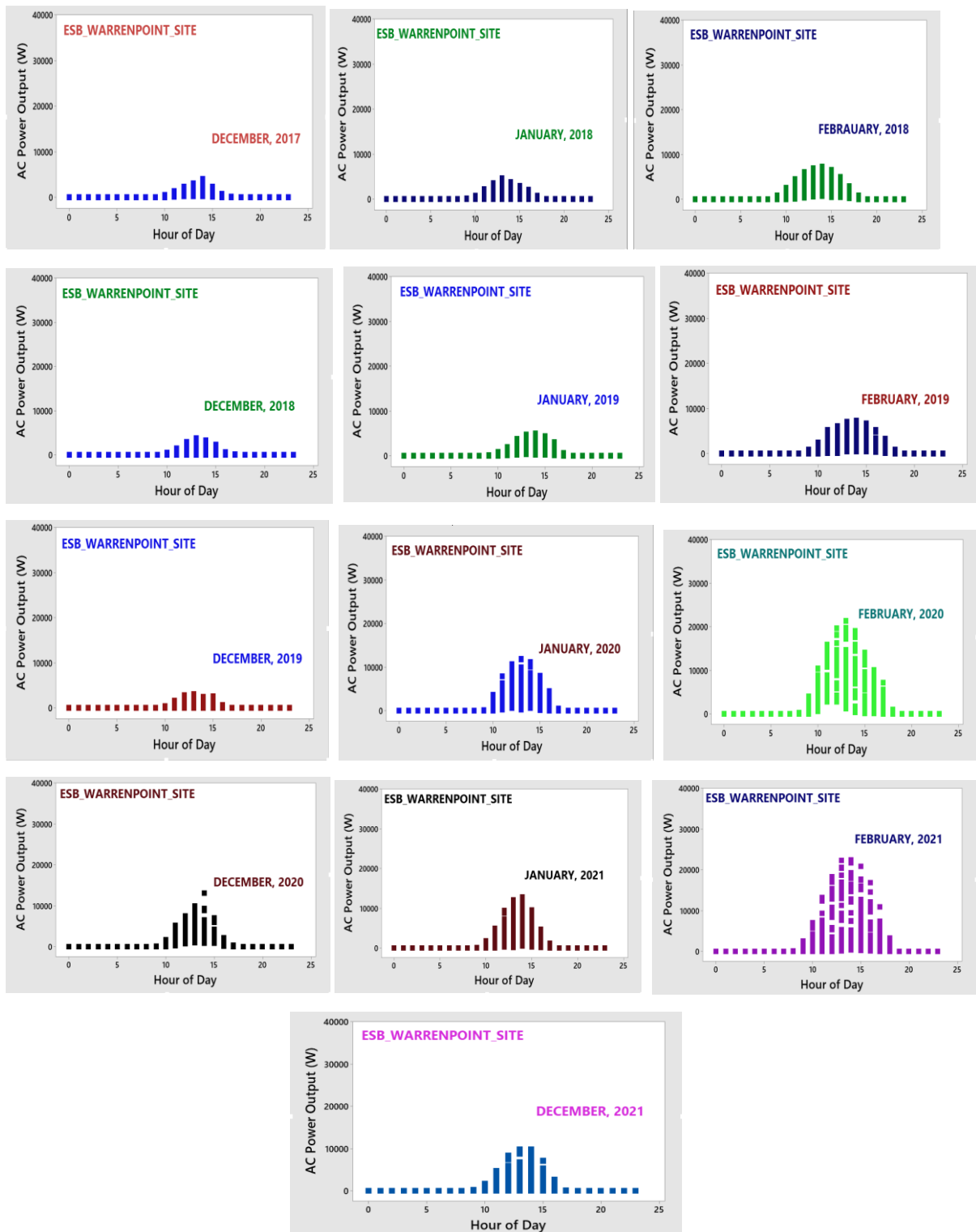**Appendix 3 (a):** AC power output profiles in the spring season at Warrenpoint from 2017 – 2021.

Appendix 3(b): AC power output profiles in the summer season at Warrenpoint from 2017 – 2021.

Appendix 3 (c): AC power output profiles in the autumn season at Warrenpoint from 2017 – 2021.

Appendix 3 (d): AC power output profiles in the winter season at Warrenpoint from 2017 – 2021.

Publications Arising From This Thesis

Conferences

Okorieimoh C.C., Norton B., Conlon M. (2020). Long-Term Durability of Solar Photovoltaic Modules. In: Scott L., Dastbaz M., Gorse C. (eds) Sustainable Ecological Engineering Design. Springer, Cham. https://doi.org/10.1007/978-3-030-44381-8_24

Okorieimoh C.C., Norton B., Conlon M. (2019). Effect of Transient Performance Changes on Photovoltaic Modules Output. 10th Annual Graduate Research School Symposium, Technological University Dublin, Ireland. 10.13140/RG.2.2.28516.94083

Okorieimoh C.C., Norton B., Conlon M. (2021). The Effects of the Transient and Performance Loss Rates on PV Output Performance. International Conference on Innovations in Energy Engineering & Cleaner Production IEECP21, Silicon Valley, San-Fransico, USA.

Okorieimoh C.C., Norton B., Conlon M. Comparison of Predicted and Measured Annual Performance of a Roof-Top Grid-Connected PV System in the Irish Climate. SEEDS 2021 Conference. Accepted to be Published in SpringerNature.

Okorieimoh C.C., Norton B., Conlon M. Reviewing The External Factors That Influence PV Output Performance in the Irish Climate. SEEDS 2021 Conference. Accepted to be Published in SpringerNature.

Journals

Okorieimoh C.C., Norton B., Conlon M. (2022). Influence of Site and System Parameters on the Performance of Roof-Top Grid-Connected PV Systems Installed in Harlequins, Belfast, Northern Ireland. International Research Journal of Engineering and Technology (IRJET), Vol. 09, Issue 02, pp.507-520. 10.13140/RG.2.2.33222.75840

Okorieimoh C.C., Norton B., Conlon M. Statistical Analyses Studying the Significance Levels and Confidence Intervals for the Temperature-Correction in Reducing the Seasonal Performance Ratios Variability of Grid-Connected Rooftop Photovoltaic Systems Installed in the Irish Climate. Undergoing a reviewing process by the Journal of Renewable and Sustainable Energy Reviews.

Okorieimoh C.C., Norton B., Conlon M. The Investigation of System Performance Assessment of 49.92 kW$_P$ of Rooftop Grid-Connected PV Systems Installed in Warrenpoint, Northern Ireland. Undergoing a reviewing process by the Journal of Current Sustainable/Renewable Energy Reports.